ResearchGate

See discussions, stats, and author profiles for this publication at: https://www.researchgate.net/publication/8013567

The Structure of Active Centers and the Ethylene Polymerization Mechanism on the Cr/SiO 2 Catalyst: A Frontier for the Characterization Methods

ARTICLE *in* CHEMICAL REVIEWS · FEBRUARY 2005

Impact Factor: 46.57 · DOI: 10.1021/cr040083s · Source: PubMed

CITATIONS
244

READS
115

5 AUTHORS, INCLUDING:

Carlo Lamberti
Università degli Studi di Torino
379 PUBLICATIONS **12,975** CITATIONS
SEE PROFILE

Giuseppe Spoto
Università degli Studi di Torino
187 PUBLICATIONS **7,029** CITATIONS
SEE PROFILE

A. Zecchina
Università degli Studi di Torino
560 PUBLICATIONS **19,745** CITATIONS
SEE PROFILE

Available from: Carlo Lamberti
Retrieved on: 20 January 2016

The Structure of Active Centers and the Ethylene Polymerization Mechanism on the Cr/SiO_2 Catalyst: A Frontier for the Characterization Methods

E. Groppo, C. Lamberti, S. Bordiga, G. Spoto, and A. Zecchina*

Department of Inorganic, Physical and Materials Chemistry and NIS Centre of Excellence, University of Torino, Via P. Giuria 7, 10125 Torino, Italy

Received July 12, 2004

Contents

* To whom correspondence should be addressed. Tel: +39011-6707860. Fax: +39011-6707855. E-mail: adriano.zecchina@unito.it.

1. Introduction

The discovery of olefin polymerization catalysts in the early 1950s by Ziegler and Natta represents a milestone in industrial catalysis. This discovery was of outstanding relevance for the industrial synthesis of polyolefins. Tremendous evolution has taken place since that moment: today, fourth generation Ziegler−Natta catalysts and metallocene-based "single-site" catalysts display activity and stereoselectivity close to those of enzymatic processes optimized by nature over millions of years. The production of polyolefins is nowadays a multibillion dollar industrial activity.

Among all of the synthetic polymers, PEs have the highest production volumes.[1] Global production currently stands at just over 40 million tons annually, making PE by far the most widely used commodity polymer.[2] PEs have been and still are so successful in competition with other plastic materials because they have clear advantages and key success factors. PEs have an excellent chemical resistance, a high impact strength, and stiffness even at low temperature. The industrial processes work at low costs and

10.1021/cr040083s CCC: $53.50 © 2005 American Chemical Society
Published on Web 01/12/2005

Elena Groppo was born in 1978 and received her degree in Material Science in July 2002 at the University of Torino, under the supervision of Dr. C. Lamberti, investigating the local structure of thin oxide films deposited on metal substrates by means of polarization-dependent EXAFS spectroscopy at LURE, ESRF, Daresbury, and Elettra synchrotrons. Since November 2002, she has started a Ph.D. in Chemistry, under the supervision of Prof. A. Zecchina, devoted to the spectroscopic characterization of the Phillips catalyst using in situ IR, Raman, UV–vis DRS, EXAFS, and XANES as the main techniques. She has coauthored six research papers and two book chapters.

Carlo Lamberti was born in 1964 and took the degree in Physics in 1988 at the University of Torino. He received a Ph.D. in solid state physics by investigating 4 K photoluminescence and EXAFS spectroscopies of the structures of the interfaces in InGaAs/InP and InGaAsP/InP quantum wells and superlattices for optoelectronics. He joined the group of Adriano Zecchina in 1992, with the role of preparing and reanalyzing X-ray absorption and diffraction experiments at synchrotron radiation facilities on zeolites and zeotypes materials. In Zecchina's group, he received a permanent position as researcher in 1998. He has performed more than 50 experiments with synchrotron and neutron sources, and he has authored and coauthored more than 150 research papers, three review articles, three book chapters, and a book that have received more than 2500 citations. In the 2001–2004 period, he has been a member of the ESRF review commitee in Chemistry.

Silvia Bordiga was born in 1964 and took the degree in Chemistry in 1988 at the University of Torino. During the period 1990–1992, she followed the Ph.D. in Chemistry, discussing her thesis in 1993. In 1995, she obtained the position of researcher in the field of physical chemistry. She has been a Professor in Physical Chemistry at the Faculty of Sciences of the University of Turin since July 2001. Actually, her teaching activities refer to heterogeneous catalysis and spectroscopies considering both theory and applications. Her scientific activities are mainly devoted to the characterization of the physical–chemical properties of oxides and zeolites with particular attention to their surface properties. She has coauthored more than 150 research and 3 review papers, which have appeared in international journals and have received more than 3000 citations.

Giuseppe Spoto (born in 1955) received his degree, under the supervision of Prof. A. Zecchina, in 1981 from the University of Torino. After some years spent performing industrial research (by the Istituto Guido Donegani in Novara, Italy) on the preparation and characterization of ceramic powders with controlled morphology, he joined, in 1986, the Physical Chemistry Group at the University of Torino where he is currently an Associate Professor of Spectroscopy. His main research interests involve the physicochemical characterization of the surface properties (including reactivity) of oxides, zeolites, and zeotypes, as pure systems or containing supported, grafted, or incapsulated metal species, by means of spectroscopic and gravimetric (or volumetric) methods and electron microscopies (HRTEM and SEM).

are environmental friendly. When PEs have lost their performance, they can be recycled for energy production.[3]

The demand for catalysts to make new varieties of PE has inspired an extraordinary effort from researchers both in industry and in academia, due to the growing commercial importance of these materials. However, a major challenge remains in rationalizing and ultimately predicting the differences in activity manifested by various catalyst formulations.

With the exception of the LDPE, which is made by a high temperature/high pressure radical process, the other types of PE (HDPE and LLDPE) are produced by using either homogeneous or heterogeneous catalysts operating at relatively low temperatures (353−453 K) and pressures (<50 bar). Three classes of olefin polymerization catalysts can be distinguished as follows: (i) Phillips type catalysts, which are composed of a chromium oxide supported on an amorphous material such as silica;[4−9] (ii) Ziegler−Natta catalysts, which consist of a transition metal compound and an activator (aluminum alkyl, MAO, etc.) whose function is to introduce an alkyl group in the coordination sphere of the metal;[1,10−14] and (iii) single-site homogeneous catalysts or supported homogeneous catalysts, like metallocene catalysts[15,16]

Adriano Zecchina was educated at the University of Turin (I), where he has been a full Professor of Physical Chemistry since 1976. He spent a year at Bath University (United Kingdom) doing research on surface spectroscopy with Prof. F. S. Stone. He has been a foreign member of the Faraday Division Council. In 1980, he was awarded with the Bourke Medal of the Faraday Society, and in 2003, he received the Fauser Plate of the Italian Chemical Society. He was president of the Italian Physical Chemistry Society from 1984 to 1988. He was a member of the International Advisory Board of Faraday Transactions from 1993 to 1996 and of the Editorial Board from 1996 to 1998. He is a member of the International Advisory Board of PCCP. His interests focus on the studies of surface chemistry using spectroscopic techniques. He has authored and coauthored more than 300 research articles and six reviews that have received more than 7000 citations. He is the coordinator of the Centre of Excellence NIS (Nanostrucured Interfaces and Surfaces) and of the Ph.D. School in Science and Technology of Materials of the Torino University.

and incompletely condensed silsesquioxane,[17] which also need an activator.

The Cr/SiO_2 Phillips catalysts, patented in 1958 by Hogan and Banks,[4] are nowadays responsible for the commercial production of more than one-third of all of the PE sold worldwide.[3,9] The success of the Phillips polymerization process originates from its diversity: Phillips catalysts, in fact, are able to make more than 50 different types of HDPE and LLDPE.[6] Furthermore, it does not require the intervention of any activators, a fact that simplifies the catalyst preparation and production process.

In this review, no attempt will be given to discuss the industrial Phillips polymerization processes. We only mention that three different industrial modes of operation for the Phillips polymerization process exist, and in this respect, we refer to the reviews of Clark[7] and Weckhuysen:[8,9] (i) the solution process, which uses an inert hydrocarbon to dissolve the polymer as it is formed; (ii) the slurry process, known as the Phillips Particle Form process (licensed by Phillips Petroleum), in which a liquid dispersant is used; and (iii) the gas phase process, generally known as the UNIPOL process (licensed by Union Carbide), which does not require any solvent or dispersant.

The industrial importance of the Phillips catalyst has attracted a great deal of academic and industrial research over the last 50 years. Despite these efforts, however, the structures of active sites on the Phillips type polymerization systems remain controversial, and still, the same questions are asked since their discovery. In the 1950s, Hogan and Banks[4] claimed that the Phillips catalyst "is one of the most studied and yet controversial system". In 1985, McDaniel, in a review entitled "Chromium Catalysts for Ethylene Polymerization",[6] stated, "we seem to be debating the same questions posed over thirty years ago, being no nearer to a common view." Nowadays, it is interesting to underline that although in the last two decades a lot of progress has been made, no unifying picture has yet been achieved.

Briefly, the still open questions remain the structure of the active sites and the exact initiation/polymerization mechanism. The difficulties encountered in the determination of the structure of the active sites of the real catalyst are associated with several factors. Among them, we mention the problem associated with the initial reduction step consisting of the reaction between the ethylene and the anchored chromate or dichromate precursors, leading to the formation of the real active sites. In fact, in this reaction, ethylene oxidation products (including H_2O) are formed, which, remaining partially adsorbed on the catalyst, make the characterization of the surface sites of the reduced Cr/SiO_2 system a highly complex problem. Fortunately, it has been established that the reduction of the oxidized precursors can be performed also with a simpler reductant like CO with formation of a single oxidation product (CO_2), which is not adsorbed on the sample.[6] This simpler reduction procedure allows us to obtain a simplified version of the catalyst, where the oxidation state of chromium and the surface hydroxylation are much better controlled. This CO-reduced catalyst, containing prevalently anchored Cr(II), has consequently been considered as a "model catalyst" and an ideal playground where the application of sophisticated in situ characterization methods could finally give the opportunity to solve the mystery of the structure of active sites and of the initiation mechanism.

Unfortunately, as it will be documented in the review, the results accumulated in the last two decades showed that the Cr(II) sites formed upon CO reduction, which are anchored to an amorphous support, are still quite heterogeneous from the structural point of view. Hence, the model character of the CO-reduced catalyst has not been fully confirmed. Similarly, despite many efforts, the exact determination of the structure of the species formed in the initiation step has been prevented so far for two reasons: (i) Only a very small fraction of the Cr(II) sites are really active in polymerization under the usually adopted experimental conditions, and (ii) the high polymerization rate (high turnover number) characterizing the active sites makes the observation of the first polymerization products troublesome (at least under normal reaction conditions). It is so surprising that all of these difficulties did not discourage the efforts for the complete characterization of this catalyst. This is for two reasons. The first is related with the outstanding importance of the ethylene polymerization reaction with the Phillips catalyst and with the mystery of the initiation mechanism not requiring activators (unlike Ziegler−Natta and metallocene systems). The second is associated with the simple character of the CO-reduced system,

where the chromium centers are nearly all under the divalent form, and, hence, still represents the nearest example of model catalyst.

The aim of this review is to illustrate, on one side, how much progress has been made in the last period on understanding the site structures and, on the other side, the strategies and the techniques that can be adopted to study the catalyst under working conditions. It will be shown that the methods adopted for the Cr/SiO_2 system have paradigmatic character and can be extended to other catalytic systems. The next section is devoted to a discussion of the surface chemistry of the silica support, which plays a key role in the anchoring of chromium species. The abundant literature on the Phillips catalyst until 1985 will be shortly reviewed in section 3, and in this respect, we refer to several excellent review papers, most notably the McDaniel one.[6] In the successive part of the paper, we will try to accurately describe the answers to the two principal questions concerning the Cr/SiO_2 Phillips catalyst (i.e., the structure of the active sites and the polymerization mechanism) given by the various researchers, collecting the recent experimental and theoretical results in the two fields of characterization (section 4) and catalytic activity (section 5). The final conclusion (section 6) is that the increasing use of sensitive and sophisticated surface characterization methods allows us to approach the final target and that the lesson derived from this study has general validity.

2. The Surface of Silica Support

The Cr/SiO_2 system is an outstanding example of a catalyst where the sites are formed by anchoring a chromium compound to the hydroxyl groups of the silica surface. For this reason, the catalyst support not only acts as a mere dispersing agent for the active chromium centers but its properties also have a relevant effect on the catalyst activity and on the polymer characteristics. In other words, the sites structure depends directly upon the surface structure and chemical properties of the support. This confers to the Cr sites unique catalytic properties, differentiating the Cr/SiO_2 system from other Cr-based catalysts. On the basis of these considerations, it is evident that a brief description of the structure of SiO_2, together with a discussion of the surface models and of the modifications induced by thermal treatments, is of vital importance to understand the anchoring process and the chromium localization. No attempt will be given to cover the whole field of the silica surface properties. In this respect, we refer to the review of Sauer et al.,[18] reporting a complete theoretical study of van der Waals complexes at surface sites in comparison with the experiment and to the Zhuravlev review,[19] where the properties of amorphous silica surfaces and their dependence from the activation procedure are deeply discussed.

Because amorphous silica acts as a support for several transition metal ions, resulting in a large number of catalytic systems playing important roles in both academic and industrial levels, the interest of the present section is not limited to the Phillips catalyst only but has a much broader impact.

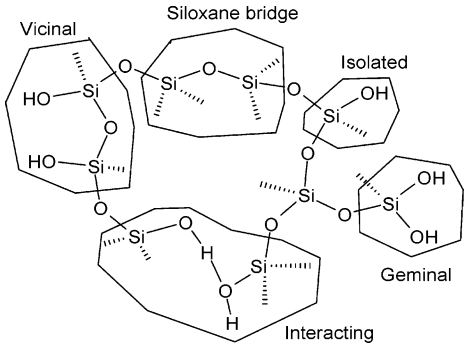

Figure 1. Structural schemes of various OH sites found at the hydrated amorphous silica surface.

Coming back to the structural problems, we recall that the rigid tetrahedron SiO_4 is the building block of all siliceous materials: from quartz, through microporous zeolites, to amorphous silica. The reason that such a relatively rigid unit is able to aggregate in so many different ways lies in the peculiar bond between two SiO_4 moieties. In contrast with the rigidity of the O−Si−O angle, the energetic costs needed to change the Si−O−Si angle in the 130−180° range are negligible. This result also explains, among the other things, the high thermal stability of the amorphous phase. Because of such flexibility, amorphous silica is easily formed and shows a great stability. It consists of a network of such building blocks with a random distribution of the Si−O−Si angle centered around 140°. Silica is classified as a nonmetallic covalent oxide,[20] where the valence electrons are localized in strong covalent bonds between Si and O.

2.1. OH Groups at the SiO_2 Surface: Experimental and Theoretical Approaches

Peripheral SiO_4 groups carry OH groups, which terminate the unsaturated valences. Different types of surface hydroxyls have been identified, differing either by the number of hydroxyl groups per Si atom or by their spatial proximity. Roughly, OH groups can be divided as follows (see Figure 1): (i) isolated free (single silanols), ≡SiOH; (ii) geminal free (geminal silanols or silanediols), =$Si(OH)_2$; and (iii) vicinal, or bridged, or OH groups bound through the hydrogen bond (H-bonded single silanols, H-bonded geminals, and their H-bonded combinations). On the SiO_2 surface, there also exist surface siloxane groups or ≡Si−O−Si≡ bridges exposing oxygen atoms on the surface.

Isolated silanols groups have been the subject of an impressive number of computational and experimental works, due to their well-characterized structural and spectroscopic features.[18,21−26] From a spectroscopic point of view, the hydroxyl group gives rise to three vibrational modes: (i) OH stretching mode, ν_{OH}; (ii) SiOH in-plane deformation, δ_{SiOH}; and (iii) SiOH out-of-plane torsion deformation, γ_{SiOH}. Only the OH stretching mode is easily observed, at 3744−3750 cm^{-1} in transmission experiments, while both the bending and the torsion modes are hidden by silica framework vibrations. When the weakly acidic OH group undergoes interaction with basic molecules

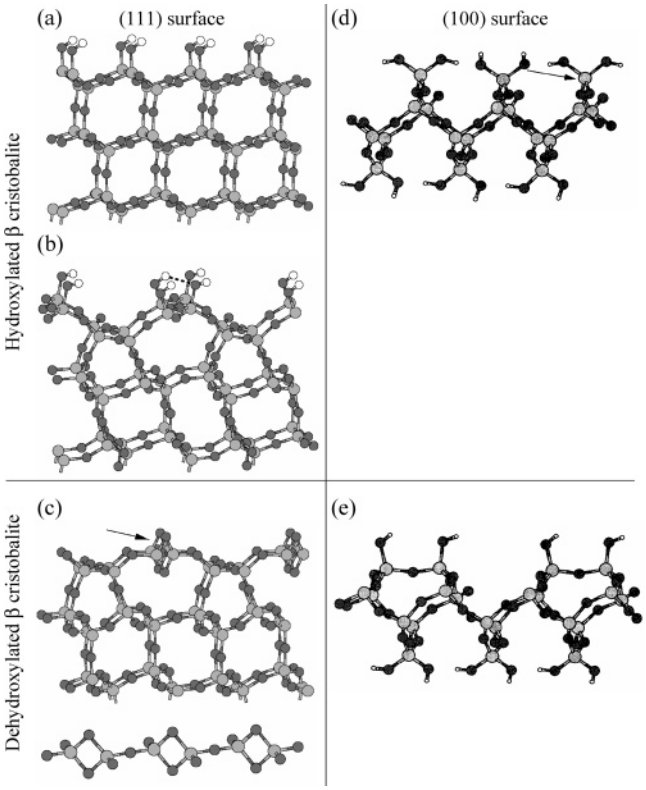

Figure 2. Optimized geometries of two hydroxylated surfaces of β-cristobalite: ideal (111) surface (a); ideal (100) surface (part d); and reconstructed (111) surface (b), where the silanols chain along the [1$\bar{1}$0] direction are dimerized, forming a weak H-bond 2.22 Å long (dashed lines). Optimized structure of the dehydroxylated reconstructed (111) surface (c) and of the (100) surface (e). In the first case, a single two-memebered ring, which lies in a plane perpendicular to the surface, is present in the unit cell, as indicated by the arrow (in the bottom of part c, the chain of two-membered rings along the [1$\bar{1}$0] direction is also reported; view from a different direction). In the second case, the condensation of vicinal silanols leads to the formation of a five-membered silicon ring. Oxygen, silicon, and hydrogen atoms are represented by black, gray, and white spheres, respectively. Adapted with permission from ref 40. Copyright 2001 American Chemical Society. Adapted with permission from ref 52. Copyright 2000 American Physical Society.

B, hydrogen-bonded adducts are formed and all of the three bands shift: the bending and the torsion mode to higher frequencies and the stretching modes to lower values.[27,28] The red shift of the stretching mode is readily measured and constitutes one of the best studied topics in IR spectroscopy because it gives a direct indication about the strength of the OH···B interaction.[26,28−34] Geminal sites have been the subject of ab initio studies.[35] ^{29}Si NMR spectroscopy shows two distinct signals for geminal and isolated hydroxyls of fully hydroxylated silica surface.[36,37] The peak intensities suggest that the population of geminal hydroxyls constitutes a substantial fraction (up to 30%) of that of isolated ones on fully hydroxylated surfaces. The computed and experimental results indicate that IR modes of geminal silanols are indistinguishable from those of isolated silanols and fall in the 3744−3750 cm^{-1} range.[38,39] Controversial conclusions are found in the literature concerning the presence[29,40] or the absence[18] of a significant H-bonding interaction between the two hydroxyls of the geminal pair.

Existing data (IR,[41−46] Raman,[47] and NMR[48−50]) on the amorphous hydroxylated silica are often rationalized by modeling the surface as an alternation of patches of the hydroxylated (100) and (111) surfaces of β-cristobalite, which is the crystalline phase of silica with a density and refractive index closest to those of amorphous silica.[40,48,49,51,52] These two main faces of β-cristobalite sustain the two types of silanol groups identified experimentally on the hydroxylated amorphous silica surface, namely, the isolated silanols, typical of the unreconstructed (111) surface,[52] and the geminal silanols, which are typical of the (100) surface.[40] The isolated silanols of the (111) face are not interacting via hydrogen bonding (Figure 2a). Geminal silanols of the (100) face interact via an H-bond directly, as evidenced by the arrow in Figure 2d. Vicinal silanols interacting via H-bonding are also present on reconstructed (111) faces, as represented in Figure 2b (dashed lines).[40,52] Surface reconstruction was performed by means of ab initio MD calculations using the Car−Parrinello scheme.[53]

2.2 Dehydroxylation of the SiO_2 Surface

2.2.1. Experimental and Theoretical Evidences on the Formation of Surface Strained Siloxane Groups

The concentration of hydroxyl groups decreases with increasing temperature of treatment and is accompanied by the parallel increase of strained siloxane groups. Zhuravlev[19,54] has shown that the number of total silanols per 100 Å^2, when the surface is hydroxylated to the maximum degree, is around 4.9, irrespective of both the kind of silica and the method of preparation. The number of geminal species is a function of the preparation method and may reach some 15% of the whole populations of isolated silanols, whereas the relative populations of isolated and vicinal sites are dependent on the thermal treatment of amorphous silica. A model of a fully hydroxylated unreconstructed SiO_2 surface, obtained using a slab of amorphous silica, created by adopting a classical MD approach,[55] and saturating the dangling bonds with OH groups, will be shown in Figure 4a. From this model, it is evident that the average OH number per 100 Å^2 is around 5 and that a fraction of them are located at distances $\leq$2−3 Å and then can interact via hydrogen bonding. Correspondingly, the IR spectrum of amorphous silica in air or treated at low temperature is characterized by a broad band in the OH stretching region (at about 3600−3100 cm^{-1}); see Figure 3b (dotted and dashed curves, respectively). On this surface, a certain fraction of geminal species is present, in agreement with the experimental results.[19,38,39] By increasing the temperature of treatment, the species interacting via hydrogen bonding react via elimination of a water molecule and form a new (possibly strained) siloxane bond, according with the reaction path in Scheme 1. Correspondingly, the samples dehydrated at high temperatures show only a very sharp IR band at about 3748 cm^{-1}, attributed to the OH stretch of either isolated or geminal surface silanols; see Figure

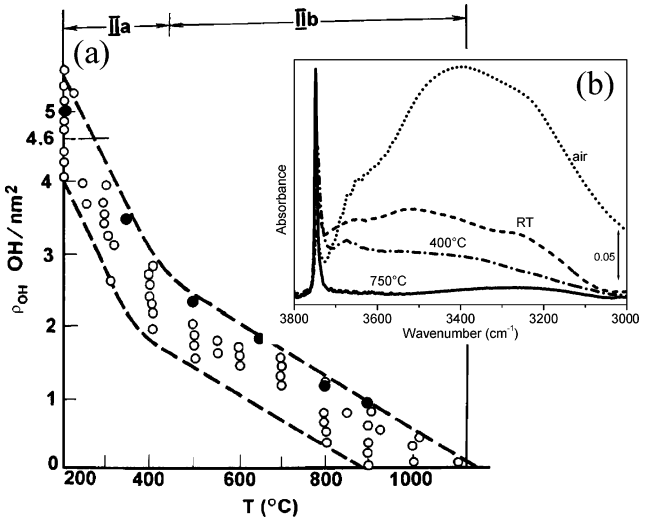

Figure 3. (a) Silanol number, ρ_{OH}, as a function of the temperature of pretreatment in vacuo for different SiO_2 samples (16 samples with different surface areas varying from 11 to 905 m^2/g). Adapted with permission from ref 19. Copyright 2000 Elsevier. Black dots are the data reported in ref 41. (b) IR spectra of amorphous silica as a function of the temperature of treatment: sample at air (dotted curve), outgassed at RT for 1 h (dashed curve), outgassed at 673 K for 1 h (dashed−dotted curve), and outgassed at 1023 K for 1 h (full curve). Unpublished spectra.

Scheme 1. Reaction between Two Adjacent Silanol Groups Interacting via H-Bonding (Dashed Line) on the Silica Surface Leading to Formation of Strained Siloxane Bonds and Molecular Water

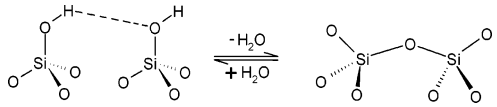

3b (full curve).[56] Already in 1967, Borello et al.,[41] combining temperature-dependent weight loss measurements under vacuum with IR measurements (evaluation of the intensity of the 3748 cm^{-1} band), found that the content of surface hydroxyls may be reduced to about one SiOH per 100 Å^2 at 1173 K (data reported as full black dots in Figure 3a). This value is in agreement with the data reviewed later by Zhuravlev[19] (open dots in Figure 3a). Such species are isolated, as the average distance between two of them on the surface is larger than 3 Å. A model of a portion of unreconstructed SiO_2 surface containing only one OH group per 100 Å^2 is shown in Figure 4b, obtained adopting a classical MD approach.[55] In such conditions, the distance between two OH groups is in the order of about 10 Å.

The model reported in Figure 4, obtained with the computationally light MD approach, contains all of the possible types of surface rings also emerging from more realistic (and computationally heavy) models that will be briefly discussed in the following. As for the purposes persecuted in this work we are just interested on the presence, and relative proportion, of surface rings of decreasing (down to two) nuclearity, vide infra Schemes 2, 6, and 7, and not to the fine details of the surface species, we will use the model reported in Figure 4 for further considerations about the chromium grafting on the amorphous silica surface. Nevertheless, few details about results obtained using more sophisticated theoretical approaches merit a detailed illustration, because they represent a frontier of computational chemistry.

More sophisticated and realistic models of the surface of amorphous silica have been reported in the theoretical works of Garofalini,[57] Huff et al.,[58] and Du et al.[59,60] adopting a MD approach and by the Bernasconi group[52,61] by means of ab initio MD calculations, using the Car−Parrinello scheme.[53] Du et al.[60] first heated and equilibrated at 8000 K, using an NVT ensemble, a bulk sample of β-cristobalite consisting of 3000 atoms with periodic boundary conditions; then, they annealed the system continuously down to 300 K. The so obtained model for bulk amorphous SiO_2 exhibits pair distribution distances with peaks at 1.61, 2.60, and 3.09 Å, for $g_{Si-O}(r)$, $g_{O-O}(r)$, and $g_{Si-Si}(r)$, respectively. These values are in excellent agreement with the corresponding experimental values extracted from neutron diffraction data: 1.608, 2.626, and 3.077 Å.[62] Also, the simulated average α_{SiOSi} (146.4°) and α_{OSiO} angles (109.3°) as well as the bulk density (2.25 g/cm^3) are in good agreement with experimental data[62] and previous theoretical results.[58] To generate a surface, in a second step, Du et al.[60] inserted a vacuum gap in the z direction of the periodic cell, which has been further relaxed at 300 K using an NPT ensemble. The resulting surface is terminated by silica rings of various sizes, among which the dominant ones are six- and five-membered rings. Some smaller rings, such as four-, three-, and two-membered rings, are also present, which are more strained and rigid. In particular, two-membered rings are found to be perpendicular to and sticking a bit out of the surface to reduce the local strain. Du et al.[60] have also observed an enrichment of the small-membered rings at the surface. Although small-membered rings are characterized by longer Si−O distances, they are more compact when compared to larger rings, resulting in an increase of density at the surface.

The picture emerging from the classical MD studies is basically confirmed by the computationally more demanding ab initio Car−Parrinello MD approach.[52,61] In fact, the so obtained model of the annealed (fully dehydroxylated) amorphous silica surface is characterized by a small density of two-membered silicon rings (about 0.5 per 100 Å^2). This result is qualitatively similar to that obtained by Du et al.[60] and is not too far from the experimental estimate on the dehydroxylated amorphous surface (0.2−0.4 per 100 Å^2).[19,41,63] In addition, underneath the two-membered silicon rings, also seven- and five-membered rings were constructed spontaneously during the ab initio MD optimization.[52,61]

The formation of strained siloxane groups, emerging from both classical and ab initio MD studies discussed above, has been experimentally observed long ago by Morrow and co-workers[64] and by Boccuzzi et al.,[42] by means of IR spectroscopy. More recently, strained siloxane groups have also been observed at the surface of a thin SiO_2 film by reflection−absorption IR spectroscopy.[65] In conclusion, it is well-assessed that (i) at the surface of amorphous silica

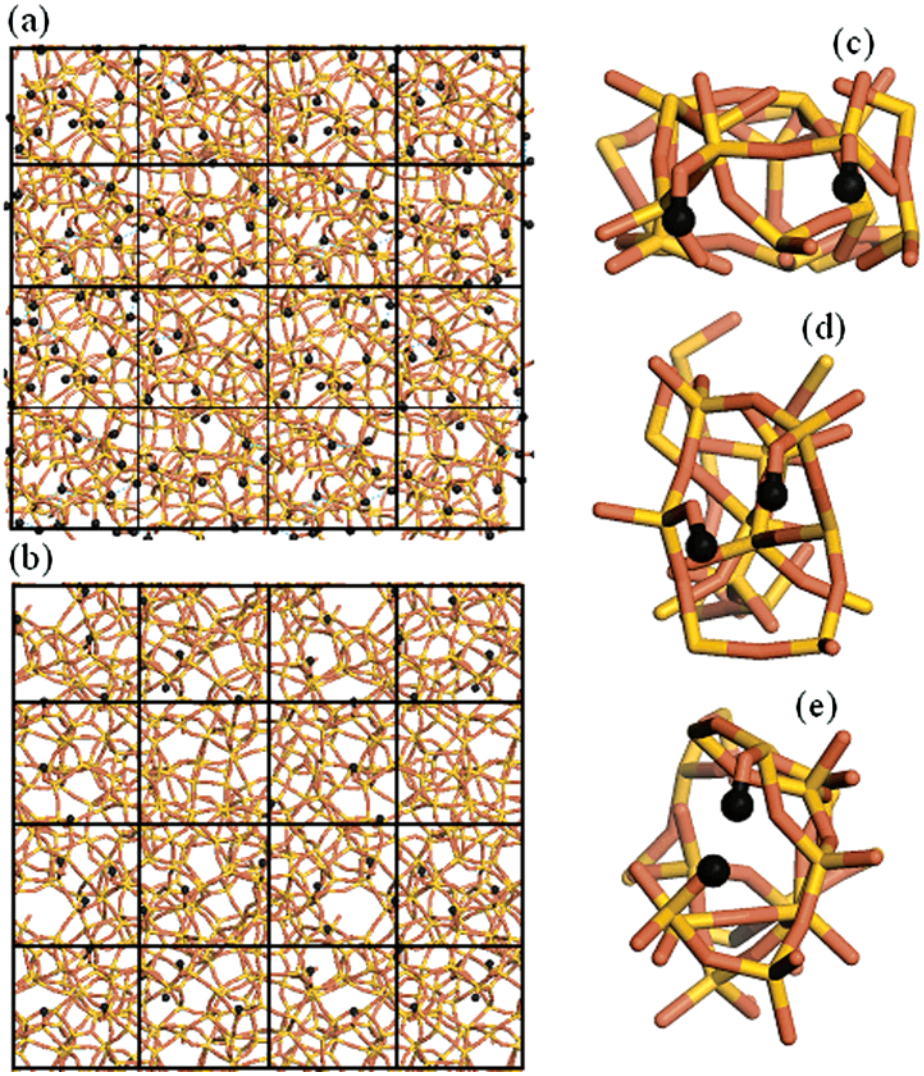

Figure 4. Model of an unreconstructed SiO_2 surface (a) fully and (b) only partially hydroxylated. The model was obtained cutting a slab of amorphous silica and saturating the dangling bonds with OH groups.[55] Each square has an area of 100 $Å^2$. Red and yellow sticks connect together silicon and oxygen atoms, respectively; black balls represent hydrogen atoms. Parts c−e report zooms in three representative cases, where adjacent hydroxyls terminate two- (vicinal), three-, and four-membered silicon open rings, respectively.

outgassed at high temperature two-membered silicon rings are present, resulting from the reaction depicted in Scheme 1 applied to two vicinal silanols as those shown in Figure 4c, and (ii) a general enrichment of low membered silicon rings is present on the dehydroxylated surface. Highly strained siloxane bridges are the only ones observable by IR.[25] In fact, they are characterized by a weak triplet of bands around 932, 908, and 888 cm^{-1}, which appear in a region of partial transparency of otherwise opaque samples; see Figure 5a, curve 1. In this figure, the two intense absorptions present at frequencies higher than 950 cm^{-1} and lower than 880 cm^{-1} are due to the bulk modes of silica. According to quantum chemical calculations performed on the $Si[OSi(OH_3)_4]$ cluster model,[66] the highest modes are basically represented by the asymmetric vibrations of the central SiO_4 tetrahedron achieved through antisymmetric stretching of the four connected Si−O−Si bridges. Conversely, the modes occurring at lower frequencies are principally due to the antisymmetric deformations of the central SiO_4 tetrahedron achieved through the symmetric stretching of the four connected Si−O−Si bridges; see the scheme reported in Figure 5b.

Vibrational modes in the gap between the high frequency and the low frequency vibrations appear once the Si−O stretching modes are perturbed by a symmetry reduction of the T_d unit. This can occur by (i) insertion of substitutional heteroatoms in the SiO_2 lattice;[66−69] (ii) Si vacancy in one neighboring $[SiO_4]$ unit;[66,70] or (iii) the presence of strained siloxane bridges, e.g., formed by H_2O removal from surface hydroxyl groups (see Scheme 1).[25,42,64,65,71−73] Computed vibrational modes appearing in Figure 5b in the gap are due to the cluster termination, i.e., to case ii, while the experimental bands at 932 (vw), 908 (m), and 888 (s) cm^{-1}, see Figure 5a, curve 1, are due to the presence of strained siloxane bridges, case iii. Such bands are very similar to those observed in the 900−800 cm^{-1} region for the ciclodisiloxane molecules, which also display two strong peaks due precisely to vibrations of the two-membered siloxane ring.[74] Similar bands, but much more intense, are observed upon dehydroxylation of the internal nests of defective silicalite.[25,71,72] The IR peaks appear upon

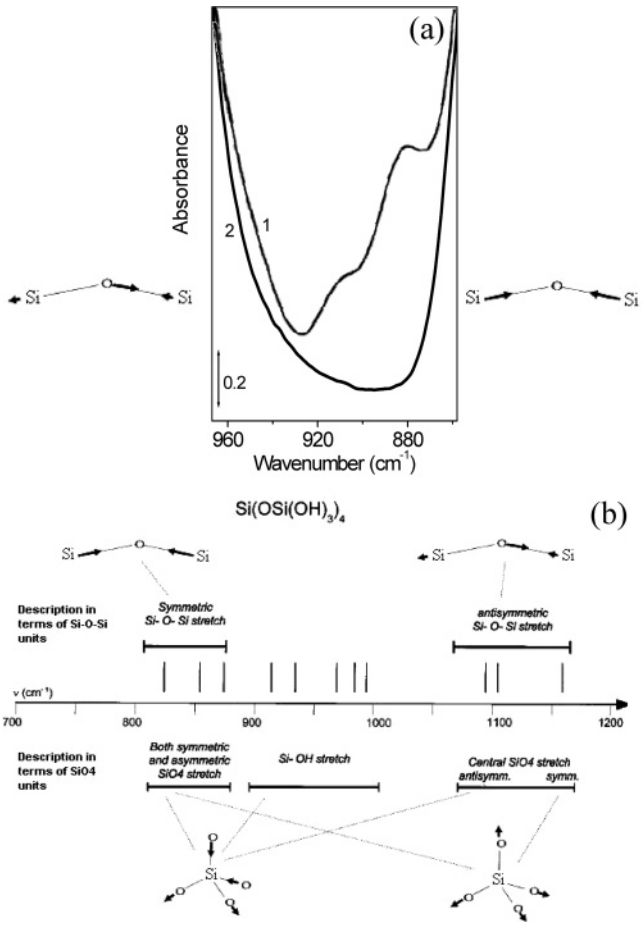

Figure 5. (a) IR spectra of an amorphous silica pellet, curve 1, and of Cr/SiO_2 catalyst (0.5 wt % Cr loading), curve 2, outgassed at 923 K and CO-reduced at 623 K. Grafting of chromium causes the relaxation of the strained siloxane bridges responsible for the absorption in the optical gap of silica. Unpublished spectra. (b) Calculated vibrational frequencies for the $Si[OSi(OH)_3]_4$ model, classified following the symmetries of the Si−O−Si unit (upper part) or according to the symmetries of the $[SiO]_4$ unit (lower part). Note that the wavenumber scale is inverted passing from the experimental spectrum (a) to the theoretical one (b). Adapted with permission from ref 66. Copyright 2001 American Chemical Society.

dehydroxylation above 773 K and disappear upon adsorption of water and other chemical species such as ammonia and methanol.[35,43−45,74,75] Whether water is interacting with other low membered rings is not well-established. The reactivity of such rings, where the surface strain is mainly located, is relevant for the scope of this review. We will see in the following section that grafted Cr(II) ions play a role similar to that of these molecules in decreasing the silica surface strain, as evident in Figure 5a, curve 2.

To simplify the problem of a correct description of surface reactivity of SiO_2, we refer again to the theoretical works of Bernasconi and co-workers,[40,52] who simulated the dehydroxylation reaction of the (100) and (111) surfaces of β-cristobalite by means of ab initio MD calculations, using the Car−Parrinello scheme.[53] They found that the dehydroxylation of the (100) surface leads to the creation of five-membered rings (see Figure 2e) and requires an energy of 42 kJ/mol, much lower than the experimental average energy of dehydroxylation (about 81 kJ/mol for temperatures in the 623−923 K range[76]). Conversely, dehydroxylation of the reconstructed (111) face provides the formation of two-membered silicon rings, as illustrated in Figure 2c (see arrow). In this case, the condensation energy is 127 kJ/mol, slightly higher than the experimental value. However, it is conceivable that the theoretical dehydroxylation energy should correspond to an average over different processes including the formation of less strained five-, four-, and three-membered silicon rings. The main limitation in assuming the β-cristobalite surface as a model for amorphous silica obviously concerns the limited variety of surface rings that cannot account for the high heterogeneity present on the surface of the amorphous phase. The surface heterogeneity of silica has been well-documented by microcalorimetry of different adsorbed molecules such as H_2O, NH_3, CH_3OH, and $(CH_3)_3COH$).[21,77−79] Moreover, the crystalline phase of silica exhibits a higher surface reactivity, a higher hydrophilic character, and a greater resistance to the dehydroxylation process than the amorphous one.[60,80] Being aware of these problems, Bernasconi and co-workers also investigated a model of fully dehydroxylated amorphous silica obtained by an annealing process performed with an ab initio MD approach,[52] already discussed above. Figure 6a reports the model of silica obtained with this method.

2.2.2. Hydroxyl/Siloxane Equilibrium

We have seen that the hydroxyl and siloxane concentrations change with thermal treatments and that they influence the SiO_2 surface strain and reactivity. For this reason, this topic merits a detailed discussion. The hydroxylation reaction at the surface of the amorphous silica has been investigated on the model of fully dehydroxylated amorphous silica proposed by Bernasconi et al.[61] described at the end of the previous section. The hydration occurs preferentially on the two-membered silicon ring present on the surface. The authors investigated two different reaction paths: (i) water is adsorbed on the Si site of the two-membered ring, which acts as an electron acceptor, and (ii) water is adsorbed on the O site of the strained ring. Even if water can physisorb on the acidic silicon of the ring, the activation energy for the ring opening and the formation of surface hydroxyls were found to be lower in the second case: 1.1 eV (106 kJ/mol) vs 0.32 eV (31 kJ/mol). This implies that the chemisorption of water is driven by the basic character of the oxygen in the ring. The ab initio Car−Parrinello MD method suffers, however, from the presence of a long-range order in the adopted model, unavoidably present when dealing with a periodic approach, which does not exist in amorphous silica.

An alternative frequently used method in the study of amorphous surfaces is the cluster model, in which relevant clusters are chosen from the amorphous surface and treated by ab initio methods. Walsh and co-workers, after having reported a study on the dehydroxylated silica surface,[81] have studied the activation barriers of water dissociative reactions with a number of clusters that represent defect sites on the amorphous SiO_2 surface.[82] They reported

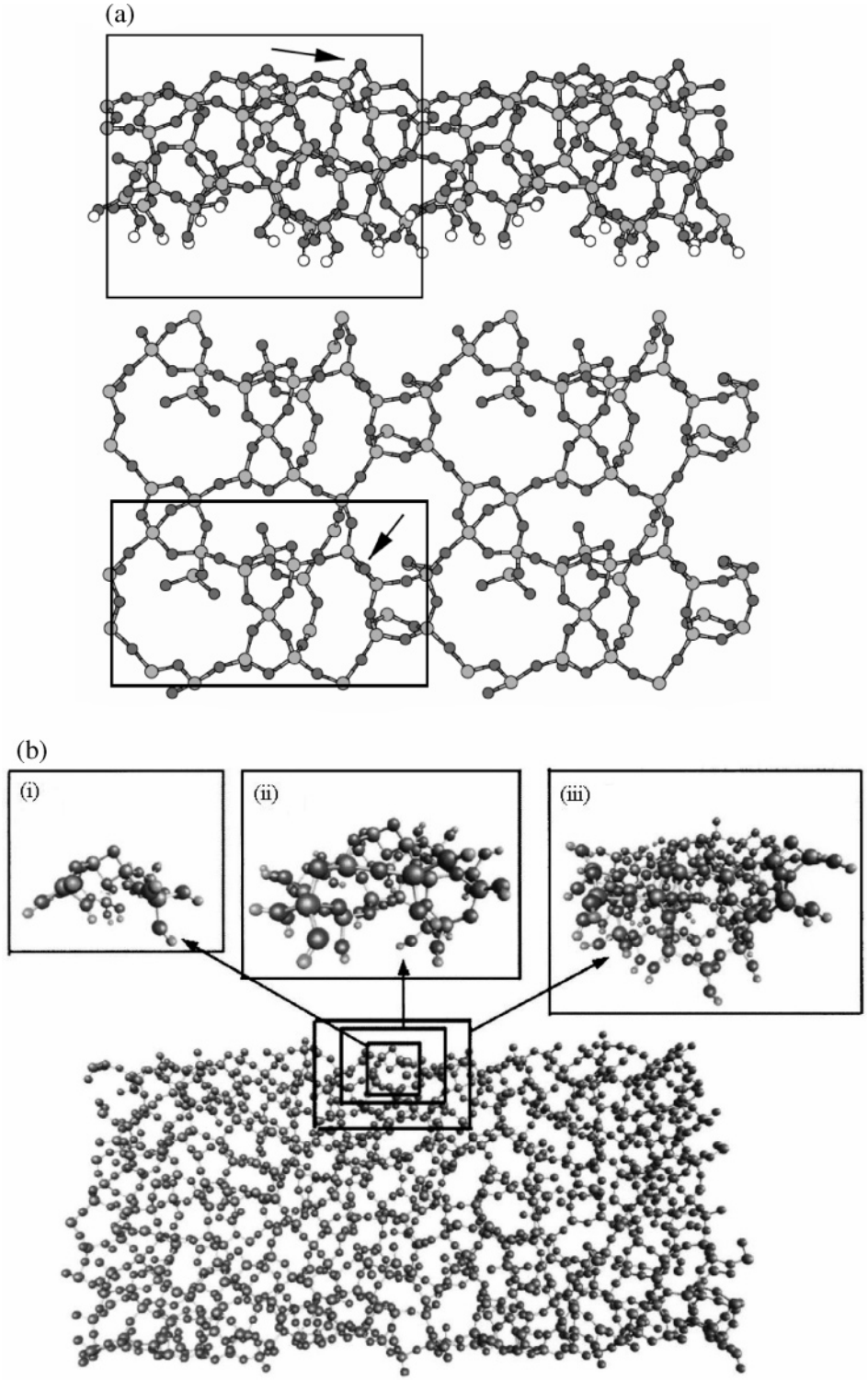

Figure 6. (a) Side (top part) and top (bottom part) view of the model of a fully dehydroxylated amorphous silica surface obtained by an ab initio Car−Parrinello MD approach. Only surface atoms are shown. The simulation cell containing 135 atoms is indicated in both panels. One two-membered ring per unit cell is present (arrow). Oxygen, silicon, and hydrogen atoms are represented by black, gray, and light gray spheres, respectively. Reprinted with permission from ref 52. Copyright 2000 American Physical Society. (b) Side view of the model of a fully dehydroxylated amorphous silica surface obtained by the hybrid QM/CM method discussed in ref 60. Panels i−iii are enlarged pictures of three QM regions constituted by an increasing number of atoms (31, 74, and 203 atoms, respectively). Reprinted with permission from ref 60. Copyright 2004 American Institute of Physics.

activation barriers ranging in the 0.7−1.1 eV interval (68−106 kJ/mol), depending on the rigidity of the investigated cluster. However, great cautions must be taken in these cases, because the absence of bonds at the end of the cluster intrinsically causes a structural relaxation that reduced the strain of the systems.[83] Consequently, smaller clusters generally overestimate the activation barrier and reaction energy.[84] In our case, the siloxane groups simulated with this approach are less strained and thus less

reactive than the actual ones. In analogy, it is worth recalling that the reactivity of Ti(IV) species embedded in zeolitic framework can be correctly evaluated only when the local strain has been sufficiently well-reproduced, either by the use of large clusters reproducing entire zeolitic cages[69,85−88] or by applying a periodic approach.[89]

Very recently, Du et al., in a communication first[59] and in a full article then,[60] developed a combined QM and CM method, which has the advantage of simulating chemical reactions involving surface atoms (treated by QM method), which are in an elastic field provided by the surrounding bulk material (treated by simpler CM method); see ref 90 for a more detailed description on the computational method. An amorphous silica slab consisting of four 3000 atom unit cells generated by the classical MD method described previously (vide supra section 2.2.1 and see Figure 6b) has been used as a model for the surface. The dimensions of such a slab allowed the authors to omit the periodic boundary constraints. The accuracy of the method can be systematically improved by increasing the size of the QM region: three QM regions of increasing dimension (31, 74, and 203 atoms, respectively) have been chosen by the authors; see the three insets in Figure 6b. As for the part of the slab treated with the CM approach, two different potentials have been tested. Both physisorption and chemisorption of water on the two-membered silicon ring have been studied in details, and the results of the hybrid QM/CM method have been compared with those obtained with cluster models, coming both from literature[82] and from new internal data reported in the same work.[60] The authors found that water−surface interaction is significantly stronger in the combined QM/CM surface approach than in the cluster one. Moreover, also the reaction barrier for water dissociation found by Du et al.[60] is much smaller than that obtained with the cluster approaches:[60,82] 0.4 eV (39 kJ/mol), to be compared with the 0.7−1.1 eV (68−106 kJ/mol). Such a barrier is well evident in Figure 7a and corresponds to the difference between the physisorption state (Figure 7b) and the transition state (Figure 7c), where a proton transfer from the water molecule to the oxygen of the strained siloxane bridge is occurring. The final state, where the strained Si_1-O_2 bond has been broken, is depicted in Figure 7d. The comparison between the hybrid QM/CM approach and the cluster one gives even more different results when the adsorption of two water molecules is taken into account. Du et al.[60] observed a cooperative effect when two water molecules approach the silica surface. They reported that water molecules spontaneously dissociate and undergo a double hydrogen transfer process that breaks the siloxane bridge. Such a reaction is not observed when the cluster model is adopted.

As far as the energetic of the phenomenon is concerned, Du et al.[60] concluded that using the larger cluster (for the QM part), inset iii of Figure 6b, and adopting the more refined potential (for the CM part), the dissociative adsorption energy of water is 1.06 eV (102 kJ/mol). This value is in fair agreement with the experimental one of 100 kJ/mol (1.04 eV) obtained by Bolis et al.[21] on a high surface area (380 m^2/g) silica outgassed at 1073 K using adsorption microcalorimetry.

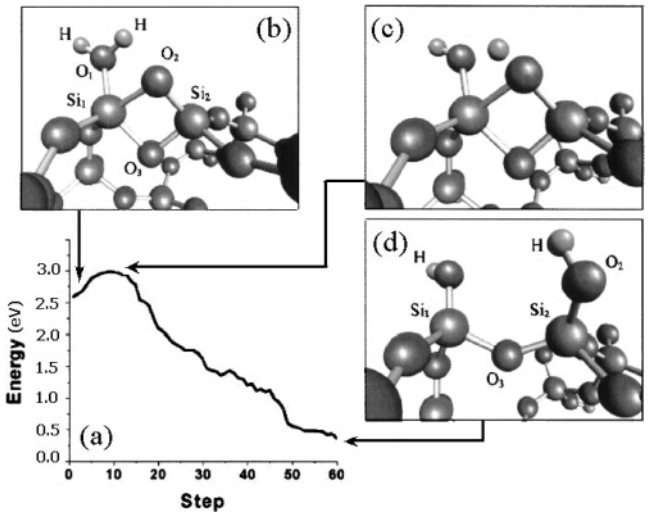

Figure 7. (a) Relative potential energy of QM atoms along the dissociation path of one water molecule with the silica surface obtained from the hybrid QM/CM method described in Figure 6b. (b−d) Snapshots of the physisorption, transition, and chemisorption states; see arrows for determining the corresponding point in the reaction path. The most relevant atoms have been labeled in parts b−d. Adapted with permission from ref 60. Copyright 2004 American Institute of Physics.

Till now, in this section, we have discussed the displacement of the equilibrium reported in Scheme 1 from the right to the left: i.e., the hydroxylation of the strained siloxane bridges by interaction with water molecules. However, in the activation process of the silica surface, the opposite path is followed. As mentioned before, Zhuravlev[19] reviewed most of the research results obtained by different authors on the properties of amorphous silica surfaces and in particular analyzed the processes of dehydration (the removal of physically adsorbed water), dehydroxylation (the removal of silanols groups from the silica surface), and rehydroxylation (the restoration of hydroxyl covering). In Figure 3a, the evolution of the total silanol number (ρ_{OH} = number of silanols per 100 $Å^2$) as a function of the temperature of pretreatment in vacuo for different silica samples has been illustrated and compared with the experimental IR spectra discussed above (Figure 3b). In this figure, the data from Borello et al.[41] are also inserted (full dots in Figure 3a), because they were obtained in very early times. It is confirmed that the decrease of ρ_{OH} with temperature is characterized by two approximately linear sections, characterized by markedly different slopes. In the first one (473−673 K), the ρ_{OH} values decrease considerably; in the second one (673−1373 K), the decrement becomes notably smaller (note that the slope of the two curves is related to the energy of desorption). Thus, the dehydroxylation of the silica surface proceeds via two stages, labeled as subregion IIa and IIb in Figure 3a. In the first subregion, the OH coverage of the silica surface is high, $1 \geq \theta_{OH} \geq 0.5$ (corresponding to $4-5 \geq \rho_{OH} \geq 2-3$ OH per 100 $Å^2$); this region is so characterized by the presence of lateral interactions (hydrogen

bonds) between the neighboring OH groups, as testified by the broad IR band around 3600−3100 cm^{-1}, which decreases in intensity passing from the first to the third curve in Figure 3b. In the subregion IIb, the coverage of the silica surface with hydroxyl groups is smaller, $\theta_{OH} < 0.5$ ($\rho_{OH} < 2-3$ OH per 100 $Å^2$); in this case, the main role is played by free isolated hydroxyl groups and siloxane bridges, as demonstrated by the sharp IR band at 3748 cm^{-1} characterizing the full line curve in Figure 3b.

In subregion IIb, the dehydroxylation occurs through the OH condensation via disordered migration of protons on the surface. At the final stage, water is evolved, owing to the interaction of two OH groups that accidentally approach each other to a distance of about 3 Å. The mechanism describing the migration of protons is not entirely clear. It probably involves the interaction of the protons at elevated temperatures with O atoms of the neighboring Si−O−Si bridges, resulting in the formation of new surface OH groups, which are displaced relative to their initial position. In other words, this mechanism can be represented as the transition from one local minimum of the potential energy into another by means of "jumps" between the neighboring siloxane bridges.[19] Once two OH groups are (or become) adjacent, the dehydroxylation process can follow the inverse path with respect to that shown in Figure 7.

The components of the silanol density (the number of free isolated OH groups, $\rho_{OH,I}$, the number of vicinal OH groups bound via the hydrogen bonds, $\rho_{OH,V}$, and the number of geminal OH groups, $\rho_{OH,G}$) on the surface of SiO_2 were determined by the method of deuterium exchange and IR spectroscopic measurements, depending on the temperature of the preliminary treatment in vacuo.[91,92] The results of experimental and theoretical studies permitted the cited author to construct an original model (Zhuravlev model) of the silica surface.[19,91,92] A graphic representation of this model is shown in Figure 8.

As mentioned before, upon dehydroxylation at progressively higher temperatures, the concentration of siloxane groups increases. An analysis has been carried out using data reported in the literature to establish the proportion of stable and strained siloxane bridges located on the surface of amorphous silica at the various dehydroxylation stages.[19,93] At present, there is still no definitive agreement on this question. Bergna[93] stated that weakened siloxane bridges are formed upon the thermally induced condensation process of vicinal silanols. Such weakened ≡Si−O−Si≡ bridges exist at temperatures up to approximately 673 K and do not possess peculiar vibrational properties. The weakened siloxane bridges could be the same reacting with methanol at RT, as reported by Borello et al.[41] Upon further dehydroxylation at $T > 673$ K, the weakened bridges likely undergo activated relaxation and become "normal". However, at the same time, dehydroxylation at high temperature leads to the formation of new highly strained siloxane species characterized by so peculiar IR vibrations to become distinguishable from those of the bulk (vide supra, curve 1 of Figure 5a).[25,42,64,71−73] At even higher temperatures, all of these strained

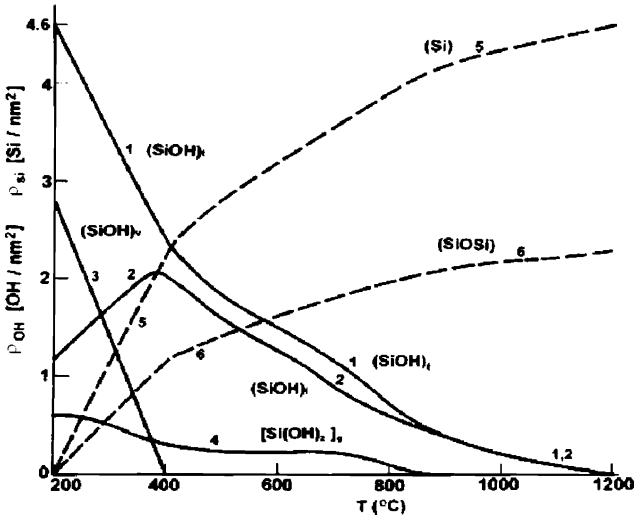

Figure 8. Distribution of the surface OH groups as a function of the temperature of pretreatment in vacuo according to the Zhuravlev model: curve 1, average concentration of the total OH groups, ρ_{OH}; curve 2, average concentration of the free isolated OH groups, $\rho_{OH,I}$; curve 3, average concentration of vicinal OH groups bound through the hydrogen bonds, $\rho_{OH,V}$; curve 4, average concentration of geminal OH groups, $\rho_{OH,G}$; curve 5, average concentration of surface Si atoms that are part of the siloxane bridges and thus free of OH groups, ρ_{Si}; curve 6, average concentration of surface Si−O−Si bridges, which are free of OH groups, ρ_{SiOSi}. Reprinted with permission from ref 19. Copyright 2000 Elsevier.

siloxane groups tend to be converted into stable siloxane bridges and rings, because of relaxation and reconstruction processes occurring at high temperatures. The process is slow, and little is known about the surface distribution of the strain among the surface siloxane bridges.

2.2.3. Summary and Basic Classification of Surface Rings

On the basis of what discussed above, the siloxane bridges formed upon dehydroxylation can be classified into several groups, depending upon the structure of the immediate surroundings. A schematic but more detailed version of the dehydration process and of the formed structures is given in Scheme 2. These

Scheme 2. Different Siloxane Bridge Structures Formed upon Dehydroxylation of the Silica Surface[a]

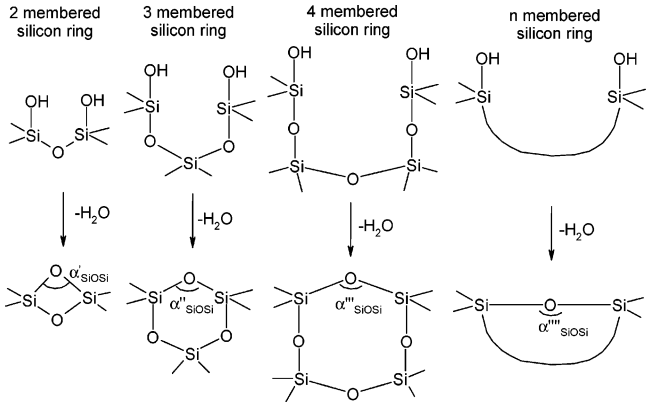

[a] The increasing dimension of silicon rings and, consequently, of the Si−O−Si angle reflects a decrease of the strain of these structures.

structures are characterized by the presence of two-, three-, four-, etc.-membered silicon open rings. The strain present in these structures decreases going from left to right, parallel to the increase of the Si−O−Si bond angle: $\alpha_{SiOSi}' < \alpha_{SiOSi}'' < \alpha_{SiOSi}''' < \alpha_{SiOSi}''''$. Taking again β-cristobalite as a simplified example, silanols attached to two-membered silicon rings can be identified both on the reconstructed (111) (see Figure 2b) and on the dehydroxylated (100) (see Figure 2e) surfaces. On the same system, also silanols belonging to three-membered silicon rings [on the hydroxylated (111) surface, see Figure 2a] and five-membered silicon rings [on the hydroxylated (100) surface, see Figure 2d] can be found. A greater variety of situations is expected in the case of amorphous silica. In the model of a fully hydroxylated unreconstructed silica surface obtained by the MD approach and reported in Figure 4a, we can find quite easily silanols belonging to two-, three-, four-, etc.-membered silicon open rings, as reported in Figure 4c−e, respectively. Similar surface configurations can be found in the more sophisticated models obtained from the Car−Parrinello quantum MD approach by Ceresoli et al.[52] (Figure 6a) and from the hybrid QM/CM approach by Du et al.[60] (Figure 6b). Of course, Scheme 2 is still oversimplified, because it does not take into consideration that the two silicon atoms directly involved in the hydroxyl condensation are also linked to other rings in a three-dimensional mode (as it is evident in Figure 4c−e and in Figure 6) and that part of the surface strain could be localized on these rings. This makes the full classification of the siloxane bridges formed upon dehydroxylation of amorphous silica surface an extremely complex task. Another point deserving a comment involves the rearrangement of the surface upon dehydroxylation. In fact, we expect that the formation of a Si−O−Si siloxane bridge, being accompanied by the decrement of the Si−Si distance, can have an influence on the Si−O−Si bridges located in the immediate vicinity and, to a smaller extent, on the rings in the nearest positions. This means that the condensation of two OH groups can influence surface structures located at distant positions. This is testified by the appearance in the 880−940 cm^{-1} region of new components due to the perturbation of the stretching modes of the [SiO_4] unit in adjacent positions (see Figure 5a).[25,42,64,71−73]

In conclusion, it has been shown that in any description of the surface of amorphous silica the hydroxylation of the surface is of critical importance. It can be stated with confidence that silica samples, outgassed at about 923 K in vacuo, are characterized by ρ_{OH} very near to one OH per 100 $Å^2$. This means that nearly all of the silanols are isolated and that their average distance is about 10 Å. In particular, for our purposes, it's important to remember that the activation temperature influences the properties of the silica support in two ways: (i) modifying the OH abundance and (ii) modifying the strain properties of the surface. The higher is the activation temperature (at least in the 673−1073 K interval), the lower is the OH population and the higher is the siloxane abundance and thus the strain on the surface. At T > 1073 K also the strained siloxane groups undergo relaxation and become gradually normal. At the same time, at T > 1073 K, the surface area of samples decreases because of sintering. These considerations may have deep consequences on the structure of chromium centers grafted on the silica surface in the Cr/SiO_2 system and therefore on the activity of the catalyst, as we will describe in the following sections. In fact, as the anchoring process involves suitably spaced OH groups, it is evident that the surface structure of silica has a great influence on the bonding and location of the anchored species.

3. Since the Beginning until 1985: A Historical Review on the State of the Art

3.1. Anchored Process and the Structure of Anchored Chromium

The Phillips Cr/Silica catalyst is prepared by impregnating a chromium compound (commonly chromic acid) onto a support material, most commonly a wide pore silica, and then calcining in oxygen at 923 K. The resulting anchored Cr(VI) catalyst is activated and thus belongs to the family of one-component polymerization catalysts, as it initiates polymerization without activators. The formation of the propagation centers takes place by reductive interaction of Cr(VI) with the monomer (ethylene). As we will describe in detail in section 5, this feature makes the Phillips catalyst unique among all of the olefin polymerization catalysts, but it also makes it the most controversial one.

As summarized previously (section 2.1), the surface of the silica used for anchoring the Cr(VI) is fully covered by hydroxyl groups (≡Si−OH). The surface silanols are only weakly acidic and hence can react with the stronger H_2CrO_4 acid with water elimination, thus acting as anchoring sites. The anchoring process is an acid−base type reaction and occurs at temperatures between 423 and 573 K. In this esterification reaction, surface hydroxyl groups are consumed, and chromium becomes attached to the surface by oxygen linkages (Si−O−Cr), in the hexavalent state (see Scheme 3).[6,8]

Scheme 3. Anchoring Reaction of Chromate on a Silica Support[a]

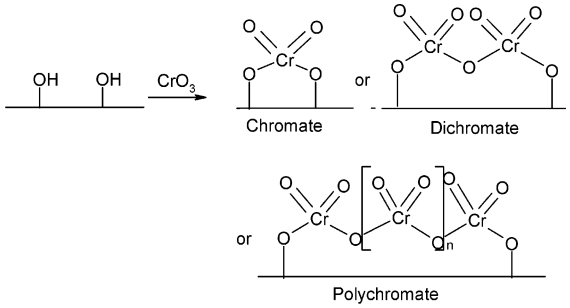

[a] Adjacent surface hydroxyl groups are consumed, and chromium attaches to the surface by oxygen linkages, either in mono-, di-, or polychromate forms.

Evidence for this anchorage reaction comes from IR, UV−vis DRS, mass spectrometry experiments, and differential thermal analysis. In particular, (i)

IR[94−96] and diffuse reflectance UV−vis spectroscopy[97] in the near-infrared region indicate a consumption of hydroxyl groups. The decrease is linear for chromium concentrations in the 0.5−2% range and stops for 5 wt % chromium content. Because the chromium loading does not cause an appreciable loss of the silica surface area, the hydroxyl concentration decrease is only due to the anchoring process.[94] (ii) Experiments with CrO_2Cl_2 and silica show the release of HCl, and the reverse reaction of dry HCl with calcined Cr/SiO_2 causes a release of chromyl chloride vapor.[98−100] (iii) The exothermal peak in the differential thermal analysis curves around 523 K shows the occurrence of an esterification reaction.[101]

The molecular structure of the anchored Cr(VI) has been a strong point of discussion in the literature, and several molecular structures (monochromate, dichromate, polychromate, etc.) have been proposed (see Scheme 3). The reason for this probably lies in the complex redox and coordination chemistry of chromium in combination with the heterogeneity of the silica surface. The nature of the silica support (e.g., specific surface area, porosity, concentration of surface hydroxyls), the chromium loading, and the activation method (e.g., maximum temperature, heating rate, total calcination time, and calcination atmosphere) can all influence the chemical state of the supported chromium.[6,8]

In the past, many authors have tried to distinguish between chromate and dichromate structures measuring the change in hydroxyl population of silica surface upon anchoring of the chromium: a chromate species should react with two hydroxyls per chromium, while a dichromate displaces only one hydroxyl per chromium. However, the results from this approach were contradictory. The number of hydroxyls lost per chromium attached is not constant but depends on the calcining temperature. Hogan[5] and McDaniel[98−100,102] concluded that the dominant chromium species are monochromates, while Krauss[103] and Rebenstorf[104] were in favor of dichromate species.

More recently, as deeply discussed in sections 4.1−4.5, the surface chemistry of chromium catalysts has been investigated by means of several spectroscopic and chemical techniques, among which are UV−vis DRS, IR, Raman spectroscopy, EPR, XAS (both in the XANES and EXAFS regions), TPR, XPS, and SIMS. For silica supports, both monochromate (on a precalcined Cab-O-Sil) and dichromate (on a precalcined sol-gel silica) have been found to be the main species after calcination. On silica, high chromium loading and high calcination temperatures are believed to favor the formation of dichromates.[8,9,97] The ratio of surface monochromate to polychromate species can be altered by changing the surface chemistry of the oxide support. For example, it has been reported that the addition of submonolayer quantities of surface titania to silica enhances the concentration of surface polychromate species and results in comparable amounts of surface monochromate and polychromate species.[105] On the other hand, the formation of surface silica on titania suppresses the concentration of surface polychromate species and increases the amounts of surface monochromate species.[106]

During the calcination process, two unfavorable processes may occur as follows: the calcination-induced reduction of surface-stabilized hexavalent chromate species into lower valent state (+5 or +3) and the creation of aggregated α-chromia (Cr_2O_3, usually in crystallized form), even if an oxidizing atmosphere is used. It can be safely hypothesized that dichromate and polichromate species, together with unreacted CrO_3, can be the preferential precursors of α-Cr_2O_3. Isolated Cr^{5+} ions are easily detectable by an EPR axially symmetric/rhombic signal with g around 2, usually denoted as the γ signal. This γ signal is generally attributed to isolated Cr^{5+} in a square-pyramidal or distorted tetrahedral coordination.[107−112] Detailed EPR studies of ^{45}Cr- and ^{53}Cr-enriched supported Cr systems and SQUID measurements showed that Cr^{5+} is present as an isolated paramagnetic ion, following the Curie−Weiss law down to 10 K.[109,113,114] The concentration of these species is very low and accounts only for a negligible fraction of mononuclear anchored species. They so play a negligible role as precursors of the active species. In conclusion, in a certain concentration range (0−2 wt %), almost all Cr is stabilized in the hexavalent state. At loadings higher than the saturation value, the excess Cr merely decomposes to the trivalent oxide Cr_2O_3.[98,100,102,115] It can be recalled that already during the anchoring process, the presence of hydrogen in the gas phase greatly favors the formation of α-Cr_2O_3, as expected because Cr(III) is the most stable state in the presence of water.

3.2. Reduction Process and the State of Reduced Chromium

As we will describe in detail in section 5, when a calcined Cr/SiO_2 catalyst is fed with ethylene at 373−423 K, an induction time is observed prior to the onset of the polymerization. This is attributed to a reduction phase, during which chromium is reduced and ethylene is oxidized.[6] Baker and Carrick obtained a conversion of 85−96% to Cr(II) for a catalyst exposed to ethylene at 400 K; formaldehyde was the main byproduct.[116] Water and other oxidation products have also been observed in the gas phase. These reactive products can partially react with surface silanols and siloxane bridges. The same can occur for reduced chromium sites. Consequently, the state of silica surface and of chromium after this reduction step is not well-known. Besides the reduction with ethylene of Cr(VI) precursors (adopted in the industrial process), four alternative approaches have been used to produce supported chromium in a reduced state: (i) thermal reduction of $Cr(VI)/SiO_2$ with CO or H_2;[94,104,117−124] (ii) photochemical reduction of $Cr(VI)/SiO_2$ with CO or H_2;[125−130] (iii) exchange of silica hydroxyls with organometallic reagents containing reduced chromium;[104,131] and (iv) ion exchange with aqueous solutions of Cr(III).[132−134]

Thermal reduction at 623 K by means of CO is a common method of producing reduced and catalytically active chromium centers. In this case, the induction period in the successive ethylene polymerization is replaced by a very short delay consistent with initial adsorption of ethylene and formation of

active precursors. In the CO-reduced catalyst, CO_2 in the gas phase is the only product and chromium is found to have an average oxidation number just above 2,[6,9,97,103,115,116] comprised of mainly Cr(II) and a very small amount of Cr(III) species (presumably as α-Cr_2O_3). Fubini at al.[117] reported that reduction in CO at 623 K of a diluted Cr(VI)/SiO_2 sample containing 1% Cr by weight yields 98% of the silica-supported chromium in the +2 oxidation state, as determined from oxygen uptake measurements. The remaining 2 wt % of the metal was proposed to be clustered in α-chromia-like particles. As the oxidation product (CO_2) is not adsorbed on the surface and CO is fully desorbed from Cr(II) at 623 K (reduction temperature), the resulting catalyst acquires a model character; in fact, the siliceous part of the surface is the same of pure silica treated at the same temperature and the anchored chromium is all in the divalent state.

The CO-reduced catalyst polymerizes ethylene much like its ethylene-reduced hexavalent parent and produces almost identical polymer.[6] Because the polymer properties are extremely sensitive to the catalyst pretreatment, this is a strong endorsement for the conclusion that Cr(II) is probably also the precursor of the active species on the commercial catalyst after reduction by ethylene. Further evidence comes from XPS experiments, which showed analogous spectra for the CO- or ethylene-reduced catalysts.[135] The situation is different for photoreduced samples. From oxygen uptake measurements, the average oxidation state of the photoreduced catalysts was +4.[5] These results suggested a photoreduction scheme in which one Cr(VI) of a dinuclear site was reduced to Cr(II), and the oxidation state of the other chromium was unchanged.[130]

Anchored Cr(II) is very reactive and adsorbs oxygen with a brilliant flash of chemioluminescence, converting the chromium back to its original orange hexavalent state[4−6,136] (see Scheme 4). The intensity

Scheme 4. Reversible Oxidation/Reduction[a] Process for the Cr/SiO_2 System

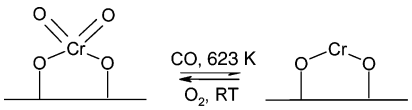

[a] Note that the stoichiometry of the scheme has not been balanced, for the sake of simplicity.

of this yellow-orange light flash decreases with an increasing reduction temperature of the catalyst and decreasing initial calcination temperature. This chemioluminescence has an orange emission line at 625.8 nm and is due to oxygen atoms (O*), which are formed at coordinatively unsaturated Cr(II) sites.[9] The easiness with which this reversal reaction occurs suggests that there is a little rearrangement during reduction at 623 K. Fubini et al.,[117] by means of calorimetric measurements, pointed out the occurrence of two distinct reoxidation processes, one very fast (i.e., little or nonactivated), and the other very slow and definitely activated, the transition between them being quite abrupt. At RT, the former is by far more important. This process can be simply thought of as the breaking of an oxygen molecule onto a chromium ion giving rise to a surface chromate (or dichromate). No activation energy is required, in particular if account is taken that π-bonded oxygen molecule (peroxidic-like structure) probably acts as the intermediate for the reaction.[137] The second reoxidation process, involving less exposed chromium centers, is activated, i.e., strongly dependent on time, pressure, and temperature. At RT, the process is very slow but fast at 623 K. This can be understood by supposing that this process involves a fraction of chromium sites not readily accessible (because partially buried into the silica framework). We shall show in the following that a fraction of less accessible sites is always present on the surface and that this fraction increases when the reduced sample is successively heated in vacuo at high temperature for a prolonged time, vide infra sections 4.1.2 and 4.2.1.

The structure of Cr(II) and to a less extent the average valence state of the reduced chromium on the silica surface have been in much dispute in the past and have been widely investigated by several spectroscopic (such as UV−vis DRS, IR, EXAFS-XANES, EPR, XPS, etc.) and chemical techniques. By UV−vis DRS spectroscopy,[9,94,117,138,139] the presence of pseudo-octahedral Cr(II), pseudo-tetrahedral Cr(II), and pseudo-octahedral Cr(III) in α-Cr_2O_3 has been inferred, with a relative concentration depending on the treatment and the support composition. Vibrational spectroscopy of adsorbed probe molecules has proven to be a powerful technique to obtain valuable information on the adsorption sites. In particular, the carbonyl IR spectra obtained by dosing CO on naked Cr sites have been used to infer the nuclearity and the oxidation state of the chromium adsorption sites, as well as their coordination environment.[71,117−124,140−146] In particular, by investigating the evolution of the IR spectra of the formed Cr^{2+}-$(CO)_n$ groups at increasing CO pressures, the divalent chromium species have been classified in different families, which differ in their degree of coordinative unsaturation and, consequently, in their ability to chemisorb CO. The assignment of the absorption bands in the carbonyl IR spectra has been controversial, and no unifying view has yet emerged (see section 4.2.1). Nitrosylic bands formed upon NO probe adsorption have also been widely studied to gain information on Cr(II) sites structure. All of these spectroscopic results will be discussed in detailed in section 4.2, because they represent a paradigmatic example of the difficulties encountered by researchers in the investigation of the structure of the Cr(II) sites.

Finally, a number of XPS works appeared in the literature, devoted to discriminate between different supported Cr ions.[135,147−149] XPS is a potentially useful technique because the electron binding energies measured by XPS increase with increasing oxidation state and, for a fixed oxidation state, with the electronegativity of the surrounding atoms. Also these data will be considered as well in section 4.5.

3.3. Modifications of Cr/SiO_2

The possibility to change the catalytic activity by altering the composition and the structure of the

active sites has been known since the seventies. The Phillips catalyst has been successfully modified either by using other support materials (such as alumina,[6] alumino phosphate,[58,150−152] MCM materials,[153−158] etc.), by adding metal alkyls as cocatalyst,[159−161] or by modifying the silica composition with titanium, fluorine, boron, or alkali metal ions.[6,105,120,162−170] Because the Phillips catalyst is highly active as such, modifications are in general used to diminish the induction period or to increase the polymerization activity, so that polymer with different qualities can be produced. All of the cited modifications of the Cr/SiO_2 catalyst lead, in general, to a polymer characterized by a lower density and a lower MW. This is of particular interest, because in certain applications of PE, it is suitable to have a certain amount of short chains to make easier the processability of the polymer.

A detailed discussion about the modified Phillips catalysts is not the aim of this work. In particular, because one of the factors which confers to the Phillips catalyst unique properties among the other Cr-based catalyst is the nature of the silica support (vide supra section 2), the modifications of the catalyst obtained by using other support materials will be not treated at all. Conversely, the investigation of the effects induced by the addition of doping atoms into the silica support can be interesting in the frame of the identification of a precise relationship between the structure of the chromium sites and the polymerization activity. For this reason, in this section, few words will be devoted to discuss the way to modify the Phillips catalyst properties by inserting other atoms as dopants into the silica support. The case of titanium will be deeply discussed, because it is by far the most studied modifier, both from a spectroscopic point of view and from a catalytic side. The recent spectroscopic investigations and the improvements in the comprehension of the catalyst structure with respect to the work of the eighties will be discussed in each subsection of section 4. Finally, in section 5.1.3, the relation between structure, polymerization activity, and polymer properties will be treated. The conclusion that can be drawn from the analysis of the reported results is that we have an instrument to "play" with the silica support in order to modify the structure of the active sites and thus the properties of the resulting polymer.

Coming to the Ti-modified Cr/SiO_2, the inclusion of small amounts of titanium on Cr/SiO_2 catalyst has been found to have a promotional effect both on polymerization activity and on the termination rate of the catalyst (vide infra section 5.1.3).[6,162,164,166−168] Numerous patents were filed in the 1970−1975 period,[165,171,172] but only few works concerning the characterization of titania-modifed Cr/SiO_2 catalyst appeared in the literature up to now.[6,105,162,164,169,170,173] Two ways of incorporating titanium onto Cr/SiO_2 catalyst have been described in the patent literature.[165,171,172] The simplest procedure involved the reaction of a titanium ester with the hydroxyl groups of the bare silica support,[165] as illustrated in Scheme 5. Following this method, which permits us to dope commercial silicas with titanium amounts up to 5−6 wt %, the silica surface is coated with a layer of titanium: thus, the method provides an efficient use of titanium, because most of it should be exposed. The second method of incorporating titanium onto the catalyst consists of the coprecipitation of hydrous titanium along with the silica gel. In this case, a higher amount of titanium is dispersed inside the bulk, and only a minor part of it is exposed on the silica surface. In both cases, chromium may attach to the titanium-modified silica surface during later impregnation and calcination. The different amount of titanium exposed on the surface with the two different methods explains why catalysts containing a surface layer of titanium usually exhibited about twice the polymerization activity of the coprecipitated samples containing the same overall titanium content.[162]

Scheme 5. Hypothesized Reaction between a Titanium Ester and the Hydroxyl Groups on the Silica Surface[a]

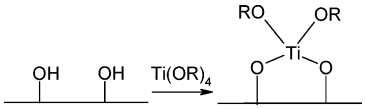

[a] Note that the stoichiometry of the scheme has not been balanced, for the sake of simplicity.

How the chromium ions attach to the silica−titania surface is not completely clear. By using XPS, optical spectroscopy, and polymerization kinetics, Pullukat et al.[165,173] concluded that the Cr(VI) became attached to two vicinal titanium atoms and that the beneficial effect derived from the resulting change in electronic environment around the chromium. However, other possible structures may be hypothesized, such as a surface chromium species bridging an isolated surface titanium site and an adjacent surface silica site or, eventually, a combination between the Pullukat structure and the last one.[105] Mc Daniel et al.[6,162] suggested that the promotional effect probably derives from the creation of Ti−O−Cr links, which change the electronic environment of the chromium active center. The proportion of Ti−O−Cr links formed, relative to Si−O−Cr links, is extremely sensitive to variations in the preparation method and determines the magnitude of the promotional effect. In particular, great differences are noticed according with the order of impregnation. When titanium is added to a silica previously impregnated with chromium, only a little promotional effect is observed, probably because the chromium remains attached to the silica and does not link up with titanium. Conversely, when the order of impregnation is reversed, i.e., titanium first, then chromium, a huge promotional effect is observed. An intermediate effect occurs when a simultaneous impregnation of chromium and titanium is performed.[162]

More recently, Rebenstorf, by means of FTIR spectroscopy,[120,170] and Ellison, by means of TPR and SIMS spectroscopy,[169] tried to better describe the structure of the chromium sites on the Ti-modified silica surface. A more systematic spectroscopic study devoted to determine the dispersion and molecular structure of $Cr/SiO_2−TiO_2$ catalysts has been performed by Jehng et al.,[105] by means of Raman, UV−

vis DRS, and EPR spectroscopies. All of these works will be discussed in more detail in section 4.

Finally, it must be noticed that the incorporation of titanium inside the silica support does not promote only the catalytic activity but also the silica sintering.[6,162] Although Cr/SiO_2 itself does not sinter below 1173 K, the titanium added by coprecipitation promotes the sintering, which occurs at temperatures below 1073 K. The more titanium present, the lower the temperature at which sintering begins. A less pronounced sintering effect is observed in the case of the presence of a surface layer of titanium. Also alkali metals (Na, Li, K, etc.) are known to promote silica sintering.[163] In general, it is accepted that the main effect of alkali metal ions is to enhance the formation and breakage of Si−O−Si bonds; thus, doping a Cr/SiO_2 catalyst with alkali metals followed by calcination at low temperatures has been found to yield the same effects on porosity and polymerization performances as calcining the undoped catalyst at higher temperatures. However, the situation is a bit more complicated than a simple shift of events at lower temperatures. McDaniel et al.[163] observed that the maximum MI value, which is related to the termination rate of the polymer chains, achievable without alkaline metal dopants, was not possible at lower temperatures with dopants. Despite the lower MI maxima, however, the effect of alkali metals could be viewed as positive in one sense. At the lower calcining temperatures such as 923 K, which is commonly used in commercial operations, the alkali metals-treated catalyst often exhibits a higher MI value than those not treated.

4. Spectroscopic Characterization of the Structure of Chromium Sites: A Review of the More Recent Literature

4.1. Diffuse Reflectance UV−Vis Spectroscopy

4.1.1. Cr(VI) Species

UV−vis DRS is a suitable technique for studying heterogeneous catalysts containing transition metal ions, as both d−d and CT transitions can be probed.[94,97,111,117,118,174−178] In the particular case of the Cr/SiO_2 catalyst, it must be noticed that the color of the samples reflects the presence of the majority species. Yellow is the characteristic color of monochromates, and orange is the color of dichromates (or polychromates); the presence of Cr(III) is revealed by a greenish shade, while Cr(II) confers a light blue color to the material. It is so clear why UV−vis DRS, frequently combined with other characterization techniques, has been widely used (i) to investigate the molecular structure of Cr(VI) anchored on SiO_2 and (ii) to address the long-standing question of the active oxidation state and structure of reduced chromium in the Phillips catalyst.

As anchored chromate and di/polychromate are the dominating species on freshly prepared sample after activation in oxygen, a short review of the electronic structure and of electronic transitions of the chromate and dichromate ions is useful. Miller et al.[179] have calculated the orbital energies of chromate ion,

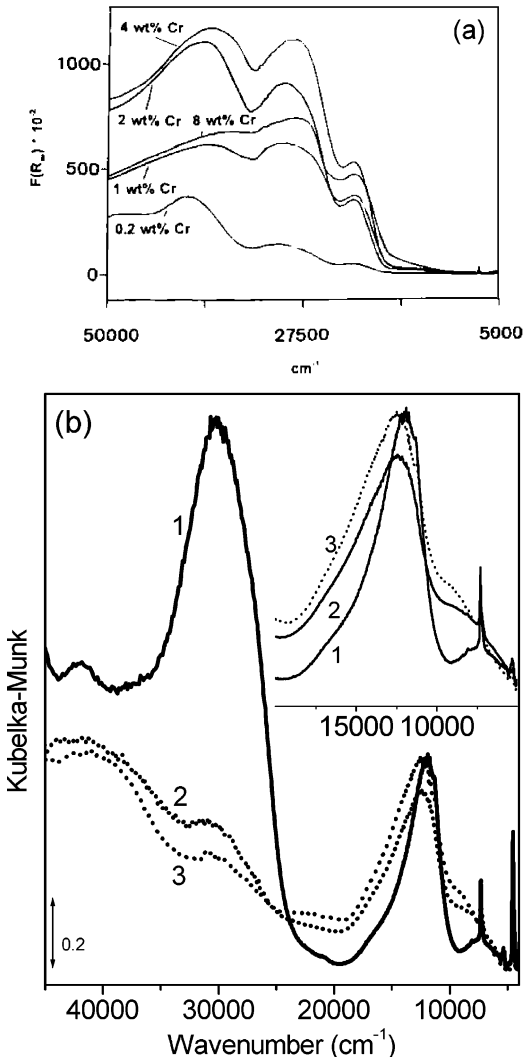

Figure 9. (a) UV−vis DRS spectra of $Cr(VI)/SiO_2$ samples at increasing chromium loadings. Reprinted with permission from ref 97. Copyright 1995 Royal Chemical Society. (b) UV−vis DRS spectra of $Cr(II)/SiO_2$ sample (0.5 wt % Cr loading) (1) reduced in CO at 623 K; (2) heated at 923 K in vacuo after reduction; and (3) heated at 1023 K in vacuo after reduction. In the inset: zoom of the d−d region. Unpublished spectra were obtained by reproducing the experimental procedure described in ref 117.

establishing that the HOMO level possesses pure oxygen character and the unoccupied MO levels are of mostly chromium character. Similarly, if we consider the chromyl chloride as a model for the anchored species, the highest filled MO are mostly localized on oxygen and chlorine atoms, while the lowest unfilled MO has mainly chromium character. Thus, in both cases, the transition of one electron from the HOMO to the LUMO levels gives rise to an intense ligand-to-metal CT absorption band in a UV−vis spectrum.

Weckhuysen et al.[8,97,138,180−184] have published several UV−vis DRS works devoted to investigate the surface chemistry of supported chromium catalysts ($Cr/SiO_2{\cdot}Al_2O_3$) as a function of the support composition (Si:Al ratio) and the Cr oxide loading. In Figure 9a, the UV−vis DRS spectra of calcined Cr/SiO_2 samples as a function of the chromium loadings are shown.[8,97] The assignment of the observed bands was made by considering the features of some relevant

Table 1. UV−Vis DRS Bands of Reference Chromium Oxide Compounds

ref compd	color	UV−vis DRS bands (cm^{-1})[a]	ref
K_2CrO_4 (solid)	yellow	21800 (s); 29400 (s); 37700 (s); 43600 (s)	8,185
$K_2Cr_2O_7$ (solid)	orange-red	19000 (s,br); 30100 (s); 38200 (s); 43600 (s)	8,185
Cr_2O_3 (solid)	green	14000 (sh); 15500 (sh); 16800 (s); 21700 (s); 28500 (s); 36500 (s)	8
CrO_4^{2-} (solution)	yellow	22700 (sh, vw); 27000 (s); 36350 (s)	8,185
$Cr_2O_7^{2-}$ (solution)	orange	22700 (sh, w); 28400 (s); 39200 (s)	8,185
CrO_2Cl_2 (gas)		18000 (w,br); 24000 (s); 38000 (s); 45000 (s,br)	185

[a] s = strong; w = weak; vw = very weak; sh = shoulder; and br = broad.

reference compounds,[8,185] reported in Table 1. From the reported data, it is evident that chromates and dichromates give rise to different absorptions in the solid state while in solution their spectra are very similar. In particular, in the solid state, the lowest CT band occurs at 21800 cm^{-1} for chromate, while it is observed at 19000 cm^{-1} for dichromate. These values are lower than those of the same species in solution. A reason for that may be the presence of more localized double bonds between oxygen and chromium in the solid compounds with respect to the solution case, where the double bonds are mainly delocalized on the four oxygen atoms. As the anchorage of Cr(VI) to the surface as chromates or dichromates should be accompanied by (i) the formation of highly covalent bonds with surface silicon and (ii) the localization of double bonds on the CrO bonds pointing outward from the surface, it has been inferred that the presence of an intense band in the 21000−25000 cm^{-1} range (see Figure 9a) in the supported state could be indicative of the presence of anchored dichromates.

Weckhuysen et al.[138,180−184] have tried to establish the monochromates/dichromates ratio on the basis of the different intensities of the CT bands present in the spectra of calcined samples (monochromates: bands at 44100, 30600, and 20300 cm^{-1}; dichromates: bands at 45500, 36600, and 25000 cm^{-1}). They have found that the nuclearity of Cr is extremely sensitive to the support type and more particularly to the specific preparation method. By analyzing the O→Cr(VI) CT transitions in UV−vis DRS spectra of the calcined catalysts, the main chromium species are shown to be a mixture of hexavalent dichromate (band in the 30000 cm^{-1} region) and monochromate (band in the 28000 cm^{-1} region) on laboratory sol-gel silica supports (700 m^2/g), while monochromate dominates on industrial pyrogenic silica supports (Cab-O-Sil, 300 m^2/g) characterized by low chromium loadings.

The ratio between surface polychromate and monochromate can be varied by altering the composition of the support and the chromium loading: on pure silica surfaces, the dichromate-to-monochromate ratio is found to increase with chromium loading[138] (see Figure 9a). In a systematic spectroscopic study, Jehng et al.[105] investigated the molecular structure of chromium sites on Ti-modified Cr/SiO_2 samples obtained in different ways. They reported that when a low amount of titanium is added by impregnation on the silica surface, the catalyst assumes an orange color, suggesting that polychromates are associated with the surface titanium sites. This observation is confirmed by the appearance of an additional UV−vis DRS band around 22000 cm^{-1}, which is not present in the case of a standard Cr/SiO_2 catalyst. The preferential interaction between the surface chromates and the surface titanium sites is consistent with the low affinity of the silica support for oxides and the high affinity of the titania support. This is confirmed by the recent work of Zhu et al.,[153] who reported that Cr/Ti-MCM-41 samples give rise to an UV−vis band around 454 nm (22000 cm^{-1}), while the corresponding Cr/MCM-41 material did not exhibit this additional band. Whether UV−vis DRS results can be used to demonstrate that Ti is altering the polychromate/chromate ratio is debatable, because it takes into account only the first coordination sphere around chromium (i.e., the oxygens). It is conceivable that the different molecular structure of chromium sites on a Ti-modified silica may induce a different activity toward polymerization (vide infra section 5.1.3).

All of the conclusions summarized so far are based on the attribution of the component in the 21000−25000 cm^{-1} region of the UV−vis DRS spectra to dichromate species. In this regard, it is however worth noticing that quoted authors[8,97,138,180−184] were perfectly aware of the risk of this interpretation, and already in the initial stages of their ongoing work, also the claim of site distortion has been made. The fact that the presence of components in the 21000−25000 cm^{-1} region cannot be univocally related to the presence of dichromate species is also testified by the fact that the chromyl chloride, which is mononuclear and has two Cr=O moieties characterized by localized double bonds, presents a very intense CT absorption at 24000 cm^{-1}, i.e., a feature very similar to that observed for the oxidized samples. We can so conclude that the determination of the molecular structure of chromium species on silica surface based on UV−vis DRS data only is to be considered with caution and that, when available, the support of other techniques is desiderable. In this regard, it is worth anticipating that the new Raman results summarized in section 4.3.2 strongly support the absence of dichromate species in low Cr-loaded Cr/SiO_2 catalyst.

From the data reviewed (and anticipated) so far, it can be concluded that the dominant oxidized species on Cr/SiO_2 samples, characterized by a chromium content in the 0−1% (by weight), is most probably the monochromate. As the concentration of the most active samples is in the 0.5−1% range, hereafter we will consider the chromate only for further considerations concerning the structure of anchored species. On the basis of Scheme 2, the anchoring of chromic acid on suitably spaced OH doublets can originate different species, characterized

by an increasing α_{OCrO} bond angle and consequently by a decreasing strain (vide supra sections 2.2.1 and 2.2.3), as illustrated in Scheme 6. These species are

Scheme 6. Cr(VI) Anchored Reaction on Silicon-Membered Rings of Increasing Dimensions (and Decreasing Strain)[a]

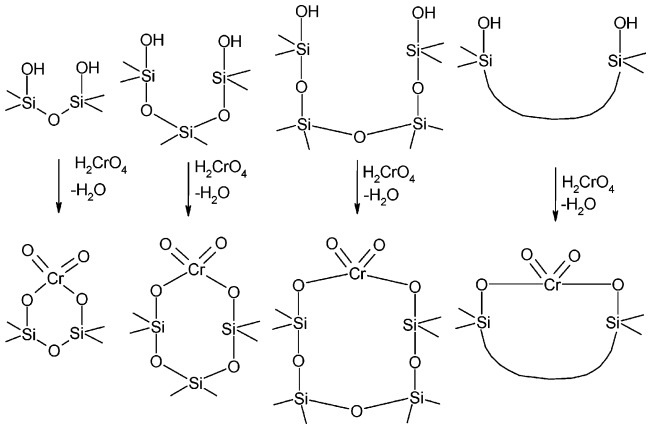

[a] Surface anchoring sites are those reported in Scheme 2. Note that when Ti is present, one or more Si atoms in the reported schemes could be substituted by a Ti atom.

expected to show very similar spectroscopic transitions and cannot be distinguished by UV−vis spectroscopy. However, a final point requires discussion here. Even assuming that monochromates are by far the dominant species on low loaded Cr(VI)/SiO_2 sample, we cannot make a definite conclusion about the final destination of a surface monochromate after CO (or ethylene) reduction. In other words, we cannot exclude that some Cr ions can be characterized by a distance less than that hypothesized in the case of a homogeneous distribution of monochromate species (about 10 Å). As we will discuss in the following sections, this may have some consequences when dealing with the polymerization mechanisms (vide infra section 5.2.1.1).

4.1.2. Cr(II) Species

Bensalem et al.[180] have investigated the CO reduction of Cr/SiO_2 (0.5 wt % Cr loading) in the 673−773 K temperature range by in situ UV−vis DRS measurements. By quantifying the concentration of Cr(VI) on silica in the presence of CO at a fixed temperature as a function of time, they proposed a kinetic model for the reduction reaction. According to their model, the first step of the reduction is the adsorption of CO on the surface at some unspecified site, resulting in its activation. The second step, the actual reduction of Cr(VI), is rate determining and occurs with formation of surface carboxylates, which decompose to CO_2 [the oxygen coming from the chromate or di(poly)-chromate species]. Thus, the reduction of Cr(VI) is accompanied by a decrease in the number of oxygens in its coordination sphere, leaving empty coordination sites, which can be used for specific adsorption and catalysis. The overall reaction order was found to be 2, in agreement with the results of Finch on the basis of TPR study.[186]

In the following, we want to focus the attention on the modification undergone by both CT and d−d

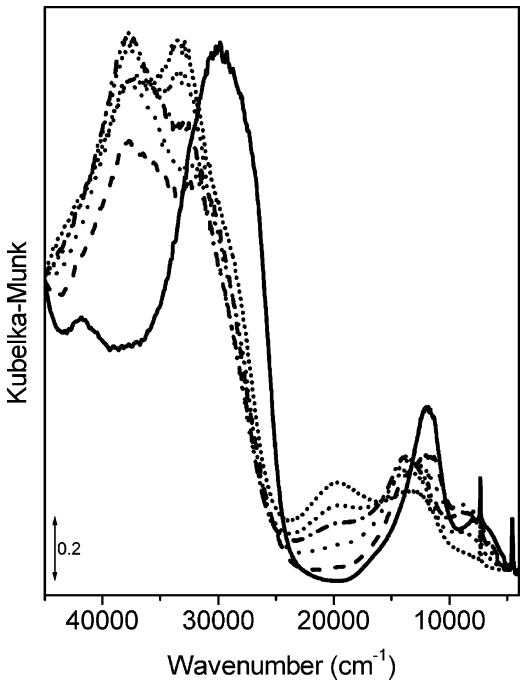

Figure 10. UV−vis DRS spectra of reduced Cr(II)/SiO_2 sample (0.5 wt % Cr loading) upon increasing dosages of CO at RT. Black solid curve, Cr(II)/SiO_2 reduced in CO at 623 K; dashed and dotted curves, increasing dosages of CO from 0.1 to 50 mbar. Unpublished spectra.

transitions upon (i) different treatment conditions, affecting the Cr(II) coordination state, and (ii) different equilibrium pressures of CO and NO probe molecules. DRS UV−vis has been widely used in the literature to study such effects.[8,117,118,187] As Cr(II)/SiO_2 catalyst is extremely sensitive to support properties, impregnation method, activation conditions, treatment procedures, etc. and as the response of DRS UV−vis instruments is intrinsically dependent on the experimental conditions (integration sphere, sample positioning, etc.), we decided to reproduce such literature experiments on an unique Cr(II)/SiO_2 sample in a consistent way, vide infra Figures 9−12. Such new experiments do not provide any new insight on the topic, as they are perfectly representative of those reported in the literature. They just allow us to better appreciate the physical and chemical effects produced by different treatment conditions and by interaction with probes, as systematic differences due to instrumental and experimental conditions have been minimized.

The UV−vis DRS spectrum of the CO-reduced Cr/SiO_2 sample (0.5 wt % Cr loading on pyrogenic silica) shows a strong absorption in the CT region (there are at least two overlapped components at about 28000 and 30000 cm^{-1}) and two bands in the d−d region, (i.e., at transition energies of about 12000 and 7500 cm^{-1}) (see Figure 9b, curve 1). Transitions in the 7000−10000 and 10000−13000 cm^{-1} regions have been previously attributed to coordinatively unsaturated Cr(II) species.[94,97,103,117,118,139] Additional broad bands at ~16000 and 19500−22000 cm^{-1} (apparently not present in the reported spectrum), whose intensities depend on the activation procedure and are absent on samples where the water deriving from Si−OH condensation is efficiently removed during the

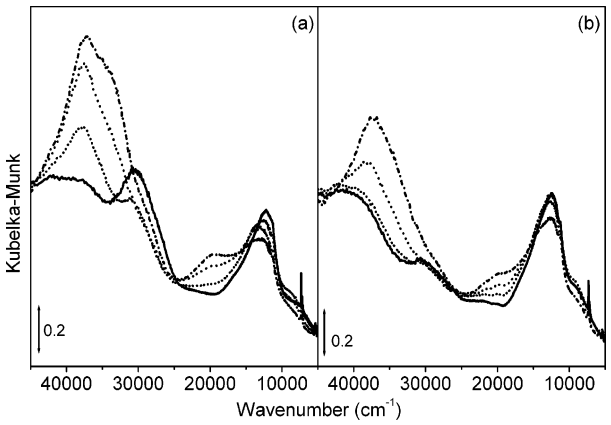

Figure 11. UV−vis DRS spectra of reduced $Cr(II)/SiO_2$ sample (0.5 wt % Cr loading) heated at high temperature after reduction upon increasing dosages of CO at RT. Black solid curve, $Cr(II)/SiO_2$ sample treated at high temperature after reduction; dotted and pointed curves, increasing dosages of CO from 0.1 to 50 mbar. (a) Sample heated at 923 K in vacuo after reduction; (b) sample heated at 1023 K in vacuo after reduction. Unpublished spectra.

thermal treatments, have been assigned to Cr(III) species in octahedral coordination (α-Cr_2O_3).[94,139] Considering that the oscillator strength of Cr(III) is much higher than that of the Cr(II) species, the presence of an even small quantity of Cr(III) species can be potentially easily detected by UV−vis spectroscopy, as shown by Groppo et al. on a high loaded Cr/SiO_2 catalyst.[115]

The spectrum illustrated in Figure 9b is characteristic of diluted samples and is independent from the type of siliceous support. In principle, the location and intensity of d−d bands should allow the determination of coordination state and of the symmetry of a transition metal ion. Unfortunately, in the Cr(II) case, no clear inference about the coordination and symmetry can be made from the comparison of the UV−vis results with the spectra of the rare Cr(II) homogeneous complexes carefully studied so far. The only safe conclusion that can be derived from the presence of a doublet in the 7500−12000 cm^{-1} region is that the Cr(II) centers are in highly distorted structure and that the ions are preferentially sensing the crystal field caused by two strong SiO^- ligands. This broad conclusion is in agreement with the Cr(II) structures, which can be derived by CO reduction from the anchored chromates of Scheme 6, as reported in Scheme 7, where the α_{OCrO} bond angle is increasing along the series together with ionicity of the Cr−O bond.

The Cr(II) structures represented in Scheme 7 do not consider surface relaxation, which is certainly occurring around the Cr(II) ions, to increase the crystal field stabilization. It is worth noticing that the IR bands at about 900 cm^{-1}, characteristic of the strained Si−O−Si siloxane bonds (vide supra section 2.2), completely disappear upon chromium grafting (see the evolution from curve 1 to curve 2 in Figure 5a). Because of this effect, it can be hypothesized that surface locations of Cr(II) are certainly present where, beside the strong SiO^-, other weaker ligands (like the oxygens of adjacent SiOSi bridges) contribute to the ligand field stabilization, vide infra eqs

Scheme 7. Different Cr(II) Structures Deriving by CO Reduction of the Anchored Chromates Reported in Scheme 6[a]

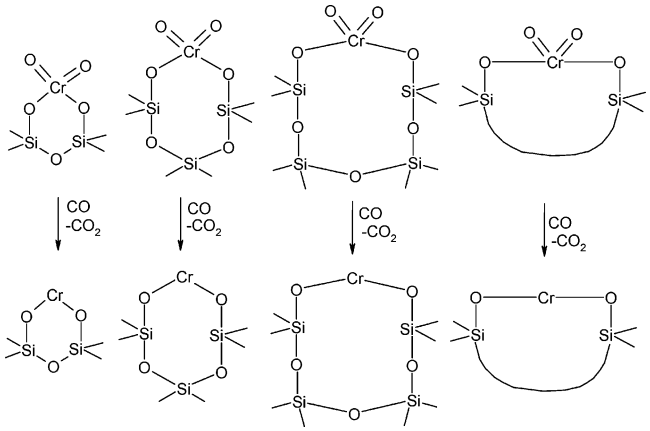

[a] Note that the stoichiometry of the scheme has not been balanced, for the sake of simplicity.

1−3. For these structures, we expect d−d transitions shifted progressively toward higher frequencies with the increase of the number of ligands. That this is the case is demonstrated by the spectra 2 and 3 reported in Figure 9b, where the effect of thermal treatments at 923 and 1023 K in vacuo on a reduced Cr/SiO_2 sample is shown. These spectra are characterized by (i) the small shift of the two d−d maxima toward energies higher than those observed in the case of a standard activation and (ii) a considerable decrease of the intensity of the CT bands. The variations induced in the d−d region of the spectrum of Cr(II) by heating at high temperature in vacuo is similar to some extent to the shifts caused by the adsorption of weak ligands, such as CO forming 1:1 or 2:1 complexes, on the standard reduced Cr(II) sample (Figures 10 and 11). In fact, the original bands are shifted to 12500 and 9000 cm^{-1}, respectively. Stronger ligands, such as NO, cause much higher shifts (Figure 12). Of particular interest is the progressive growth of the tail on the high frequency side of the 12500 cm^{-1} maxima upon increasing the temperature of the thermal treatment (Figure 9b, inset). This suggests that absorption centered at about 15000 cm^{-1} is increasingly contributing. Considering that the octahedral $[Cr(H_2O)_6]^{2+}$ complex absorbs at about 16000 cm^{-1},[188] we suggest that we are in the presence of Cr(II) ions sunk in the silica matrix and thus characterized by a greater number of ligands in the coordination sphere.

These results suggest that the thermal treatment at high temperature decreases the population of the grafted Cr(II) sites characterized by highest coordinative unsaturation and favors the partial penetration of the ions into the flexible silica framework, with subsequent stabilization of more coordinated Cr species, containing siloxane bridges in the coordination sphere.[117,143] An additional result is that the oxygen of the siloxane bridge behaves as a very weak ligand, as hypothesized before. This interpretation explains also the considerable change in the CT region of the spectrum (Figure 9b). In fact, the energy and the intensity of a CT band are related both to the donor character of the ligand and to the acceptor

power of the metal. The greater the oxidizing power of the metal ion and the reducing power of the ligand group, the lower the energy at which the CT bands appear and the lower their intensity. Under the same donor character of the ligands (oxygens), the acceptor power of the sunk Cr(II) sites decreases, due to the increasing number of ligands.

The assignment given so far is further demonstrated by the study of the spectroscopic modifications induced by the interaction of Cr(II) with CO as a probe molecule. Figure 10 shows the evolution of UV−vis spectra of the Cr(II)/SiO_2 system as a function of CO pressure. Upon increasing CO pressure at RT, we observe the consumption of the two d−d bands described before (12000 and 7500 cm^{-1}) and the intermediate growth of two bands shifted at higher transition energies (14000 and 8600 cm^{-1}). Analogously, in the CT region, the consumption of the CT band at 28000−30000 cm^{-1} occurs, accompanied by the growth of a new intense band at 37700 cm^{-1}. The clear appearance of two isosbestic points at 10000 and 13100 cm^{-1} indicates a 1:1 transformation Cr(II) + CO → Cr(II)···CO. Further increase of the CO pressure leads to the disappearance of the 14000−8600 cm^{-1} doublet and to the formation of a new absorption centered at 20000 cm^{-1}. The isosbestic point at 16000 cm^{-1} ensures that we are dealing with the addition of a second CO molecule, following a Cr(II)···CO + CO → Cr(II)···$(CO)_2$ process. It is interesting to observe that CO dosage has an effect partially similar to that induced by a thermal treatment after reduction, as discussed before (see Figure 9b). This confirms that the ligands, which enter in the chromium coordination sphere upon heating at high temperature, are quite weak. The Cr(II)···CO + CO → Cr(II)···$(CO)_2$ transformation is accompanied by the appearance of a CT component at about 33400 cm^{-1}. These two-step features, which will be discussed again in the complementary FTIR section (see section 4.2.1), can be resumed as follows. The adsorption of CO, being accompanied by the increase of the coordination number due to the formation of mono- and dicarbonyl species, causes a shift of the d−d transitions toward the values more typical of the octahedral coordination, as happens when chromium ions are naked into the silica framework. Furthermore, in the presence of CO (electron donor molecule), more energy is requested to transfer electrons from O to Cr; as a consequence, the O→Cr CT transition shifts at higher frequencies (from 28000 to 30000 to 33700 cm^{-1}). At increasing CO pressure also the CO→Cr(II) CT transition becomes visible (band at 33400 cm^{-1}).

The sequence of spectra obtained upon CO dosage on Cr(II)/SiO_2 activated at high temperature (see Figure 11a,b) confirms the previous assignment. In fact, the samples show a decreased tendency to add CO molecules, as it is evident both in the CT and in the d−d regions (compare with the spectra reported in Figure 10).

From all of these data, the following picture about the structure of the Cr(II) is emerging. Several types of Cr(II) sites are present on the amorphous silica surface. All of the grafted Cr(II) species have a

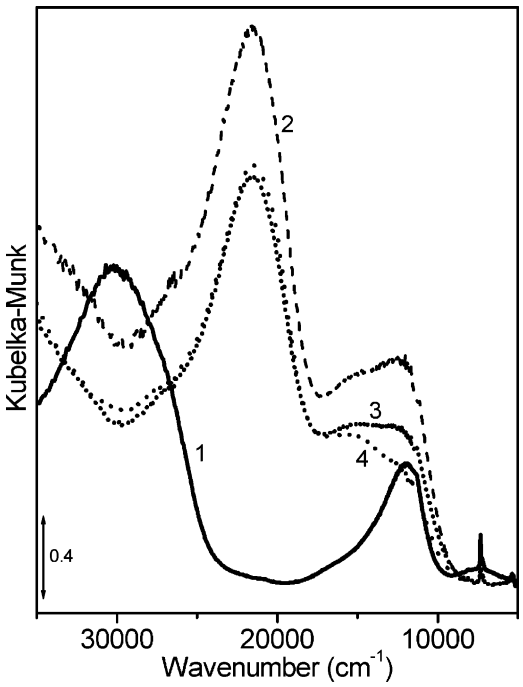

Figure 12. UV−vis DRS spectra of NO adsorption on a reduced Cr(II)/SiO_2 sample (0.5 wt % Cr loading). Curve 1, sample reduced in CO at 623 K; curve 2, NO interaction at RT with the same sample; curve 3, NO interaction at RT with the same sample after treatment at 923 K in vacuo after reduction; and curve 4, NO interaction with the same sample at RT after treatment at 1023 K in vacuo after reduction. Unpublished spectra were obtained by reproducing the experimental procedure described in refs 117 and 118.

coordination sphere constituted by two strong SiO^- ligands. When the strong SiO^- ligands belong to the smallest cycles, they form with Cr(II) an angle α_{OCrO} near to tetrahedral value. In this case, we speak of pseudo-tetrahedral structure. The O−Cr bond is expected to be quite covalent. The angle α_{OCrO} gradually grows when the cycle dimension increases, and for large cycles, it is approaching 180° (Scheme 7). In this case, we can speak of pseudo-octahedral complexes. Because of surface relaxation, a variable number of weak siloxane ligands is also present in the coordination sphere of the Cr(II) ions. On the standard reduced sample, Cr(II) sites in distorted tetrahedral environment are by far the most abundant species, characterized by a high adsorption activity. Nevertheless, a little fraction of more saturated Cr(II) sites, unable to coordinate CO molecules, is contemporarily present, as demonstrated by the permanence of a residue of the unperturbed d−d bands at the maximum CO coverage and of the broad absorption in the 20000−15000 cm^{-1} range observed for the sample before CO dosage. The tetrahedral-like sites are protruding on the surface; hence, they are expected to be preferentially affected by thermal treatments and to undergo structural rearrangement, leading to more coordinated Cr(II) species (increase of the number of siloxane ligands in the coordination sphere). This process can be described as a sinking of Cr(II) into the siliceous matrix. The pseudo-octahedral sites, being less protruding, are certainly interacting with oxygens of siloxane rings in an

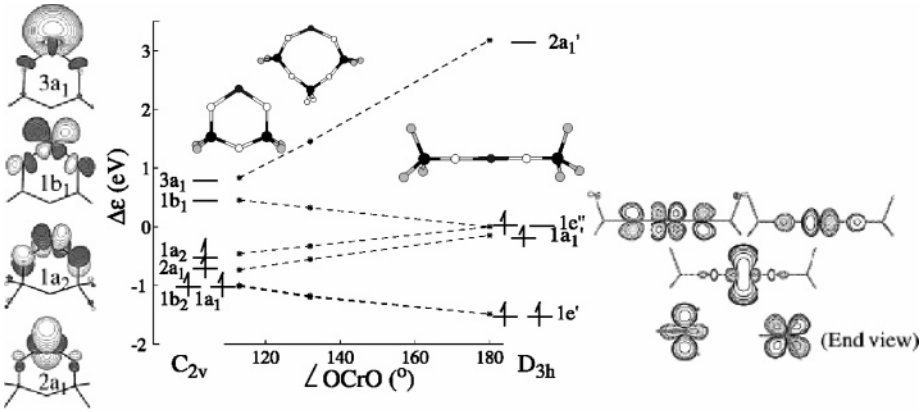

Figure 13. Walsh diagram of the MOs with mainly Cr 3d and 4s character for mononuclear Cr(II) cluster models with the α_{OCrO} bond angle in the tetrahedral-to-octahedral range. Orbital energies are shown relative to the mean energy of the HOMO and LUMO in the ground state. The elements are coded in a gray scale according to increasing atomic number, H (white) < O < F< Si < Cr (dark gray). Reprinted with permission from ref 191. Copyright 2002 Elsevier.

adjacent position. A more pronounced ionicity and resistance to thermal treatments is foreseen. Intermediate behavior can be hypothesized for intermediate structures. The same behavior, analyzed by means of IR spectroscopy, will be discussed in section 4.2.1.

Analogous features have been reported in the past about NO adsorption on the reduced Cr/SiO_2 system.[118,187] Note that the adsorption of NO, which is a $\sigma-\pi$ acceptor ligand stronger than CO, has a more profound effect on the UV−vis spectrum (see Figure 12, curve 2). It is a matter of fact that upon NO adsorption, the d−d band at 7400 cm^{-1} is completely destroyed and substituted by a complex absorption with components at about 13000 and 15000 cm^{-1}; the intense CT band at about 30000 cm^{-1} disappears in favor of a strong band at 21000 cm^{-1}. The distinct upward shift of low frequencies component of the original d−d doublet is caused by the insertion of two strong NO ligands into the coordination sphere of Cr(II) species. The reaction occurs in a single step; no evidence has been obtained so far of the presence of a mononytrosil intermediate, probably because the dinitrosyl compound is by far the most stable compound. The strong CT band at 21000 cm^{-1}, responsible for the yellow color of the sample after NO adsorption, is located at a frequency exceptionally low for a CT and too high for a d−d transition. Inorganic complexes with a similar electronic structure (for example, CN^- and O_2^-, which differ from NO by one or two electrons, respectively) present low energy CT absorption, even if not so intense. Such bands are usually accounted for in the literature by an electronic transition in which an appreciable mixing of metal and ligand orbitals occurs, as in transition metal complexes where strong π-acceptor ligands are involved. In comparison with the CO case, the differences between the standard and the sample heated at high temperature after reduction are less pronounced in the case of NO; compare curves 3 and 4 with curve 2 in Figure 12. This is due to the stronger nature of NO, which is able to extract the chromium centers from the surface by displacing the weaker ligands, thus uniforming different Cr(II) sites.

In conclusion, we can schematically represent the structure of Cr(II) sites as $(SiO)_2Cr^{II}L_n$, where L represents a weak ligand and n is a not fully known figure, which increases upon activation at high temperature. The adsorption of CO and NO at RT on grafted Cr(II) sites is accompanied by a modification of their coordination number, following reactions 1 and 2:[189]

$$(SiO)_2Cr^{II}L_n \xrightarrow{CO} (SiO)_2Cr^{II}L_{n'}(CO) \xrightarrow{CO} (SiO)_2Cr^{II}L_{n''}(CO)_2 \quad (1)$$

$$(SiO)_2Cr^{II}L_n \xrightarrow{2NO} (SiO)_2Cr^{II}L_{n''}(NO)_2 \quad (2)$$

where $n \geq n' \geq n''$. Actually, the scheme has only a qualitative character, because it does not take into consideration that the α_{OCrO} angle can vary in a wide interval, as discussed above. Furthermore, we have to consider that the adsorption of molecules is always associated with a surface relaxation phenomenon. The relaxation may occur starting from an increment of the Cr−L distance to a complete displacement of the ligand L, as we will discuss in detail in the following sections. For the moment, it's important to notice that UV−vis DRS spectroscopy is a very sensitive technique, because it is able to give information not only on the oxidation state of the chromium ions but also on their environment. Of special importance is that little modifications in the coordination sphere of chromium sites (such as the presence of weaker ligands) may cause spectacular changes in both CT and d−d regions.

4.1.3. Theoretical Calculations

Recently, Espelid and Børve performed detailed ab initio calculations on the number, energy region, and electric−dipole oscillator strength of the observable electronic transitions of grafted Cr(II),[190,191] which aid in the assignment of the UV−vis spectra discussed above. In agreement with the considerations developed in the previous paragraph, they constructed cluster models of coordinatively unsaturated mononuclear and dinuclear Cr(II) sites, changing from pseudo-tetrahedral to pseudo-octahedral geometries as a function of the α_{OCrO} bond angle (Figure 13). In particular, the mononuclear Cr(II) species were rep-

resented by three cluster models (Figure 13): a pseudo-tetrahedral site, **T**, with an angle of 116° (left); a pseudo-octahedral site, **O**, with an angle of 180° (right); and a site with an intermediate α_{OCrO} bond angle (135°), **I** (center).

Concerning the mononuclear Cr(II) case, a Walsh diagram for the MOs with considerable chromium 3d and 4s character is shown in Figure 13, for clusters displaying a α_{OCrO} bond angle in the tetrahedral-to-octahedral range. Starting from the pseudo-tetrahedral cluster model **T**, the authors identified two sets of excitations. The first one corresponds to excitation of an electron from one of the four singly occupied d type MO localized on Cr(II) into the LUMO and is responsible for two bands at transition energies of 8400 and 12300 cm^{-1} ($1b_1 \leftarrow 1a_2$ and $1b_1 \leftarrow 1a_1$, respectively). These excitations closely correspond to the pair of d−d bands in the 8000−13000 cm^{-1} interval observed on Cr(II)/SiO_2 (see Figure 9b, full line curve). The second set of excitations (29000−30000 cm^{-1}) has a mixed d−d and metal-to-ligand CT character, resulting in high transition energies and large oscillator strengths. This excitation closely corresponds to the strong CT absorption observed on Cr(II)/SiO_2 centered in the 28000−30000 cm^{-1} interval (see Figure 9b, full line curve).

In Figure 13, it is evident that the energy gap between $1b_1$ and $1a_2$ orbitals decreases with increasing α_{OCrO} bond angle. On going from pseudo-tetrahedral sites **T** (116°) to sites with greater α_{OCrO} angles (**I**, 135°), modest shifts of the d−d bands to lower transition energies and a decrease in the associated oscillator strength have been calculated. The trend of converging orbital energies continues to full degeneracy at the linear pseudo-octahedral site, which gives rise to a single d−d band at a transition energy in the range 7000−8000 cm^{-1}. Because the transition is electric−dipole forbidden and, moreover, at least partly overlapping with a relatively strong band from the tetrahedral sites, it may be difficult to identify, on an experimental ground, pseudo-octahedral chromium sites on the Cr/SiO_2.

When we compare the theoretical results with the experimental observations, essentially two complex absorptions centered at 12000 and 7500 cm^{-1} with intensities ratio 5:1, the following considerations can be made: (i) There is a reasonable correspondence between the calculated frequencies of **T** sites and the experimental frequencies. However, the observed oscillator strength ratio (5:1) greatly differs from the calculated one (1:1). (ii) The correspondence between the observed frequencies and those calculated for **I** species is less favorable, although the oscillator strength ratio is now coinciding with the observed one. (iii) No absorption is observed at about 7000 cm^{-1}, where **O** sites are expected to absorb.

Considering that the calculated frequencies are obtained on $(SiO)_2Cr(II)$ sites not interacting with external oxygens of siloxane ligands, we can conclude that the observed spectra can be explained in terms of $(SiO)_2Cr^{II}L_n$ **T** and **I** sites. The possible presence of comparable amounts of pseudo-octahedral Cr(II) species **O** cannot be excluded, because the intensities of the associated d−d bands can be very weak.

4.2. IR Spectroscopy

IR spectroscopy has been widely used to study the reduced Cr(II)/SiO_2 system, while it is scarcely useful in the characterization of the oxidized form of the catalyst. In fact, the vibrational manifestations of Cr=O species fall in a region obscured by the intense modes of the silica support. In the so-called "silica window", see Figure 5, only a band at 905 cm^{-1} becomes pronounced with increasing the chromium loading and this band was assigned to a dehydrated chromium oxide surface species.[96] Raman spectra do not suffer from the same problems encountered in the IR, because the vibrational modes of silica in the 1300−200 cm^{-1} range are much weaker (vide infra Figure 21). Consequently, the vibrational features of surface Cr(VI) species will be treated in section 4.3, where the results of Raman spectroscopy will be discussed.

Concerning the characterization of chromium sites in the reduced Cr(II)/SiO_2 system, a lot of work has been made with the method of probe molecules.[143] Vibrational spectroscopy of adsorbed probes, in fact, has proven to be a powerful technique for characterizing supported metal-based catalysts, both with respect to acidity and coordination environment.[143,192] Of course, it must be kept in mind that different probe molecules can give different answers (depending upon the interaction strength) and that this method is not absolute, because the probing process is necessarily associated to a perturbation of the surface. This is the reason that it is always preferable to use more than one molecule to probe the structure of surface sites. In the context of Phillips catalyst, various diatomic and triatomic gases (NO, CO, CO_2, and N_2O) have been used as adsorbates to discriminate between different chromium species. Nevertheless, despite the application of advanced spectroscopy over more than two decades, a unifying picture of the microscopic composition of the Phillips catalyst in the reduced state is still wanted.

For the reasons already discussed in section 4.1.2 for UV−vis spectroscopy, to better appreciate the effects on the IR spectra of adsorbed probe molecules, catalyst treatment procedures (affecting surface OH population and chromium coordination), equilibrium pressure, and adsorption temperature, we decided to reproduce literature experiments on two sets of Cr/SiO_2 samples (1.0 and 0.5 wt % for CO and NO adsorption, respectively) prepared in consistent ways, vide infra Figures 14−19.

4.2.1. Interaction of CO

IR spectroscopy of adsorbed carbon monoxide has been used extensively to characterize the diluted, reduced Cr/Silica system.[118−124,130,145,146] CO is an excellent probe molecule for Cr(II) sites because its interaction is normally rather strong. The interaction of CO with a transition metal ion can be separated into an electrostatic, a covalent σ-dative, and π-back-donation contributions, the first two causing a blue shift of the $\tilde{\nu}_{CO}$ (with respect to that of the molecule in the gas phase 2143 cm^{-1}), while the last causes a red shift.[193−199] From a measurement of the $\tilde{\nu}_{CO}$ of a

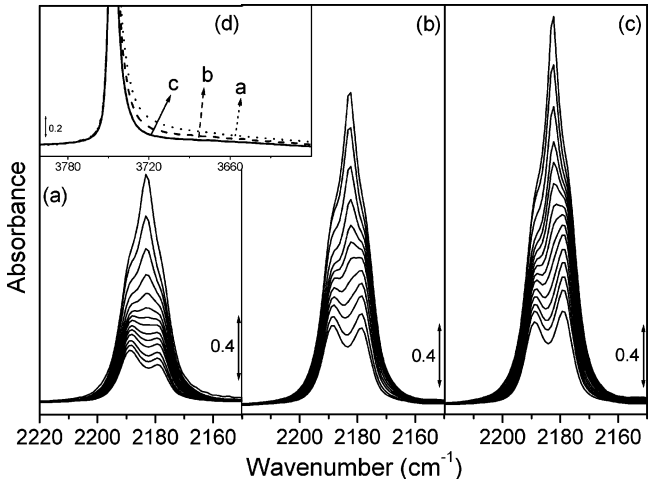

Figure 14. (a–c) Effect of decreasing OH population (obtained by increasing the activation time at 923 K: 90, 120, and 180 min, respectively) on the IR spectra of CO adsorbed at RT on $Cr(II)/SiO_2$ samples (1.0 wt % Cr loading) in the C–O stretching region. Curves from top to bottom: effect of gradual lowering of the CO pressure (from 30 to 10^{-3} Torr). Part (d) quantifies the decrease of the OH population by reporting the IR spectra in the O–H stretching region, collected before CO dosage on the three samples. Curves a–c of part (d) refer to the samples resulting in the spectroscopy reported in parts (a–c), respectively. Unpublished spectra.

given Cr(II) carbonyl complex, information is so obtained on the nature of the Cr(II)···CO bond.

4.2.1.1. Interaction of CO at RT. Figure 14 shows the spectra of CO adsorbed at RT on $Cr(II)/SiO_2$ samples characterized by a decrease of the OH population (see Figure 14d, showing the gradual reduction in the intensity of the tail of the silanol OH stretching peak, obtained by increasing the activation time at 923 K). Notice that these sequences, although corresponding to the same concentration of Cr(II), have intensities in the order c > b > a, so indicating without any doubt that increasing dehydroxylation has a beneficial effect on the adsorption capacity of Cr(II) species. At low equilibrium pressure, the spectra show two bands at 2180 and 2191 cm^{-1}, with an intensity ratio that goes from 1:1.5 to 1.5:1 upon decreasing the OH content. Upon increasing the CO pressure, the 2191 cm^{-1} component grows up to saturation without frequency change. Conversely, the 2180 cm^{-1} component evolves into an intense band at 2184 cm^{-1} and a shoulder at 2179 cm^{-1}. The bands at 2191, 2184, and 2179 cm^{-1}, which are the only present at RT for pressure lower than 40 Torr, are commonly termed "the RT triplet" and are considered the fingerprint of the $Cr(II)/SiO_2$ system. A new band at around 2100 cm^{-1} appears at RT only at higher CO pressure. As this peak gains intensity at lower temperature, it will be discussed further on (section 4.2.1.2).

The interpretation of these spectra given in the literature can be summarized as follows. The 2191 cm^{-1} peak is the stretching mode of CO σ-bonded on a Cr(II) site possessing a high polarizing ability, named as the B site in refs 118, 123, 124, 146, 200, and 201. The 2180 cm^{-1} peak is the stretching mode of CO adsorbed on Cr(II) sites possessing some d-π bonding ability. These sites are named as A sites in refs 118, 123, 124, 146, 200, and 201. Upon increasing the CO pressure at RT, the 2191 cm^{-1} band gradually increases and reaches a saturation plateau, suggesting that at RT Cr_B^{II} sites can only coordinate one CO ligand and that Cr_B^{II} is an isolated site, as an increase of the surface coverage is not able to perturb the $\tilde{\nu}_{CO}$ of the Cr_B^{II}···CO complex.[143,202,203] Conversely, the 2180 cm^{-1} peak is gradually replaced by the 2184–2178 cm^{-1} doublet. This behavior has been interpreted in terms of the easy addition of a second CO molecule with formation of a dicarbonylic species. Thus, the doublet at 2184–2178 cm^{-1} may be assigned to the symmetric and antisymmetric modes of a dicarbonyl formed at Cr_A^{II} sites.[124,146] This elementary interpretation is not straightforward, because the more intense band of the doublet is located at higher frequency, in contrast with all known cases of dicarbonyls.[198,199,204–207] The explanation can lie in the prevailing σ character of the bond between chromium and CO, which may allow a negative sign for the coupling constant of the two carbonyls. This interpretation has some implications. First, it is evident that Cr_A^{II} sites are more coordinatively unsaturated than Cr_B^{II} sites, as they are able to coordinate at RT a second CO molecule. A second deduction is that Cr_A^{II} sites have a higher tendency to give d-π interactions. The absence of bands at $\tilde{\nu}$ < 2000 cm^{-1} demonstrates that no bridging CO structures are formed upon CO dosage at RT.[204,208]

In conclusion, the examination of the $\tilde{\nu}_{CO}$ bands in the 2200–2178 cm^{-1} region at RT reveals that Cr(II) sites are distributed in two basic structural configurations, namely, Cr_A and Cr_B. These results confirm the view illustrated before about the structural complexity of the Cr(II) system (vide supra section 4.1.2). Cr_A sites seem to correspond to the first family of chromates represented in Scheme 7, while Cr_B sites correspond to a family characterized by a larger α_{OCrO} bond angle. It is important to underline here that when we speak about Cr_A and Cr_B sites, we are referring to two families of structures instead of simply two different well-defined sites. This aspect will be widely discussed in section 4.6.

Once that the RT triplet has been assigned, the question is why, at a constant chromium concentration, the CO spectra are a function of the degree of dehydroxylation of the sample (Figure 14a–c). We have already discussed the different results that one can obtain by different activating procedures (see section 2.2), and we will see in section 5.1.1.3 that there is a precise relationship between the activity of the catalyst and its calcining temperature. In Figure 14, it is evident that the effect of a prolonged activation treatment is two-fold: (i) the overall intensity of the triplet increases, and (ii) the relative intensity ratio of the bands at 2191 and 2184–2178 cm^{-1} increases in favor of the 2184–2178 cm^{-1} doublet. We can explain this behavior by considering that although the chromium is fully attached to the silica support upon activation at 573 K, a prolonged activation procedure and/or a higher activation temperature causes a gradual dehydration of the silica surface, as hydroxyl groups condense to release water

(Scheme 1). Remaining hydroxyls may somehow interfere with the active sites. Two explanations can be advanced. Following the first one, hydroxyl groups behave as ligands in the coordination sphere of Cr(II), like in the structure represented in Scheme 8, and

Scheme 8. Interaction between a Cr(II) and an Isolated Adjacent Silanol

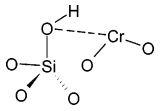

hence shield their potential adsorptive activity. Only their elimination by dehydroxylation allows the formation of additional coordination vacancy, allowing Cr(II) species to adsorb a second CO molecule.

The second explanation is that the hydroxyls are not directly involved at all in the coordination sphere of Cr(II) and that simply their presence merely decreases the surface strain.[6] On hydroxylated surfaces, a high fraction of Cr(II) is buried into the surface layers (fully coordinated by the oxygen of adjacent Si−O−Si bridges) and is not available for adsorption of ligands. Dehydroxylation is accompanied by surface rearrangement and appearance of strain (vide supra section 2.2). Some of the buried (fully coordinated) chromium sites are forced to emerge on the surface in order to decrease the surface strain, according with the Scheme 9, thus becoming

Scheme 9. Effect of Surface Dehydroxylation on the Local Environment of Isolated Cr(II) Species

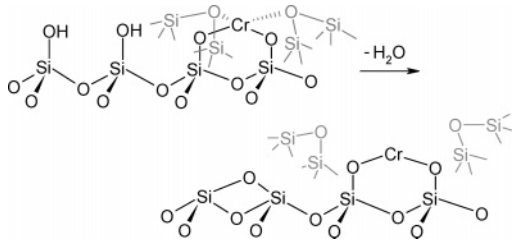

coordinatively more unsaturated and free for the adsorption of ligands. The two explanations are not mutually exclusive, and the two effects could be simultaneously present. Whatever the explanation, it is ascertained that upon a prolonged activation procedure, (i) a greater number of chromium sites, previously hampered by OH groups, become active in adsorbing CO molecules, and this justifies the increase of the intensity of all of the components of the triplet; and (ii) the fraction of Cr(II) sites characterized by a more coordinatively unsaturated environment increases, so explaining the increase of the relative intensity of the 2184−2178 cm^{-1} doublet, formed on Cr_A^{II} site.

The beneficial effect of the increase of the activation temperature on the number of less coordinated chromium sites reaches a maximum and then turns into the opposite effect. In fact, by heating the reduced sample at high temperature in vacuo, a dramatic reduction of the triplet intensity is observed (see Figure 15b,c). Although the intensity of all of the triplet is enormously depressed by the thermal treatment, the effect on A and B sites is not the same. In

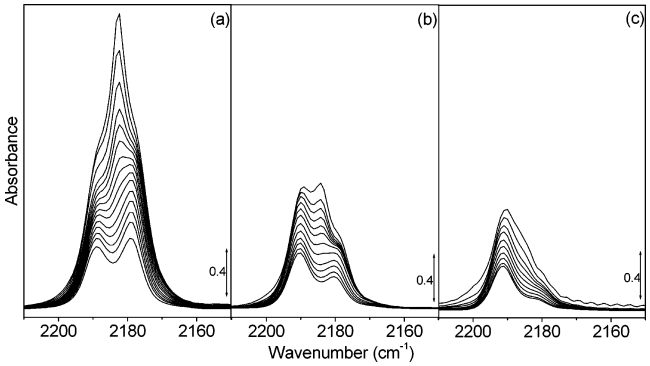

Figure 15. IR spectra of CO adsorbed at RT on a Cr(II)/SiO_2 (1.0 wt % Cr loading). Curves from top to bottom: effect of gradual lowering of the CO pressure. (a) Cr(II)/SiO_2 sample activated at 923 K and reduced in CO at 623 K; (b) same sample subsequently treated at 923 K in vacuo after reduction; and (c) same sample subsequently treated at 1023 K in vacuo after reduction. Unpublished spectra were obtained by reproducing the experimental procedure described in ref 146.

fact, the fraction of sites able to coordinate two CO molecules at RT (Cr_A^{II}) is preferentially decreased if compared to the standard case (Figure 15a), while Cr_B^{II} sites seem to be almost unaffected by the thermal treatment. Furthermore, it is worth noticing that little variations are present in the frequency values of all carbonyl bands, in the order of 1 cm^{-1}. These observations confirm the interpretation given in section 4.1.2, i.e., a thermal treatment at high temperature after reduction favors a complex rearrangement of the surface and is associated with restructuring of the most coordinatively unsaturated Cr(II) ions, to increase the crystal field stabilization with insertion of siloxane ligands and subsequent sinking into the silica surface. The overall number of the Cr_A^{II} sites able to coordinate two CO molecules is consequently specifically decreased.

A final comment on the experiments illustrated in Figures 14 and 15 can be summarized as follows. The silica surface undergoes complex transformations upon thermal treatments in the 723−923 K interval. The structure of anchored Cr(II) complexes reflects these transformations. After activation treatments in the 723−923 K interval, the concentration of the OH groups gradually decreases and the number of chromium centers able to coordinate probe molecules increases. Upon high temperature treatment after reduction, a sinking of the Cr(II) centers into the silica framework occurs, with subsequent loss of adsorption capacity. As discussed above (vide supra sections 3.1 and 3.2), the chromium centers can become available again by a new oxidation at 923 K followed by reduction at 623 K.

Ultraviolet photoreduction of Cr/SiO_2 in CO atmosphere is less efficient in reducing the supported chromium as is thermal reduction.[130] Short UV exposures produce a linear Cr^{4+}(CO) carbonyl species, which gives rise to a band at 2206 cm^{-1} and which is totally absent in the case of thermal reduction. Long UV exposures produce, together with the already discussed triplet (now at 2190, 2184, 2178 cm^{-1}) other two carbonyl bands at 2212 and 2099 cm^{-1}. The authors report the IR spectra at a CO equilibrium

pressure of 755 Torr and after evacuation at RT. The two additional bands are not stable upon evacuation at RT. The high frequency bands have been assigned by Kohler and Ekerdt[130] in terms of a *mer*-$Cr^{2+}(CO)_3$ species of C_{2v} symmetry, responsible for the bands at 2212 cm^{-1} [$(A_1)_1$, w], 2190 cm^{-1} [B_2, s], and 2178 cm^{-1} [$(A_1)_2$, s], and for a linear $Cr^{2+}(CO)$, responsible for the band at 2184 cm^{-1}. As far as the band at 2099 cm^{-1} is concerned, it has been assigned to a carbonyl bridging between two chromium centers. Notice that, following this interpretation, the bands of the common triplet have been assigned differently from those discussed so far.[118,123,124,146,200,201]

The interpretation of the 2212, 2190, and 2178 cm^{-1} bands in terms of the vibrational modes of a single species makes odd with the remarkable difference in the stability of the 2212 cm^{-1} band vs that of the 2190 and 2178 cm^{-1} ones upon RT evacuation. Moreover, the 2212 cm^{-1} band has never been observed on low Cr loading samples (up to 1 wt %) upon thermal reduction in CO, while it appears, together with UV−vis features of Cr_2O_3 oxide,[115] when higher Cr-loaded samples are considered. An alternative assignment of the 2212 cm^{-1} band could be consequently in terms of a Cr(III)···CO complex. As for the band at 2099 cm^{-1}, it is observed at high CO equilibrium pressure or at low adsorption temperature also on thermally reduced Cr/SiO_2 samples. An alternative interpretation will be reported in the next section.

4.2.1.2. Interaction of CO at 77 K. If a quite unifying picture has been achieved in the interpretation of the CO RT triplet, different views are still present concerning the low temperature spectra of CO on $Cr(II)/SiO_2$. The remarkable sequence of spectra illustrated in Figure 16a−c corresponds to increasing coverages of CO adsorbed at 77 K on $Cr(II)/SiO_2$ after thermal treatments at increasing temperature. This sequence is the low temperature counterpart of that shown in Figure 15. These characteristic and complex spectra are greatly independent upon the silica used to support the chromium phase (pirogenic silica, aerogel, xerogel). For this reason, they can be considered as a highly reproducible fingerprint of the system. Focusing the attention on the standard case (Figure 16a), the IR bands can be clearly divided into two groups, depending on the CO equilibrium pressure. At very low equilibrium pressure (P_{CO} < 50 Torr, bottom curve in Figure 16a) only the RT triplet is present. Upon increasing the pressure, a second series of intense bands in the 2140−2050 cm^{-1} region (i.e., at $\tilde{\nu}$ lower than $\tilde{\nu}_{CO}$ gas) grows up at the expenses of the bands formed in the first phase. This behavior, together with the multiplicity of peaks, suggests that the bands in the 2140−2050 cm^{-1} interval belong to polycarbonylic species formed by the addition of further CO molecules to the species responsible for the triplet at 2191−2179 cm^{-1}. The first band appears at 2100 cm^{-1} with a FWHM close to that of the high temperature triplet. As previously anticipated, this band can be observed also on RT spectra for CO pressures higher than 50 Torr. This band is immediately followed by a second component at 2045 cm^{-1}, which initially grows in the same way. Then two other components follow, centered at 2120 and 2035 cm^{-1}, the last one being initially only a shoulder of the 2045 cm^{-1} peak. Upon increasing the CO pressure, the intensity of the 2120, 2100, and 2035 cm^{-1} peaks increases, while the 2045 cm^{-1} component remains quite unaltered. Finally, it must be noticed that at high CO pressure a new component appears at high frequencies, at about 2200 cm^{-1}. Although this last band is growing, it cannot be assigned to multicarbonylic species, according to refs 146 and 209 (on the basis of the considerations reviewed in the following).

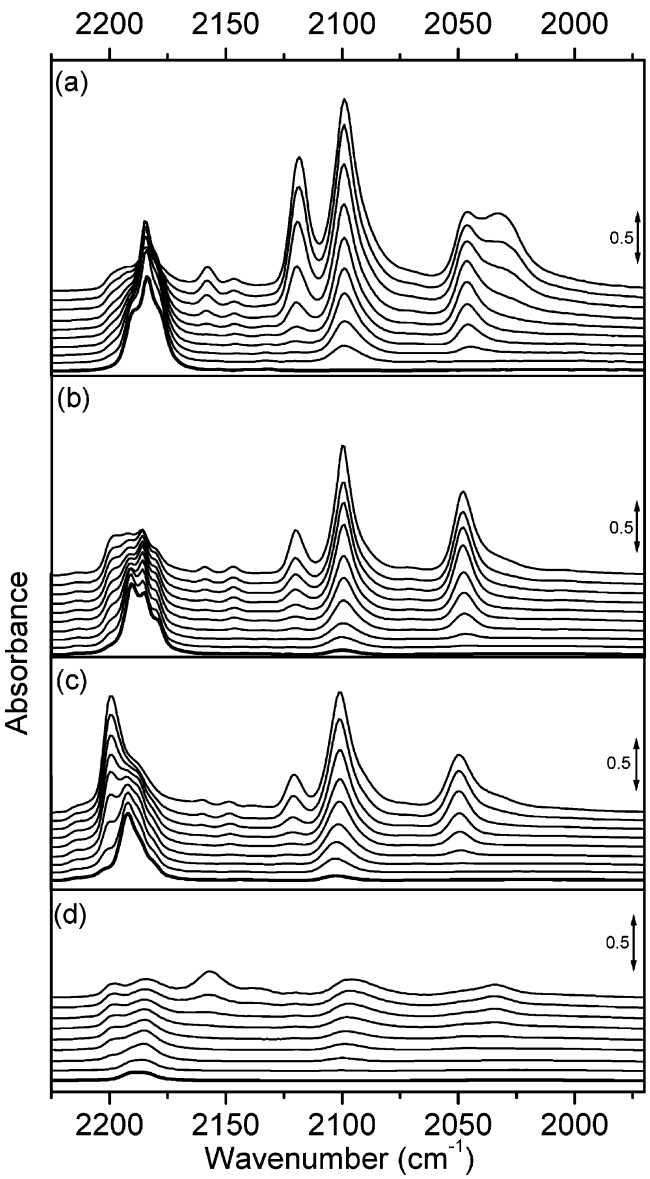

Figure 16. Effect of gradual lowering of the CO pressure (curves from top to bottom) on IR spectra of CO adsorbed at 77 K on a $Cr(II)/SiO_2$ sample (1.0 wt % Cr loading). (a) $Cr(II)/SiO_2$ sample activated at 923 K and reduced in CO at 623 K; (b) same sample subsequently heated at 923 K in vacuo after reduction; (c) same sample subsequently heated at 1023 K in vacuo after reduction; and (d) $Cr(II)/SiO_2$ sample activated at 773 K and reduced in CO at 623 K. Unpublished spectra were obtained by reproducing the experimental procedure described in ref 146.

The IR spectra obtained at 77 K have already been thoroughly discussed in the past, and their assign-

ment has caused an interesting controversy in the specialized literature. In particular, the most crucial question associated with the whole set of low frequency bands is why the addition of further CO ligands causes such a dramatic shift toward lower frequencies and an equally dramatic increase of the integrated intensity. About the attempts to answer this problem, we have already mentioned the works of Zecchina et al.[94,117,118,144] and of Rebenstorf et al.,[119−122,145] which proposed two radically different interpretations of the carbonyl bands at 77 K for thermally reduced Cr/SiO_2. As the same double interpretation is still persisting also in the more recent literature,[191] we think that it is useful to summarize the recent works by dividing them in terms of the basic interpretations mentioned before, i.e, (i) interpretation based on the formation of bridged species on Cr(II)−Cr(II) pairs and (ii) interpretation based on multiple CO addition on isolated Cr(II) sites. It is useful to remember that isolated centers derive from CO reduction of surface monochromates, while paired Cr(II)−Cr(II) centers mainly derive from reduction of dichromate precursors. It is so clear that a correct interpretation of the spectra of CO adsorbed on the reduced Cr/SiO_2 system could also give us information about the oxidized precursors, thus offering a complementary picture to that obtained from DRS UV−vis spectroscopy (vide supra section 4.1.1).

4.2.1.2.1. Interpretation Based on Pairwise Distribution of Cr(II). Following the first interpretation,[119−122,145] the formation of low frequency bands is simply described as due to CO bridges formation on adjacent chromium centers, as schematically depicted in Scheme 10. Bridge interactions are indeed

Scheme 10. Schematic Picture of CO Bridged Addition to Cr(II)−Cr(II) Pairs[119−122,145]

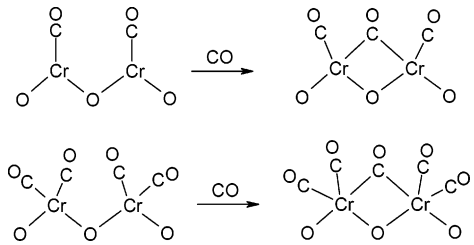

known from the spectroscopy of cluster carbonyls to lower the frequency of the involved CO groups.[204,208] The four low frequency bands can be divided in two pairs (2100−2045 and 2120−2033 cm^{-1}) according to the different evolution upon increasing CO pressure. This implies that two distinct families of Cr(II)−Cr(II) pairs exist. These families would not only differ for the number of ligands but also for the Cr(II)−Cr(II) distance.

This hypothesis is intrinsically weak for several reasons. The main one is that the low frequency bands are always the same independently upon the original chromium concentration. This result is in conflict with the hypothesis of pairwise distribution of the Cr(II) sites, because we know that the concentration of the dichromate precursors tends to zero when the Cr(II) concentration decreases (while conversely the relative intensity of the low frequency bands remains substantially unaltered with respect to the fingerprint triplet). The second weakness resides in the intensity of the low frequency bands. In fact, it is well-known that the absorption coefficient of CO bridged species is approximately one-fifth of the linear ones.[204,208] This would imply that in the high coverage spectra reported in Figure 16a (top curve) more than 90% of the CO molecules are in bridged configuration. Furthermore, as the adsorption enthalpy of a bridged CO is usually rather high, we should expect that bridged species appear since low CO coverages, contrarily to the experimental observation. Another problem is related to the fact that it is difficult to accept that only two rather well-defined Cr(II)−Cr(II) distances (corresponding to the 2100−2045 and 2120−2033 cm^{-1} peaks) are present on an amorphous material like SiO_2. Finally, the last element of weakness is that related to the partial transformation of the RT triplet (due to terminal species, as discussed before) into the low frequency bands, a fact that cannot be easily accounted for by the formation of bridged species.

4.2.1.2.2. Interpretation Based on Multiple CO Addition to Isolated Cr(II) Sites. This interpretation[118,123,124,146,209] is based on the hypothesis that at low temperature/high pressure we have further insertion of CO into the coordination sphere of isolated Cr(II) ions, assumed as the dominant species, following the Scheme 11. Following this hypothesis,

Scheme 11. Schematic Picture of CO Addition to Isolated Cr(II) Species, According to the Multiple CO Addition Model[118,123,124,146,209]

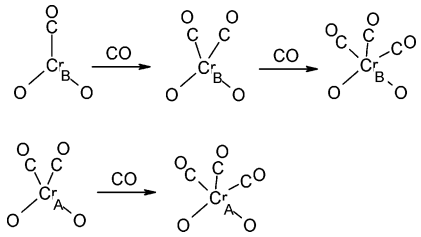

the added CO molecules have a character of linear species and no bridged carbonyls are involved. Three different types of isolated mononuclear Cr(II) ions have been proposed; the assignments for IR bands are shown in Scheme 12. The isolated Cr(II) ions, labeled A, B, and C, are characterized by an increasing number of oxygen ligands. The Cr_A^{II} and Cr_B^{II} sites are those responsible for the RT triplet, as discussed above. Cr_C^{II} is almost inactive to CO at RT. The Cr_A^{II} and Cr_B^{II} families are able to coordinate further CO ligands at low temperature/high pressure, suggesting that the involved Cr_A^{II} and Cr_B^{II} species are both highly coordinatively unsaturated (although at different degrees). The weak shoulder at ∼2200 cm^{-1} (observable only at high CO pressure) indicates that at this stage CO ligands are also filling a third family of unsaturated and weaker sites (Cr_C^{II} family). The high stretching frequency has to be interpreted in terms of increased contribution of the polarization forces (which are long-range forces) with respect to chemical forces (important only at appropriate bonding distances). This suggests that the CO ligand cannot fully approach the Cr_C^{II} center, because of

Scheme 12. Schematic Assignment of the Carbonyl Bands as a Function of the CO Pressure and/or Adsorption Temperature, According to the Multiple CO Addition Model[118,123,124,146,209]

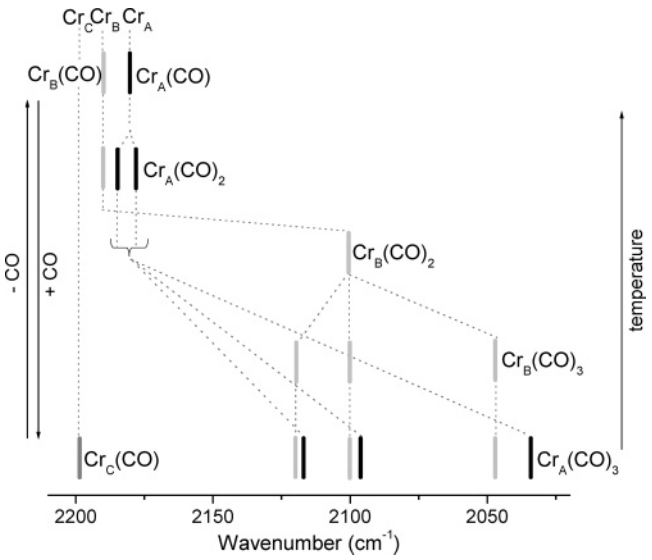

some steric hindrance,[117,118,144,146] or that the ionic charge on chromium center is largest on Cr_C^{II} sites. The two hypotheses are not mutually exclusive.

This interpretation overcomes some of the weakness of the pairwise distribution model mentioned before, because (i) the intensity decrement of the original triplet is well-explained; (ii) as no bridging species are present, the considerations about the intrinsic low intensity of the stretching mode of bridging CO do not hold; and (iii) as the Cr(II)−Cr(II) pairs are not playing a role, the invariant character of the low frequency band upon the chromium concentration is well-understood.

This interpretation is however facing a new problem. If the low frequency bands are not due to bridging species, which is the explanation of the distinct downward shift of the $\tilde{\nu}_{CO}$ bands upon CO addition and of their strong intensity as well? Authors of quoted works[118,123,124,146,209] tried to overcome this point by explaining that upon CO ligand insertion into the coordination sphere of Cr(II), the resulting Cr(II)···CO bonds have an increased d-π character (a fact that explains the simultaneous lowering of the $\tilde{\nu}_{CO}$ and the increment of the specific intensity). Indeed, metal carbonyls of the type $M(CO)_nX_2$ (M = Cr, Fe, Mn, Ni, W, etc. and X = Br, Cl, etc.), characterized by substantial d-π back-donation, have bands in the same frequency range and with similar intensity patterns.[204] However, as an increase of the d-π interaction must be associated also with an increase of the strength of the Cr···CO bond, this seems to be in apparent contradiction with the fact that these species are easily reversible, even at 77 K. Note that this is not the only case of carbonyl complexes characterized by low $\tilde{\nu}$(CO) and low adsorption enthalpy.[198,199] Zecchina et al.[146] believed to have solved this apparent contradiction by abandoning the hypothesis of a surface process depicted as a simple ligand insertion into a preexisting coordinative vacancies. Conversely, they thought that the real process is better explained as a ligand displacement reaction of the type reported in eq 3

$$(SiO)_2Cr^{II}L_{n,n-1}(CO)_{1,2} \xrightarrow{CO} (SiO)_2Cr^{II}L_{n-1,n-2}(CO)_3 + 1{,}2L \quad (3)$$

where the insertion of the additional CO is associated with the simultaneous expulsion of a weakly bonded surface ligand L (presumably, the bridging oxygen of the siloxane groups).[189] In other words, the adsorption of CO is accompanied by local relaxation, a fact that is not unknown in surface science. On this basis, it is evident that although the Cr(II)···CO bond is strong, the CO removal is easy. In fact, the total enthalpy of the process can be small, because the positive enthalpic contribution of the formation of strong CO bonds is partially canceled by the negative contribution of the displacement of the L ligands [ensuring crystal field stabilization to the naked Cr(II) sites].

Summarizing, at low coverage, CO molecules probe a surface where no Cr(II) sites exhibit an actual high coordinative unsaturation, owing to the presence of weak ligands L in their coordination sphere. As a result, the geometry of the carbonyl adducts cannot be optimized resulting in a nonefficient d-π contribution to the overall interaction, explaining the positive $\Delta\tilde{\nu}$(CO) shifts observed in such conditions (RT triplet). Upon increasing the coverage, either by increasing the equilibrium pressure or by decreasing the adsorption temperature, the insertion of additional CO ligands into a preexisting carbonyl adduct occurs via displacements of weak ligands L, eq 3. This has an energetic cost that explains while the overall adsorption enthalpy of the additional CO insertion is low, justifying the high reversibility of polycarbonyl species. On the other hand, once the weak ligands L have been displaced, the geometry of the resulting polycarbonyl species can be optimized resulting in the activation of the d-π contribution to the Cr(II)···CO interaction and explaining both the negative $\Delta\tilde{\nu}$(CO) shifts and the high intensities of the corresponding IR bands. Note that the ligand displacement occurs with the insertion of the third (second) CO molecule on Cr_A^{II} (Cr_B^{II}) sites, being not observed (in the pressure/temperature ranges investigated) for the Cr_C^{II} sites.

This explanation is in line with the structure of the silica surface and of anchored chromium. Additional proofs arise from the discussion of the effect of high temperature treatments on the low frequency bands. Figure 16b, which is the low temperature counterpart of Figure 15b, reports the IR spectra at 77 K of increasing coverages of CO on a Cr/SiO_2 system heated at 923 K in vacuo after reduction. Upon increasing CO pressure, the RT triplet is consumed less than in the standard case, suggesting that a lower fraction of chromium sites is able to add further CO molecules. Also the intensity ratio of the low frequency bands is different from the situation previously discussed. In particular, we notice the almost total disappearance of the lower band at 2035 cm^{-1} and a strong decreasing of the intensity of the 2120 cm^{-1} component. A similar and more evident behavior is shown also by the sample treated at 1023 K

after reduction (Figure 16c). The band at about 2200 cm^{-1}, previously assigned to a monocarbonylic species on a Cr_C^{II} site, gains progressive intensity with respect to the standard case (Figure 16a). These results confirm that vacuum thermal treatments at high temperatures convert Cr_A prevalently into Cr_C species and partially into Cr_B species, thus favoring the partial penetration of the ions into the silica framework. This conclusion is in agreement with the UV−vis DRS results shown in Figure 11b as compared to those shown in Figures 11a and 10.

The comparison between Figure 16a−c, together with the considerations outlined before about the adsorption of CO at RT, gives us the opportunity to advance an assignment of the CO bands in the 2140−2050 cm^{-1} region, as reported in Scheme 12. Almost three families of chromium sites able to coordinate CO molecules can be found on the Phillips catalyst, whose distribution is a function of the thermal history of the sample. One of them (Cr_C^{II}) is particularly coordinated and is able to form monocarbonyl species only at low temperature. The other two (Cr_A^{II} and Cr_B^{II}) are more coordinatively unsaturated and thus are able to coordinate up to three CO molecules at low temperature/high pressure, giving rise to tricarbonyl species characterized by very similar vibrational manifestations. Nevertheless, these two chromium sites show a different propensity to form tricarbonyl species. Cr_B^{II} sites, which at RT form monocarbonyl species only (band at 2191 cm^{-1}), add very fast a second and a third CO molecule upon increasing the CO pressure. The band at 2100 cm^{-1}, which is the first to grow decreasing the temperature (and which is observed also at RT when a high CO pressure is dosed), may be interpreted as the vibrational feature of a dicarbonyl species on Cr_B^{II} sites, where the partner band is weak and is buried in the residual room triplet or where the partner band is IR inactive (because the CO angle between the CO groups is approaching 180°).[144,204,207] In both cases, it is clear that Cr_B^{II} sites are the first to form carbonyl complexes with significant d-π character. The formation of the tricarbonyl on Cr_B^{II} sites follows very rapidly, giving bands at 2120, 2100, and 2048 cm^{-1}. Conversely, the addition of a third CO molecule on Cr_A^{II} sites is more difficult, even if they are able to coordinate two CO molecules at RT. This is testified by the band at 2035 cm^{-1}, which is the last to grow up. These experimental observations have been considered by Zecchina et al.[146,209] as a further confirmation that the CO adsorption cannot be explained as a simple ligand insertion into a preexisting coordination vacancy but requires the intervention of ligand displacement; see eq 3. Notwithstanding the fact that Cr_A^{II} sites possess two coordination vacancies available at RT, the displacement of a ligand to give a third vacancy is more difficult than for Cr_B^{II} sites.

Finally, Figure 16d shows the effect of a low activation temperature on the Cr/SiO_2 system, confirming the interpretation given to the spectra reported in Figure 16a−c. In fact, by comparing these spectra with the previous ones (see Figure 16a−c), we notice a dramatic decrease in the intensity over the whole CO absorption range. Now two bands at 2156 and 2137 cm^{-1}, present even in the previous spectra but with a not comparable intensity, dominate the entire CO region. These two bands are associated with CO hydrogen-bonded to silanols, and this is confirmed by the consumption of the OH stretching band at ~3750 cm^{-1} and by the simultaneous growth of a band at ~3660 cm^{-1} due to the CO-perturbed OH vibration (not shown for brevity)[28,146,210] and to CO physically adsorbed on the silica surface, respectively.[146,210−215] The RT triplet has lost its intensity and is quite broad and not well-resolved. Upon increasing the CO pressure, we observe the growth of a band at ~2200 cm^{-1} [previously assigned to a Cr_C^{II}(CO) species] and the appearance of two broad little bands in the low frequencies region, at ~2095 and ~2035 cm^{-1}. These results confirm what was anticipated previously (vide supra 4.2.1.1), i.e., a low temperature activation procedure does not allow chromium ions to reach a high coordinative unsaturation, both for a direct interference by OH groups (see Scheme 8) and for a less strained environment (see Scheme 9). It is important to remember that a high unsaturation in the coordination sphere is the first condition to obtain a high polymerization activity, and this explains why there is a precise relationship between the activity of the catalyst and its calcining temperature, as we will see in the following (vide infra section 5.1.1.3).

Also the addition of doping atoms onto the Cr(II)/SiO_2 surface influences the aspect of the IR spectra of CO adsorbed at low temperature. Rebenstrorf[120,170,216] reported a systematic study on the influence of fluorine, titanium, boron, and alkali metals on the IR spectra of CO at low temperatures. Without entering in the spectra interpretation (already criticized above, vide supra section 4.2.1.2.1), the experimental evidence resulting from these works is that the introduction of doping atoms strongly decreased the bonding ability of chromium species toward CO.

4.2.1.3. Theoretical Calculations. Despite the enormous amount of experimental works on chromium carbonyls published so far, very few works appeared until now concerning theoretical calculation of the vibrational properties of such species. This lack is fundamentally due to two main reasons. First, the level of complexity needed to approach the bare silica surface with theoretical methods has already been underlined in section 2. Cr anchoring represents a significant further increase in system complexity. Moreover the amorphous nature of the support prevents the direct use of periodic codes and makes the adoption of cluster models compulsory. This introduces a relevant degree of subjectivity in the choice of the clusters mimicking the chromium sites environment. The second reason concerns the computational problems that one has to face when dealing with clusters containing transition metal ions. The bonds between CO and transition metals pose a challenge to quantum mechanical methods.[217] Qualitatively, the metal−CO bond is usually described in terms of an electrostatic contribution (Stark effect), a ligand-to-metal σ donation and a metal-to-ligand π back-donation (vide supra), with 5σ

and 2π (also denoted as π^*) constituting CO's donating and accepting MOs, respectively. A quantitative description needs to include all of these aspects, which is hard to accomplish. Espelid and Børve[191] have recently explored the structure, stability, and vibrational properties of carbonyls formed at low valent chromium bound to silica by means of suitably chosen cluster models and DFT.[218] These models, although reasonable, do not take into consideration neither the complexity of the silica surface (section 2) nor the structural situations of anchored Cr(II) discussed in sections 4.1.2 and 4.2.1.2; hence, they must be considered as a useful basis for discussion. They found that the pseudo-tetrahedral mononuclear Cr(II) site (see Figure 13) is characterized by the highest coordination energy and is able to adsorb two molecules of CO even at low pressure.[191]

Concerning the vibrational properties of the various surface sites, the authors were not able to reproduce the substantial blue shift of the experimental RT triplet with none of the considered model structures and Hamiltonians.[191] However, the authors provided an interpretation of the IR spectrum of CO adsorption on the $Cr(II)/SiO_2$ system on the basis of the frequency shift of the carbonyl bands, one with respect to each others. They concluded that the RT triplet may be explained as the manifestation of a dicarbonyl species on a pseudo-tetrahedral mononuclear Cr(II) site, together with a monocarbonyl species formed at a similar site with a nondisplaceable oxygen donor. This interpretation is consistent with that presented above (vide supra section 4.2.1.1). They explained the low temperature evolution of the CO spectra in terms of terminal dicarbonyl species and tricarbonyl species with one bridging CO, of dinuclear Cr(II) complexes. This interpretation is similar to that based on pairwise distribution of Cr(II) presented above (vide supra section 4.2.1.2.1)[119−122,145] and disagree with the interpretation given by Zecchina et al.[118,123,124,146,209] (vide supra section 4.2.1.2.2).

It is however difficult to consider the simulation of chromium carbonyls on the silica surface a closed question of quantum chemistry. This statement is suggested by the non-negligible disagreement between experimental and calculated C−O stretching shifts [$\Delta\tilde{\nu}$(CO), defined as the difference between the $\tilde{\nu}_{CO}$ of the adsorbed molecule and that of the free one], the former being a blue shift in the 48−37 cm^{-1} range for the monocarbonyl complexes, [118,120−124,146,209] where the latter[191] predicts a red shift in the −45 to −49 cm^{-1} interval or a much smaller blue shift, in the 5−15 cm^{-1} interval, depending on the adopted level of theory: a pure generalized gradient-corrected DFT method[218] (DFT1 in that work) or hybrid B3-LYP[219−221] (DFT2 in that work) method, respectively.

Limitation on the accuracy of ab initio values computed with a cluster approach can arise from several, eventually coexisting factors: (i) cluster construction, (ii) cluster size, (iii) cluster termination, (iv) adopted basis sets, (v) adopted Hamiltonian, and (vi) inability to properly consider long-range effects. Point (i) represents a serious problem for the simulation of amorphous systems as the choice of the cluster is not straightforward. To overcome this problem, Espelid and Børve have tried an impressive large number of clusters in order to reproduce the population of local environments of Cr on the silica surface.[191] Particular attention has been devoted to study the effect of a modification of the α_{OCrO} angle, in the 116−180° range (vide supra section 4.1.3, Figure 13, and Scheme 7). It is however a matter of fact that a systematic study on the cluster size effect, point (ii), is still missing. This implies that second and higher shell contributions are neglected; a feature that prevents to take into account the effects of weak ligands such as neighboring siloxane bridges or silanol groups; see eq 3. Moreover, simulated clusters are not able to take into account the presence of local strain at the silica surface, due to siloxane bridges, as deeply discussed in sections 2.2 and 4.2.1.2. Also cluster terminations can play a role, point (iii). The here reviewed ab initio $\Delta\tilde{\nu}$(CO) values have been obtained with −F terminations.[191] This could seem to be strange, on a chemical ground, as no fluorine species are present on the real system. This choice has been justified by the authors on the basis of the analogy with the difluorosilanol molecule (two terminal F), which describe the surface acidity of the silanol groups at the silica surface better than the silanol molecule (two terminal H).[222] The basic electronic properties of this model were validated by comparison to a much larger cluster in which the anchoring site was represented by two singly deprotonated hydroxosilasesquioxane clusters.[223] It is however evident that the high electronegativity of this termination causes an electron deficiency on the neighboring O atoms, which, in turn, subtracts a further charge to the Cr. This results in an increase of the electric field generated by the cation and in a depression of its d-π back-donation ability: both features playing a synergic role in increasing the computed $\Delta\tilde{\nu}$(CO). If more usual terminations, like −H or −OH, are used, important red shifts are obtained (in the −32 to −17 cm^{-1} range) at the B3-LYP[219−221] level of theory.[224,225] Coming to point (iv), a systematic study on the evolutions of the computed values vs improved basis sets is still missing. It is however worth noticing that high quality basis sets have been employed by Espelid and Børve.[191] The Hamiltonian, point (v), has been shown to be a crucial factor as, on the same clusters, the switch from a pure generalized gradient-corrected DFT method to the hybrid B3-LYP method resulted in a switch from red to blue shifts for $\Delta\tilde{\nu}$(CO).[191] The problems faced in the attempt to simulate the $\Delta\tilde{\nu}$(CO) for silica supported Cr carbonyls seem even more serious when it is noticed that the B3-LYP[219−221] level of theory is able to correctly reproduce the sign of the frequency shift for a large numbers of Cr carbonyls hosted in cryogenic matrices.[226,227] Of course, we are dealing here with a much easier computational problem as the choice of the clusters is perfectly defined. Finally, long-range interactions, point (vi), that in principle require a periodical approach to be perfectly reproduced, can represent a serious problem for amorphous systems, for which the absence of long-range order makes the use of such computational approaches extremely difficult.

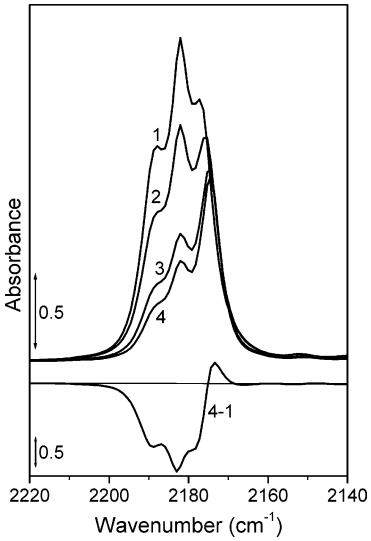

Figure 17. IR spectra of ethylene dosage at RT on a Cr(II)/SiO_2 sample (1.0 wt % Cr loading) activated at 923 K, reduced in CO at 623 K, and precontacted with 30 Torr of CO. Curve 1, spectrum before ethylene dosage; curves 2−4, increasing partial pressures of ethylene. In the bottom, the difference between curve 4 and curve 1 is reported, showing the depletion of the CO RT triplet and the appearance of the band at 2174 cm^{-1}, due to the formation of a CO/C_2H_4 mixed complex. Unpublished spectra were obtained by reproducing the experimental procedure described in ref 123.

4.2.1.4. Interaction between CO and Ethylene. Finally, to complete the picture about the interaction of CO with Cr/Silica, the interaction between CO and ethylene at RT is illustrated in Figure 17 as an example of formation of mixed complex. The starting spectrum (curve 1) is the well-known CO triplet at RT. When the partial pressure of ethylene is gradually increased into the IR cell containing CO (curves 2−4), we observe the depletion of the peaks of the Cr(II)···$(CO)_n$ complexes and the simultaneous formation of a new carbonyl band at 2174 cm^{-1} (more evident in the difference spectrum curve 4−curve 1). The given interpretation is as follows.[123,209] Cr_B^{II} ions simply undergo a ligand displacement, following reaction 4:

$$Cr_B(CO) + C_2H_4 \rightarrow Cr_B(C_2H_4) + CO \qquad (4)$$

and this explains the rapid decrease of the CO band at 2191 cm^{-1}. $Cr_A^{II}(CO)_2$ first forms a mixed complex, responsible for a CO stretching vibration at 2174 cm^{-1}, following reaction 5:

$$Cr_A(CO)_2 + C_2H_4 \rightarrow Cr_A(CO)(C_2H_4) + CO \quad (5)$$

At a second stage (not reported in Figure 17), the mixed complex undergoes a ligand displacement and a diolefin complex $Cr_A^{II}(C_2H_4)_2$ is formed, following reaction 6:

$$Cr_A(CO)(C_2H_4) + C_2H_4 \rightarrow Cr_A(C_2H_4)_2 + CO \quad (6)$$

The rapid decrease in the 2174 cm^{-1} intensity monitors the latter process; spectra were not reported here in Figure 17. There is however a fraction of $Cr_A(CO)$-C_2H_4 complex, which is reluctant to undergo CO displacement, as it is evident in the spectra reorted by Ghiotti et al.[123] from the permanence of the band at 2174 cm^{-1}. As we will describe in section 5.3.1, CO acts as a strong poison of the ethylene polymerization activity.

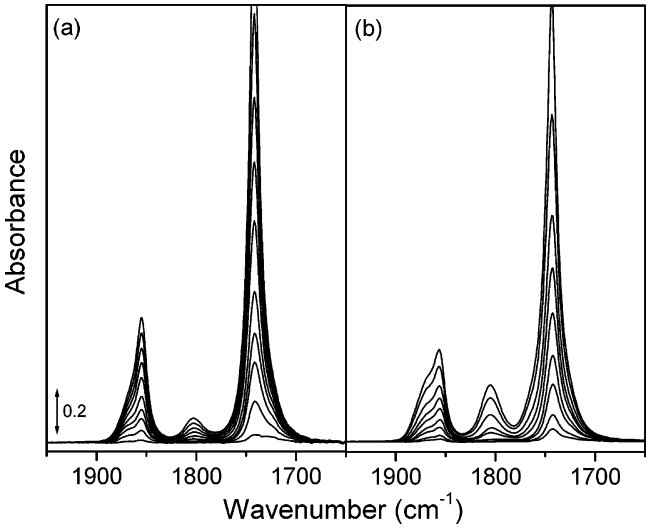

Figure 18. IR spectra of the adsorption at RT of small doses of NO on (a) a Cr(II)/SiO_2 sample (0.5 wt % Cr loading) activated at 923 K, reduced in CO at 623 K, and on (b) the same sample subsequently heated at 923 K in vacuo. Unpublished spectra were obtained by reproducing the experimental procedure described in ref 187.

4.2.2. Interaction of NO

The Cr(II)···NO link can be considered in terms of a donation from the lone pair of the NO^+ ligands together with a synergic back-donation from occupied metal d orbitals to the unoccupied π^* orbitals of NO^+. Depending on the coordinative unsaturation of the adsorbing sites, mono- or dinitrosyl complexes can be formed, the former characterized by a single $\tilde{\nu}_{NO}$, the latter by a doublet due to the in-phase and out-of-phase stretching motions of the two N−O stretching.[146,178,187,228] In some cases, nitrosyl complexes of higher nuclearity can be formed.[175,229]

The high coordinative unsaturation of Cr(II) centers in the reduced Cr/SiO_2 system is further confirmed by the interaction with NO, as reported in Figure 18. At RT, the spectra are characterized by three main peaks. The dominant 1856 and 1743 cm^{-1} peaks, evolving in a parallel way upon increasing NO pressure, have been associated by Zecchina et al.[118,144,146,187] with dinitrosylic species formed on highly coordinatively unsaturated Cr(II) sites. As a single doublet is observed, the authors concluded that, unlike CO, NO does not differentiate the two families of Cr_A^{II} and Cr_B^{II} sites. The stability of the dinitrosyl complexes was suggested to be due to the cooperative effect between the two unpaired electrons, which is responsible for the formation of a MO delocalized over the whole complex. The formation of a strong bond between NO and adsorbing centers is consistent with the irreversible nature of the NO species at RT, as a heating at 573 K in vacuo is required to remove the 1856−1743 cm^{-1} bands. The high stability of the dinitrosylic complexes also explains why the Cr(II) + 2NO → Cr(II)···$(NO)_2$

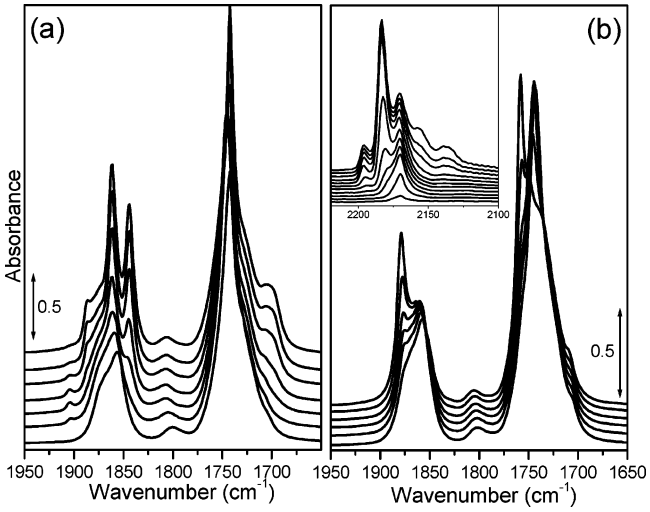

Figure 19. (a) IR spectra of NO adsorbed at 77 K on a $Cr(II)/SiO_2$ sample (0.5 wt % Cr loading) activated at 923 K and reduced in CO at 623 K. Curves from bottom to top: effect of gradual lowering of the temperature from RT to 77 K. (b) NO/CO interaction on the same sample. Bottom curve: pure NO at RT. Successive curves from bottom to top: effect of dosing increasing amounts of CO at 77 K. In the inset: evolution of the spectra in the CO stretching region during the same experiment. Unpublished spectra were obtained by reproducing the experimental procedure described in ref 146.

equilibrium is totally displaced to the right at RT, preventing the observation of the intermediate Cr(II)···(NO) within the time and pressures sampling of the reported experiment. This fact is not unusual for nitrosylic adducts formed on surface transition metal ions.[228]

The coordination of a single NO molecule appears to be only possible when a single coordination vacancy is present. The peak around 1810 cm^{-1} has been assigned to mononitrosylic species formed on C type families.[118,144,146,187] This band is not hindered by oxygen preadsorption at RT, meaning that the involved chromium ions do not react with molecular oxygen at RT.

Figure 18b shows the effect of a thermal treatment at 923 K after reduction on the RT spectra of adsorbed NO. Upon thermal treatments at high temperature, we observe the growth of the relative intensity of the band related with the formation of mononitrosylic species on C type families (1810 cm^{-1}), at the expense of the 1743−1856 cm^{-1} pair, related to dinitrosylic species on Cr_A^{II} and Cr_B^{II} families. As already discussed in the case of CO adsorption (vide supra section 4.2.1), this spectroscopic evidence reflects a decrease of the number of more unsaturated chromium centers, favoring their partial penetration into the flexible silica framework.

Lowering the temperature to 77 K (see Figure 19a), a third NO ligand is inserted and a distorted trinitrosylic species with approximate C_{3v} symmetry is formed; this additional NO ligand is suggested to be distinctly different with respect to the others, which remain strongly coupled. The entrance of the third NO into the coordination sphere of Cr(II) is testified by the appearance of a new peak at 1845 cm^{-1} and by a shift toward high frequency of the modes of the two coupled NO (now at 1862 and 1745 cm^{-1}). Besides these manifestations, we observe also the formation of weak IR bands located at ∼1700, 1905, 1887, and 1875 cm^{-1}. These bands have been interpreted as due to the formation of a few types of tetranitrosylic species with two $NO^{\delta+}$ and $NO^{\delta-}$ (bent) species, as a consequence of the excess electron density accumulation at the chromium centers.[146,230,231]

It is important to stress that CO and NO give different and complementary information about the surface structure of Cr/SiO_2. In the case of CO, we have observed that the formation of polycarbonylic species is accompanied by an abrupt decrease of the CO stretching frequency. As discussed above, this has been interpreted by Zecchina et al.[118,123,124,146,209] in terms of an increased d-π contribution in the Cr−CO ligand and of a simultaneous decrease of the electrostatic interaction with the oxygens of adjacent siloxane bridges. Instead, in the case of NO, already after the first adsorption stage the dinitrosylic species show frequencies lower than that of NO gas, thus indicating a substantial d-π overlap. NO, being a stronger ligand than CO, immediately displaces the chromium centers from the silica surface, so that the final dinitrosylic complexes do not remember the starting situation (i.e., Cr_A^{II} and Cr_B^{II} sites give nearly identical species).

Similar results have been obtained dosing CO at 77 K after the formation of $Cr_{A,B}(NO)_2$ complexes, to form CO/NO mixed species; see Figure 19b. We can observe that the entrance of CO into the coordination sphere of the dinitrosylic complex shifts upward the NO frequencies (bands at 1879 and 1758 cm^{-1}), exactly as found for the entrance of the third weaker NO ligand. Simultaneously, in the CO region, a band at 2170 cm^{-1} appears, followed by the more intense 2183 cm^{-1} peak and by a less intense component at 2196 cm^{-1}.

4.3. Raman Spectroscopy

4.3.1. Standard Raman Studies

It is well-recognized that Raman spectroscopy successfully provides the surface structural information of the supported metal oxide catalysts because of its ability to discriminate between different metal oxide species that may simultaneously be present in such systems.[96,97,232−237] Wachs and co-workers[96,232−234] have proposed from Raman spectroscopic studies that the surface structures of supported metal oxides under ambient conditions, where the catalyst is covered by adsorbed water, resemble the metal oxide species in aqueous solution. Upon dehydration, not only desorption of adsorbed water takes place but decomposition of the aqueous metal oxide clusters also occurs, which results in the formation of dehydrated surface metal oxide species on the support surface. Therefore, the Raman spectra of supported metal oxides under dehydrated conditions differ strongly from those obtained under hydrated conditions.

Raman spectroscopy has been widely used to characterize the SiO_2-supported Cr(VI) oxide species, as a function of chromium loading and calcination

temperature, in air and in vacuo. The identification of Raman bands for these systems is partially hampered by the presence of a rising baseline due to luminescence from the silica support, which has been well-documented.[8,96,97,232] Wachs et al.[97,232] observed a number of $\tilde{\nu}$(Cr=O) bands in the 800−1000 cm^{-1} region. The Raman spectrum of hydrated Cr/SiO_2 is characterized by a single Raman band at 895 cm^{-1} at low chromium loadings, while increasing the chromium content, a complex series of bands appears at 380, 850, 900, and 960 cm^{-1}. The first band is assigned to dichromate species, while at increasing chromium loadings Raman spectra have been interpreted in terms of formation of surface polychromates species.

Hardcastle et al.[232] have shown that variation of calcination temperature dramatically changes the Raman spectrum of Cr/SiO_2, which is related to the dehydroxylation of SiO_2 at high temperatures (vide supra section 2.2). Only a single strong Raman band characteristic of the dehydrated surface chromium oxide species on the silica support was observed at 986 cm^{-1} (see Figure 20a). The assignment of this band can be made by considering the Raman and IR spectra of chromium oxide reference compounds. Table 2 summarizes the Raman and IR band positions of the most relevant reference compounds.[96,185,239] The Cr(VI) cation can be surrounded by four [CrO_4^{2+}-(aq)], three ($CsCrO_3Br$), two (CrO_2Cl_2, CrO_2Br_2), or one ($CrOF_4$) terminal oxygens.[185,240] The tetrahedrally coordinated chromium cation can also be dimeric [$(NH)_4Cr_2O_7$], trimeric ($K_2Cr_3O_{10}$), and tetrameric ($K_2Cr_4O_{13}$).[239] Finally, crystalline CrO_3 possesses a chain structure of CrO_4 tetrahedra with two terminal Cr=O bonds and two bridging Cr−O bonds for each Cr(VI) cation. From the comparison of the spectrum of Figure 20a with the data of Table 2, it is inferred that the position of the 986 cm^{-1} band is consistent with the symmetric stretching mode of a terminal CrO_2 unit (see, e.g., CrO_2Cl_2 and CrO_2Br_2). However, a dioxo structure (O=Cr=O) would give rise to a symmetric and an antisymmetric stretching mode, the former being more intense in the Raman and the latter strongly allowed in the IR spectrum.[241] Furthermore, the antisymmetric stretching vibrational mode should occur at a higher wavenumber than the symmetric one. The absence in the spectra reported in Figure 20a of a band attributable to the antisymmetric mode implies that, if present, this mode has a lower Raman intensity than the symmetric mode. Authors[96,234,242] affirm that the Raman active CrO_2 surface species should be isolated, since no strong Raman bands due to Cr−O−Cr or O−Cr−O (with both oxygen bridging to other two chromium cations) linkages are observed in the 820−880 cm^{-1} interval. This suggests that on a diluted sample, the surface chromium is present primarily as a monomeric species upon calcination and indicated that surface dimers, trimers, and tetramers are not stable on the silica support under conditions that cause surface dehydroxylation. It is however worth noticing that all conclusions based on the absence of expected Raman bands have to be considered with caution owing to the intrinsically poor signal/noise ratio of conventional experiments. Much more definitive conclusions will be reached in the new Raman spectra reported in the following section, where innovative experimental conditions have been adopted. Conversely, conventional experimental conditions al-

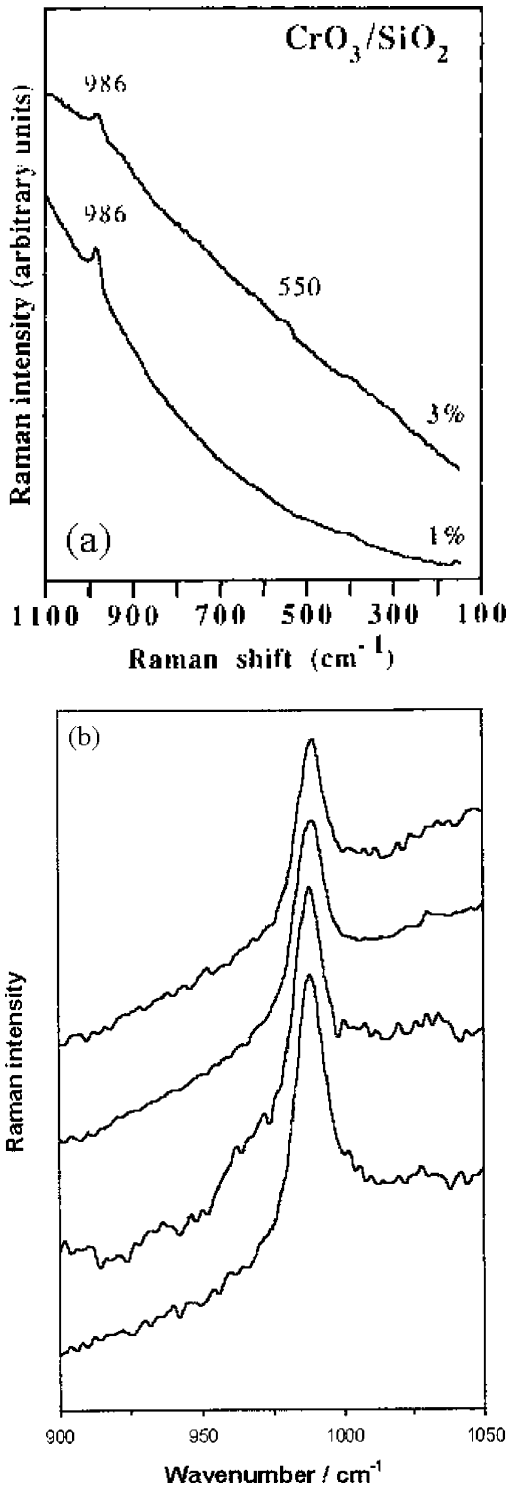

Figure 20. (a) Raman spectra of 1 and 3 wt % Cr(VI)/SiO_2 under dehydrated conditions, obtained by using a 514.5 nm laser line. Reprinted with permission from ref 96. Copyright 1993 Elsevier. (b) Raman spectra of 1 wt % Cr(VI)/SiO_2, obtained by using a 476.5 nm laser line, subjected to thermal treatments at increasing temperatures from bottom to top: 723, 823, 873, and 923 K. Note that the abscissa axis has been inverted in the two parts of the figure. Reproduced with permission from ref 238. Copyright 2003 Royal Society of Chemistry.

Table 2. Raman and IR Band Positions (in cm^{-1}) of Several Chromium Oxide Reference Compounds[a]

$CrOF_4$ [185]		CrO_2Cl_2[b] [185]		$CsCrO_3Br$[b] [185]		CrO_4^{2-} (aq) [185]	$(NH_4)_2Cr_2O_7$ [239]		$K_2Cr_3O_{10}$ [239]		$K_2Cr_4O_{13}$ [239]		CrO_3 [239]		
Raman	IR	Raman	IR	Raman	IR	Raman	Raman	IR	Raman	IR	Raman	IR	Raman	IR	assignment
1028	1028														$\tilde{\nu}$(CrO)
		994(4)	995(s)						980(2)	986(s) 972(s)	982(1)	982(vs) 976(vs)	1003(2)		$\tilde{\nu}_{as}(CrO_2)$
		984(10)	990(m)						961(3) 945(7)	960(s) 945(vs)	957(4)	945(vs)	975(9)	979(vs) 967(m) 945(m)	$\nu_s(CrO_2)$
				955(6) 947(4) 933(6)	954(vs) 942(vs)	884	946(3)	955(vs) 937(vs)	930(1)	934(vs)	936(1)				$\tilde{\nu}_{as}(CrO_4)$/ $\tilde{\nu}_{as}(CrO_3)$
				908(10)	906(ms)	847	904(10)	906(ms) 884(ms)	903(6)	900(s) 865(m)	906(2) 887(6) 872(5)	903(s) 879(s)			$\tilde{\nu}_s(CrO_4)$/ $\tilde{\nu}_s(CrO_3)$
							770(0)	795(s) 762(w)	761(5)	775(s) 740(s)		728(vs)		894(vs)	$\tilde{\nu}_{as}$(CrOCr)
									818(10)	827(s)	818(10)	819(s)			$\tilde{\nu}_s$(OCrO)
							560(2)	567(w)	562(1) 518(2)	552(ms) 516(m)	572(1) 518(2) 490(2)	570(m) 510(w) 480(m)	563(1) 498(10)	491(m)	$\tilde{\nu}_s$(CrOCr)
		357(5)	356(m)						378(2)	383(w) 372(w)	380(1)	390(w) 378(w)			$\delta(CrO_2)$
				369(4) 360(4) 242(3)	369(w) 360(w) 245(w) 237(w)	368 348	370(5)		358(1)	357(m)	332(1)	338(s) 315(w)			$\delta(CrO_4)$/ $\delta(CrO_3)$
													377(1)	376(w)	$\delta(CrO_2\|\|$ OCrO)
							217(4)						332(0.5)	318(w)	δ(OCrO)
		211(3)	211(w)		209(w) 204(w)				262(1) 230(2) 212(3)		235(2) 216(2)		284(3)	235(w)	$\delta(CrO_2\perp$ OCrO)

[a] For Raman modes, the number in brackets reports the relative intensities, while for IR modes the following nomenclature has been adopted: vs = very strong; s = strong; ms = medium strong; m = medium; w = weak; and vw = very weak. Reproduced with permission from ref 96. Copyright 1993 Elsevier. [b] Only the chromium oxide vibrations are shown.

lowed several authors to unequivocally single out the presence of polychromate species on the dehydrated alumina, titania, and zirconia surfaces.[96] Kim et al.[234] found that at loadings higher than about 3 wt % the formation of aggregated Cr_2O_3 phase occurs.

In a recent work,[238] Dines and Inglis have reported a Raman study on Cr(VI) oxide species supported on silica, silica−alumina, alumina, and titania surfaces as a function of chromium loading and calcination temperature, reporting experimental spectra characterized by a better signal-to-noise ratio (see Figure 20b and compare with Figure 20a) with respect to those obtained in the earlier works discussed above.[96,234,242] The Raman spectra of Cr/SiO_2 system obtained in controlled atmosphere by using an excitation λ of 476.5 nm show a single well-defined band at 990 cm^{-1}, which is analogous to the 986 cm^{-1} one observed in previous studies[96,234,242] (Figure 20a) and which has thus been attributed to the symmetric CrO stretching vibration associated with terminal Cr=O bonds of the surface chromium species. After having performed a baseline subtraction aimed to eliminate the fluorescence background, authors claimed the existence of a weak shoulder at the high energy tail of the main peak, centered at 1004 cm^{-1}, which has been attributed to the expected antisymmetric Cr=O stretch. The manipulation of the raw experimental data needed to appreciate this shoulder, as well as the borderline signal-to-noise ratio of the data around 1004 cm^{-1}, makes the claimed observation of the antisymmetric Cr=O stretching rather questionable. To support this weak experimental evidence, Dines and Inglis[238] complemented their work with ab initio calculations performed on a model, involving CrO_4 bridging across a siloxane group, yielded $\tilde{\nu}_s$(O=Cr=O) at 983 cm^{-1} and $\tilde{\nu}_{as}$(O=Cr=O) at 1010 cm^{-1}, respectively, in fair agreement with the experimental data. Other chromate vibrations, involving Cr−O stretching and O=Cr−O deformation, were predicted to be strongly mixed with vibrations of the support, giving rise to composite modes, which have a much lower Raman intensity.

The observed $\tilde{\nu}$(O=Cr=O) vibrations reveal which type of terminal chromium−oxygen bond the surface species possess or whether these species are isolated or polymerized. Information about the Cr−O-support interaction, however, has not been obtained since Cr−O support vibrations, which are expected to be found below 800 cm^{-1}, have not been observed in the Raman spectra. This result is not anomalous; in fact, metal−oxygen support vibrations have also never been observed for other supported metal oxide systems, e.g., supported rhenium oxide, molybdenum oxide, and tungsten oxide.[243] The absence of a Raman

mode associated with SiOCr(VI) structures indicates a partly ionic character of the Cr−O support bond, which results in a very low Raman intensity because of the decrease of the polarizability.

As already anticipated at the end of section 4.1.1, the addition of a low amount of titanium into the silica support greatly affects the molecular structure of the surface chromium sites. Jehng et al.[105] showed that the Raman spectra of Ti-modified Cr/SiO_2 samples, obtained with different techniques, are very similar to that of Cr/TiO_2 and may be explained in terms of the presence of polymeric chromium species mainly on the TiO_2 phase. The preference for the TiO_2 support in comparison with SiO_2 was confirmed by heating a physical mixture of TiO_2 and Cr/SiO_2, which revealed that the surface chromate species migrated from the silica support to the titania support after calcination at 773 K.

However, as in the case of the UV−vis DRS study, the Raman technique is not able to provide direct information about the structure of chromium sites on a Ti-modified Cr/SiO_2 and in particular cannot discriminate between the possible coordinations of this surface species, i.e., a Cr species coordinated to two isolated surface titanium sites, a Cr species bridging an isolated titanium site, and an adjacent surface silica site or a combination of both. In fact, as previously discussed, Raman spectroscopy is not able to directly monitor the Cr−O support bonds.

4.3.2. New Highlights

On the basis of a critical examination of the limitations[96,97,234,242] (Figure 20a) and recent improvements of the literature results by Dines and Inglis[238] discussed above (Figure 20b), we report here new Raman experiments that allowed us to strongly improve the signal-to-noise ratio of the Raman spectra collected on the $Cr(VI)/SiO_2$ system.[244] Improvements came by optimizing both the laser wavelength and the silica support, as discussed in the following.

In the last years, it has been demonstrated that a laser excitation λ, which falls near the energy required for an electronic transition of the material, may lead to a remarkable increase in the intensity of Raman bands if the resonance occurs. The resonance Raman spectroscopy has been widely used to identify the local structure of titanium,[66−68,245,246] iron,[247] and vanadium[248,249] in microporous and mesoporous molecular sieves. Moreover, it has also been demonstrated that the use of a high energy line as an exciting source of Raman spectroscopy can avoid the fluorescence interference from silica materials.[245,250] On the basis of these principles, we collected Raman spectra by using an excitation λ of 442 nm (22600 cm^{-1}). In this way, we eliminated the fluorescence problems, and at the same time, we took advantage of the resonance effect. By looking at Figure 9a, in fact, it is evident that this laser excitation λ falls into an intense CT absorption, so that resonance occurs.

The result obtained following this experimental approach on a 0.5% $Cr(VI)/SiO_2$ sample, after oxidation at 923 K, is shown in Figure 21a, curve 1. A remarkable narrow and very well-resolved peak at

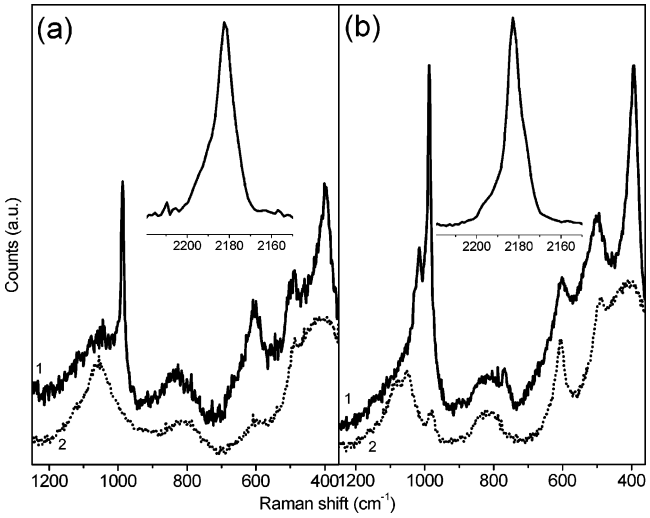

Figure 21. (a) Raman spectra of 0.5 wt % $Cr(VI)/SiO_2$, obtained by using a 442 nm laser line, after oxidation at 923 K (curve 1, collected in oxygen atmosphere) and after reduction in CO at 573 K (curve 2, collected in CO atmosphere). The inset reports spectrum 2 in the CO stretching frequency region. Unpublished results. (b) Raman spectra of 0.5 wt % $Cr(VI)/SiO_2$-aerogel, obtained by using a 442 nm laser line, after oxidation at 923 K. Curves 1 and 2 and the inset are as in part a. Adapted with permission from ref 244. Copyright 2005 American Chemical Society.

985 cm^{-1} (FWHM = 10 cm^{-1}) grows on the rising baseline of the silica support. On the higher energy tail of the dominant band an unresolved weak shoulder is observed around 1000 cm^{-1} (scarcely appreciable in the large wavenumber scale adopted in Figure 21a). This component appears at a frequency very close to that obtained by deconvolution of the baseline subtracted experimental data of Dines and Inglis.[238] On the basis of what has been discussed so far, it can be understood why the quality of the spectra reported by Dines and Inglis[238] (Figure 20b) is intermediate between the earlier ones[96,97,234,242] (Figure 20a) and the new one, here reported for the first time (Figure 21a). In fact, Dines and Inglis,[238] using a λ of 476.5 nm (21000 cm^{-1}) start to enter into the resonant conditions, being the excitation line in the low energy tail of the absorption spectrum of the sample (Figure 9a). Conversely, the Raman spectra reported in Figure 20a, being collected with a λ of 514.5 nm (19400 cm^{-1}), are out of the absorption edge and thus of the resonant conditions. Note that the limited spectral interval used by Dines and Inglis[238] (Figure 20b) does not allow a precise estimation of the improvement in the signal-to-noise ratio with respect to earlier spectra (Figure 20a); for the same reason, it is also difficult to evaluate the fluorescence background present when the Cr/SiO_2 system is measured with that excitation line.

Also reported in Figure 21a (curve 2) is the Raman spectrum obtained on the CO-reduced catalyst in the CO atmosphere. The intense band due to the chromate stretching vibration totally disappeared, as expected, and no evidence of SiOCr(II) modes is present. In the CO stretching region (see the inset of Figure 21a), an intense band centered at 2182 cm^{-1}, accompanied by a broad tail at higher frequencies (2190−2195 cm^{-1}), is observed. To the best of our

knowledge, this is the first time that Cr(II) carbonyls, formed at the surface of the Cr/SiO_2 systems, have been detected by Raman spectroscopy. These are the Raman counterparts of the well-known IR RT triplet previously discussed (see section 4.2.1 and Figure 14).

A further improvement has been obtained by repeating the same Raman experiments on a Cr(VI)/SiO_2 sample prepared by anchoring Cr(VI) on a silica aerogel monolite about 2 mm thick. Such a support is chemically equivalent to a standard aerosil, as testified by IR spectroscopy (spectra not reported for brevity) showing O−H and Si−O stretching bands comparable to those observed in Figures 3b and 5a, respectively. The aerogel monolites are perfectly transparent from the visible to the near-IR region of the electromagnetic spectrum and present very good Raman scattering properties. These peculiar optical properties arise from the coupling of (i) the absence of absorbing bands (as all pure SiO_2 materials) and of (ii) the absence of intragrain scattering processes, which is the main reason for light attenuation in the common powdered silica. In other words, aerogel monolites exhibit an optical behavior very close to that of a homogeneous liquid phase. Moreover, its porous nature allows us to work with a sample having a surface area comparable with (or even greater than) that of commonly used amorphous aerosil. When chromium is grafted on this peculiar support, great improvements appear in the Raman spectrum, as evident in Figure 21b (curve 1). This spectrum is particularly intense and more structured than those presented in Figures 20 and 21a. It is dominated by the sharp and well resolved band, now at 987 cm^{-1}, which grows on the structured background of the aerogel system. Beside this band, other two well resolved components at 1014 and 394 cm^{-1}, that is, in the regions where the $\tilde{\nu}_{as}$(O=Cr=O) and δ(O=Cr=O) modes are expected, are observed here for the first time. As was the case for the Raman spectrum collected on the Cr(VI)/SiO_2-aerosil system (Figure 21a), a shoulder at about 1000 cm^{-1} is observed. The presence of two signals in the frequency region where the $\tilde{\nu}_{as}$(O=Cr=O) mode is expected (well defined band at 1014 cm^{-1} and weak shoulder around 1000 cm^{-1}) could be a consequence of the heterogeneity of the Cr(VI) supported on the amorphous SiO_2 (see section 4.6). The Raman spectrum 1 reported in Figure 21b is thus the first experimental complete vibrational characterization of the Cr(VI) species supported on a siliceous matrix. The absence of any other narrow bands in the 800−900 cm^{-1} region, also when the silica fluorescence background has been minimized and the Raman scattering from chromium species enhanced, definitely excludes a significant presence of polymeric chromium species, at least at low chromium loadings, as already suggested (but not safely demonstrated) in the past,[96,234,238,242] and in contrast with the case of Cr(VI) anchored on other oxide supports.[96,235,236,238,251,252]

Both Raman (compare the insets of parts a and b of Figure 21) and IR spectroscopies (spectra not reported for brevity) testify that the same kind of carbonyl species are formed on the reduced Cr(II) cations irrespective of the used support (silica aerosil or aerogel). The spectroscopy of CO adsorbed on Cr(II) is sufficiently rich, in terms of spectra modification induced by both temperature and pressures variations (vide supra section 4.2.1), to conclude that the formal equivalence of the Cr(II) carbonyls reflects the equivalence of type and population of surface Cr(II) species on both supports. It is finally worth anticipating that the ethylene polymerization performed on both supports results in a very similar time dependence of the in situ IR spectra monitored under comparable conditions (vide infra section 5.3.1), which basically reflects a similar catalytic activity of the two systems. In other words, the Cr/SiO_2−aerogel system represents the ideal material for spectroscopic investigations in both visible and NIR regions, without being appreciably different, on a catalytic level, from the classical Cr/SiO_2−aerosil system.

4.4. XAS (XANES and EXAFS)

XAS spectroscopy (both XANES and EXAFS), because of their atomic selectivity, represent techniques of choice in the characterization of highly diluted species[253−255] such as chromium atoms on the Phillips catalyst. Moreover, the short mean free path of the photoelectron (which is the probe of XAS spectroscopy) limits the sensibility of the technique to a few Ångstroms around the absorbing atom. This implies that unlike XRD, no long-range order is required and structural information can be obtained from amorphous systems also.

4.4.1. XANES

XANES provides information on both electronic state and local symmetry around the absorbing atom.[97,115,177,178,228,256−259] Like many transition metals, chromium exhibits a wide range of oxidation states (from 0 to +6) and also of coordination geometries in its compounds (cubic, octahedral, tetrahedral). K-edge absorption spectra for various chromium compounds have been reported in the past.[260−262] From these studies, the following basic information can be derived.

(i) An intense preedge peak and a shoulder in the rising absorption edge appear in the XANES spectra of tetrahedrally coordinated chromium compounds of different oxidation states: Cr(IV), Cr(V), and Cr(VI). These typical absorption features have often been observed in the XANES spectra of other transition metal compounds with tetrahedral coordination geometry, such as Mn,[263,264] Ti,[66,265] and V.[260,266] Following the MO theory,[267] the preedge absorption line has been assigned to the electron transition $Cr1s \rightarrow 3t_2$ (mainly d origin), whereas the shoulder in the absorption edge was assigned to the electron transition $Cr1s \rightarrow 4t_2$ (mainly p origin). Alternatively, by using atomic theory,[260] the preedge line was attributed to the dipole forbidden transition Cr(1s)→3d, which actually corresponds to the $Cr1s \rightarrow 3t_2$ transition in MO theory. This forbidden transition gains additional intensity through the mixing of 3d and 4p orbitals, caused by the breakdown of inversion symmetry due to structure distortion, which is maximum when a T_d like geometry is present.

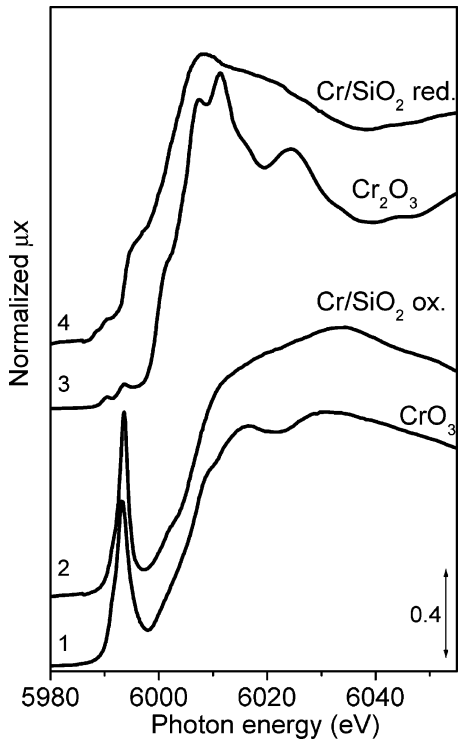

Figure 22. High resolution XANES spectra of the Cr/SiO_2 Phillips catalyst after oxidation at 773 K (curve 2) and subsequent reduction in CO at 623 K (curve 4). For comparison, also the spectra of CrO_3 (curve 1) and of Cr_2O_3 (curve 3) model compounds are reported. Adapted with permission from ref 115. Copyright 2005 Elsevier.

(ii) The energy position of the chromium K-edge, corresponding to the minimum energy required to promote a 1s electron to the continuum, is very sensitive to the chromium oxidation state, to the electronegativity of the nearest neighbor atoms, and to the coordination geometry. These results have been confirmed by recent studies,[262,268−270] which demonstrated that there is a direct correlation between the energy position of the edge and/or the preedge and the valence state of the chromium center. This means that in principle, it should be possible to use the position of the Cr−K edge and preedge transitions to determine the average chromium valence state and coordination geometry in unknown compounds, by using data collected for reference compounds.

Figure 22 reports the high resolution XANES spectra of the Cr/SiO_2 catalyst (4 wt % Cr loading) after oxidation at 773 K (curve 2) together with that of the catalyst after reduction in CO at 623 K (curve 4). For comparison, also the XANES spectra of CrO_3 (curve 1) and of α-Cr_2O_3 (curve 3), where chromium species have a well-defined oxidation state (+6 and + 3, respectively), are reported. Similar spectra have been previously published by Weckhuysen et al.[97] on a Cr/SiO_2 sample with almost the same chromium loading. From a first view, it is clear that the spectrum of the oxidized catalyst is very similar to that of CrO_3, both in the preedge and in the edge regions. This confirms that chromium species anchored on the silica surface as Cr(VI) in a tetrahedral-like coordination geometry and well agrees with the literature data based on different spectroscopic laboratory techniques, such as UV−vis (section 4.1.1), Raman (section 4.3.2), and XPS (vide infra section 4.5.1).[8,96,138,139,271,272] It is important to notice that a Cr(VI) in a T_d like symmetry is basically compatible with both chromate and dichromate structures, vide supra Scheme 3, i.e., XANES alone is not able to discriminate between different chromium molecular structures. Recently, the XANES technique has been applied to determine the coordination structure of chromium in mesoporous siliceous materials, such as MCM-41[273,274] and MCM-48.[274] Also in these cases, chromium has been found to anchor as Cr(VI) with a distorted tetrahedral coordination, giving rise to XANES spectra very similar to that reported in Figure 22.

As far as the CO-reduced catalyst is concerned, the remarkable red shift of the edge, with both respect to the oxidized sample (about 6.5 eV) and respect to the α-Cr_2O_3 reference (about 2.0 eV), suggests that the CO-reducing process converts Cr(VI) into chromium species in an oxidation state lower than +3, given by the simultaneous presence of Cr(II) (mainly) and Cr(III) species.[97,115] The preedge peak associated with tetrahedral Cr(VI) species totally disappears and is substituted by a distinct feature at about 5996 eV. It is worth noticing that a similar shoulder has been observed for the $[Cr(OCOCH_3)_2\ H_2O]_2$·Cr(II) model compound in planar square coordination.[115,262] As a shoulder around 5995 eV is extrapolated from the CO-reduced Cr/SiO_2 catalyst reported in Figure 7 of ref 97, we can put forward that the 5995.9 eV component is a fingerprint of the Cr(II) species in an almost 4-fold coordination state. Weckhuysen et al.,[97] observing that the feature at about 5996 eV is less evident for Cr/SiO_2·Al_2O_3 and Cr/Al_2O_3 samples, inferred the following order of reduction of chromium species on different supports: SiO_2 > SiO_2·Al_2O_3 > Al_2O_3.

From the XANES spectrum of the CO-reduced sample, two evidences confirm that a detectable amount of Cr_2O_3 clusters is present, due to the relatively high chromium loading (4 wt %): (i) The shoulder at 5995.9 eV is less pronounced than that observed for the $[Cr(OCOCH_3)_2$·$H_2O]_2$ model compound, and (ii) the presence of an unstructured absorption is in the 5990−5993 eV range (a region where preedge features of α-Cr_2O_3 appears). The presence of an aggregated chromium phase on samples characterized by such a high chromium content (4 wt %) perfectly agrees with the literature discussed so far.[9,71,94,103,116−120,123,124,138−146]

Figure 23 reports the effects of the in situ polymerization on the XANES spectra of the Cr/SiO_2 catalyst, both for the CO-reduced, part a, and for the ethylene reduced, part b, systems. The XANES spectrum of the CO-reduced catalyst after polymerization at RT (dashed curve in Figure 23a) is very similar to the spectrum collected prior to polymerization (full black line). Only a slight increase in the intensity of the white line (first resonance after the edge, evidenced in Figure 23 by an arrow) can be observed, which reflects a modest increase of the average coordination of Cr ions. Also a weak erosion of the fingerprint shoulder at about 5996 eV, char-

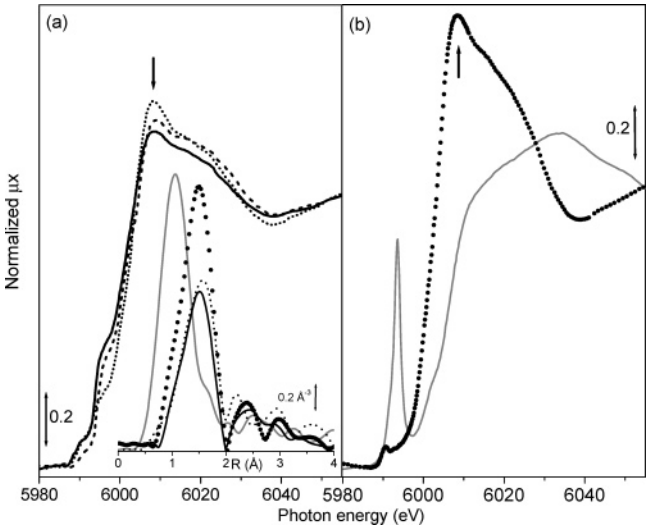

Figure 23. Effect of in situ ethylene polymerization on the XANES spectra. (a) Polymerization on the model CO-reduced Cr/SiO_2 Phillips catalyst: reduced Cr/SiO_2 (black solid line), after polymerization at RT (dashed line) and after polymerization at 373 K (dotted line). (b) Polymerization on the $Cr(VI)/SiO_2$ Phillips catalyst: oxidized Cr/SiO_2 (gray solid line) and Cr/SiO_2 reduced directly in ethylene at 523 K (scattered circles). The arrow indicates the white line. The inset of part a: FTs of k^2-weighted Cr K-edge EXAFS spectra of the Cr/SiO_2 catalyst. Symbols are as in parts a and b. Adapted with permission from ref 115. Copyright 2005 Elsevier.

acteristic of Cr(II) species, is observed. A stronger modification of the XANES features is obtained by conducting the polymerization on the CO-reduced system at 373 K (dotted curve in Figure 23a). In this case, the erosion of the fingerprint shoulder at about 5996 eV is more evident. These results confirm that the number of Cr(II) sites involved in the polymerization reaction at RT and low ethylene pressure is very low (vide infra section 5.1.2.2), so that the XANES spectrum after polymerization reflects the majority of inactive chromium sites and only little modifications are present with respect to the sample prior the polymerization. By contacting the CO-reduced catalyst with ethylene at 373 K, a larger fraction of Cr(II) sites becomes active in the polymerization, explaining the partial disappearance of the fingerprint shoulder at 5996 eV. Of course, we have to remember that we are in the presence of a fraction of Cr_2O_3 clusters (which has been quantified by the authors of ref 115 to be about 40%), so that the XANES spectrum is better described as a mixture of aggregated Cr(III) species, unreacted Cr(II) species, and chromium sites in a higher oxidation state (presumably IV) in interaction with the polymer chains (vide infra section 5.2.1).

The conclusions outlined before are further on demonstrated by looking at the XANES spectrum obtained on a Cr/SiO_2 sample reduced directly in ethylene at 523 K (scattered dots in Figure 23b). In this case, we observe the depletion of the preedge peak characteristic of Cr(VI) in a T_d like geometry and the shift of the edge absorption toward lower values with respect to the oxidized starting point, confirming that ethylene reduces Cr(VI) during the polymerization reaction. Unfortunately, as discussed before, the situation is complicated by the presence of a fraction of clustered Cr(III) ions, so that it's difficult to estimate the average oxidation state of chromium on the industrial catalyst. However, by comparing the spectrum of the ethylene-reduced catalyst with that of the CO-reduced system after polymerization (dashed and dotted curves in Figure 23a), observations can be made as follows: (i) the white line intensity grows up remarkably, reflecting a much higher increase of the average chromium coordination, and (ii) the Cr(II) fingerprint feature at 5996 eV is totally absent, suggesting that almost all isolated chromium species have been involved by the polymerization reaction. Of course, this does not mean that all of the Cr(II) sites are active in the polymerization. A large heterogeneity is expected among the isolated Cr species at this stage,[275] including active Cr sites carrying the polymer chains, Cr sites just perturbed by a polymer generated elsewhere, Cr sites still in interaction with reduction products, or, eventually, Cr sites carrying some "deactivating precursors" (such as "Cr−cyclopentane" structures, which have been found to be inactive with respect to polymerization,[276] vide infra section 5.2.4.2).

For the reduced catalyst, where no reduction products are supposed to be present, Groppo et al.[115] measured the decrease of the Cr(II) fingerprint at 5996 eV (Figure 23) and used this value to estimate an upper limit of the number of Cr(II) sites active in the polymerization. By comparing the integrated area of the 5996 eV band in the case of the CO-reduced catalyst after polymerization at RT with that measured before polymerization, the authors estimated that a fraction of about 25% of the original Cr(II) sites was involved in the polymerization. Analogously, when the polymerization is performed on the CO-reduced catalyst at 373 K, about 55% of the initial Cr(II) sites are estimated to be involved in the polymerization. Groppo et al.[115] concluded that even if these values do not correspond directly to the fraction of actually active sites, they suggest the order of magnitude of the active sites, which is probably near to 10% of the Cr(II) sites.

In conclusion, XANES technique is able to provide useful information about the oxidation state, the coordination geometry of chromium sites on an amorphous support such as silica, and to give a quantitative upper limit of the number of Cr(II) sites involved in the polymerization process on the CO-reduced catalyst. Nevertheless, it is not sufficient to overcome some problems, such as the chromate/dichromate question or the oxidation state of the chromium centers during the polymerization.

4.4.2. EXAFS

Figure 23 (inset of part a) reports the k^2-weighted, phase uncorrected, FT of the EXAFS function of a 4 wt % Cr/SiO_2 catalyst, collected by Groppo et al.[115] together with the XANES spectra reported in Figure 23a,b. In this regard, please note that distances extracted from such data are typically 0.2−0.3 Å shorter than the actual ones, which are obtained only when the appropriate phase correction is applied. Distances obtained after a best fit of the EXAFS data

are phase-corrected and thus reflect the actual ones. The oxidized catalyst (gray solid curve) exhibits a dominant contribution centered at 1.06 Å, clearly due to the short Cr=O double bonds, and a minor shoulder clearly visible at higher distances (1.55 Å), due to longer Cr−O single bonds. As anticipated in the previous section, Weckhuysen et al.[97] performed a XANES/EXAFS study on an analogous Cr/SiO_2 system with 4% Cr loading by weight. By performing a curve fitting of the Cr K-edge EXAFS spectra collected for calcined Cr/SiO_2, two Cr−O distances were obtained, at 1.53 and 2.05 Å with a similar coordination number, ca. 2.1. Also, a higher shell signal was observed and attributed by the authors to a Cr−Cr contribution that was found at 3.1 Å, with a coordination number of 0.5.[97] The authors provided two possible explanations. A polychromate ion may be attached on the silica surface upon calcination, characterized by both bridging and terminal Cr atoms with two different Cr−O distances (2.05 and 1.65 Å, respectively). Alternatively, the 1.53 Å distance is representative of polychromate, while the 2.05 Å reflects the presence of Cr(III) oxides.[97]

In a more recent work,[115] another interpretation has been suggested. The signal of the $Cr(VI)/SiO_2$ system is clearly a complex one as two families of species are present, resulting in three kinds of contributions: Cr=O and Cr−O of isolated Cr(VI) and Cr−O of clustered Cr(III). The short Cr=O bond is expected to be in the 1.5−1.6 Å range,[97,277] while the Cr−O bonds in α-Cr_2O_3 occur in the 1.96−2.01 range.[278] As far as the Cr−O single bonds of the hexavalent species are concerned, a much shorter distance with respect to that in α-Cr_2O_3 is expected, owing to the absence of d electrons. Note that in CrO_3, Cr−O single bond distances occur at 1.75 Å.[277] This remarkable heterogeneity in distances implies, in k-space, the superimposition of sinusoidal signals with a remarkable difference in periodicity. Under such conditions, the experimental $\chi(k)$ function is rapidly killed by out-of-phase signals and shows only noise for k values higher than 7 $Å^{-1}$. On this basis, Groppo et al.[115] suggested that also the Cr−O and Cr−Cr contributions detected in ref 97 come from aggregated Cr_2O_3 particles. This interpretation is supported by the more recent EXAFS experiment of Wang et al.[273] on a much more diluted Cr/MCM-41 sample (in the 0.35−1.7 wt % range), performed in fluorescence mode. Under such diluted conditions, only a single peak is observed in the phase uncorrected |FT| of the oxidized samples at 1.23 Å and no vestiges of the high R component in the data of Wang et al.[273] are present.

Upon reduction in CO at 623 K, Groppo et al.[115] report experimental $\chi(k)$ data showing a significant signal up to 11 $Å^{-1}$. The corresponding k^2-weighted, phase-uncorrected, FT shows an almost symmetric peak, centered at 1.51 Å, while the strong Cr=O signal is totally destroyed (see full black curve in the inset of Figure 23a). After reduction, the Cr−O distances of the isolated species have undergone a significant elongation owing to the increased ionic radius of Cr(II) with respect to that of Cr(VI) and are now much closer to those of the clustered species.[115]

After the polymerization reaction (dashed and dotted curves in the inset of Figure 23a, respectively), the intensity of the peak of the FT in the 0.7−2.0 Å interval increases in the order: CO-reduced catalyst (black full line) < CO-reduced catalyst after polymerization at RT (dashed line) < CO-reduced catalyst after polymerization at 373 K (not reported) < ethylene-reduced catalyst (scattered circles). EXAFS is unable to discriminate between Cr−O and Cr−C first shell contributions owing to the negligible difference in electrons of the scattering atoms. However, as a change of the Cr-to-support interactions is not expected, the increase of the peak at 0.7−2.0 Å has been attributed to an increase of the average number of C atoms entering in the first coordination shell of isolated Cr species upon polymerization.[115]

In conclusion, although XANES and EXAFS spectroscopies are potentially useful techniques in order to understand the local structure of chromium sites on the silica surface, only semiquantitative information has been extracted so far; there is still a lack of knowledge in this field and numerous progresses could be done. Limitations arise from the fact that only high chromium loaded samples have been investigated, where the unavoidable presence of a fraction of clustered Cr_2O_3 particles influences the XANES features and prevents any structural EXAFS data analysis on the samples after polymerization. It is therefore evident that the next generation of XANES/EXAFS experiments on this catalyst must mandatorially be performed in fluorescence mode on more diluted samples. This implies the design and the realization of new cells able to work in fluorescence mode and to double the performances of the transmission mode cells.[279]

4.5. Other Techniques

4.5.1. XPS and SIMS

Ultrahigh vacuum spectroscopic techniques are potentially very powerful for microscopic characterization of catalysts in general, as they provide direct information originating from the atoms and molecules on the surface. In particular, XPS is a good surface science method for measuring the oxidation states of the transition metal ions in a thin surface layer of supported oxide such as polyolefin catalysts, including, e.g., Phillips catalyst,[8,106,135,147−149,280] Ziegler−Natta catalyst,[281] and metallocene catalyst.[282] Also the metal−support interaction can be deduced. As was the case for the binding energy (BE) of Cr1s electrons discussed in the XANES section (4.4.1), the BE of the Cr2p levels increases with increasing chromium oxidation state and for a certain oxidation state with increasing electronegativity of the surrounding atoms; for these reasons, it is frequently used as a criterion for identifying the oxidation state of the surface chromium species supported on the Phillips catalyst.[8,135] On the other hand, the FWHM value of the Cr2p components reflects the distribution of the chromium species in its corresponding oxidation state, which also gives valuable information, especially for discriminated aggregated and bulky chromium oxide from the surface-stabilized and

highly dispersed chromium species.[283] Both qualitative and quantitative information of surface chromium species in mixed oxidation states can be obtained by XPS spectroscopy.

However, XPS, like the other surface science techniques, presents some limitations. In industrial catalysts, the active phase is usually hidden inside a porous high surface area support (e.g., silica), out of reach for surface spectroscopies. For XPS, the surface sensitivity is restricted by the typical mean photoelectron escape depth to about 20 Å.[281] Moreover, the catalyst supports are in general nonconductive, and thus, the sample will charge when applying electron or ion-releasing techniques such as XPS, SIMS, or ion scattering. For XPS experiments, the sample charging results in a blue shift for the XPS band position, due to the presence of an additional macroscopic electrostatic potential. Charge effects can be, at least, partially compensated by the use of an electron gun that artificially restores the missing negative charge due to escaping XPS and Auger electrons. For polycrystalline samples, this compensation is critical, as each grain receives a different X-ray photon flux, resulting in a different charging effect. The same holds for the compensation electrons received from the electron gun. As a result, the charging/compensating effects cannot be perfect for each sampled grain, causing an instrumental broadening of the XPS peaks. To avoid these complications, Thüne et al. prepared a surface science model sample for the Phillips catalyst, by impregnating flat Si(100) conducting single-crystal substrate covered by amorphous silica with aqueous CrO_3 solution.[271,272,284−287] After impregnation of 1 Cr/100 Å^2 (2.5 wt %), the $Cr2p_{3/2}$ maximum appears at 580.0 eV. Upon calcination at 723 K, the BE increases to 581.3 eV. This value is in excellent agreement with the 581.6 eV measured by Merryfield et al.[135] for a 1.1 wt % Cr/SiO_2 (0.42 Cr/100 Å^2) catalyst calcined in dry air at 923 K. From these results, the authors concluded that the shift in $Cr2p_{3/2}$ BE proves the anchoring of Cr to their SiO_2/Si(100) model support upon calcination. The high BE of surface chromate is a unique feature of the silica support, whereas chromate on other oxidic supports such as Al_2O_3[288,289] or SnO_2[290] shows $Cr2p_{3/2}$ maxima close to 580 eV.

After impregnation, the same authors[271,272,287] found a linear correlation between the XPS $Cr2p_{3/2}$ intensity and the chromium loading (as expected for a molecular dispersion) up to a loading of 2.0 Cr/100 Å^2 (5.0 wt %), while the relation was not true for loading of 4.0 Cr/100 Å^2 (10.0 wt %). They explained this feature considering the picture proposed by Weckhuysen et al.[8] of hydrated chromium on silica and supported by Groppo et al.[115] with XAS technique. At loadings of 4.0 Cr/100 Å^2, it is reasonable to expect some Cr_2O_3 clustering, resulting in a decreased dispersion of the impregnated chromium and therefore in a slightly reduced visibility in XPS. In addition, chromium partially desorbs from the silica surface, especially in the case of high initial chromium loadings and high calcination temperatures.

Comparable results have been obtained by Liu et al.[283,291] on an industrial Cr/SiO_2 catalyst with 1 wt % of Cr loading (i.e., 0.4 Cr/100 Å^2). The BE value of 581.8 eV for the surface chromium species in an oxidation state of VI on the calcined catalyst was reported to be 2.6 eV higher than that of 579.2 eV for the bulk CrO_3. The shifting in $Cr2p_{3/2}$ BE demonstrated that this surface chromium is surface-stabilized chromate species (including monochromate, dichromate, and polychromates). Such an increase in BE is acceptable when the chromium species becomes isolated on a silica surface with weak acidity, since the electron extracting effect from the oxygen atoms on silica is stronger than it would be in the CrO_3 lattice.[135] This effect could be further strengthened by the increasing strain in the surface siloxane groups due to the successive dehydroxylation upon calcination.[6]

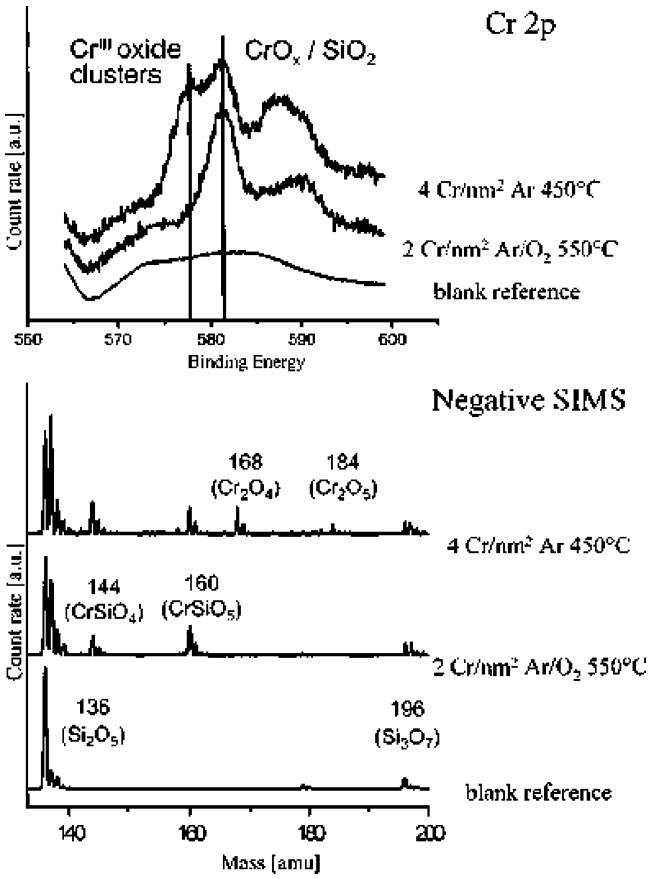

Figure 24. Cr2p XPS spectra (a) and negative SIMS spectra (b) of a blank reference (bottom), a $CrO_x/SiO_2/Si(100)$ sample activated in O_2 at 823 K (middle), and a $CrO_x/SiO_2/Si(100)$ sample activated in vacuo at 723 K (top). Reprinted with permission from ref 272. Copyright 2001 American Chemical Society).

SIMS has been used by Thüne et al.[272] to elucidate the structure of the surface chromate anchored to the silica surface. Figure 24 shows the XPS and SIMS spectra of two model catalysts with a different chromium loading and a blank reference. The catalyst with a 2 Cr/100 Å^2 loading has been calcined at 823 K in O_2 and shows in the XPS spectrum only the $Cr2p_{3/2}$ peak at 581.4 eV, as expected for anchored chromate. The catalyst with an initial loading of 4 Cr/100 Å^2 has been treated at 723 K in the absence of O_2, thus showing both anchored chromate and reduced Cr(III) [$Cr2p_{3/2}$ peak at 577.7 eV, close to the 577.6 eV value found by Merryfield et al.[135] for highly

dispersed Cr(III) oxide on silica], as the loading exceeds the saturation coverage of silica. The negative SIMS spectrum of the calcined catalyst shows two additional fragments with respect to the blank reference, assigned to $CrSiO_4^-$ (mass, 144 amu) and $CrSiO_5^-$ (mass, 160 amu). The second catalyst shows again two additional fragments, assigned to $Cr_2O_4^-$ and $Cr_2O_5^-$ (masses, 168 and 184 amu, respectively).[272] The key observation is that the calcined catalyst shows only $Cr_1Si_1O_x$ fragments, while on the second sample, where a part of the chromium was forced to form clusters, Cr_2O_x fragments are easily detectable. Combining the XPS and SIMS techniques, the authors concluded that this is a strong evidence that chromate can only anchor to the silica surface as a monomer[272] thus confirming, on their model catalyst, the results coming from Raman experiments (vide supra section 4.3.2). Conversely, SIMS analysis conducted on Ti-modified Cr/SiO_2 samples detected mixed Si−Cr fragments,[169] indicating that some of the chromium was in close contact with the support, and Cr_2O_5 fragments, indicating the possible presence of dichromate or polychromate species. Mixed Cr−Ti families of fragments were also observed, indicating the existence of Cr−Ti second shell neighbors on the surface. Similar results have been obtained also on Mg-doped catalysts, showing mixed Cr−Mg families of fragments.[169]

The XPS technique has also been applied to study the interaction of the Phillips catalyst with ethylene. Merryfield et al.[135] collected XPS spectra on a calcined $Cr(VI)/SiO_2$ catalyst (1.1 wt %) before and after addition of ethylene at 453 K. The spectrum obtained contacting the calcined catalyst with ethylene ($Cr2p_{3/2}$ peak at 577.1 eV) closely resembled that obtained contacting the CO reduced model catalyst with ethylene. This value suggests reduction from Cr(VI) to Cr(II) ($Cr2p_{3/2}$ peak at 576.6 eV) by ethylene and that the electron density on the Cr(II) is decreased by ethylene.

Similar results have been obtained by Liu et al.,[291] by contacting an industrial $Cr(VI)/SiO_2$ catalyst with ethylene at RT for a prolonged time. They reported a shift of $Cr2p_{3/2}$ peak to lower BE as well as the relatively increasing of peak intensity, indicating the reduction of surface chromium species by ethylene. Deconvolution of the spectrum of the $Cr2p_{3/2}$ core level revealed the coexistence of three oxidation states. The first chromium species (BE = 580.6 eV, FWHM = 7.8 eV, and atomic concentration = 47.8%) was ascribed to surface chromate species. This implied that about one-third of the chromate species was reduced to chromium species in a lower oxidation state during the RT ethylene treatment. The second chromium species (BE = 577.0 eV, FWHM = 4.2 eV, and atomic concentration = 39.3%) was assigned to surface-stabilized trivalent Cr(III). The third chromium species (BE = 576.0 eV, FWHM = 3.3 eV, and atomic concentration = 12.9%) was ascribed to surface-stabilized divalent chromium species, chemically bonded to the silica surface.[291] This assignment is supported by the report of Merryfield and co-workers, who prepared a standard $Cr(II)/SiO_2$ catalyst with a BE value of 576.6 eV and a FWHM value of 5 eV for the $Cr2p_{3/2}$ level.[135] Weckhuysen et al.[9] reported the same $Cr2p_{3/2}$ BE value at 576.0 eV for the divalent chromium species supported on silica. Gazzoli et al.[149] identified a divalent chromium species with a $Cr2p_{3/2}$ BE of 576.0 ± 0.2 eV on a CO-reduced CrO_x/ZrO_2 catalyst. On the basis of these results, Liu et al.[291] concluded that already during the induction period on the Phillips catalyst, a redox reaction occurs between the surface chromate and the ethylene at RT, resulting in the formation of Cr(II) surface species. Under such conditions, the simultaneous formation of hydrocarbon species was also observed, as will be described in detail in section 5.1.1.

The XPS technique has been extended also to systems carrying a considerable amount of the polymer, in an attempt to gain information on the structures of chains attached to the catalytic centers. In particular, Thüne et al.[271] reported the XPS spectra of a $Cr(VI)/SiO_2/Si(100)$ model catalyst with a loading of 1 Cr/100 Å^2 (2.5 wt %) after polymerization at 433 K. The C1s component at 284.4 eV is intense and narrow (FWHM = 1.5 eV) and is almost symmetrical. From these observations, the authors concluded that only one carbon species was present after polymerization, the CH_2 carbon of PE.

In conclusion, the XPS data confirm that reduction of anchored Cr(VI) species by means of both C_2H_4 or CO leads to Cr(II) species. Finer information about the structure of the oxidized and reduced species seems not within the potentialities of the technique. In particular, the XPS results alone are not able to resolve the controversy involving the chromate/dichromate ratio. However, the smart combination between XPS and SIMS allowed quoted authors to formulate strong hypotheses in this field[272] complementing the results obtained with UV−vis (section 4.1.1) and Raman (section 4.3.2) spectroscopies.

4.5.2. Distribution of Surface Chromium Species

Different analytical methods have been used to directly map the distribution of surface chromium species on Phillips catalyst and related systems. Rahman et al.[288] reported chromium dispersion images, with a spatial resolution of the order of micrometers, from a CrO_x/Al_2O_3 catalyst by using the PIXE microanalytical technique. Because energetic protons can penetrate the surface layers (up to about 30−50 μm) and the X-rays produced can be detected from such depths, the PIXE technique provides information about elemental concentration. Schmidt et al.[292] mapped the distribution state of surface chromium species on a CO-reduced CrO_x/SiO_2 catalyst by means of SEM/EDS techniques. In both cases, the systems were characterized by a relatively high chromium loading (4.4−5.0 wt %). Conversely, the EPMA method with high resolution makes it possible to directly map the distribution state of the chromium species on a Phillips catalyst with relatively low chromium loading.[283,291] Liu et al.[283] performed EPMA measurements combined with XPS technique on an industrial Phillips catalyst with 0.4 Cr/100 Å^2 loading (about 1.0 wt %), to obtain an image of the surface state of the catalyst in the calcined form. They demonstrated that the chromium species mostly

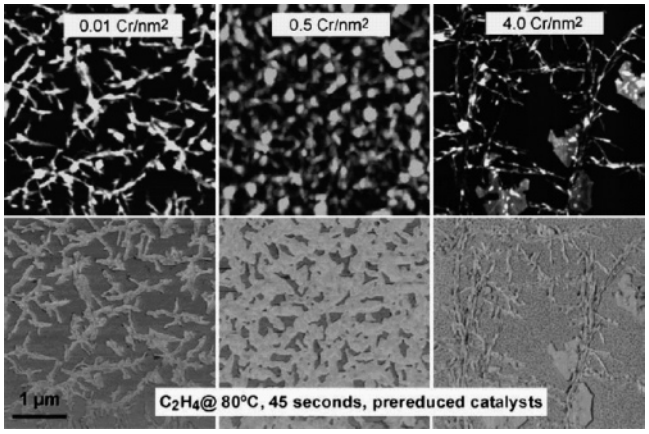

Figure 25. AFM images (5×5 μm^2) of the $CrO_x/SiO_2/Si$ model catalyst (Cr loading as indicated) after treatment with ethylene for 45 s at 353 K. The bright fractal-shaped features in the height-contrast (top) and phase-contrast images (bottom) are PE islands (10−25 nm high) resembling the parts on the catalyst with high polymerization activity. Dark regions (height images) are bare silica surfaces with (almost) no catalytic activity in the time frame of the experiment. Reprinted with permission from ref 287. Copyright 2004 Elsevier.

dispersed uniformly on the surface of each catalyst particle, accompanied by the existence of a few local aggregates of chromium species in sizes of 200−300 nm. These species were supposed to be microcrystal particles of Cr_2O_3. One year later, the same authors tried to investigate the phenomena occurring during the induction time in the ethylene polymerization reaction by means of EPMA technique.[291] They found that by treating a calcined catalyst (1 wt % Cr loading) with ethylene at RT for a prolonged time (2 h), a small extent of surface chromium agglomeration is induced. EPMA images revealed, in fact, few large aggregation areas in sizes of several micrometers on the catalyst surface. These results suggested that the reactions occurring during the induction period most probably induced the surface aggregation of chromium species in some extent.[291]

In an attempt to visualize the distribution of the polymerization activity on the model catalyst in the early stages of reaction, van Kimmenade et al. have very recently applied AFM on the single-crystal supported model of the heterogeneous Phillips polymerization catalyst described before, performing polymerization experiments at 353 K with very short polymerization times.[287] This study revealed that the catalytically active centers are not homogeneously distributed over the silica surface but form islands, with shape and size dependent on the exact catalyst pretreatment (see Figure 25). At 0.01 Cr/100 $Å^2$ (0.025 wt %) loading, they observed fractal-shaped PE islands ranging between 100 and 150 Å in height and covering about 20% of the catalyst surface. At 0.5 Cr/100 $Å^2$ (1.25 wt %) loading, more than the 80% of the catalyst surface is covered with a 200−500 Å PE film. The polymer morphology of a 4 Cr/100 $Å^2$ (10 wt %) loaded sample resembles again the 0.01 Cr/100 $Å^2$ case: roughly 30% of the catalyst surface is covered with a 100−150 Å PE film. Note that in this case a high fraction of clustered Cr_2O_3 species is present.[272] These results suggest that the active polymerization sites are not homogeneously distributed on a submicrometer scale but can be concentrated in patches that represent only a small portion of the entire silica surface.

4.6. Comprehensive Points on the Characterization Techniques

On the basis of the whole literature reviewed above, we are now able to summarize the main results concerning the structure of oxidized and reduced anchored chromium sites obtained in the last period by means of the application of an impressive number of physical techniques.

(i) No doubt exists concerning the oxidation state of chromium species on the calcined Cr/SiO_2 system. UV−vis DRS, Raman, XANES, and XPS techniques state that Cr(VI), traces of Cr(V), and a small portion of Cr_2O_3 clusters are formed on calcined surfaces of the Phillips catalyst. Their relative amounts and coordination geometries strongly depend on the support type and composition, on the chromium loading, and on the activation procedure. Among all of the spectroscopic techniques here reviewed, UV−vis DRS,[8,97,117,118,138] Raman spectroscopy,[96,232,234,238,242,244] XANES spectroscopy,[97,115] and the combined XPS/SIMS approach[272] have been revealed to be by far the most useful in the identification of the molecular structure of chromium on the silica surface. On the basis of a critical examination of the results presented so far, it can be stated that the dominant oxidized species on the Cr/SiO_2 catalyst with 0.5−1% (by weight) chromium loading is the monochromate. Increasing the chromium loading, the monochromate/dichromate ratio decreases and an appreciable fraction of Cr_2O_3 forms. Another way to change the mono/dichromate ratio is represented by the addition of doping atoms, like Ti, into the silica support.[105]

(ii) For low loaded Cr samples, CO reduction mainly converts Cr(VI) into Cr(II). The CO-reduced Cr/SiO_2 catalyst is constituted by ∼98% of Cr(II);[117] hence, it is highly homogeneous from the point of view of the valence state.

(iii) Conversely, the structure of anchored Cr(II) ions is still extremely heterogeneous. This Cr(II) structural variability is favored by the amorphous nature of the silica support and can be influenced by the thermal treatments. In fact, on the surface of the amorphous silica support (see section 2), numerous locations of the anchored Cr(II) ions are conceivable, which differ in the number, type, and position of surface ligands. Figure 26 tries to basically represent this complex situation. The central part is a top-view of the partially dehydrated unrelaxed silica surface already reported in Figure 4b (and obtained by a MD approach), where three Cr(II) ions have been grafted in different positions on two vicinal oxygens. In the upper part of the figure, a lateral view of the same model is shown. From this picture, it is evident that some Cr(II) ions are protruding out of the surface more than others, depending on the geometry and the strain of their environment. Different possible coordinative situations of Cr(II) centers are reported in the three zoomed inserts of the picture. All of the Cr(II) ions are grafted to the silica surface through

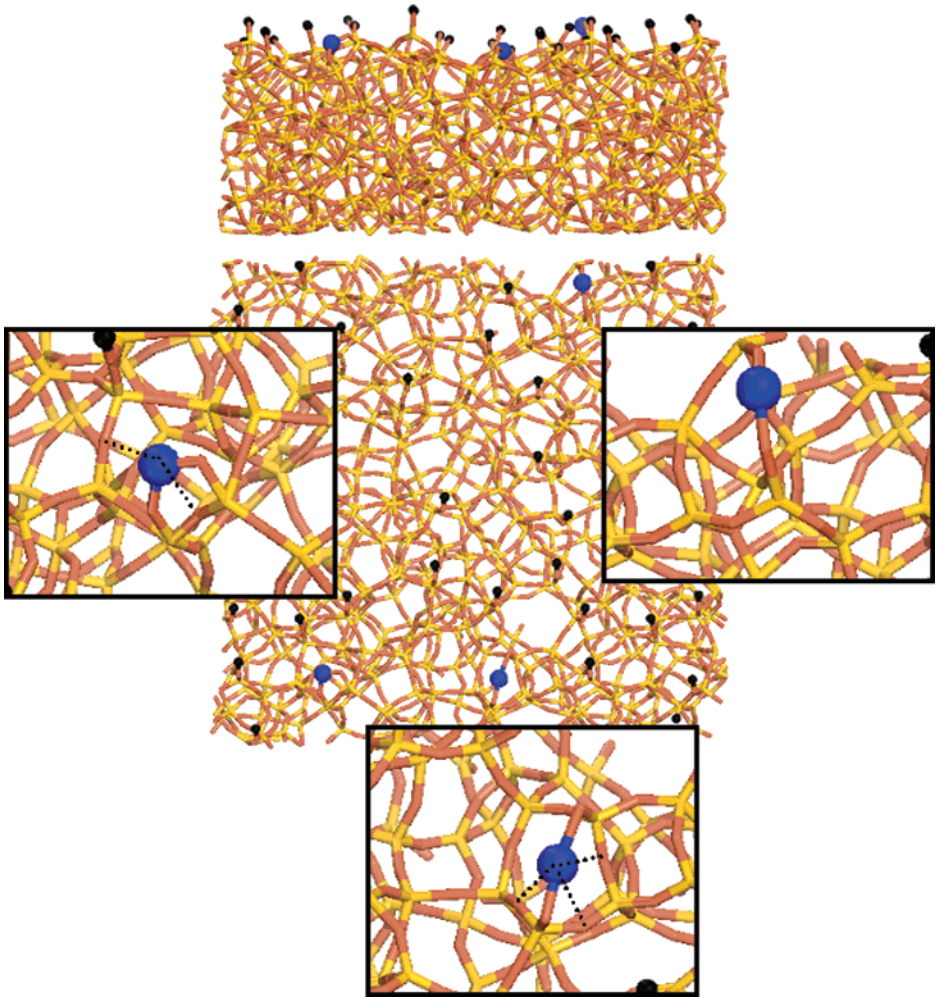

Figure 26. Representation of the Cr/SiO_2 surface obtained by grafting Cr(II) ions on the partially hydroxylated SiO_2 surface represented in Figure 4b: lateral (top of the figure) and top visions (central part of the figure). In the zoomed inserts are clearly visible the different environments of the three chromium ions. Red and yellow sticks connect together silicon and oxygen atoms, respectively; black balls represent hydrogen atoms, while the big blue balls represent Cr(II) ions. Dotted lines show the interaction between Cr(II) ions and weak ligands L.

two strong SiO ligands, but they differ in the type, number, and position of additional weaker ligands, such as siloxane bridges or (more rarely) residual OH groups. When the strong SiO ligands belong to small silicon-membered rings, they form with Cr(II) ion an angle near to the tetrahedral value (left inset in Figure 26). The resulting O−Cr bond is quite covalent. Upon increasing the ring dimensions, we pass from a pseudo-tetrahedral structure to a pseudo-octahedral one (inset in the bottom of Figure 26), characterized by less strain and a higher ionicity of the resulting O−Cr bond, through intermediate structures (right inset in Figure 26). UV−vis spectroscopy[117] has demonstrated that the tetrahedral-like sites, being more protruding on the surface, are preferentially affected by thermal treatments and undergo structural rearrangements, leading to more coordinated Cr(II) species. Conversely, the octahedral-like sites are more stable.

(iv) Even if it has been demonstrated that monochromates are the dominant species on low loaded $Cr(VI)/SiO_2$ samples,[244,272] we cannot make a definite conclusion about the final destination of surface Cr(II) after reduction. On the basis of calculation merely based on the chromium percentage and the silica surface area, we expect that surface Cr(II) species lie on the silica support as isolated species with an average distance of 10 Å, as shown in Figure 26. However, we cannot exclude that a fraction of Cr(II) species could be located at lower distances. This means that even if the two chromium sites do not formally constitute a dichromate-like structure (and thus do not show spectroscopic manifestations of a dichromate, as discussed in the previous sections), their proximity may play a role in determining the polymerization mechanism.

(v) IR spectroscopy of probe molecules has been revealed to be the most sensitive and useful technique in order to discriminate between different Cr(II) sites on the silica surface.[118−124,145,146,209] By analyzing these results, the structure of the Cr(II) sites has been schematically formulated as $(SiO)_2Cr(II)L_n$, where L is a weak ligand (≡SiOSi≡ siloxane bridge or OH group) and n can vary from 0 (completely unsaturated Cr site) to 4 (completely saturated Cr site).[118,123,124,146,209] For example, in Figure 26, $n = 2$ for the chromium ion in the left inset, $n = 3$ for the chromium ion in the bottom inset, while the Cr ion in the right inset is completely protruding out of the surface and so represents the site more

favorable for molecule adsorption. In the insets, the interaction between Cr and L ligands is evidenced by dotted lines. To increase the complexity of the emerging picture, we remember that Cr(II) ions could also graft to the surface via two geminal OH groups. Thus, we can distinguish several chromium structures, characterized by a fixed number n of weaker ligands L in a surface complex but differing in the type of ligand (siloxane bridges or OH groups) and in the position of chromium (vicinal or geminal oxygens). This means that we are potentially in the presence of a wide distribution of chromium species, with a different structure of the first coordination sphere, a different degree of ionicity, and a different surface strain.

(vi) It is reasonable to suggest that the number of Cr(II) sites with $n = 0$ or 1 is low and that their abundance depends strongly on the activation temperature and procedure. In particular, a high temperature treatment after reduction favors the penetration of the Cr(II) ions into the flexible silica framework, increasing the number of sites characterized by a high n value. In other words, Cr(II) becomes progressively shielded by surface siloxane and loses its coordinative unsaturation and adsorption capacity. On this basis, a lower activation temperature could be suggested in order to increase the number of more coordinatively unsaturated sites. However, as under these conditions a more hydroxylated surface is obtained (vide supra section 2.2), more OH groups are in coordination spheres of Cr(II) centers, so suppressing their adsorption ability. These considerations justify why the samples activated at intermediate temperature (around 923 K) are the most active. In fact, in these conditions, dehydroxylation is maximized while thermal deactivation is still low.

(vii) Focusing the attention on the coordination sphere of the Cr(II) sites, it is concluded that they differ from each other for the number of the effective coordination vacancies, v. The greater is v, the more unsaturated is the Cr(II) site and more molecules can be adsorbed on it. However, it must be noted that v does not coincide necessarily with the maximum number of adsorbed molecules, because the weak ligands L can be more or less easily displaced from their position when stronger ligands (e.g., NO) interact with the chromium center and its environment, vide supra eq 3. Of course, the displacement of a weak ligand may require simultaneously a high coverage of the adsorbed ligand and a certain activation energy. This could explain the necessity to slow the temperature to 77 K to insert a third CO ligand into the Cr(II) coordination sphere but also their easy removal, as discussed in section 4.2.1.2.[146,209] The displacement of one or more weak ligands may happen not only with CO and NO but also with the ethylene monomers during the initial stages of the polymerization reaction. This means that, if the Cr(II) sites characterized by $n = 0$ and 1 are certainly the most active species in the polymerization, also the sites with $n > 1$ could become active, provided that the energy required to displace the weak ligands L is not so great and the ethylene pressure is sufficiently high.

5. Catalytic Activity

5.1. Polymerization on the Phillips Catalyst: A Review of Literature, Problems, and Perspectives

5.1.1. Industrial Catalyst (Ethylene Reduced Catalyst)

The Phillips catalyst is known to be highly active for ethylene polymerization with or without a preliminary activation step using organometallic cocatalysts[160,161,293,294] or other reducing agents (e.g., CO[117,295] and H_2[101,296]). In the absence of any reducing agent, the ethylene polymerization on the Phillips catalyst at low temperature (<423 K) usually presents an induction period (also called "dormant period"), without measurable activity.[6,7,135] This is thought to be due to the slow reduction of Cr(VI) by ethylene leading to the formation of Cr(II) active site, accompanied by formation of byproducts such as formaldehyde.[116]

The ability of the Phillips catalyst in polymerizing ethylene without the intervention of any activator makes it unique among all of the olefin polymerization catalysts. It is generally accepted that for catalytic reactions involving olefin insertion and oligomerization (e.g., Ziegler−Natta catalysts), the metal active site must possess one alkyl or hydride ligand and an available coordination site (see structure I in Scheme 13).[1,15,16] Very frequently, the active

Scheme 13. Scheme of the Initiation Mechanism in Ethylene Polymerization According to a Ziegler−Natta Like Behavior

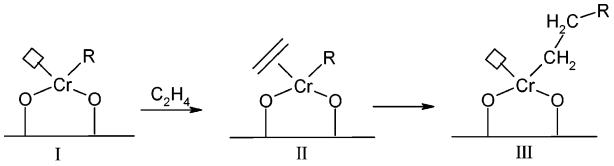

catalyst is prepared in situ, from a transition metal compound not having the active ligand, and an activator (aluminum alkyl, MAO, etc.) whose function is to introduce an alkyl group in the coordination sphere of the metal. The first step is the insertion of a monomer molecule into a vacant position of the metal site (structure II in Scheme 13), via a d-π interaction. The second step is a migratory insertion reaction that extends the growing alkyl chain by one monomer unit, thereby regenerating the vacant coordination site at the metal center (structure III in Scheme 13).[1,15,16] This means that if a Ziegler−Natta like polymerization mechanism is assumed also for the Phillips catalyst, ethylene has to play three important roles simultaneously and/or successively: (i) as a reduction agent, reducing the chromate species in an oxidation state of +6 into coordinatively unsaturated active chromium precursor in a lower oxidation state; (ii) as an alkylation agent, alkylating the potential active chromium species resulting in the formation of active sites; and (iii) as a propagation agent, acting as a monomer for chain propagation of the active sites.

On this basis, the problems associated with polymerization mechanism on the industrial catalyst will be divided into five parts. Part 5.1.1.1 will deal with the reactions occurring during the induction time, which leads to the formation of the catalytic centers and evolution of ethylene oxidation products. Part 5.1.1.2 will be devoted to discuss the problems associated with the low number of catalytic sites and with the high TOF of the polymerization reaction. In part 5.1.1.3, the problems associated with the activation procedure will be discussed, while in part 5.1.1.4 the problems related to the effect of the presence of foreign molecules such as H_2 and CO on polymerization activity will be treated. Finally, in part 5.1.1.5, some information about the morphology of the produced PE particles will be given.

5.1.1.1. Induction Time. Reduction and successive alkylation might account for the presence of the induction period for Phillips-catalyzed ethylene polymerization without using any other reducing agent. The induction time becomes shorter with (i) increasing calcining temperature, (ii) increasing reaction temperature, and (iii) increasing ethylene concentration.[135] In particular, the lower the polymerization temperature is, the longer the induction period is. When the polymerization temperature goes below 323−333 K, there is almost no activity no matter how long the catalyst contacts ethylene atmosphere. The induction period is considered infinitely long in this case.[6,135] Which reaction is occurring and whether the insertion of the first ethylene monomer initiates or not during the induction period are still unclear.[6,7,135] For characterization purposes, the most critical problem is the presence of ethylene oxidation products, which, being adsorbed on the chromium sites, make the determination of structure of the species formed during the first stages of the polymerization reaction a very complex problem. It has been suggested that the sites formed during the reduction step undergo rapid poisoning by oxidation products and that subsequent reactivation by ethylene can be slow, thus becoming responsible for the time-delayed site activation. For this reason, the conventional spectroscopic investigations of the early stages of ethylene polymerization (mostly by IR method) were performed prevalently on the model $Cr(II)/SiO_2$ catalyst, mostly CO-prereduced (vide infra sections 5.1.4 and 5.3.1). However, notwithstanding the simpler structure of the model CO-reduced system, measurements performed on this catalyst were limited by the short lifetime of the initial species, rapid encapsulation of the catalytic species, and low temporal resolution of traditional IR instruments (vide infra sections 5.1.4 and 5.3.1). The insufficient understanding of the induction period also hindered the real comprehension of the mechanisms concerning the polymerization process.[209]

The kinetic behavior of Phillips-catalyzed ethylene polymerization is quite different from that observed in other olefin polymerization processes with Ziegler−Natta type catalysts and metallocenes. With these last catalyst systems, the catalytic site activation is almost instantaneous and the polymerization rate quickly rises to a maximum, followed by either a rapid or a slow rate decrease due to site deactivation and/or diffusion-limited intraparticle monomer mass transfer. Conversely, after the induction period, the polymerization rate with Phillips-type catalysts starts to increase steadily with time until it reaches a stationary level. The steady increase in polymerization rate with time suggests that the concentration of active catalytic species, probably derived from Cr(II) is not constant but increases with time. Zacharov and Yermakov[297,298] reported that the increase in the reaction rate of Cr/SiO_2 was due to the increase in the number of propagation centers measured by the radio tracer technique during polymerization. Unfortunately, whether this increase in the number of propagation centers was caused by fragmentation or chemical change in the catalytically active species was not discussed.[297,298] It is believed that the time varying polymerization rate also affects the MW distribution of PE, because the polymer chain length is dependent on the chain propagation rate. In general, MW distribution of PE made over supported chromium oxide catalysts is much broader than that made over other catalysts, such as Ziegler−Natta and metallocene catalysts.[6]

Notwithstanding the fact that modeling of Ziegler−Natta or metallocene-catalyzed ethylene polymerization processes have been quite extensively studied, little has been published so far on the modeling of the polymerization kinetics for the Phillips type catalysts. A possible reason lies probably in the complexity of the redox and coordination chemistry of chromium in combination with the heterogeneous silica surfaces. In the past, McDaniel et al.[299,300] reported that upon dosage of different poisons (such as oxygen, methanol, acetylene, butyl mercaptan, or diethyl sulfide) the polymerization activity of the Cr/SiO_2 catalyst diminished but mainly through a lengthening of the induction time. In other words, the initiation reactions (reduction and/or alkylation) are more inhibited by the poison than the polymerization itself. If it is assumed that these poisons serve as mild oxidizing agents, the observed inhibition can be explained in terms of a reoxidation of the Cr(II) active species immediately after the initial reduction from Cr(VI) by ethylene, which may perhaps then be reduced again by the ethylene. In conclusion, at least one of the initiation reactions, reduction of Cr(VI) by ethylene or subsequent alkylation, must be inhibited. Very recently, this conclusion has been confirmed by Choi et al.,[301] who have proposed a two-site kinetic model for a silica-supported chromium oxide catalyst for ethylene polymerization to explain the presence of an induction period and to model the polymer MW distribution. To model the induction period, they proposed that (i) Cr(VI) is first reduced to the catalytically active species Cr(II) by reacting with two ethylene monomers (M); (ii) aldehyde is produced as a reaction byproduct (P) when Cr(VI) is reduced to Cr(II); (iii) the reduced Cr(II) site is temporarily poisoned by the aldehyde (P) and so is unable to initiate polymerization [$Cr_T(II)$]; and (iv) the temporarily deactivated or poisoned chromium site [$Cr_T(II)$] is slowly reactivated by ethylene-assisted alkylation (see Scheme 14). Qualitatively, the poisoning reaction

Scheme 14. Two-Site Kinetic Model of the Reactions Occurring during the Induction Time of Ethylene Polymerization, as Proposed by Choi et al.[301a]

Reduction of Cr(VI)	$Cr(VI) + 2M \longrightarrow Cr(II) + P$
Poisoning of active site	$Cr(II) + P \xrightarrow{fast} Cr_T(II)$
Site transformation	$Cr_T(II) \xrightarrow{slow} Cr(II)$
Chain propagation	$Cr(II) + M \longrightarrow Cr(II) - polymer$
Chain transfer	$Cr(II) - polymer + M \longrightarrow Dead\ polymer$

[a] M = ethylene monomer; P = reaction byproduct; and $Cr_T(II)$ = temporarily deactivated Cr site.

might be very fast and the site reactivation reaction might be the rate determining step for the polymerization. To model the MW distribution broadening, each active chromium site is assumed to have the same propagation activity but different monomer chain transfer ability.

Liu et al.[291] have recently studied an industrial Phillips catalyst engaged in the induction period through interaction with ethylene at RT, by the combination of surface analytical methods (XPS, TPD, and EPMA). They found that even during the induction period under interaction with ethylene atmosphere at RT, surface chromate species were partially reduced into Cr(III) and Cr(II) species (vide supra section 4.5.1). Furthermore, they observed the alkylation of the potential active chromium species (corresponding to the formation of active sites after the reduction step) as well as the initiation of the insertion of the first ethylene monomer. Most probably, the formaldehyde molecules coordinatively adsorbed on the active sites, which cannot be desorbed under such mild conditions, and hindered the formation of long polymer chains thus solely permitting ethylene oligomerization. From these studies, it is inferred that not only reduction but also alkylation as well as initiation have already occurred in the induction period. On this basis, a mechanism concerning the reactions occurring during the induction period on the Phillips catalyst at RT was proposed.[291] The Cr(II) species coordinated with one formaldehyde and one ethylene is supposed to be the active site precursor for the alkylation as well as subsequent initiation of the first ethylene insertion.

According to McDaniel[6] and Weckhuysen,[9] the first hydrocarbon species produced upon interaction of ethylene with the catalyst is the most important fingerprint of the catalyst itself and can be used as crucial criterion for a reconsideration of the initiation mechanisms proposed in the literature. Liu et al.,[280] in a successive study on the same system discussed above, found that the first hydrocarbon species formed during the induction period is propene, while the expected dimer of ethylene, butene, is only the second hydrocarbon species formed. The conversion of ethylene into higher olefins with both odd and even numbers of carbon atoms is a well-established phenomenon, which is believed to proceed by ethylene metathesis. This indicates that coordination of formaldehyde on surface-stabilized divalent chromium species most probably results in the formation of a new kind of active precursor for olefin metathesis,

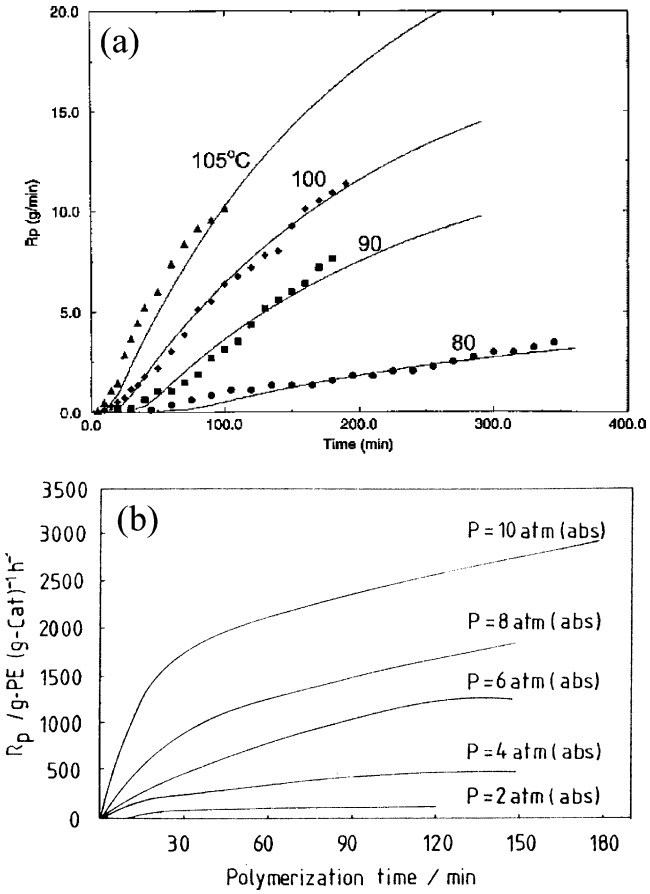

Figure 27. (a) Polymerization rates at different reaction temperatures: symbols refer to experimental data, while lines are the simulations made with the model reported by Choi et al.[301] Reprinted with permission from ref 301. Copyright 2004 Wiley. (b) Polymerization rates as a function of time for different ethylene pressures at 353 K. Reprinted with permission from ref 302. Copyright 1991 Elsevier.

rather than a polymerization active precursor. A conversion of ethylene metathesis into ethylene polymerization from the induction period to normal polymerization period can be expected after the desorption of formaldehyde at a higher temperature. In our opinion, the most important achievement of the study of Liu et al.[280] is that the activation period can be divided into two parts. In the first one, metathesis products and intermediates are dominating, while in the second one regular oligomerization/polymerization Ziegler type intermediates take over.

As already anticipated, the induction time and the polymerization rate depend both on the reaction temperature and on the ethylene pressure. Figure 27a shows the polymerization rate profiles at 353, 363, 373, and 378 K, as experimentally measured by Choi et al.[301] (dots). In the same work also a model able to predict the activity is presented (lines in Figure 27a). It is evident that both the experimental data and the model calculations show that the induction period becomes shorter at higher temperatures. The pressure of monomer was found to affect both the shapes of the rate−time profiles and the values of the polymerization rates; see Figure 27b. At low ethylene pressure (2 atm), the polymerization rate increases with increasing polymerization time

until a more or less limiting constant value was obtained. However, at higher ethylene pressures the polymerization rates failed to reach limiting values and continued to increase with time, the effect being more marked at higher pressures. The change in polymerization rate with time can be explained by (i) a change in the reactivity of active centers, (ii) a change in the number of active centers, and (iii) a change in their accessibility (or a change in the availability of monomer because of diffusion limitations). Wang et al.,[302] by applying a ^{14}CO radiolabeling technique, determined that only a fraction comprised between 3.2 and 7.3% of chromium is active and that this value increases with ethylene pressure. On the basis of their results, they exclude that the change in polymerization rate with time is due to an increase in the number of active centers species and explained the behavior by either a chemical effect relating to changes in the site activities or by a physical effect due to changing availability of monomer in the reaction phase (diffusion limitation). As already mentioned, the propagation step is highly dependent on ethylene pressure (first-order behavior). Conversely, the rate of termination is less dependent on ethylene concentration. This means that varying the ethylene pressure, it is possible to tune the MW of the final polymer, i.e., the chain length. In fact, by increasing the ethylene pressure, the propagation increases without greatly affecting termination and the net result is the formation of long polymer chains. Conversely, working in low ethylene pressure conditions, the propagation rate is lower (in front of a termination rate almost constant), so that shorter chains are produced.

5.1.1.2. Low Concentration of Active Sites and High Turnover Number: Obstacles for Sites and Initiation Species Characterization. The comprehension of the real polymerization mechanism in the Phillips catalyst is further on hampered both by the very low concentration of the active sites and by the very high polymerization rate. Concerning the number of active sites, only a small fraction of the chromium, typically 0.01−10% under realistic conditions,[5] is reported to be active for polymerization, depending on the total chromium content,[7] on the ethylene pressure,[302] and on the method used for active site determination.[303] In contrast to the situation encountered in the Ziegler−Natta polymerization, there have been comparatively few publications concerning the experimental determination of active center concentration in Phillips type polymerization systems.

In the past, some researchers have tried to determine the number of active sites by measuring the number of chains formed during polymerization and assuming that each site makes one chain. However, as a site terminates and reinitiates chains continuously, this approach has strong limits.[6] Hogan reported a value of 2.5×10^{-5} mol active Cr sites/g.[5] This value corresponds to a substantial fraction of the total chromium number (certainly larger than 10% of the total for a 1 wt % Cr loaded system). Zacharov at al.,[297,298] using a radio tagging technique, found only about 1% of the chromium to be active, but they used a Cr/Silica calcined at a lower temperature than that used by Hogan.[5] So the two studies are not necessarily in conflict. Yermakov and Zacharov,[193] by using labeled methanol as a quenching agent, determined the number of active centers at relatively low polymerization rates to about 0.2% of total chromium content. Again, the different polymerization conditions make difficult the comparison with Hogan's value.[5]

Poisoning studies are often used to estimate the number of active centers on a catalyst.[5,133,299,300,304,305] Ideally, the poison chemisorbs irreversibly onto the active site in a one-to-one stoichiometry and blocks further catalytic activity at that site. Thus, the activity is "titrated" against increments of poison added. However, sometimes, the poison also adsorbs onto other sites that are not active, so the technique is only good when the selectivity of the poison for the active site is appropriate. This is not the case of the Phillips catalyst; nevertheless, the technique can give an upper limit of the active site concentration. However, caution should be taken when conclusions are drawn from such poisoning studies. According to the method used to evaluate the polymerization activity (maximum rate of polymerization, average ethylene consumption over a certain length of time, etc.), McDaniel et al.[299,300] concluded that the amount of chromium involved in polymerization can vary from almost 0 up to 100% of the total chromium content. They explained the difficulty to obtain a single value for the active site concentration by the fact that, under high ethylene pressure and relatively high reactor temperature, the poisoning is not selective or strong enough to serve as a titrant. From all of these studies, the only safe conclusion is that the site concentration is likely lower than 10%.

The low concentration of the real active sites makes their spectroscopic characterization very difficult. Furthermore, any measurements of the global properties of the catalyst (for example, its average oxidation state) yield a result, which is not necessarily related to the active centers of the catalyst.[6,9,193]

In addition to the problem of active sites, the turnover number for the insertion reaction is extremely high, making the observation of the species involved in the first stages of the polymerization even more difficult. The maximum activity of Cr/SiO_2 operating at 353 K (approximately the operating temperature of commercial reactors) was reported by Zacharov and Yermakov to be 5.0×10^5 g(PE)/(h mol Cr atm), a value that corresponds to a TOF of about five C_2H_4 molecules per second.[303] Assuming that, in first approximation, the polymerization rate is proportional to the ethylene pressure, we can estimate that at a pressure of 20 Torr the TOF is about 0.1 C_2H_4 molecule per second. A comparable activity was reported for $CrO_3/SiO_2-Al_2O_3$ at 0.001% Cr loading and 500 psi C_2H_4.[7] Eden et al.[304,306] reported, for a polymerization conducted at 373 K and at an ethylene pressure of 180 Torr on a Cr/SiO_2 catalyst calcined at 873 K, a TOF of 1.0 C_2H_4 molecules/s (which corresponds to about 0.5 C_2H_4 molecules/s at 20 Torr). Recently, Amor Nait Ajjou et al.[307−309] determined the polymerization activity of a one-

component olefin polymerization catalyst obtained through thermal transformation of a dialkyl Cr(IV) structure. At 353 K, the activity was of 5.9×10^6 g(PE)/(h mol Cr atm) (TOF $\approx$ 60 C_2H_4 molecules/s, which corresponds to about 1.6 C_2H_4 molecules/s at 20 Torr). The higher activity of this catalyst, if compared with the Phillips catalyst for which it was proposed as a model, has been attributed to a higher fraction of active sites, due to its relatively homogeneous nature.

Thüne et al.[272,284,287] estimated the amount of PE formed per chromium atom in their model CrO_x/SiO_2/Si(100) catalyst (see section 4.5) measuring the thickness of PE film grown in a definite time by means of AFM profile scans. The model catalyst (with a chromium loading of 1.0 Cr/100 Å^2 and activated at 923 K) produces a 420 nm thick film of PE in 1 h, corresponding to 42 μg per hour (at 433 K and atmospheric pressure). As the catalyst contains 1 Cr/100 Å^2, the activity corresponds to about 250 g of PE per mmol of chromium per hour or to a nominal TOF of 2.5 ethylene molecules/(Cr atom s) (which corresponds to about 0.06 C_2H_4 molecules/s at 20 Torr).

5.1.1.3. Activation Procedure and Catalytic Activity. McDaniel and Welch[310] report that the polymerization activity of supported chromium oxide catalysts is strongly dependent upon the activation temperature, although the induction time is little affected. It is also reported that the polymer MW tends to decrease as a higher catalyst calcination temperature is used. In particular, the activity toward polymerization is found to increase as a function of the calcination temperature from 773 K to reach a maximum at 1198 K and then declines. Sintering, which destroys the surface area and porosity of the silica support, has been invoked as responsible for the decline at $T > 1198$ K.[6,310] Now we know that sinking of the chromium centers into the siliceous matrix is another important factor (see sections 4.1.2, 4.2, and 4.6). As formation of surface chromate and dichromate esters is complete below 773 K, it is argued that the activation procedure must achieve some other necessary purpose. As described in detail in section 2.2, within the temperature range of increasing activity, gradual dehydroxylation of the surface is observed, even if it is important to realize that even at 1198 K there is a residual population of isolated hydroxyls.[310]

McDaniel[6] stated that there is a strong reverse correlation between the hydroxyl population on the silica surface and the catalyst activity and termination rate. On this basis, the hypothesis that these hydroxyls coordinate to the active centers and actively participate to the initiation process looks unrealistic or overestimated. We are so forced to hypothesize that hydroxyls are not directly involved at all and that the inverse correlation mentioned before simply reflects some other important change on the silica surface, induced by dehydroxylation. It is a matter of fact that dehydroxylation of pure silica above 773 K results, in fact, in strained siloxane rings by condensation of paired hydroxyl groups (vide supra sections 2.2 and 4.6). It is a wide spread opinion that the presence of these strained siloxane rings after activation is a clear indication that dehydroxylation is associated with surface strain. By analogy, it can be hypothesized that dehydroxylation may interfere with chromium centers, making them more reactive.

5.1.1.4. Effect of the Presence of Foreign Molecules (CO, O_2, H_2, etc.) on Catalytic Activity. We have already mentioned the poisoning studies performed by McDaniel et al.,[299,300] vide supra section 5.1.1.2. To summarize, ethylene polymerization over Cr/Silica catalysts is strongly inhibited by carbon monoxide, oxygen, methanol, triethylamine, and acetylene. Furthermore, the initiation reactions are inhibited more strongly than the polymerization itself.

Different is the case of hydrogen. The addition of hydrogen during catalytic olefin polymerization generally moderates the MW of the produced polyolefin.[1,6] With Ziegler−Natta and Cp_2Cr/Silica catalysts, hydrogen shortens the chains by hydrogenation and this is the main method of MW control; the result is a saturated polymer containing very few vinyl end groups.[311,312] In contrast to the dramatic effect of hydrogen on Ziegler−Natta and on Cp_2Cr/Silica systems, the Phillips type catalysts generally exhibit only a minor response to hydrogen. Surprisingly, there is no evidence of hydrogenation on the Cr/Silica catalyst, i.e., the produced polymers possess vinyl termination and suffer only a minor decrease in the chain length.[5] In addition, while the Ziegler−Natta and the chromocene catalysts' activities are generally depressed in the presence of hydrogen,[313] the Phillips catalysts respond with an increase in catalyst activity.[314] The reason for the observed acceleration of ethylene polymerization in the presence of hydrogen is still not clear. One possibility is that hydrogen revives deactivated sites, or it is possible that hydrogen causes propagation sites that are less active (or inactive) in its absence to become more active. Furthermore, the effect of adding hydrogen in the feed may be understood in terms of dissociative chemisorption of hydrogen at strained siloxane defects to give SiOH and SiH and subsequently activation of suitably positioned Cr(II) sites.

5.1.1.5. Polymer Morphology. SEM and AFM have been widely used to study the morphology of the polymer formed on the Phillips catalyst. The SEM micrographs of polymer particles produced by Cr/SiO_2 at different productivity levels did not resemble those of catalyst particles, which were fractured inhomogeneously.[302,315] McDaniel[6] had already reported that the Phillips type catalyst fragments during polymerization, each catalyst particle providing a polymer particle of approximately the same shape but some 1000 times larger. Fragmentation can arise as a consequence of the forces produced within the pore structure of the silica by the growing polymer chains. He suggested from porosimetric analyses of catalyst ash produced at different polymer yields that the ultimate silica fragments size may be 0.1−1 μm diameter or even smaller.[6] Fragmentation was complete within the first few minutes of polymerization and was not the rate controlling step. This suggests

that the gradual increase in the polymerization rate of Cr/SiO_2 with time described before (vide supra section 5.1.1.1 and Figure 27) must be due to the chemical change of catalytically active species. In other words, all Cr(VI) species cannot be reduced by ethylene to catalytically active Cr(II) at the same time but reduced gradually during polymerization.[315]

AFM has been used more recently to study the morphology of polymer particles. Thüne et al.[284] applied AFM on the single-crystal model of the heterogeneous Phillips polymerization catalyst described before (vide supra section 4.5.1) for visualizing the morphology of the PE growing on the catalyst. AFM provides detailed insight into the lateral distribution of the polymerization activity (see Figure 28). After 10 min of polymerization on a 2 Cr/100 $Å^2$ loaded catalyst, the system was covered by a 80 nm thick film, in which paraffins coexist with polymer. Increasing the polymerization time to 30 min, the surface contains spherulites of approximately 50 μm in diameter, which contain pronounced nucleation centers from which lamellae grow sheaflike. The average film thickness is on the order of 250 nm. After 60 min of reaction, the average layer thickness is about 420 nm. The nucleation centers, although clearly recognizable, have been covered by a domelike structure of PE lamellar crystals.[284]

Di Croce et al.[316] have very recently characterized the surface morphology of the polymer formed on a model Phillips catalyst, elaborated by spin coating a trivalent chromium precursor on a silicon wafer. The polymerization was conducted at 433 K for approximately 60 min in 2 bar of ethylene. Domelike structures were observed, with a diameter of about 30 μm and a height of about 450 nm. Each dome is characterized by a lamellar structure. The lamellae, distinctly separated one from the others, are aligned almost parallel and are agglomerated in bundles.[316]

5.1.2. CO-Reduced Model Catalyst

As said before (vide supra section 3.2), the CO-reduced system is active in ethylene polymerization and the resulting polymer is generally considered almost the same with respect to that obtained with the industrial catalyst. As done for the latter in section 5.1.1, in the present section, we will discuss the presence of a short induction time (section 5.1.2.1), the problems connected with the low concentration of active sites and the high TOF (section 5.1.2.2), and the morphology of the formed polymer particles (section 5.1.2.3) on the CO-reduced catalyst. When possible, clear comparisons with the industrial system will be made.

5.1.2.1. Induction Time. It is a general opinion that the CO-prereduced Cr/SiO_2 catalyst does not present an induction time, being the Cr(II) sites immediately active in the ethylene polymerization already at temperatures as low as 300 K.[6] In Figure 29, the polymerization rate (evaluated as the integrated IR absorption of CH_2 groups of the growing polymer chains, band at 2925 cm^{-1} in the inset) as a function of time is shown. The polymerization has been conducted at 300 K and 20 Torr of C_2H_4. It is evident that, in the first stages of the reaction (first

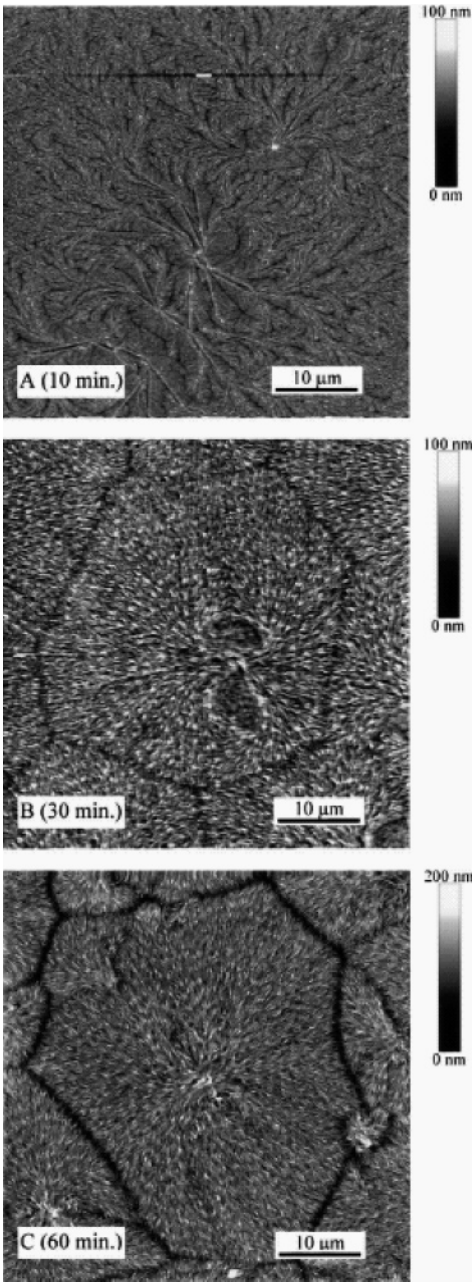

Figure 28. AFM images of the PE films formed on the $CrO_x/SiO_2/Si$ model catalyst at different polymerization times. The small stripes are stacks of lamellar crystals. They form the well-known spherulite superstructure when they crystallize from the melt. Depending on the layer thickness, the spherulite growth stops at different stages of development. Reprinted with permission from ref 284. Copyright 1999 Elsevier.

20 s in our experiment), a short delay is still present also for the reduced catalyst. This delay is consistent with the initial adsorption of ethylene and with the formation of active precursors and suggests that an energy barrier has to be overcome before starting the polymerization.

5.1.2.2. Concentration of Active Sites and Turnover Number. Several attempts have also been made on the reduced Cr/SiO_2 catalyst to determine the number of active sites. McDaniel et al.[6] tried to determine the concentration of the active sites by contacting a CO-prereduced catalyst with ^{13}C-en-

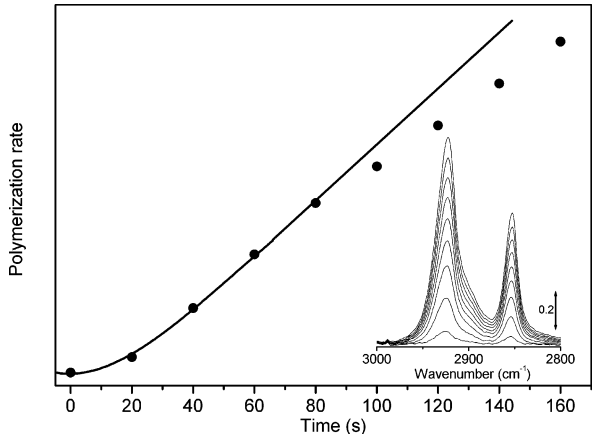

Figure 29. Polymerization rate (evaluated as the integrated IR absorption of CH_2 groups, band at 2925 cm^{-1}, of the growing polymer chains; see inset) as a function of time for $Cr(II)/SiO_2$ samples activated at 923 K and reduced in CO at 623 K. The polymerization was conducted at 300 K and in the presence of 20 Torr of C_2H_4. Scattered circles, experimental integrated areas; full line, polynomial fit on the first five experimental points. The slow decrease of the polymerization rate at higher polymerization times is due to the decrease of the ethylene pressure. Unpublished data.

riched ethylene at 195 K, the temperature at which no polymerization occurs. The labeled ethylene excess was pumped off and replaced by natural ethylene at the same temperature. When the temperature was raised, polymerization began and presumably the labeled ethylene started the polymer chains. Analyzing the resulting polymer by ^{13}C NMR, they found that about 10% of the chromium sites was active. Ghiotti et al.[123] measured the number of alkyl chains produced on a reduced Cr/SiO_2 sample by means of IR spectroscopy. From the intensity of the band at 1660 cm^{-1}, originated after oxidation of the polymer and assigned to aldehydic species, they evaluated that the number of active sites reaches about 10% of the total chromium content.

Myers et al.,[133,305] by means of poisoning experiments with hydrogen sulfide, determined that the active fraction of chromium was about 34% of the total chromium content in the catalyst. A few years later, McDaniel et al.[299] tried to see if the polymerization activity could be "titrated" by dosing various amounts of CO onto the reduced catalyst before charging it into the reactor. Five polymerization experiments have been performed by dosing C_2H_4 on five Cr/SiO_2 catalysts characterized by a poisoning ratio of CO/Cr ranging between 0.01 and 0.25 and compared with the polymerization reaction performed on the unpoisoned catalyst. Authors found that the CO/Cr ratio does not affect either the kinetics of the polymerization, which were the same in all of the cases, or the induction time, while a progressive but not linear decrease in activity has been observed. Reporting the average polymer yield against the amount of CO preadsorbed onto the catalyst, they found that the yield was almost reduced to half of the initial value for the lowest CO/Cr ratios (up to 0.05), while a further increase of the preadsorbed CO molecules has a much smaller effect on the polymerization yield. This behavior, commonly seen in poisoning experiments where the poison/site ratio is significantly smaller than unit, is usually explained as a decreasing selectivity of the poison. In other words, at low CO/Cr ratios, the poison concentrates on the active centers, while at higher CO/Cr ratios, the adsorption of poison becomes less selective. From these data, the authors suggested that up to 6% of the total chromium could be active.[299] Not always the frontier between active and inactive sites can be unequivocally draft, and different families of sites, characterized by a spread in the TOF, have to be hypothesized. Accepting this view, a slightly different explanation of this poisoning experiment has been put forward by the authors. The sites poisoned at low CO/Cr ratios are now the most active ones, while the poison will act on the less active chromium sites at higher CO/Cr ratios only. According to this second interpretation, the percentage of chromium involved in the polymerization has been determined to be much higher: 20−50%. As a results, authors concluded that caution should be taken when conclusions are derived from such poisoning experiments.[299,300]

Kantcheva et al.[317] estimated the number of active sites in a reduced catalyst by integrating the absorbance of the $\tilde{\nu}_{as}(CH_2)$ band (as shown in Figure 29) and knowing the number of ethylene molecules added to the IR cell. The concentration of active sites estimated at the start of ethylene polymerization (1.2×10^{19} sites/g = $2.0\ 10^{-5}$ mol/g) corresponds approximately to the number reported by Hogan (2.5×10^{-5} mol active Cr sites/g) in the case of an industrial Cr/SiO_2 catalyst.[5] As already anticipated in the discussion of the XANES data (section 4.4.1), Groppo et al.[115] estimated an upper limit of the number of active Cr sites on the CO-reduced catalyst by measuring the decrease of the integrated area of the Cr(II) fingerprint feature at 5996 eV. Authors estimated that a fraction of about 25% (55%) of the original Cr(II) sites has been involved in the polymerization at 300 K (373 K). The same authors have also estimated the fraction of engaged Cr sites from IR experiments by quantifying the intensity of the CO triplet, in the 2191−2178 cm^{-1} range, before and after polymerization. Also, in this case, the obtained values are to be considered as upper limits of the active chromium sites. The decrease in the intensity of the CO RT triplet after polymerization is due, in fact, to the loss of chromium sites able to coordinate CO molecules, among which we can distinguish Cr sites carrying some deactivating (or less active) precursor species and Cr sites carrying the polymer chains (the actual active sites). The obtained numbers are 35% (52%) for polymerization conducted at 300 K (373 K), in quantitative agreement with those deduced from XANES spectroscopy. As the estimations obtained with both approaches yield upper limits, Groppo et al.[244] suggested that the order of magnitude of the active sites is probably near to 10% of the Cr(II) sites.

In conclusion, the vast majority of results point toward a fraction of site not far from 10%. This view is in contrast with the results of Bade et al.[318] showing, by GPC analysis of the polymer formed with an ethylene to chromium molar ratio of 1.0 on a

reduced Cr/Silica sample, that only 0.1% of the chromium is active. It must be noticed, however, that the low number of active sites could be a consequence of the adopted conditions: RT and low ethylene pressure, as suggested by the absence of fragmentation of the silica support at the end of the experiment. The great spread in the estimated fraction of active sites on the CO-reduced catalyst mirrors the spread already discussed in the case of the industrial, ethylene-reduced, catalyst (see section 5.1.1.2).

Concerning the polymerization activity, Myers et al.[133] reported a TOF of 0.58 C_2H_4 molecules/s for a polymerization conducted at 323 K in an ethylene pressure of 100 Torr on a Cr/SiO_2 catalyst (oxidized at 1173 K and reduced in CO at 673 K). Rebenstorf[319] obtained, at a temperature of 353 K and at an ethylene pressure of 500 Torr, a TOF of about 0.44 C_2H_4 molecules/s. Szymura et al.[320] reported a polymer yield of 25.5 g (PE)/g (catalyst) for a 300 m^2/g silica loaded with 5 wt % Cr, during polymerization at 300 K and atmospheric pressure over a CO-prereduced catalyst. This value corresponds to a TOF of about 0.26 C_2H_4 molecules/s at atmospheric pressure. Of course, it is very difficult to compare these three values, because they have been obtained in different conditions of temperature and pressure on catalysts characterized by different chromium concentrations and different activation procedures. Nevertheless, we can try to convert reported TOF values[133,319,320] into the expected TOF values for a polymerization reaction conducted in conditions typical of spectroscopic characterization experiments, i.e., RT and low ethylene pressure (20 Torr). As the spread in the temperature adopted in the three experiments is quite small (300−353 K), in this simple conversion, the temperature effects can be neglected. By assuming that the concentration of active sites is 10% for all samples and hypothesizing a direct relationship between TOF and ethylene pressure, the converted TOF values range in the 0.5−1.2 C_2H_4 molecules/s interval.

5.1.2.3. Polymer Morphology. SEM studies on the CO-reduced Cr/SiO_2 catalyst after polymerization revealed that the shape of the PE particles is quite similar to that of catalyst particles and that fragmentation occurs at a smaller extent if compared with the industrial case.[315] The morphology of the polymer particles may have consequences on the MW and on the density of the produced PE. This means that contrary to the common view, the polymer obtained with the model catalyst may be a little different from the polymer obtained in industrial conditions. For example, the MW of PE prepared with CO-reduced Cr/SiO_2 is reported to be higher than that of PE prepared with industrial Cr/SiO_2.[315] Kim et al. interpreted this fact claiming that the heterogeneous nature of active sites of the CO-reduced Cr/SiO_2 is responsible for the different MW distribution.[315] The same authors also found that the density of the PE produced with CO-reduced Cr/SiO_2 increased with polymerization time, while that of PE produced with industrial Cr/SiO_2 decreased. Nevertheless, in the whole investigated polymerization time, the former lies always below the latter. This indicates that the differences in the active sites and in the mode of catalyst fragmentation also affect the aggregation of PE chain segments.

5.1.3. Modifications of Cr/SiO_2 Catalyst

In this section, few words will be devoted to discuss the differences between the standard Cr/SiO_2 catalyst and the Ti-modified one, in terms of induction time and polymerization activity (section 5.1.3.1) and of morphology of the resulted polymer (section 5.1.3.2).

5.1.3.1. Induction Time and Polymerization Activity. As anticipated in section 3.3, the inclusion of small amounts of titanium into Cr/SiO_2 catalyst has a promotional effect on both the polymerization activity and the termination rate.[6,162] Concerning the first point, Mc Daniel et al. reported that titanium increases the activity of the catalyst both by shortening the induction time and by allowing higher polymerization rates.[6,162] The shortened induction time may be explained by considering that the neighboring titanium atoms, and the consequent changes in electron density around the chromium atoms, might cause the reduction of Cr(VI) to be more rapid or the removal of the oxidation products might be facilitated. This is also suggested by the increase in polymerization rate. The promotional effects survive up to a calcining temperature of about 1073 K, above which sintering of the support occurs (vide supra section 3.3).

5.1.3.2. Polymer Morphology. PEs samples made with the Ti-modified Cr/SiO_2 catalysts generally present higher MI values than PEs made with standard catalysts. In addition, the Ti-modified catalysts yield PE that has a higher shear response and a broader MW distribution.[164,166,168,173] This means that the relative rates of propagation and termination must be different for the two catalysts. Mc Daniel et al.,[6,162] by plotting the relative MI potential (which reflects the termination rate) against the titania concentration, concluded that the presence of titanium increases the termination rate. The magnitude of these effects is greater when titanium is present as a surface layer than when it is dispersed in the catalysts bulk. This phenomenon is explained by Pullukat et al.[164] by considering that the increase in the electron density at the chromium atoms, induced by the presence of titanium, destabilizes the Cr−C bond facilitating termination over propagation. This interpretation is supported by previous observations by Hogan[321] who, based on the orientation of the terminal propylene groups, concluded that the chromium atoms are positive relative to the growing polymer chain. If this is true, then an increase in electron density at the chromium site might weaken the bond to the growing polymer and favor termination over propagation.

5.1.4. Initiation Mechanism as Investigated by IR Spectroscopy in the 1980s

The high TOF and the low concentration of the active sites have limited the application of traditional spectroscopic techniques to observe the species involved during the initiation mechanism. In 1988, Ghiotti et al.[123] carried out ethylene polymerization

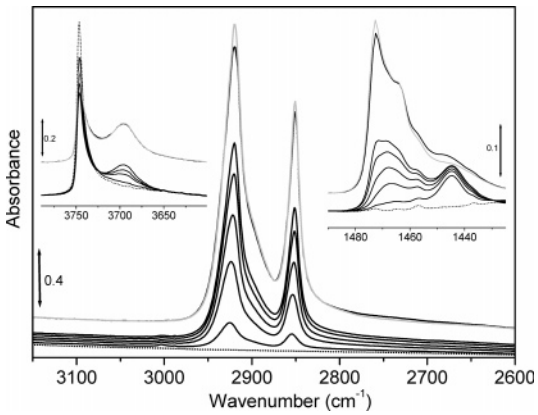

Figure 30. Time-resolved FTIR spectra of ethylene polymerization reaction on a 1.0 wt % Cr/silica sample oxidized at 923 K and CO reduced at 623 K (ethylene pressure = 10 mbar). CH_2 stretching (central part), OH stretching (left inset), and CH bending (right inset) regions are reported. Dashed curve, Cr/SiO_2 sample before contact with ethylene; full lines, polymer growth at increasing polymerization time (last spectrum after 3 min of contact). Gray line: after subsequent adsorption of 30 Torr of CO. Unpublished spectra were obtained by reproducing the experimental procedure described in ref 123.

on the CO-reduced Cr/SiO_2 system at RT and at low pressure. The idea was that short contact times and low pressures should yield short length chains thus allowing the study of the initial steps of polymerization reaction. The IR spectra, reproduced in Figure 30, are characterized by two bands at 2920 and 2851 cm^{-1}, growing with time in a parallel way at nearly constant rates, which are readily assigned to the antisymmetric and symmetric stretching vibrations of CH_2 groups of living polymeric chains growing on the silica external surface. In the bending region (right inset), two bands at 1472 and 1465 cm^{-1} were assigned to the bending modes of CH_2, the former being typical of crystalline PE, the latter being common to both the crystalline and the molten phase.[322] Furthermore, a broad band centered around 2750 cm^{-1} grows at increasing polymerization times. This band disappears upon contact with CO (gray curve in Figure 30) and is accompanied by the increase of the methylene stretching absorptions at 2920 and 2851 cm^{-1}. These features were explained by the assumption of an agostic interaction between the CH_2 groups and the Cr ion.[123,323] In the OH stretching region (left inset), it is evident that the presence of the polymer perturbs an increasing fraction of the silanols. The interaction between the polymer chains and the surface silanols from the spectroscopic point of view resembles a H-bonding interaction,[28] in that a new broad absorption appears at about 3698 cm^{-1}. Note that, assuming that on a dehydroxylated 1 wt % Cr/SiO_2 sample we have about 1 OH/100 $Å^2$ (vide supra section 2.2) and about 0.5 Cr/100 $Å^2$ (vide supra section 4.6), the average distance between an OH group and a chromium center is about 5−6 Å. This means that not very long chains are required to have an agostic interaction.

From Figure 30, it is evident that no absorption due to terminal groups (for instance CH_3 groups) can be seen, even in the early stages of polymerization, although the corresponding modes have extinction coefficients larger than those of CH_2. Analogously, no spectroscopic evidence of carbene species can be observed in the series of spectra. For these reasons, the chains were suggested to have a cyclic structure (which explains the absence of CH_3 groups) and to be very long even after short polymerization times.[123,323] However, it has been argued that as the TOF can be very high (in agreement with refs 133, 319, and 320), the strong absorption of the long polymer in CH_2 stretching and bending regions may mask the weak absorption of initially formed products. In fact, by considering the TOF values estimated before in these conditions (vide supra section 5.1.2.2) the Cr(II) centers can insert from 30 up to 70 ethylene molecules during the time needed to perform a conventional IR spectrum with a high signal-to-noise ratio (60 s). Consequently, the absence of CH_3 groups is not conclusive to establish the cyclic nature of the initially formed species and hence to understand the initial steps of the reaction.

Another important observation has to be made here. In the firsts spectra of the series reported in Figure 30, the two methylenic bands at 2920−2851 cm^{-1} appear slightly asymmetric, with a broad tail at higher frequencies. This feature becomes less evident at increasing polymerization times, since the intensity of the CH_2 bands increases. At least two different explanations can be advanced. (i) It is reasonable to suppose that a methylene group next to a low valent chromium would be influenced by the presence of the chromium itself and thus exhibits a distinct difference in the stretching frequency with respect to that of a methylene group in the middle of the polymer chain. (ii) The second possibility involves the metallacycle mechanism (vide infra section 5.2.4). The CH_2 belonging to the small and strained rings present in the first stages of the polymerization may be characterized by stretching frequencies higher than that of CH_2 belonging to linear infinite polymeric chains. As the polymerization proceeds, the strain of the cyclic structures decreases and the CH_2 groups become indistinguishable from those of long linear chains. On the basis of the data reported in Figure 30, it is not possible to make a choice between the two alternatives, which are not mutually exclusive.

The presence of methylenic bands shifted at higher frequency in the very early stages of the polymerization reaction have been reported also by Nishimura and Thomas.[95] To overcome, in part, the intrinsic nonuniformities of the Phillips catalyst, they prepared a "model" Cr/silica catalyst by grafting Cr(VI) ions from CrO_2Cl_2 onto OH groups of the silica support. As the vapor of CrO_2Cl_2 selectively reacted with vicinal OH groups of the silica surface, the environment of chromium atoms is more uniform, and the activity of the sample for ethylene polymerization is improved. The author reported that the first pair of CH_2 peaks (after 10 s from ethylene dosage) appears at 2930−2860 cm^{-1}; during the next 10 s, the two peaks shift to lower frequencies and become slightly sharper; finally, after 30 s of contact with ethylene, the peaks begin to appear at the normal positions. Dosing C_2D_4 on the polymer formed after

10 s of contact with ethylene (and thus characterized by the peaks at 2930−2860 cm^{-1}), they observed the shift of these peaks at lower frequencies. As new C_2D_4 inserts between the α-carbon of the preexisting polymer chain and the Cr−metal bond, the CH_2 initially neighboring the metal ion is displaced into the middle of polymer chains. On the basis of their results, the authors concluded that the pair of bands at 2930−2860 cm^{-1}, which appear only during the first stages of polymerization, are attributable to CH_2 groups directly bound to the chromium. After the initiation reaction is complete, only the 2920−2850 cm^{-1} pair of bands, due to CH_2 groups in the middle of the chains, grows in intensity. However, no clear evidences can exclude the second explanation mentioned before.

A few years later, Spoto et al.[71,146] reported an ethylene polymerization study on a Cr/silicalite, the aluminum free ZSM-5 molecular sieve. This system is characterized by localized nests of hydroxyls,[25,26,324] which can act as grafting centers for chromium ions, thus showing a definite propensity for the formation of mononuclear chromium species. In these samples, two types of chromium are present: those located in the internal nests and those located on the external surface. Besides the doublet at 2920−2850 cm^{-1}, two additional broad bands at 2931 and 2860 cm^{-1} are observed. Also in this favorable case, no evidence of CH_3 groups was obtained.[71,146] The first doublet is assigned to the CH_2 stretching mode of the chains formed on the external surface of the zeolite. These peaks are extremely narrow if compared with those obtained on Cr/silica. This feature reflects the crystalline nature of the silicalite support and thus the more regular and homogeneous structure of chromium sites. In other words, the amorphous nature of silica support favors the growth of polymers with a much broader MW distribution. The bands at 2931 and 2860 cm^{-1} were assigned by Spoto et al.[71,146] to CH_2 modes of polymeric chains growing on chromium sites located inside the zeolite framework. Because of the spatial hindrance caused by the framework walls, polymeric chains initiated at internal chromium centers cannot grow freely and only very short chains can be obtained. The CH_2 stretching frequencies are shifted with respect to those of the infinite chains formed on the external surface. The presence of these broad bands confirms the observations made before about the asymmetry of the CH_2 bands for ethylene polymerization on the Cr/silica samples. Even if the experiment does not allow to make a choice between the two possible explanations outlined before, it is important to stress here that the species present during the initiation stage of the ethylene polymerization could be characterized by IR manifestations distinguishable from those of the infinite polymeric chains.

5.2. Ethylene Polymerization Mechanism on Cr/SiO_2 Catalyst

5.2.1. Introduction

In the following, a concise review of the literature-proposed models for the ethylene coordination, initiation, propagation, and termination steps on the Phillips catalyst will be presented (section 5.2.1.1). From this discussion, the extraordinary complexity of the species that can be be formed, at least in principle, during the first steps of the ethylene polymerization will be evident. The experimental and mechanicistic deductions on the ethylene coordination step are compared with ab initio calculations (section 5.2.1.2).

5.2.1.1. Ethylene Coordination, Initiation, Propagation, and Termination Steps: A Concise Review. Despite the commercial significance of the polymerization reaction and the amount of related research, which has been reported in the literature, no general agreement concerning the structure of the really active catalytic sites and initial polymerization mechanism exists. It is generally accepted that the catalyst produces PE where the individual polymer molecules have one methyl and one vinyl group.[5,6] The predominant termination mechanism is so suggested to occur via β-hydrogen elimination (see Scheme 15). This mechanism fits well (but not exclusively) with the known chemistry of metal alkyls.[6] Quick-kill experiments have identified the presence of methyl groups during the early stages of reaction but the absence of any vinyl centers; this has been taken as indicative of methyl groups formation during initiation and vinyl group production upon termination.[6,101] It is worth underlining that unfortunately, also these studies do not give details about the length of the chains in the "early stages of reaction".

Scheme 15. Termination Mechanism via β-Hydrogen Elimination

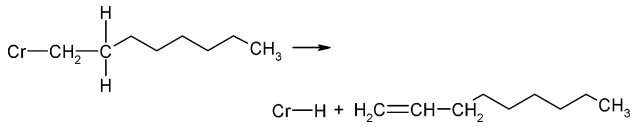

Two types of mechanisms are generally accepted for the propagation of transition metal-catalyzed olefin polymerization systems: the Cossee[325] and the Green−Rooney[326] mechanisms. The Cossee mechanism requires a vacant coordination site on the metal center in the position adjacent to the growing alkyl chain. A monomer molecule π-coordinates to the metal and then inserts into the alkyl chain, which grows of one monomer unit (see Scheme 13). The Green−Rooney mechanism requires two vacant coordination sites at the metal center. The growing polymer chain first eliminates an α-hydrogen to produce a metal−carbene species. An ethylene molecule then coordinates at the remaining vacant site, followed by addition across the metal−carbene double bond in a metathesis type reaction to form a metallacycle species. Reductive elimination causes the ring opening, thus producing an alkyl chain that has been extended by one monomer unit, together with the restoration of the original vacant coordination sites at the metal center.

Although the standard Cossee type mechanism is especially suited for the Ziegler−Natta polymerization processes[1,15,16] (where an alkyl group is preliminarily inserted into the coordination sphere of the transition metal center through the intervention of

Scheme 16. Initiation Mechanisms Proposed in the Literature for the CO-Reduced Cr/SiO_2 Catalyst[a]

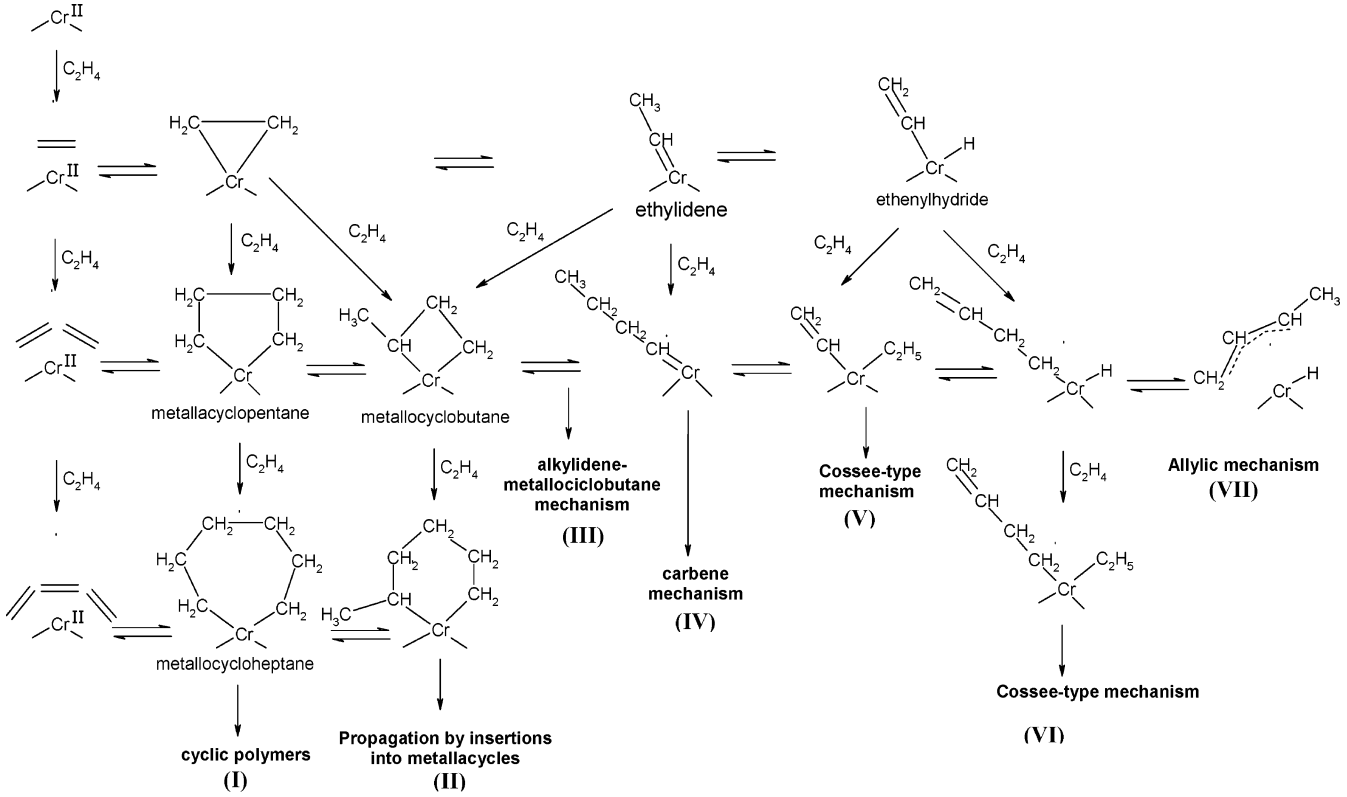

[a] In the vertical direction, the evolution of the initial species upon addition of one ethylene molecule is represented. In the horizontal direction, all of the possible isomeric structures characterized by an average C_2H_4/Cr ratio equal to 1, 2, and 3 are reported.

an activator), the standard Cossee[325] type of propagation mechanism is assumed to be valid also for the Cr/SiO_2 system. The structure of the active species of the working catalyst has therefore often been expected to be the last reported in Scheme 13. In the absence of any activator providing the alkyl group, the main problem is to explain the initiation of the first chain. The crucial point of the initiation mechanism on CO-reduced Cr/SiO_2 system has stimulated a great debate, and several hypotheses have been advanced. In the following, we will describe the single-site mechanisms of this type proposed in the literature, depicted in Scheme 16.

All mechanisms proposed in Scheme 16 start from the common hypotheses that coordinatively unsaturated Cr(II) site initially adsorbs one, two, or three ethylene molecules, via a coordinative d-π bond. Supporting considerations about the possibility to coordinate up to three ethylene molecules come from Zecchina et al.,[327] who recently showed that Cr(II) is able to adsorb and trimerize acetylene giving benzene (see Figure 31).

Concerning the oxidation state of the active chromium sites, it is important to notice that although the Cr(II) form of the catalyst can be considered as "active", as it initiates the polymerization of ethylene without an induction period, +2 is unlikely to be the oxidation state of the propagating site.[6,314,328] Suggestions for mechanisms involving Cr−H or Cr−C bond formation require formal oxidation of chromium, via oxidative addition either of a surface hydroxyl group or of ethylene itself or by rearrangement of π-coordinated ethylene to an alkylidene or

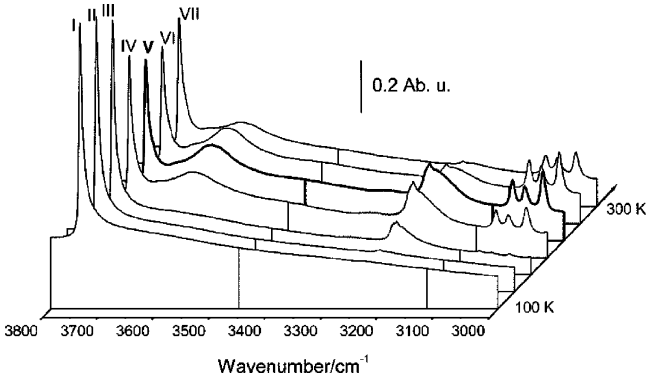

Figure 31. IR spectra in the O−H and C−H stretching regions showing the pressure/temperature-dependent interaction of acetylene on the CO-reduced Cr/SiO_2. Spectra I and II were collected at 100 K before and after C_2H_2 dosage, respectively; spectra III and IV were collected in the 100−200 K range; spectrum V (bold) was collected at 200 K; spectra VI and VII were collected in the 200−300 K range. The triplet at 3092, 3070, and 3038 cm^{-1} corresponds to the typical CH triplet of the aromatic ring of benzene. Reprinted with permission from ref 327. Copyright 2003 Royal Society of Chemistry.

metallacyclic form.[329] In all of these proposed reactions, the metal formally becomes Cr(IV) as it is converted into the active site. These hypotheses are supported by studies of the interaction of molecular transition metal complexes with ethylene.[330,331] Furthermore, it has been noted that the average oxidation state of chromium after polymerization is always grater than +3.[7] Groppo et al.[115] have recently reported that the XANES feature at 5996 eV typical of Cr(II) species is progressively eroded upon in situ

ethylene polymerization (vide supra section 4.4.1, and Figure 23a).

From Scheme 16, the extraordinary complexity of the species that can be formed, at least in principle, during the initiation step can be appreciated. It is important to underline that the number of possible initiation mechanisms can be greater than the 7 indicated in the Scheme 16, because several mechanisms can be found not only coming from top to bottom in a vertical way, but also following a zigzag path. Furthermore, most of the species here reported could be in equilibrium during the early stages of the polymerization reaction, increasing the complexity of the scenario. Nevertheless, all of the mechanisms can be depicted by the more general Scheme 17, where

Scheme 17. General Scheme of the Initiation Step in Ethylene Polymerization on the Phillips Catalyst[a]

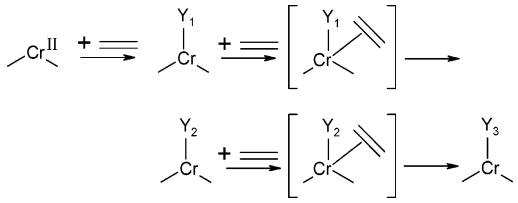

[a] Y_1 can be a $(C_2H_4)_n$ complex containing 1, 2, or 3 coordinated molecules, and the Y_2 species can be one of those reported in Scheme 16.

Y_1 can be a $(C_2H_4)_n$ complex containing 1, 2, or 3 coordinated molecules and the Y_2 species can be the metallacyclopentane (mechanism I), the metallacyclobutane (mechanism II), the ethylidene (mechanism III), or the ethenylhydride (mechanisms IV, V, and VI). By comparing the last scheme with Scheme 13, illustrating the initiation mechanism for Ziegler–Natta like catalysts, it is once again evident that in the Phillips catalyst ethylene itself is able to create an alkyl type activating species or Y_2. After the creation of Y_2 groups (initiation), the mechanism proceeds via insertion of ethylene with formation of the precursor represented in square brackets in Scheme 17. This model explains the first-order behavior with respect to the monomer pressure.[104,140,332–336]

So far, we have considered only mechanisms involving a single Cr(II) ion, because the Cr centers have been found to be isolated, at least for low Cr loadings, vide supra sections 4.3.2 and 4.5.1. However, as anticipated in section 4.6, the presence of Cr(II) multiplets, characterized by a Cr–Cr distance lower than the 10 Å merely calculated on the basis of the chromium percentage and of the silica surface area, cannot be excluded. This means that even if the two chromium sites do not formally constitute a dichromate-like structure (i.e., they are not bridging a common O atom), their proximity may play a role in determining the polymerization mechanism. For example, it can be hypothesized that an eventual cyclic intermediate formed initially (mechanisms I and II in Scheme 16) can also evolve into Cr(II)–$(CH_2)_n$–Cr(II) species, where the chain is anchored to two different chromium centers. This mechanism is quite similar to that proposed in 1981 by Rebenstorf and Larsson,[104] involving the formation of a Cr(II)–$(CH_2)_n$–Cr(II) cycle centered on the two Cr(II) of a dinuclear site. In these conditions, chromium species carry only a linear chain and the system differs from all the structures "double bridged" illustrated up to now. We will consider these possibilities in the following, by reporting also the theoretical results concerning ethylene polymerization on dymeric structure, which must be taken as the starting point to evaluate the possible differences in terms of energetic of the polymerization reaction when dealing with isolated chromium sites or with vicinal chromium species.

5.2.1.2. Ethylene Coordination Step: Theoretical Calculations. The recent ab initio calculations performed by Espelid and Børve[276,337,338] have shown that ethylene may coordinate in two different ways to the reduced pseudo-tetrahedral mononuclear Cr(II) species, either as a molecular complex or covalently bound to chromium. At longer Cr–C distances (2.36–2.38 Å), an ethylene–chromium π-complex forms (structure 3a in Figure 32), in which the four d electrons of chromium remain high spin coupled and the coordination interaction is characterized by donation from ethylene to chromium. Repulsion to Cr3d prevents the formation of an efficient donation bond, so that the CT is very modest and, correspondingly, the BE is a mere −68 kJ/mol. Cr(II) species in a pseudo-tetrahedral geometry (see Figure 13) may adsorb up to two equivalents of ethylene. The two ethylene molecules coordinate in trans position to an ester oxygen ligand, giving rise to a square-planar diethylene complex (structure 3π in Figure 32). The BE of the second ethylene molecule has been calculated to be comparable to the first one (−54 kJ/mol). Taking the loss of entropy into account, the authors concluded that both mono- and diethylene complexes can be present in appreciable amounts. In the case of a pseudo-octahedral Cr(II) site (see again Figure 13), the enthalpy for coordinating a third ethylene molecule is just enough to make up for the entropy loss. Taking the modest exothermicity of the covalently bound triethylene complex into account, a considerable ethylene pressure is probably required for it to form in appreciable amounts, even at RT. Nevertheless, this is not a serious obstacle as far as initiation is concerned, since it needs to take place only once at each site.

On the pseudo-tetrahedral Cr(II) site, only the monoethylene complex was found to undergo a transformation to covalently bound complex, characterized by a shorter Cr–C distance (about 2.02 Å), in which the donation bond is supplemented by back-donation from Cr3d into the π^* orbital of the olefin. This implies that chromium formally gets oxidized to Cr(IV), adopting a triplet spin state. This second binding mode dominates when the coordination site has more flexibility, i.e., at increasing α_{OCrO} bond angle.

Coming to a dinuclear chromium site, Espelid and Børve[338] have computed three different ethylene coordination structures. (i) Ethylene has been found to form a donation bond of −40 kJ/mol to either of the chromium atoms at the dinuclear site (structure 1a in Figure 33). (ii) This structure acts as a precursor to a covalently bound complex, which is realized

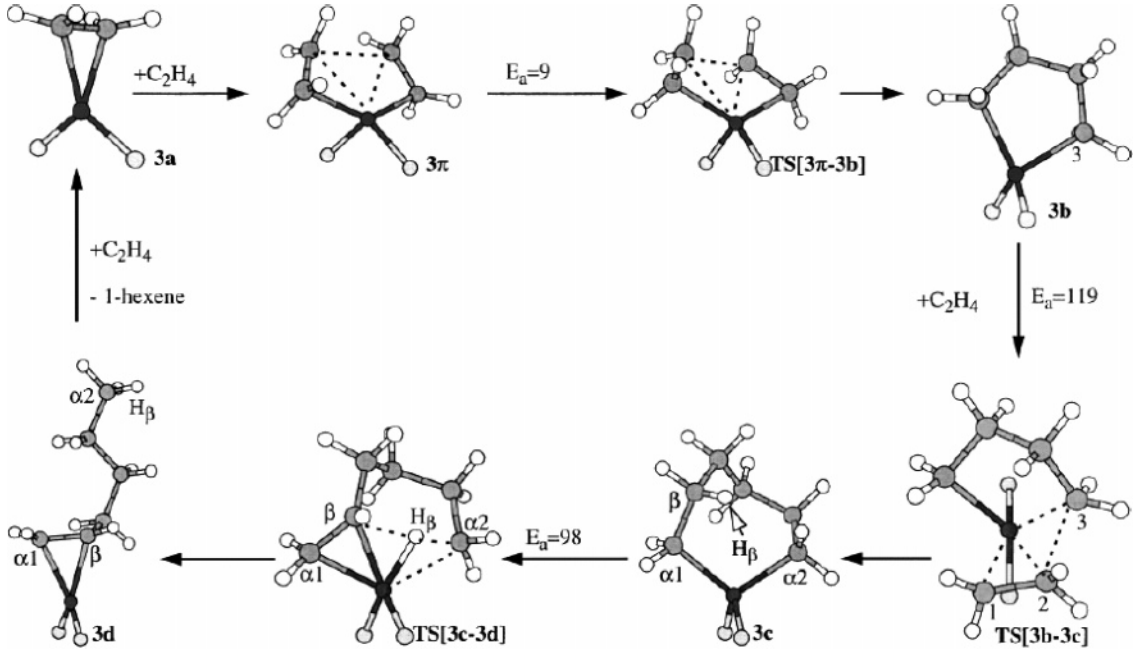

Figure 32. For the tetrahedral $CrO_3Si_2H_4$ mononuclear cluster, here only partially reproduced as a −O−Cr−O− fragment of the ring, the stationary points along the reaction path from a monoethylene complex covalently bound to chromium (structure 3a) to 1-hexene production are reported. The activation energies (E_a) required for reaching the transition states (TS) are reported in kJ/mol. Reproduced with permission from ref 337. Copyright 2000 Elsevier.

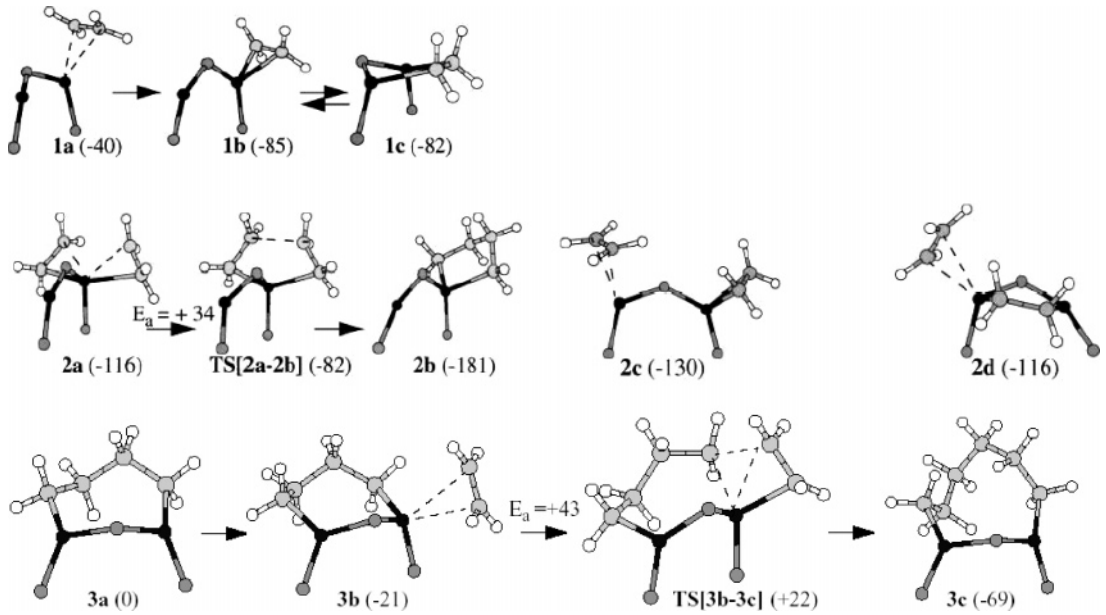

Figure 33. Starting from the same $Cr_2O_4(SiH_2)_2$ dinuclear cluster, here only partially reproduced as a −O−Cr−O−Cr−O− fragment of the ring, different coordinations of one (structures 1a−c) and two (2a,c,d) ethylene molecules, together with chromacyclopentane (2b), μ-butano (3a), and μ-hexano (3c) structures, are reported. Also reported are the TS between structures 2a and 2b (isomerization reaction) and structures 3a and 3c (insertion reaction). As for the latter, also the intermediate coordination of a third ethylene molecule to the preexisting μ-butano complex (3a) is reported in structure 3b. In both cases, the activation energy (E_a) required for the reaction is reported. For structures involving one and two ethylene molecules (first two rows), the number in round brackets represents the stability of the adduct computed with respect to the free reactants. As for the structures reported in the third row, the formation energies have been rescaled by −174 kJ/mol, referring now to structure 3a as the zero level. All energies are expressed in kJ/mol. Adapted with permission from ref 338. Copyright 2002 Elsevier.

at a closer approach of ethylene to chromium (structure 1b in Figure 33). The energy of this covalently bound ethylene complex has been computed to be −85 kJ/mol, relative to free reactants. (iii) A third coordination mode is available, in which ethylene is suspended between the two chromium atoms of the dinuclear species, giving rise to μ-ethano complex (structure 1c in Figure 33). In this structure, which is stable by −82 kJ/mol relative to free reactants, each chromium is in oxidation state III. Starting from the complex 1b in Figure 33, a second ethylene molecule can covalently bound on the same chromium site with an energy of coordination of −31 kJ/mol (structure 2a in Figure 33). Alternatively, a second

ethylene molecule may molecularly adsorb onto the second chromium atom of the dymeric species (structure 2c in Figure 33), with an energy gain of −45 kJ/mol, and then may convert into a covalently bound complex, with a further gain of −9 kJ/mol. Finally, a second ethylene molecule has been found to coordinate molecularly to the μ-ethano complex 1c in Figure 33 with an energy of −35 kJ/mol, resulting in the structure 2d reported in Figure 33.

5.2.2. Cossee Model for Initiation and Propagation

In the following, the experimental results supporting the Cossee model[325] for initiation and propagation will be shown, together with the proposed mechanisms (section 5.2.2.1). In section 5.2.2.2, the theoretical calculations involving the Cossee model will be presented.

5.2.2.1. Experimental Results and Proposed Mechanisms. To solve the problem of the initiation of the first polymer chain, Hogan[5] suggested that polymer chains were initiated by monomer insertion into a Cr−H bond. The resulting metal−alkyl species then propagates via a Cossee mechanism.[325] A prerequisite for this scheme is that there must be a Cr−H bond present prior to the onset of polymerization. Some groups have suggested that surface silanol groups provide a source of additional hydrogen atoms.[333,339] Hydride transfer may occur between a silanol group and a supported Cr(II) ion to yield an O^{2-} species and a Cr(IV)−H bond, into which the first ethylene can insert (see Scheme 18a).[333] Alternatively, it has been proposed that ethylene adsorption directly onto a surface silanol group is followed by its coordination to an adjacent chromium ion along with the migration of a proton from the silanol group onto the metal center (see Scheme 18b).[339]

Scheme 18. Two Initiation Mechanisms Involving Hydrogen Transfer from a Silanol Group (a) Directly to the Cr(II) Ion or (b) to Adsorbed Ethylene

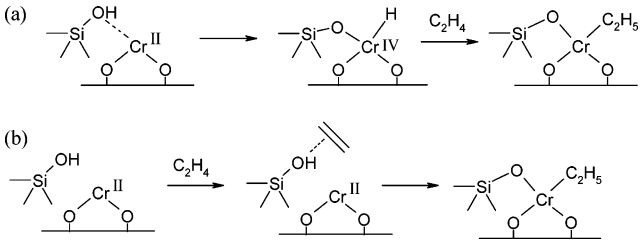

However, the inverse correlation between activity and hydroxyl concentration[6] discussed before (see section 5.1.1.3) and the fact that excellent catalysts can be obtained with systems completely dehydroxylated by chemical means[310] (e.g., by fluorination) make the mechanisms reported in Scheme 18 unlikely. The only viable direction is to hypothesize that the starting structure for polymerization may evolve directly from a reaction between ethylene and the divalent chromium species, as anticipated in Scheme 16.

The initial presence of a Cr−H bond could be explained on the basis of the rearrangement of one ethylene molecule to an ethenylhydridochromium(IV) structure, by means of hydrogen transfer to the metal (mechanisms V and VI in Scheme 16).[140] Ethylene may then be inserted in either the chromium−hydride or the chromium−ethenyl bond, following a classical Cossee mechanism. Alternatively, the chain initiation may arise from the interaction of two adsorbed ethylene molecules on a single chromium site to form an allylic species metal (mechanism VII in Scheme 16).[6,340] The chain would then grow at the chromium−ethenyl or chromium−allyl bond, respectively, and the extra hydrogen would shift to the same atom as a hydride. Such a hydride could also be involved in the initiation of polymerization.

5.2.2.2. Theoretical Calculations Involving the Cossee Model. Espelid and Børve[276] analyzed the hydrogen transfer reaction from a silanol to an ethylene that is already covalently coordinated to chromium, resulting in the formation of a four-coordinated monoalkylchromium(IV) structure. They found that for a pseudo-tetrahedral Cr(II) cluster model (see Figure 13), the proton affinity is about 644 kJ/mol, to be compared with the deprotonation reaction of a silanol group, which requires some 1400 kJ/mol. The feasibility of proton transfer thus depends on mechanisms for stabilizing the cation and anion produced, such as a favorable Madelung potential, polarization of neighboring atoms, and Coulomb attraction between the ions formed. The authors found that the structural flexibility as well as the polarizability of the chromium site may change the hydrogen transfer reaction from being endothermic into being exothermic by about the same amount. Furthermore, they found that hydridochromium(IV) structures have a very low stability.[276]

Concerning the Cossee type propagation mechanism, the ab initio calculation of Espelid and Børve[276,337,338] suggests that insertion into the chromium−hydride bond is easy, while the next insertion presumably takes place in the chromium−ethenyl bond. The structure is a model of a dialkylchromium site, since there is no tendency for the alkenyl to act as a bidentate ligand. Direct insertion into the chromium−ethyl bond was also investigated, and the barrier for insertion was found inconsistent with high catalytic activity toward polymerization. These conclusions are in line with the lack of activity recently reported by Amor Nait Ajjou et al.[308,309] for a dialkylchromium species anchored to silica by two oxygen ester linkages.

5.2.3. Carbene Model for Initiation and Propagation

In the following, the experimental results supporting the carbene model[123,314,317,326,334] for initiation and propagation will be shown, together with the proposed mechanisms (section 5.2.3.1). In section 5.2.3.2, the theoretical calculations involving the carbene model will be presented.

5.2.3.1. Experimental Results and Proposed Mechanisms. Starting from the coordination of only one ethylene molecule, a carbene mechanism has been proposed,[326] via formation of an ethylidene−chromium(IV) species through a metal-catalyzed transfer of hydrogen between the carbon atoms in ethylene (mechanisms III and IV in Scheme 16).

Kantcheva and co-workers[317] suggested a carbene mechanism for the CO-reduced Cr/SiO_2 catalyst on the basis of IR spectroscopy results. They assigned a band at 3016 cm^{-1} in the initial polymerization stage to $\tilde{\nu}_{CH}$ of Cr=CH−R groups. This mechanism does not need an extra hydrogen for initiation. Previously, Ghiotti et al.[123] proposed an alternative carbene mechanism, where the carbene was formed during a reversible hydrogen abstraction from the α-CH_2 groups to a surface oxygen atom. The catalytic cycle was completed by a shift of a proton from the new hydroxyl group backs to its carbon atom. Their support for the carbene species was the observation of a weak broad IR absorption band at about 2750 cm^{-1}, which was assigned to the $\tilde{\nu}_{CH}$ mode of a carbene group in agostic interaction with the active center. Contrary to the former carbene mechanism,[317] the latter[123] avoids hydrogen scrambling, concurring with the conclusion of McDaniel and Kantor[341] that no hydrogen shift occurs during the propagation reaction. Al-Mashta et al.[342,343] presented spectral evidence for the formation of an ethylidene species during the early stages of ethylene polymerization on sulfated anatase; they assumed that these species were formed from ethylene itself without the need for an extra hydrogen atom. Another possibility is that carbene species are generated via the dissociative adsorption of ethylene onto two adjacent chromium sites.[140] A second ethylene molecule then forms an alkyl chain bridge between the two chromium sites; this can subsequently propagate via either the Cossee or the Green−Rooney mechanism.

Recently, Amor Nait Ajjou et al.[307−309] prepared a working catalyst through thermal transformation of dialkylchromium(IV) structure, accompanied by release of the corresponding alkane, as reported in Scheme 19. The stoichiometry of this conversion is

Scheme 19. Thermal Transformation of a Dialkylchromium(IV) Structure Leads to the Formation of a Working Catalyst[307−309]

$$(\equiv SiO)_2Cr(CH_2CMe_3)_2 \xrightarrow{347\ K} (\equiv SiO)_2Cr=CHCMe_3 + CMe_4$$

in accordance with a carbene starting structure. According to this alternating alkylidene/metallacyclobutane mechanism,[314,317,328,334] which has precedent in the ethylene polymerization catalyzed by a Ta(III) neopentylidene complex,[344] chromium alkylidenes may undergo [2 + 2] cycloaddition to give chromacyclobutane intermediates. The latter rearranges to form new alkylidenes via a 1,3-H shift. The slow step in this proposed mechanism is the 1,3-H shift, because the [2 + 2] cycloaddition to Cr(IV) alkylidenes has been shown to be virtually barrierless.[345]

5.2.3.2. Theoretical Calculations Involving the Carbene Model. The theoretical calculation, again by Espelid and Børve,[276,337,338] revealed that the [2 + 2] cycloaddition between an incoming ethylene and the carbene species proceeds without an energy barrier. Conversely, the intramolecular hydrogen transfer between the two α-carbons in the chromacyclobutane moiety, which leads to the isomeric butylidenechromium structure, is associated with high activation energies, irrespective of the α_{OCrO} angle characterizing the site. Therefore, the regeneration of an alkylidene species is considered to be an unlikely propagation mechanism. Nevertheless, we can also suppose that, after the formation of the metallacyclobutane species, the new ethylene monomers insert directly into the metallacycles, generating larger rings.[334] In this way, the regeneration of the carbene functionality is avoided.

5.2.4. Metallacycles Model for Initiation and Propagation

In the following, the experimental results supporting the metallacycles model for initiation and propagation will be shown,[104,140,146,209,346,347] together with the proposed mechanisms (section 5.1.4.1). In section 5.1.4.2, the theoretical calculations involving the metallacycles model will be presented.

5.2.4.1. Experimental Results and Proposed Mechanism. Another possible initiation mechanism that avoids additional hydrogens includes formation of chromacyclopentane by coordinating two ethylene molecules to chromium metal (mechanism I in Scheme 16). As already discussed in section 5.1.4, as Ghiotti et al.[123] did not obtain IR spectral evidence indicating the presence of vinyl or methyl groups in the firsts stages of polymerization, they believed that terminal groups were not present in the polymer chains, i.e., the chains formed cyclic structures with both ends attached to the active site. They proposed two structures, a metallacycle involving only one Cr ion or a PE chain bridged over two nearby chromium ions. The second cyclic structure, first proposed by Rebenstorf and Larsson,[104] was also supported some years later by Zielinski et al.[140]

Support for the metallacyclic structure has recently been obtained from reactions between organometallic chromium complexes and ethylene where five-membered metallacycles are formed.[346] Further insertions may then take place to one of the two chromium−carbon single bonds, thus forming larger metallacycles. The metallacyclic species may propagate as such until termination occurs by hydrogen transfer from one of the β-methylene groups to the opposite α-carbon, thus forming linear polymer chains with one methyl and one vinyl end group as expected.

Several studies report the formation of 1-hexene in the early stages of ethylene polymerization.[308,340,346,347] Jolly and co-workers[346] recently reported that homogeneous chromium-based catalysts may show high selectivity with respect to trimerization of ethylene to 1-hexene. They proposed a mechanism involving chromacyclic intermediates, some of which have been isolated and structurally characterized. The key of this mechanism is suggested to lie in the relative stability toward intramolecular β-H-transfer of the metallacyclopentane ring as compared to the metallacycloheptane ring. Ruddick and Badyal[347] studied the desorbing species on a prereduced Phillips catalyst using mass spectrometry and concluded that only 1-hexene was formed. After the prereduced catalyst was exposed to C_2D_4, only fully deuterated 1-hexene mass fragments were observed, indicating activity without hydrogens from surface silanol groups. The

formation of 1-hexene has been proposed to proceed via metallacyclic intermediates; this involves coordination of two ethylene molecules to form a chromacyclopentane species. Another ethylene molecule then inserts into the ring to produce a highly reactive chromacycloheptane, which can undergo decomposition to form 1-hexene. The formation of 1-hexene ceases as the catalysis goes on, suggesting a change in the occupation of these sites to polymerization. Hence, a site that is active for 1-hexene formation might also turn out to be active with respect to polymerization. If 1-hexene is produced, as suggested, via a chromacyclopentane species, then it is possible that the initiation of polymerization may also proceed via this intermediate.

Recently, Giannini et al.,[331] investigating the chemistry of the calix[4]arene tungsten(IV) system, discovered a variety of olefin rearrangements, which are very close to those often supposed to occur on metal oxides. In particular, the rearrangements of ethylene lead to the formation not only of alkylidenes and alkylidynes but also of metallacycles structures, such as metallacyclopropane and metallacyclopentane. The peculiarities of the oxygen set of donor atoms of a calix[4]arene structure make the comparison with a metalla-oxo surface particularly appropriate.[331,348]

5.2.4.2. Theoretical Calculations Involving the Metallacycle Model. The calculations of Espelid and Børve[276,337] on the isolated pseudo-tetrahedral Cr(II) cluster (see Figure 13) have shown that only a very low barrier (9 kJ/mol) separates the double ethylene π-complex (vide supra section 5.2.1.1 and see structure 3π in Figure 32) from forming a chromacyclopentane structure (complex 3b in Figure 32). In the same way, the triethylene π-complex, which forms on the pseudo-octahedral Cr(II) sites, may undergo ring fusion reactions, either to form a chromacyclopentane structure with a coordinating ethylene molecule or, alternatively, to form a chromacycloheptane species. Rearrangement of the monoethylene complex to either ethylidenechromium or ethenylhydridochromium, on the other hand, is much less favorable for thermodynamical reasons, as described previously (section 5.2.3.2). Hence, it appears likely that according to the quantum mechanical calculations, chromacyclopentane or chromacycloheptane are the dominating initial species at the mononuclear Cr(II) site.

Unfortunately, the calculated energy barrier (119 kJ/mol) for the direct insertion of one ethylene molecule into chromacyclopentane (structure 3b in Figure 32) to give chromacycloheptane (structure 3c in Figure 32) is very high (comparable to that of regeneration of an alkylidene species in the carbene mechanism, vide supra section 5.2.3.2) and seems to be an obstacle in assuming the metallacyclopentane as the probable initiation species. Conversely, the direct insertion of ethylene into a Cr−C bond takes place with a lower barrier in the case of chromacycloheptane, provided that the triethylene π-complex assumes a square-planar conformation.

Decoordination of the olefin from the chromium complex may be expected to compete with the generation of chromacyclopentane/chromacycloheptane derivative only for short 1-alkenes and at low monomer concentrations. The calculated high barrier (219 kJ/mol, which is 100 kJ/mol higher than the barrier toward ethylene insertion) to β-H-transfer within a chromacyclopentane implies that the formation of 1-butene along this path is negligible. Conversely, starting from a chromacycloheptane structure (complex 3c in Figure 32), the corresponding β-H-transfer to form a covalently coordinated 1-hexene (structure 3d in Figure 32) was found to be 98 kJ/mol, a value comparable and even lower than the barrier to direct insertion of a monomer to the ring. This suggests that 1-hexene may be expected to form quite readily in the early stages of polymerization, accordingly with the experimental observations.[347]

From these observations, it seems that the pseudo-tetrahedral Cr(II) cluster could provide an accessible route to the propagation reaction. However, we are faced with the following problems: (i) if the triethylene complex does not assume a square-planar conformation, the free energy of the transition state associated with the propagation step is too high to comply with the observed activity toward polymerization; (ii) pseudo-tetrahedral Cr(II) sites would catalyze the formation of 1-alkenes over polymers; and (iii) the initial formation of chromacycloheptane structure seems to rely on a high partial pressure of ethylene. Although the industrial process uses a high ethylene pressure, this does not seem to be required in order to initiate polymerization without an induction period.[314,334] It is, however, interesting to note that given an external steric factor to keep the four-coordinated Cr(IV) species in a square-planar configuration, high activity toward polymerization would probably result. An oxygen donor is a candidate "steric factor", as suggested by Amor Nait Ajjou and Scott,[334] provided that the donor becomes displaced upon ethylene complexation.

More favorable energetic values have been found when the dinuclear structure is taken into account.[338] The energy gain from fusing two ethylene monomers makes the chromacyclopentane formed on only one of the two chromium atoms of the dinuclear structure (structure 2b in Figure 33) the most stable intermediate. However, the tetrahedral arrangement of ligands around chromium atom renders this structure an unlikely starting point for further ethylene insertion, exactly as happens in the case of the mononuclear structure. On the other hand, the analogous μ-butano structure (structure 3a in Figure 33), formally obtained by allowing one of the α-carbons in the chromacyclopentane structure previously discussed (structure 2b in Figure 33) to migrate to the adjacent chromium center, is essentially isoenergetic with the chromacyclopentane species attached to only one of the chromiums belonging to the dinuclear site. This structure, which displays two Cr(III)-alkyl coordination sites at a distance of 3.07 Å, has been computed to have a stability of −174 kJ/mol relative to isolated monomers and naked cluster.

The coordination energy of an ethylene monomer to either of the resulting trivalent chromium centers in the μ-butano structure described so far (structure 3a in Figure 33) is a mere −21 kJ/mol, resulting in

the adduct reported in structure 3b in Figure 33. The energy change associated with extending the bridging alkano ligand from four to six carbon atoms (thus passing from a seven-membered ring, structure 3a in Figure 33, to a nine-membered ring, structure 3c in Figure 33) has been computed to be −69 kJ/mol, with a barrier for the insertion of 43 kJ/mol relative to the π-complex (structure 3b in Figure 33).

By comparing the theoretical results dealing with the metallacycle model obtained in the two cases of a mononuclear[276,337] and a dinuclear[338] chromium site, it seems that the dinuclear site provides a more viable starting structure for polymerization. The calculated energy barrier for the direct insertion of one ethylene molecule into chromacyclopentane to give chromacycloheptane in the case of the mononuclear chromium site (119 kJ/mol, see Figure 32) is almost three times greater than that calculated to extend the bridging alkano ligand from four to six carbon atoms in the case of a dinuclear chromium site (43 kJ/mol, from structure 3a to 3d in Figure 33). These results demonstrate that the energy profile along a polymerization path is greatly affected by the structure of the chromium site (vide infra section 5.3.2). From the review of the overall works of Espelid and Børve,[223,276,337,338] it can be concluded that the energy barriers involved in the polymerization reaction via metallacycle mechanism may be lowered by the proximity of two chromium sites, even if they do not constitute a formal dinuclear site.

5.3. Is It Possible to Identify the Polymerization Mechanism? Recent Results and Reflections for the Future

5.3.1. C_2H_4 Initiation Mechanism as Investigated by IR Spectroscopy: More Recent Results

Up to now, we have presented the initiation mechanisms and the precursor structures proposed in the literature in the past decades. Unfortunately, experimental studies have failed in providing conclusive evidence that any of these species are present on the working catalyst's surface. As already mentioned before (section 5.1.2.2), the fraction of active sites is invariably low, making spectroscopic identification very difficult.[5] On the other hand, any measurement of the bulk properties of the catalyst (for example, its average oxidation state) yields a result which is not necessarily of relevance to the active sites.[193] However, mechanistic tests have been used to rule out certain propagation mechanisms. As an example, a role of surface protons in forming an initiating Cr−H bond is doubtful since high activities are found for highly dehydroxylated and fluorinated silica supports.[6,310] An alternating alkylidene−metallacycle mechanism was considered improbable because of the failure to observe isotope scrambling during the polymerization of labeled ethylenes.[341] However, the failure to observe methyl chain termination during polymerization is inconclusive for a metallacycle mechanism, since, if the TOF is high, their abundance is very low as compared to the methylene backbone units (vide supra section 5.1.4).[123,318]

The high polymerizing rate of a small fraction of low coordinated chromium sites represents the major obstacle for the study of the initiation step. This means that, to be able to identify the firsts species in the polymerization reaction using a spectroscopic technique the time needed to perform the measure must be shorter than the short lifetime of the very active species formed during the initiation. Progresses in this direction can be achieved either by improving the time response of the instrument or by finding means able to slow the reaction speed, or both. Furthermore, the spectroscopies adopted must be sensitive because it should be potentially able to identify species formed on a very low fraction of sites (for instance in the 0−10% interval).

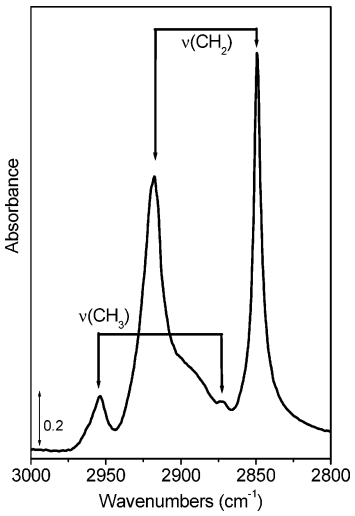

Figure 34. IR spectrum of tritriacontane ($CH_2/CH_3 = 31/2$). Unpublished spectrum.

Among all of the spectroscopic techniques here reviewed, IR spectroscopy is the most versatile and has been surely the most used in the attempt to identify the precursors of the ethylene polymerization, being able to directly discern between the vibrational manifestations of different species even under operando conditions. IR spectroscopy is, in principle, able to distinguish between all of the structures illustrated in Scheme 16. In this respect, we briefly focus the attention on the fact that, among all of the proposed mechanisms, the only one not involving species characterized by methyl groups is the metallacycle mechanism (see path I of Scheme 16). In this case, in fact, all of the initiation species are characterized only by methylenic groups, belonging to rings of increasing dimension. Being the stretching modes of methyl groups almost two times more intense than CH_2 stretching modes, we expect that methyl groups, if present, should be visible in the first stages of polymerization, when the chain length is modest, i.e., the ratio CH_2/CH_3 is relatively small. In Figure 34, the spectrum of tritriacontane, a hydrocarbon with a linear chain characterized by a $CH_2/CH_3 = 31/2$, is reported. It is evident that, even when the ratio CH_2/CH_3 is greater than 15, the methyl groups are perfectly visible by IR spectroscopy (bands at 2954 and 2849 cm^{-1}) and not hidden by the CH_2 bands.

We have already discussed the time-resolved IR spectra of ethylene polymerization reported by Ghiotti et al.[123] and by Spoto et al.[71] We have also seen

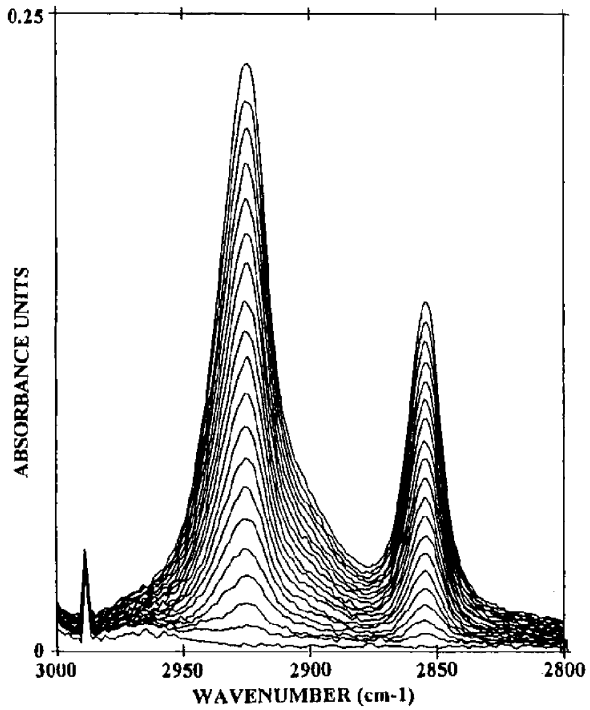

Figure 35. Fast time-resolved spectra of the ethylene polymerization reaction on a CO-reduced Cr/SiO_2 sample. Initial ethylene pressure, 10 Torr. Last spectrum after 15 s. Reprinted with permission from ref 146. Copyright 1994 Elsevier.

that traditional IR measurements failed in the determination of the species formed in the firsts stages of the polymerization reaction. In 1994, Zecchina et al.[146] tried to overcome the problem of very fast reaction speed by collecting fast time-resolved spectra of ethylene polymerization. Fast FTIR spectra can be obtained by reducing the spectral resolution (proportional to the movable mirror translation) and by collecting the interferograms without performing the FT. The latter will be performed at the end of the experiment.[146,349−353] The sequence of spectra collected every 0.75 s is reported in Figure 35; the last spectrum was collected after only 15 s from the ethylene injection into the cell. Following the considerations outlined before about the number of ethylene molecules inserted per second at each chromium center at RT and pressure of about 0.02 atm (not far from one molecule per second), the detection of the presence of alkyl groups in the initiation stage was conceivable. From the sequence of spectra reported in Figure 35, it is evident that even if the time used to perform the measure was extremely short, the spectra did not show evidence of alkyl precursors formation. From this experiment, the metallacycle hypothesis received strong (but not fully conclusive) support.

A different approach to identify the species formed during the initiation step was followed by Vikulov et al.[354] They decreased the rate of ethylene polymerization by injecting sequential small doses of ethylene (5×10^{17} molecules, corresponding approximately to 50% of the total number of chromium atoms in the sample) into the IR cell. By decreasing the reaction rate in this manner, the possibility of observing spectra relevant to the initial step of the

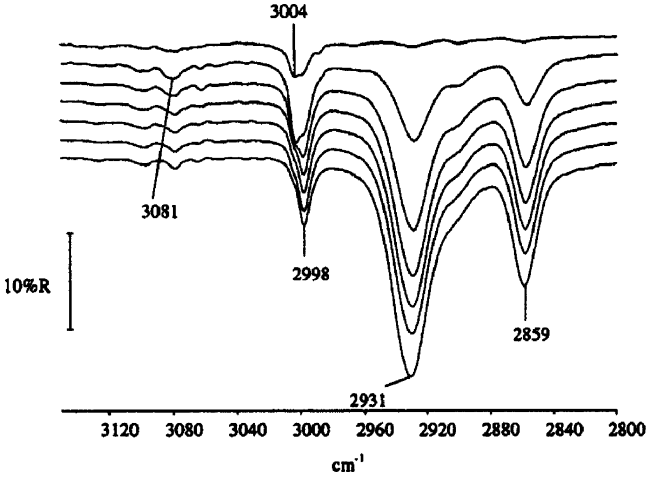

Figure 36. DRIFT spectra of the ethylene polymerization reaction on CO-reduced Cr/SiO_2 sample in the $\tilde{\nu}_{CH}$ region, recorded every 20 s after one large ethylene injection. Reprinted with permission from ref 318. Copyright 1998 Elsevier.

polymerization was improved. Nevertheless, the authors observed only π-adsorbed ethylene on Cr(II) centers at the beginning of the reaction, whose stretching and bending modes give rise to two bands at 3000 and 1448 cm^{-1}. A year before, Ghiotti et al.,[124] studying the coadsorption of CO and ethylene on the same system, observed similar bands at 3006 and 1445 cm^{-1}, the shift in the ethylene frequencies being caused by the perturbation of CO. Considering the fact that the spectrum of the polymer observed after introducing the very first doses of ethylene and that of polymer formed on the same catalyst at much higher initial pressure of ethylene were quite similar, the authors concluded that the number of active sites on the surface was very low and that this (together with the high TOF) was the reason why no indications of any initialization step were observed.

A few years later, Kantcheva et al.[317] employed the sequential injection of even smaller doses of ethylene than those reported by Vikulov et al.,[354] enabling the monitoring of the reaction path in even more detail. A weak band at 3016 cm^{-1} was inferred to be due to $\tilde{\nu}_{CH}$ of an ethylidene species, formed directly from π-adsorbed ethylene molecules without the need of a hydrogen donor. During the early stages of polymerization, the polymer chains were suggested to have a linear structure with a methyl group and a carbene group at opposite ends. No sign of $\tilde{\nu}(CH_3)$ modes was however observed. It was suggested that the polymer chain grows by insertion of ethylene molecules into the Cr=C bond, accompanied by the formation of a metallacycle compound, following an alternate alkylidene−metallacycle mechanism (see path III of Scheme 16).

DRIFTS has been used by Bade et al.[318] to study the reduced Cr/SiO_2 polymerization catalyst during reaction with ethylene at RT and at 373 K. The method was found to give excellent signal-to-noise ratio in the $\tilde{\nu}_{CH}$ region, together with much easier sample preparation as compared to transmission methods. The DRIFT spectra in the $\tilde{\nu}_{CH}$ region recorded every 20 s after one large ethylene injection are shown in Figure 36. When ethylene is added to

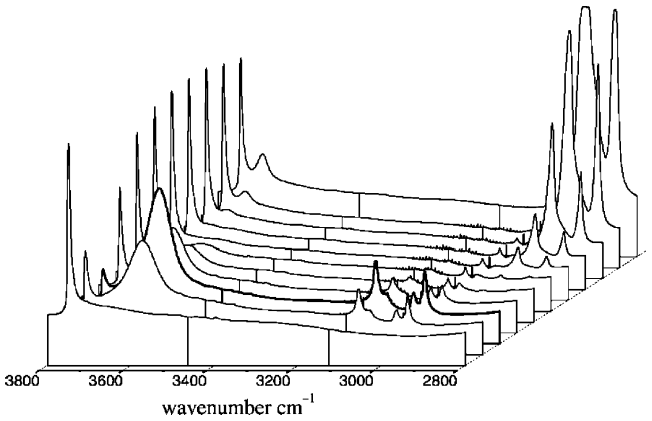

Figure 37. Temperature-resolved ethylene polymerization on CO-reduced Cr/SiO_2 catalyst in the 100−300 K range in the O−H and C−H stretching regions. The first spectrum refers to the sample at 100 K prior to contact with ethylene. Successive spectra refer to the temperature (and pressure) increase. The last but two spectrum refers to the sample at 300 K, the last but one spectrum has been recorded after 15 min at 300 K, and the last one was recorded after subsequent evacuation at 300 K. Adapted with permission from ref 209. Copyright 2003 Elsevier.

the catalyst at ambient temperature, two kinds of coordinated ethylene were detected. Relatively stable ethylene−chromium complexes were formed prior to polymerization, which are stable during the polymerization and give bands at 2998 cm^{-1} [assigned to $\tilde{\nu}_s$(CH)[317,354]] and at 3079 and 3098 cm^{-1}, assigned to $\tilde{\nu}_{as}$(C−H).[318] A "transient" band at 3004 cm^{-1} was assigned to an ethylene coordinated to chromium in a labile position before incorporation in the PE chain. This position could either be on active chromium sites or on inactive sites close to an active chromium site. The intensity of this band is reduced simultaneously to the growth in the intensity of bands coming from the polymer formed. A weak band around 2663 cm^{-1} was suggested to be an overtone or combination band of CH_2 deformation modes of coordinated ethylene. Saturation of the catalyst with a nonpolymerizing olefin such as isobutene showed that isobutene coordinates in a similar manner as ethylene does. Again, no peaks that can be assigned to chromium−carbene fragments or to methyl groups were observed.

Very recently, Bordiga et al.[209] have designed and performed new experiments allowing to collect FTIR spectra at low temperature, which is an experimental condition where the polymerization rate is so highly depressed to hopefully allow the detection of the species formed in the initiation stage. Time-, pressure-, and temperature-dependent FTIR spectra collected in the 173−300 K range on the CO-reduced Cr/SiO_2 catalyst in ethylene atmosphere (see Figure 37), showed, at the lowest temperatures (i) the adsorption of ethylene on silanols and (ii) the formation of C_2H_4 π-complexes, characterized by vibrational manifestations very similar to those reported by Bade et al.[318] (bands at 3072 and 3005 cm^{-1}). The successive increment of temperature (173−300 K range) did not affect the Cr(II)···C_2H_4 adducts but resulted in the slow and progressive start of the polymerization reaction. Even if the chain growth was extremely lowered, FTIR spectra, although successful in showing clearly the spectroscopy of molecular precursors, did not show any peculiarity that could be associated to well-defined initiation species (for instance containing CH_3 groups).

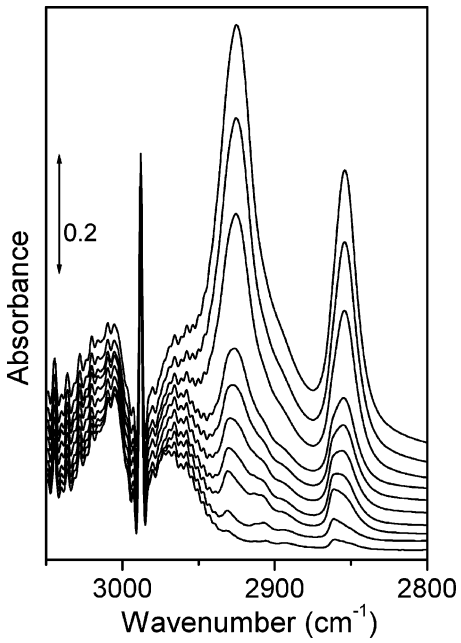

Figure 38. Temperature-resolved ethylene polymerization on CO-reduced Cr/SiO_2 catalyst in the 100−300 K range in the presence of preadsorbed CO. Reprinted with permission from ref 209. Copyright 2003 Elsevier.

In the same work,[209] the speed of the polymerization reaction was further on slowed saturating the catalyst with CO before ethylene injection. In the 100−130 K range, ethylene formed mixed Cr(II)···(CO)(C_2H_4) complexes, characterized by a sharp band at 2175 cm^{-1} in the CO region (vide supra the similar experiment performed at RT and reported in Figure 17) and by a shift in the symmetric C−H stretching band at 2998 cm^{-1} upward to about 3001 cm^{-1}.[318] Increasing the temperature, ethylene gradually displaced CO and the polymerization started but with a rate much slower than on samples without CO pretreatment. The low reaction speed allowed the observation of new features that could not be evidenced in the usual polymerization experiments (see Figure 38), presumably because the reduced rate allowed the observation of shorter olygomeric chains.[209] At the lowest reaction times, the $\tilde{\nu}(CH_2)$ peaks were located at 2931 and 2860 cm^{-1}, i.e., at values distinctly different from those observed in the normal experiments (2920 and 2851 cm^{-1}). Only after prolonged contact time these new components were overshadowed by the usual bands of the long polymeric chains. The study of the reaction in the presence of a poison probably allowed the observation of the $\tilde{\nu}(CH_2)$ modes of the first products of the polymerization.

New improvements have been recently reached by applying the same approach of the experiment reported in Figure 37 (polymerization at increasing temperature from 77 K to RT) to the Cr/SiO_2−aerogel system described previously (vide supra section 4.3.2). As already discussed in that point, the SiO_2−aerogel support is completely transparent in the IR region,

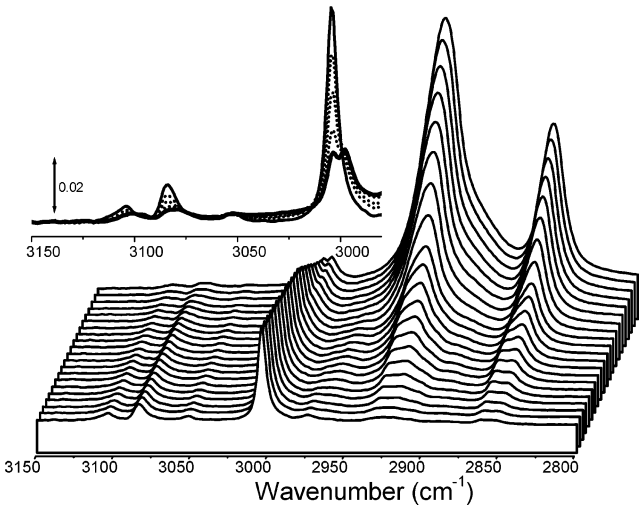

Figure 39. Temperature-resolved ethylene polymerization on CO-reduced Cr/SiO_2-aerogel catalyst in the C−H stretching region. The inset reports a zoom on the C−H stretching region associated with the ethylene π-coordinated to Cr(II). Unpublished results were shown by Zecchina in the keynote lecture "Ethylene Polymerization Mechanism on the Cr/SiO_2 Phillips Catalyst: 30 Years of Scientific Debate, Recent Results and Perspectives" presented at EuropaCat VI, Innsbruck, Austria, August 31−September 4, 2003.

so that it is possible to work in transmission mode with very thick pellets. Furthermore, it presents a surface area higher than that of common aerosil supports. It is so clear that the adoption of SiO_2−aerogel as a support allows to increase the number of chromium sites crossed by the IR beam by more than 1 order of magnitude, thus increasing the probability to detect the very weak bands such as those expected from the species present in the first stages of the reaction. The results of this approach are shown in Figure 39. The time evolution of the spectra in the CH_2 stretching region is basically the same observed in the case of the standard Cr/SiO_2−aerosil sample (Figure 37), thus confirming that the two systems are perfectly comparable on the catalytic side (vide supra section 4.3.2). Nevertheless, two differences are immediately evident: (i) the vibrational manifestations of C_2H_4 π-bonded to chromium sites (bands at frequencies higher than 3000 cm^{-1}, see inset in Figure 39) are enormously enhanced in the case of the Cr/SiO_2−aerogel; (ii) in the first stages of the polymerization, two new peaks located at 2931 and 2860 cm^{-1} are clearly evident, analogously to those shown for the first time by Bordiga et al.,[209] when polymerization was further on slowed by CO poisoning (see Figure 38).

Starting with discussing the first point, an intense and almost symmetric band at 3004 cm^{-1} appears at the lowest reaction times, accompanied by two components at 3084 and 3104 cm^{-1} (see black full line curve in the inset in Figure 39). The intensities of these bands gradually decrease as polymerization proceeds and new bands appear at 2998, 3078, and 3096 cm^{-1} (see bold line curve in the inset in Figure 39). Some of these bands have been previously reported also by Bade et al.[318] and by Bordiga et al.[209] and assigned to the $\tilde{\nu}_s$(C−H) and $\tilde{\nu}_{as}$(C−H) of an ethylene molecule π-bonded to Cr(II) species. As discussed before, Bade et al.[318] assigned the band at 3004 cm^{-1} to an ethylene coordinated to a Cr site in a labile position and the bands at 2998, 3079, and 3098 cm^{-1} to a more stable ethylene−chromium species. The evolution of the spectra as a function of the ethylene pressure, reported in Figure 39, suggests another interpretation. The band at 3004 cm^{-1} (and its partners at 3084 and 3104 cm^{-1}) belongs to the $\tilde{\nu}_s$(C−H) of a diethylene π-bonded complex, which survives only until the monomer pressure is sufficiently high. It is worth noticing that the intensity of these bands remains quite unaltered during the first stages of the polymerization reaction, suggesting that these bands are related with spectator species, i.e., with Cr sites not involved in the polymerization. As the polymerization reaction proceeds, and the monomer pressure decreases, the set of bands at 3004, 3084, and 3104 cm^{-1} evolves in the new set of bands at 2998, 3078, and 3096 cm^{-1}, which belong to a mono-ethylene complex.

Coming to the second point, it is clear that the use of the SiO_2−aerogel support strongly enhances the possibility to detect the initial species (compare Figure 39 with Figure 37, where the two bands at 2931 and 2860 cm^{-1} were not present, even if the experimental setup was the same). Furthermore, the fact that the same "anomalous" CH_2 bands reported in the case of a polymerization conducted in the presence of CO (see Figure 38) appear also in the absence of CO poison, excludes that their origin is in some way due to the presence of CO and confirms the attribution in terms of intermediate species.

In conclusion, the new experiment discussed above demonstrates that SiO_2−aerogel materials may be interesting supports for metal-based catalysts, and in particular for Cr/SiO_2 catalyst, to improve the spectroscopic investigation of both the supported metal structure and of the catalytic activity.

5.3.2. General Considerations about the Possibility to Identify the Precursor Species

After having presented the more recent results in the field of the identification of the polymerization mechanism on the Phillips catalyst, a reflection on the possibility to identify the precursor species is now required. The transition from the "reduced Cr(II) + coordinated ethylene" system toward the "polymerized" system surely passes through several intermediates states, whatever is the followed reaction path. Returning to Scheme 16, we can imagine that each of the several hypothesized intermediate states is characterized by its own equilibrium energy and is separated from the adjacent states by specific energy barriers. We have tried to represent pictorially this concept in Figure 40, where we have transformed the complex pattern of reaction paths into a network of potential "holes and barriers", by substituting each intermediate species with a potential hole of different depth separated by adjacent intermediate species by specific energy barriers of different heights. Once the first ethylene molecule is adsorbed on the Cr site, it falls in the potential hole represented at the crossing of the first row and the first column of Figure 40, forming a π-bonded complex (vide supra section 5.2.1.1). This precursor will then evolve to a first

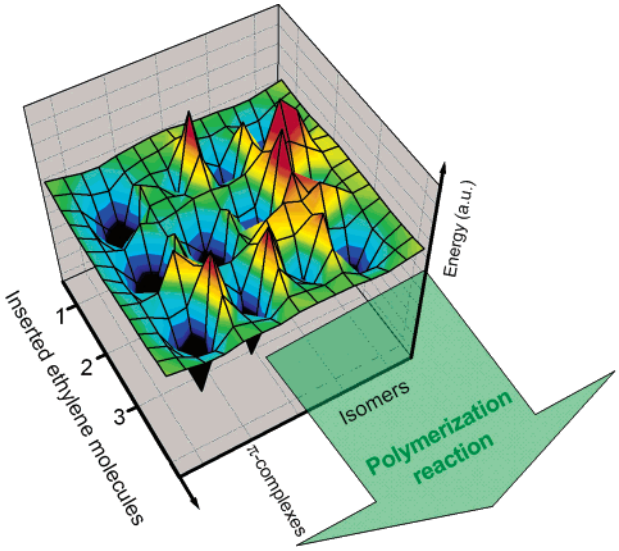

Figure 40. Qualitative representation of the energetics of the initiation mechanisms reported in Scheme 16. The intermediate species have been represented by a potential hole of different depth, mutually separated by specific energy barriers of different heights. Energy values for both holes and barriers are arbitrary in depth and height and have been coded in a colored scale from dark blue to red coming from negative to positive values. Coming from top to bottom, the insertion of one, two, and three ethylene molecules has been represented. From left to right, the π-complexes and the possibile isomeric structures characterized by an average C_2H_4/Cr ratio equal to 1, 2, and 3, respectively, have been represented by potential holes. The polymerization reaction takes place upon addition of further ethylene molecules, as suggested by the green arrow.

chemisorbed species represented by one of the potential holes in the first row (colum higher than one). It is then reasonable to imagine a living equilibrium between the occupancy of such holes according to hole depths and ratios between barrier height and thermal energy (kT). This equilibrium condition holds till a second ethylene molecule is adsorbed on the site. When this happens, the system jumps into a hole of the second row (column higher than one) and a new living equilibrium occurs and so on. From jump to jump, the system passes from the initial phases illustrated in Figure 40 to the proper polymerization reaction, represented by the green arrow. According to the experiment of Zecchina et al.[327] (see Figure 31), it is of course also possible to imagine the adsorption of two or three ethylene molecules on the same Cr site before the system is able to evolve into a chemisorbed state. According to this hypothesis, the starting point will be located in the hole in the second or third row, first column.

The identification, with spectroscopic methods, of a precursor species in the first steps of the reaction is favored when it lies in a hole of the potential energy profile and if the transition to the following state is governed by a relatively high energy barrier. Unfortunately, such intermediate species, being the less reactive, are also the less relevant in the transition from oligomerization to polymerization. We are thus in the presence of an intrinsic and unavoidable contradiction as the spectators will always be more easily detected than the relevant intermediate states.

It is reasonable to suppose that chromium sites possessing different structures are characterized by different energy profiles so that groups of different plots such as that reported in Figure 40 should be considered. This is confirmed by the theoretical calculation of Espelid and Børve,[223,276,337] who demonstrated that the energy barrier associated with the elongation of the bridging alkano ligand in a chromacycle structure from four to six carbon atoms is greatly different when dealing with a mononuclear or with a dinuclear chromium site (compare Figure 32 with Figure 33). Changes in the energy profile may occur even by passing from a Cr_A^{II} to a Cr_B^{II} mononuclear site (vide supra section 4.2.1.1 for the nomenclature definition). This means that, even if the reaction mechanism is the same, intermediate species, which can be observed on one site, could not be detected on a site with a different structure (because less energetically stable and/or separated from the successive intermediate by a less intense energy barrier). Furthermore, the same energy profile can be run along the reaction path with a different velocity at different reaction temperatures, the temperature being one of the factors which governs the overcoming of the energy barriers.

On the basis of these observations, it is clear that the challenge to identify the species present in the first stages of the polymerization reaction, if from one side, can be faced with the development of new strategies and the adoption of more sensitive characterization methods (as described in section 5.3.1) from the other side is also unavoidable linked to energetic and kinetic factors. These final considerations are not to be taken in a pessimistic way. We must only be aware that, sometimes, the impossibility to identify an intermediate species could be a consequence of the kinetics of the process and that a possible way to overcome the problem may lie with the ability to find a way to change the kinetic factors that govern the entire reaction. The problem of identifying, by means of IR spectroscopy, intermediate transient species in chemical reactions, just mentioned here in section 5.3.2 for the Phillips catalyst, has been treated in detail, using a large number of examples, in ref 355.

6. Open Questions and Perspectives

In sections 1−5, we have illustrated in detail the efforts made in the past decades to discover the structure of the active sites of the Phillips catalyst and to try to solve the mystery of the initiation step, which is unique among the polymerization catalysts because it proceeds without activators. From the survey of the literature, it can be safely concluded that many progresses have been achieved in the understanding of the surface structure and catalytic activity of the Cr/SiO_2 system. In particular, concerning the surface structure, the points appear now firmly established as follows. (i) Preliminary knowledge of the surface structures present on dehydroxylated silica is mandatory in order to understand the Cr/SiO_2 system, since the silica support plays an important role in determining the properties of chromium structures. (ii) The comparison with the

organometallic chemistry of Cr(II) complexes is vital for understanding the processes occurring at the surface of the Cr(II)/SiO_2 system. (iii) On Cr(VI)/SiO_2 diluted samples (up to 1 wt % Cr loading), the predominant anchored species are monochromates. (iv) The CO-reduced system is suitable for structural and mechanistic investigations. (v) On a CO-reduced diluted sample, chromium is prevalently isolated and in the divalent state. The average Cr(II)−Cr(II) distance, in the case of an up to 1 wt % Cr(II)/SiO_2 system, is about 10 Å. (vi) Because of the amorphous character of the support, different families of Cr(II) structures however are present on the surface, which can be identified via accurate spectroscopic methods and classified into three distinct families (Cr_A^{II}, Cr_B^{II}, and Cr_C^{II}). (vii) The vast majority of Cr(II) sites is highly coordinatively unsaturated and can adsorb up to three CO, three NO, and three acetylene molecules. (viii) The relative proportion of the different Cr(II) sites can be altered by means of suitable activation procedures. If a high temperature treatment is performed after reduction, a substantial fraction of low coordinative sites is transformed into more shielded species. (ix) The use of appropriate doping atoms (such as Ti) is a reliable mean to tune the nuclearity of surface Cr species.

As far as the polymerization activity is concerned, results have been achieved as follows. (i) The activity of different Cr(II) sites toward polymerization is distributed in a wide interval (the more shielded species being probably inactive). In other words, the heterogeneity of chromium structures is reflected in a heterogeneity of activity behavior. (ii) The initiation step proceeds by ethylene coordination on Cr(II) with the formation of d-π complexes. (iii) The residual hydroxyl groups present on the silica surface do not play a direct role in the initiation phase. (iv) Ab initio modeling is starting to play a fundamental role in the elucidation of surface structures and of adsorption, initiation, and polymerization mechanisms. (v) The use of appropriate doping atoms (such as Ti) is a reliable mean to tune the polymerization reaction in terms of induction time, activity, and morphology of the resulting polymer.

Despite all of these achievements, several questions still remain unanswered. In particular: (i) The precise structure of the three different families of Cr(II) sites (Cr_A^{II}, Cr_B^{II}, and Cr_C^{II}) on the CO-reduced catalysts is still under investigation. Furthermore, it cannot be excluded that a minor fraction of Cr(II) sites is less distant than 10 Å, even if they formally do not constitute a dymeric structure bridging a common O atom. (ii) The precise structure and relative abundance of the most active sites are still unknown, probably because they are present in low concentrations. (iii) The relation between the structure of Cr(II) sites and the TOF is still an open problem. (iv) The role of surface strain in Cr(II)/SiO_2 system activated at high temperature in influencing the activity is not completely clarified, even if the more recent information suggests that the effect is not negligible. (v) The determination of the species formed in the initiation steps is still at the infancy.

From the comparison of the achievements and open problems, new perspectives are emerging. In particular, the results collected in the review demonstrate that the synergic use of different and complementary spectroscopic techniques can provide more and more detailed information about the structure of chromium on the amorphous silica surface. The challenge for the future is the identification of the precise relationship between catalyst activation procedure, structure of chromium sites, and catalytic activity. Pursuing this goal, new, more sensitive characterization methods and more finalized strategies for the study of the really active sites must be adopted, not only from an experimental but also from a theoretical point of view. The more extended use of in situ spectroscopic investigations under conditions as close as possible to the real catalytic conditions is the first logical step. Among the new strategies, the intelligent modification of silica support via introduction of foreign atoms (like Ti, Zr, etc.), aimed to modify the electronic properties of Cr, or the use of crystalline silica support, aimed to modify the surface strain of Cr species and to reduce the surface heterogeneity, can represent innovative paths. These new studies are encouraged by the fact that most of the open problems mentioned above are not characteristic of the Cr/SiO_2 system. In fact, similar questions are commonly encountered for the vast majority of catalysts, since direct experimental observation of working centers and intermediates is invariably absent in the literature. This is the reason that the description of the achievements obtained in the characterization, of the encountered problems and of the perspectives, is of general validity.

7. Abbreviations

AFM	atomic force microscopy
amu	atomic mass unit
B3-LYP	hybrid Hamiltonian developed by Becke, Lee, Yang, and Parr
BE	binding energy
CM	classical mechanics
C_p	cyclopentadienyl
CT	charge transfer
DFT	density functional theory
DRIFTS	diffuse reflectance Fourier transform spectroscopy
DRS	diffuse reflectance spectroscopy
E_a	activation energy
EDS	energy dispersive X-ray spectroscopy
EPMA	electron probe microanalysis
EPR	electron paramagnetic resonance
EXAFS	extended X-ray absorption fine structure spectroscopy
FT	Fourier transform
FTIR	Fourier transformed infrared spectroscopy
FWHM	full width at half maximum
GPC	gel permeation chromatography
HDPE	high density polyethylene
HOMO	highest occupied molecular orbital
I	Cr cluster model characterized by an α_{OCrO} = 135°, from refs 190 and 191
IR	infrared
L	weak ligand
LDPE	low density polyethylene
LLDPE	linear low density polyethylene
LUMO	lowest unoccupied molecular orbital

MAO	methylalumoxane
MD	molecular dynamic
MI	melt index
MO	molecular orbital
MW	molecular weight
NIR	near infrared
NMR	nuclear magnetic resonance
O	cluster model of Cr in a pseudo-octahedral symmetry ($\alpha_{OCrO} = 180°$), from refs 190 and 191
P_{CO}	CO equilibrium pressure
PE	polyethylene
PIXE	proton-induced X-ray emission
QM	quantum mechanics
RT	room temperature
SEM	scanning electron microscopy
SIMS	secondary ions mass spectroscopy
SQUID	superconducting quantum interference device
T	cluster model of Cr in a pseudo-tetrahedral symmetry ($\alpha_{OCrO} = 116°$), from refs 190 and 191
T	temperature (in K)
TOF	turnover frequency
TPD	temperature-programmed desorption
TPR	temperature-programmed reduction
TS	transition state
UV-vis	ultraviolet−visible spectroscopy
XANES	X-ray absorption near edge structure spectroscopy
XAS	X-ray absorption spectroscopy
XPS	X-ray photoelectron spectroscopy
XRD	X-ray diffraction
$g_{A-B}(r)$	pair distribution function for atoms A and B
α_{OCrO}	angle O−Cr−O
α_{SiOSi}	angle Si−O−Si
ν_{AB}	A−B stretching mode
$\tilde{\nu}_{AB}$	A−B stretching frequency
$\tilde{\nu}_{as}(AB)$	frequency of the antisymmetric stretching mode of the AB unit
$\tilde{\nu}_{s}(AB)$	frequency of the symmetric stretching mode of the AB unit
δ_{ABC}	A−B−C in-plane bending mode
γ_{ABC}	A−B−C out-of-plane tortion mode
λ	laser excitation wavelength
$\Delta\tilde{\nu}(CO)$	variation of the C−O stretching frequency with respect to that in the gas phase
θ_{OH}	hydroxyl surface coverage
ρ_{OH}	average concentration of the total OH groups
$\rho_{OH,I}$	average concentration of the free isolated OH groups
$\rho_{OH,V}$	average concentration of the vicinal OH groups
$\rho_{OH,G}$	average concentration of the geminal OH groups
ρ_{SiOSi}.	average concentration of surface Si−O−Si bridges
ρ_{Si}	average concentration of surface Si atoms that are part of the siloxane bridges

8. Acknowledgments

Acknowledgments are due to C. Prestipino and F. Cesano for the unpublished DRS UV−vis spectra reported in Figure 10 and to G. Ricchiardi, A. Damin, and J. G. Vitillo for fruitful discussions on the theoretical results. Thanks are due to D. Scarano and G. Ghiotti for discussions on the experimental literature. A. Damin and C. Prestipino are also gratefully acknowledged for the Raman (Figure 21) and XAS (Figures 22 and 23) experiments, respectively. The latter have been performed at the GILDA BM8 beamline of the ESRF facility in Grenoble (France): The whole beamline staff (in particular, F. D'Acapito, F. La Manna, and F. D'Anca) is acknowledged.

9. References

(1) Böhm, L. L. *Angew. Chem. Int. Ed.* **2003**, *42*, 5010.
(2) Morse, P. M. *Chem. Eng. News* **1999**, *77*, 20.
(3) Theopold, K. H. *Chemtech* **1997**, *27*, 26.
(4) Hogan, J. P.; Banks, R. L. U.S. Patent 2,825,721, 1958.
(5) Hogan, J. P. *J. Polym. Sci.* **1970**, *8*, 2637.
(6) McDaniel, M. P. *Adv. Catal.* **1985**, *33*, 47.
(7) Clark, A. *Catal. Rev.* **1970**, *3*, 145.
(8) Weckhuysen, B. M.; Wachs, I. E.; Shoonheydt, R. A. *Chem. Rev.* **1996**, *96*, 3327.
(9) Weckhuysen, B. M.; Schoonheydt, R. A. *Catal. Today* **1999**, *51*, 215.
(10) Ziegler, K. Belgian Patent 533,362, 1954.
(11) Ziegler, K.; Holzkamp, E.; Martin, H.; Breil, H. *Angew. Chem.* **1955**, *67*, 541.
(12) Natta, G. *J. Polym. Sci.* **1955**, *16*, 143.
(13) Natta, G. *Angew. Chem. Int. Ed.* **1956**, *68*, 393.
(14) Wilke, G. *Angew. Chem. Int. Ed.* **2003**, *42*, 5000.
(15) Brintzinger, H. H.; Fischer, D.; Mulhaupt, R.; Rieger, B.; Waymouth, R. M. *Angew. Chem. Int. Ed.* **1995**, *34*, 1143.
(16) Theopold, K. H. *Eur. J. Inorg. Chem.* **1998**, 15.
(17) Duchateau, R. *Chem. Rev.* **2002**, *102*, 3525.
(18) Sauer, J.; Ugliengo, P.; Garrone, E.; Saunders, V. R. *Chem. Rev.* **1994**, *94*, 2095.
(19) Zhuravlev, L. T. *Colloid Surf. A* **2000**, *173*, 1.
(20) Duffy, J. A. *Bonding, Energy Levels and Bands*; Longman Scientific & Technical: 1990.
(21) Bolis, V.; Fubini, B.; Marchese, L.; Martra, G.; Costa, D. *J. Chem. Soc. Faraday Trans.* **1991**, *87*, 497.
(22) Ugliengo, P.; Garrone, E. *J. Mol. Catal.* **1984**, *54*, 439.
(23) Mortier, W. J.; Sauer, J.; Lercher, J. A.; Noller, H. *J. Phys. Chem.* **1984**, *88*, 905.
(24) Stave, M. S.; Nicholas, J. B. *J. Phys. Chem.* **1993**, *97*, 9630.
(25) Bordiga, S.; Ugliengo, P.; Damin, A.; Lamberti, C.; Spoto, G.; Zecchina, A.; Spano, G.; Buzzoni, R.; Dalloro, L.; Rivetti, F. *Top. Catal.* **2001**, *15*, 43.
(26) Bordiga, S.; Roggero, I.; Ugliengo, P.; Zecchina, A.; Bolis, V.; Artioli, G.; Buzzoni, R.; Marra, G.; Rivetti, F.; Spano, G.; Lamberti, C. *J. Chem. Soc., Dalton Trans.* **2000**, 3921.
(27) Pimentel, G. C.; McClellan, A. L. *The Hydrogen Bond*; Freeman: San Francisco, 1960.
(28) Paze, C.; Bordiga, S.; Lamberti, C.; Salvalaggio, M.; Zecchina, A.; Bellussi, G. *J. Phys. Chem. B* **1997**, *101*, 4740.
(29) Knözinger, H. In *The Hydrogen Bond. Recent Developments in Theory and Experiments*; Shuster, P., Zundel, G., Sandorfy, C., Eds.: North-Holland: Amsterdam, 1976; Vol. 3, p 1263.
(30) Knözinger, H. Infrared spectroscopy for the characterization of surface acidity and basicity. In *Handbook of Heterogeneous Catalysis*; Ertl, G., Knözinger, H., Weitkamp, J., Eds.; Wiley-VCH: Whenheim, 1997; Vol. 2, p 707.
(31) Zecchina, A.; Bordiga, S.; Spoto, G.; Scarano, D.; Spano, G.; Geobaldo, F. *J. Chem. Soc., Faraday Trans.* **1996**, *92*, 4863.
(32) Zecchina, A.; Geobaldo, F.; Spoto, G.; Bordiga, S.; Ricchiardi, G.; Buzzoni, R.; Petrini, G. *J. Phys. Chem. B* **1996**, *100*, 16584.
(33) Zecchina, A.; Lamberti, C.; Bordiga, S. *Catal. Today* **1998**, *41*, 169.
(34) Bolis, V.; Busco, C.; Bordiga, S.; Ugliengo, P.; Lamberti, C.; Zecchina, A. *Appl. Surf. Sci.* **2002**, *196*, 56.
(35) Ferrari, A. M.; Ugliengo, P.; Garrone, E. *J. Phys. Chem.* **1993**, *97*, 2671.
(36) Bronnimann, C. E.; Zeigler, R. C.; Maciel, G. E. *J. Am. Chem. Soc.* **1988**, *110*, 2023.
(37) Morrow, B. A.; Gay, I. D. *J. Phys. Chem.* **1988**, *92*, 5569.
(38) Hoffman, P.; Knözinger, E. *Surf. Sci.* **1987**, *188*, 181.
(39) McFarlan, A. J.; Morrow, B. A. *J. Phys. Chem.* **1991**, *95*, 5388.
(40) Iarlori, S.; Ceresoli, D.; Bernasconi, M.; Donadio, D.; Parrinello, M. *J. Phys. Chem. B* **2001**, *105*, 8007.
(41) Borello, E.; Zecchina, A.; Morterra, C. *J. Phys. Chem.* **1967**, *71*, 2938.
(42) Boccuzzi, F.; Coluccia, S.; Ghiotti, G.; Morterra, C.; Zecchina, A. *J. Phys. Chem.* **1978**, *82*, 1298.
(43) Morrow, B. A.; Cody, I. A. *J. Phys. Chem.* **1976**, *80*, 1998.
(44) Morrow, B. A.; Cody, I. A. *J. Phys. Chem.* **1976**, *80*, 1995.
(45) Morrow, B. A.; Cody, I. A. *J. Phys. Chem.* **1976**, *80*, 2761.
(46) Burneau, A.; Gallas, J.-P. Vibrational spectroscopies. In *The Surface Properties of Silica*; Legrand, A. P., Ed.; Wiley: New York, 1998; p 147.
(47) Humbert, B. *J. Non-Cryst. Solids* **1995**, *191*, 29.
(48) Chuang, I. S.; Maciel, G. E. *J. Phys. Chem. B* **1997**, *101*, 3052.
(49) Chuang, I. S.; Maciel, G. E. *J. Am. Chem. Soc.* **1996**, *118*, 401.
(50) Hommel, H.; Legrand, A. P.; Doremiéux, C.; d'Espinose de la Caillerie, J.-B. NMR spectroscopies. In *The Surface Properties of Silica*; Legrand, A. P., Ed.; Wiley: New York, 1998; p 235.
(51) Legrand, A. P. On the silica edge. In *The Surface Properties of Silica*; Legrand, A. P., Ed.; Wiley: New York, 1998; p 1.
(52) Ceresoli, D.; Bernasconi, M.; Iarlori, S.; Parrinello, M.; Tosatti, E. *Phys. Rev. Lett.* **2000**, *84*, 3887.

(53) Car, R.; Parrinello, M. *Phys. Rev. Lett.* **1985**, *55*, 2471.
(54) Zhuravlev, L. T. *Langmuir* **1987**, *3*, 316.
(55) Accelrys Inc., Materials Studio Getting Started code, San Diego, CA, 2002.
(56) Note that the absorption coefficient of the O−H stretching of interacting silanols strongly increases with the increase of the interaction strength, as a consequence of the increase of the dipole moment of the OH group. This means that the stronger the hydrogen bond interaction is the greater is the absorption coefficient and thus the corresponding IR band intensity. As a consequence, the much higher integrated area of the band in the 3600−3100 cm^{-1} range, due to silanols in mutual H-bond interaction, with respect to that of isolated silanols at 3748 cm^{-1} (Figure 3b), does not reflect a much higher concentration of the former vs the latter, as clearly documented by the quantitative data reported in Figure 8.
(57) Garofalini, S. H. *J. Non-Cryst. Solids* **1990**, *120*, 1.
(58) Huff, N. T.; Demiralp, E.; Cagin, T.; Goddard, W. A. *J. Non-Cryst. Solids* **1999**, *253*, 133.
(59) Du, M. H.; Kolchin, A.; Cheng, H. P. *J. Chem. Phys.* **2003**, *119*, 6418.
(60) Du, M. H.; Kolchin, A.; Cheng, H. P. *J. Chem. Phys.* **2004**, *120*, 1044.
(61) Masini, P.; Bernasconi, M. *J. Phys.: Condens. Mater.* **2002**, *14*, 4133.
(62) Wright, A. C. *J. Non-Cryst. Solids* **1994**, *179*, 84.
(63) Grabbe, A.; Michalske, T. A.; Smith, W. L. *J. Phys. Chem.* **1995**, *99*, 4648.
(64) Morrow, B. A.; Devi, A. *J. Chem. Soc., Faraday Trans. 1* **1972**, *68*, 403.
(65) Chiang, C. M.; Zegarski, B. R.; Dubois, L. H. *J. Phys. Chem.* **1993**, *97*, 6948.
(66) Ricchiardi, G.; Damin, A.; Bordiga, S.; Lamberti, C.; Spano, G.; Rivetti, F.; Zecchina, A. *J. Am. Chem. Soc.* **2001**, *123*, 11409.
(67) Bordiga, S.; Damin, A.; Bonino, F.; Ricchiardi, G.; Zecchina, A.; Tagliapietra, R.; Lamberti, C. *Phys. Chem. Chem. Phys.* **2003**, *5*, 4390.
(68) Bordiga, S.; Damin, A.; Bonino, F.; Ricchiardi, G.; Lamberti, C.; Zecchina, A. *Angew. Chem. Int. Edit.* **2002**, *41*, 4734.
(69) Bordiga, S.; Damin, A.; Bonino, F.; Zecchina, A.; Spano, G.; Rivetti, F.; Bolis, V.; Prestipino, C.; Lamberti, C. *J. Phys. Chem. B* **2002**, *106*, 9892.
(70) Damin, A.; Ricchiardi, G.; Bordiga, S.; Zecchina, A.; Ricci, F.; Spano, G.; Lamberti, C. *Stud. Surf. Sci. Catal.* **2001**, *140*, 195.
(71) Spoto, G.; Bordiga, S.; Garrone, E.; Ghiotti, G.; Zecchina, A.; Petrini, G.; Leofanti, G. *J. Mol. Catal.* **1992**, *74*, 175.
(72) Zecchina, A.; Bordiga, S.; Spoto, G.; Marchese, L.; Petrini, G.; Leofanti, G.; Padovan, M. *J. Phys. Chem.* **1992**, *96*, 4985.
(73) Ferrari, A. M.; Garrone, E.; Spoto, G.; Ugliengo, P.; Zecchina, A. *Surf. Sci.* **1995**, *323*, 151.
(74) Bunker, B. C.; Haaland, D. M.; Ward, K. J.; Michalske, T. A.; Smith, W. L.; Binkley, J. S.; Melius, C. F.; Balfe, C. A. *Surf. Sci.* **1989**, *210*, 406.
(75) Bunker, B. C.; Haaland, D. M.; Michalske, T. A.; Smith, W. L. *Surf. Sci.* **1989**, *222*, 95.
(76) Brinker, C. J.; Tallant, D. R.; Roth, E. P.; Ashley, C. S. *J. Non-Cryst. Solids* **1982**, *82*, 117.
(77) Fubini, B.; Bolis, V.; Cavenago, A.; Ugliengo, P. *J. Chem. Soc., Faraday Trans.* **1992**, *88*, 277.
(78) Fubini, B.; Bolis, V.; Cavenago, A.; Garrone, E.; Ugliengo, P. *Langmuir* **1993**, *9*, 2712.
(79) Bolis, V.; Cavenago, A.; Fubini, B. *Langmuir* **1997**, *13*, 895.
(80) Fubini, B. Health effects of silica. In *The Surface Properties of Silica*; Legrand, A. P., Ed.; Wiley: New York, 1998; p 415.
(81) Wilson, M.; Walsh, T. R. *J. Chem. Phys.* **2000**, *113*, 9180.
(82) Walsh, T. R.; Wilson, M.; Sutton, A. P. *J. Chem. Phys.* **2000**, *113*, 9191.
(83) Du, M. H.; Wang, L. L.; Kolchin, A.; Cheng, H. P. *Eur. Phys. J. D* **2003**, *24*, 323.
(84) Penev, E.; Kratzer, P.; Scheffler, M. *J. Chem. Phys.* **1999**, *110*, 3986.
(85) Damin, A.; Bonino, F.; Ricchiardi, G.; Bordiga, S.; Zecchina, A.; Lamberti, C. *J. Phys. Chem. B* **2002**, *106*, 7524.
(86) Damin, A.; Bordiga, S.; Zecchina, A.; Lamberti, C. *J. Chem. Phys.* **2002**, *117*, 226.
(87) Bonino, F.; Damin, A.; Bordiga, S.; Lamberti, C.; Zecchina, A. *Langmuir* **2003**, *19*, 2155.
(88) Bonino, F.; Damin, A.; Ricchiardi, G.; Ricci, M.; Spanò, G.; D'Aloisio, R.; Zecchina, A.; Lamberti, C.; Prestipino, C.; Bordiga, S. *J. Phys. Chem. B* **2004**, *108*, 3573.
(89) Damin, A.; Bordiga, S.; Zecchina, A.; Doll, K.; Lamberti, C. *J. Chem. Phys.* **2003**, *118*, 10183.
(90) Du, M. H.; Cheng, H. P. *Int. J. Quantum Chem.* **2003**, *93*, 1.
(91) Zhuravlev, L. T. *Pure Appl. Chem.* **1989**, *61*, 1969.
(92) Zhuravlev, L. T. *Colloid Surf. A* **1993**, *74*, 71.
(93) Bergna, H. E. *The Colloid Chemistry of Silica*; American Chemical Society: Washington, DC, 1994.
(94) Zecchina, A.; Garrone, E.; Ghiotti, G.; Morterra, C.; Borello, E. *J. Phys. Chem.* **1975**, *79*, 966.
(95) Nishimura, M.; Thomas, J. M. *Catal. Lett.* **1993**, *21*, 149.
(96) Vuurman, M. A.; Wachs, I. E.; Stufkens, D. J.; Oskam, A. *J. Mol. Catal.* **1993**, *80*, 209.
(97) Weckhuysen, B. M.; Schoonheydt, R. A.; Jehng, J. M.; Wachs, I. E.; Cho, S. J.; Ryoo, R.; Kijlstra, S.; Poels, E. *J. Chem. Soc., Faraday Trans.* **1995**, *91*, 3245.
(98) McDaniel, M. P. *J. Catal.* **1981**, *67*, 71.
(99) McDaniel, M. P. *J. Catal.* **1982**, *76*, 17.
(100) McDaniel, M. P. *J. Catal.* **1982**, *76*, 29.
(101) Groeneveld, C.; Wittgen, P. P. M. M.; Kersbergen van, A. M.; Hestrom, P. L. M.; Nuijten, C. E.; Schuit, G. C. A. *J. Catal.* **1979**, *59*, 153.
(102) McDaniel, M. P. *J. Catal.* **1982**, *76*, 37.
(103) Krauss, H.-L.; Stach, H. *Z. Anorg. Allg. Chem.* **1975**, *414*, 97.
(104) Rebenstorf, B.; Larsson, R. *J. Mol. Catal.* **1981**, *11*, 247.
(105) Jehng, J. M.; Wachs, I. E.; Weckhuysen, B. M.; Schoonheydt, R. A. *J. Chem. Soc., Faraday Trans.* **1995**, *91*, 953.
(106) Vuurman, M. A.; Hardcastle, F. D.; Wachs, I. E. *J. Mol. Catal.* **1993**, *84*, 193.
(107) O'Reilly, D. E.; MacIver, D. S. *J. Phys. Chem.* **1962**, *66*, 276.
(108) O'Reilly, D. E.; Santiago, F. D.; Squires, R. G. *J. Phys. Chem.* **1969**, *73*, 3172.
(109) Cordischi, D.; Campa, M. C.; Indovina, V.; Occhiuzzi, M. *J. Chem. Soc., Faraday Trans.* **1994**, *90*, 207.
(110) Cordischi, D.; Indovina, V.; Occhiuzzi, M. *J. Chem. Soc., Faraday Trans.* **1991**, *87*, 3443.
(111) Weckhuysen, B. M.; Wachs, I. E.; Schoonheydt, R. A. *Stud. Surf. Sci. Catal.* **1995**, *91*, 151.
(112) Weckhuysen, B. M.; Schoonheydt, R. A.; Mabbs, F. E.; Collison, D. *J. Chem. Soc., Faraday Trans.* **1996**, *92*, 2431.
(113) Weckhuysen, B. M.; Deridder, L. M.; Grobet, P. J.; Schoonheydt, R. A. *J. Phys. Chem.* **1995**, *99*, 320.
(114) Cordischi, D.; Indovina, V.; Occhiuzzi, M. *Appl. Surf. Sci.* **1992**, *55*, 233.
(115) Groppo, E.; Prestipino, C.; Cesano, F.; Bonino, F.; Bordiga, S.; Lamberti, C.; Thune, P. C.; Niemantsverdriet, J. W.; Zecchina, A. *J. Catal.* **2005**, in press.
(116) Baker, L. M.; Carrick, W. L. *J. Org. Chem.* **1968**, *33*, 616.
(117) Fubini, B.; Ghiotti, G.; Stradella, L.; Garrone, E.; Morterra, C. *J. Catal.* **1980**, *66*, 200.
(118) Ghiotti, G.; Garrone, E.; Della Gatta, G.; Fubini, B.; Giamello, E. *J. Catal.* **1983**, *80*, 249.
(119) Rebenstorf, B. *Acta Chem. Scand. A* **1977**, *31*, 877.
(120) Rebenstorf, B. *J. Mol. Catal.* **1991**, *66*, 59.
(121) Rebenstorf, B. *Acta Chem. Scand. A* **1989**, *43*, 413.
(122) Rebenstorf, B. *J. Mol. Catal.* **1989**, *56*, 170.
(123) Ghiotti, G.; Garrone, E.; Zecchina, A. *J. Mol. Catal.* **1988**, *46*, 61.
(124) Ghiotti, G.; Garrone, E.; Zecchina, A. *J. Mol. Catal.* **1991**, *65*, 73.
(125) Pershin, A. N.; Shelimov, B. N.; Kazansky, V. B. *Kinet. Katal.* **1979**, *20*, 1298.
(126) Pershin, A. N.; Shelimov, B. N.; Kazansky, V. B. *Kinet. Katal.* **1981**, *22*, 1526.
(127) Kazansky, V. B. *Kinet. Katal.* **1983**, *24*, 1338.
(128) Anpo, M.; Tanahashi, I.; Kubokawa, Y. *J. Phys. Chem.* **1982**, *86*, 1.
(129) Shelimov, B. N.; Elev, I. V.; Kazansky, V. B. *J. Catal.* **1986**, *98*, 70.
(130) Kohler, S. D.; Ekerdt, J. G. *J. Phys. Chem.* **1994**, *98*, 4336.
(131) Zecchina, A.; Spoto, G.; Bordiga, S. *Faraday Discuss. Chem. Soc.* **1989**, *87*, 149.
(132) Przhevalskaya, L. K.; Shvets, V. A.; Kazansky, V. B. *J. Catal.* **1975**, *39*, 363.
(133) Myers, D. L.; Lunsford, J. H. *J. Catal.* **1986**, *99*, 140.
(134) Lunsford, J. H.; Fu, S. L.; Myers, D. L. *J. Catal.* **1988**, *111*, 231.
(135) Merryfield, R.; McDaniel, M. P.; Parks, G. *J. Catal.* **1982**, *77*, 348.
(136) Morys, P.; Gorges, U.; Krauss, H. L. *Z. Naturforsh. B* **1984**, *39*, 458.
(137) Morys, P.; Gerritze, R.; Krauss, H. L. *Z. Naturforsch. B* **1977**, *31*, 774.
(138) Weckhuysen, B. M.; Verberckmoes, A. A.; DeBaets, A. R.; Schoonheydt, R. A. *J. Catal.* **1997**, *166*, 160.
(139) Weckhuysen, B. M.; Deridder, L. M.; Schoonheydt, R. A. *J. Phys. Chem.* **1993**, *97*, 4756.
(140) Zielinski, P.; Lana, I. G. D. *J. Catal.* **1992**, *137*, 368.
(141) Zielinski, P. A.; Szymura, J. A.; Lana, I. G. D. *Catal. Lett.* **1992**, *13*, 331.
(142) Kim, C. S.; Woo, S. I. *J. Mol. Catal.* **1992**, *73*, 249.
(143) Zecchina, A.; Scarano, D.; Bordiga, S.; Spoto, G.; Lamberti, C. *Adv. Catal.* **2001**, *46*, 265.
(144) Garrone, E.; Ghiotti, G.; Morterra, C.; Zecchina, A. *Z. Naturforsh. B* **1987**, *42*, 728.
(145) Rebenstorf, B.; Larsson, R. *Z. Anorg. Allg. Chem.* **1981**, *478*, 119.
(146) Zecchina, A.; Spoto, G.; Ghiotti, G.; Garrone, E. *J. Mol. Catal.* **1994**, *86*, 423.

(147) Cimino, A.; Cordischi, D.; Derossi, S.; Ferraris, G.; Gazzoli, D.; Indovina, V.; Minelli, G.; Occhiuzzi, M.; Valigi, M. *J. Catal.* **1991**, *127*, 744.
(148) Cimino, A.; De Angelis, B. A.; Luchetti, A.; Minelli, G. *J. Catal.* **1976**, *45*, 316.
(149) Gazzoli, D.; Occhiuzzi, M.; Cimino, A.; Minelli, G.; Valigi, M. *Surf. Interface Anal.* **1992**, *18*, 315.
(150) McDaniel, M. P.; Johnson, M. M. U.S. Patent 4,364,842, 1980.
(151) McDaniel, M. P.; Johnson, M. M. *J. Catal.* **1980**, *101*, 446.
(152) McDaniel, M. P.; Johnson, M. M. *Macromolecules* **1987**, *20*, 446.
(153) Zhu, Z. D.; Chang, Z. X.; Kevan, L. *J. Phys. Chem. B* **1999**, *103*, 2680.
(154) Zhu, Z. D.; Wasowicz, T.; Kevan, L. *J. Phys. Chem. B* **1997**, *101*, 10763.
(155) Zhu, Z. D.; Hartmann, M.; Maes, E. M.; Czernuszewicz, R. S.; Kevan, L. *J. Phys. Chem. B* **2000**, *104*, 4690.
(156) Ulagappan, N.; Rao, C. N. R. *Chem. Commun.* **1996**, 1047.
(157) Zhang, W. Z.; Pinnavaia, T. J. *Catal. Lett.* **1996**, *38*, 261.
(158) Weckhuysen, B. M.; Rao, R. R.; Pelgrims, J.; Schoonheydt, R. A.; Bodart, P.; Debras, G.; Collart, O.; Van Der Voort, P.; Vansant, E. F. *Chem.-Eur. J.* **2000**, *6*, 2960.
(159) Bade, O. M.; Blom, R.; Ystenes, M. *Organometallics* **1998**, *17*, 2524.
(160) Bade, O. M.; Blom, R. *Appl. Catal. A* **1997**, *161*, 249.
(161) Bade, O. M.; Blom, R.; Ystenes, M. *J. Mol. Catal. A* **1998**, *135*, 163.
(162) McDaniel, M.; Welch, M. B.; Dreiling, M. J. *J. Catal.* **1983**, *82*, 118.
(163) McDaniel, M. P.; Witt, D. R.; Benham, E. A. *J. Catal.* **1998**, *176*, 344.
(164) Pullukat, T. J.; Hoff, R. E.; Shida, M. *J. Polym. Sci,: Polym. Chem. Ed.* **1980**, *18*, 2857.
(165) Pullukat, T. J.; Shida, M. U.S. Patent 3,780,011, 1973.
(166) Conway, S. J.; Falconer, J. W.; Rochester, C. H.; Dows, G. W. *J. Chem. Soc., Faraday Trans.* **1989**, *85*, 71.
(167) Conway, S. J.; Falconer, J. W.; Rochester, C. H.; Dows, G. W. *J. Chem. Soc., Faraday Trans.* **1989**, *85*, 79.
(168) Conway, S. J.; Falconer, J. W.; Rochester, C. H.; Dows, G. W. *J. Chem. Soc., Faraday Trans.* **1989**, *85*, 1841.
(169) Ellison, A.; Overton, T. L. *J. Mol. Catal.* **1994**, *90*, 81.
(170) Rebenstorf, B.; Sheng, T. C. *Langmuir* **1991**, *7*, 2160.
(171) Hogan, J. P.; Witt, D. R. U.S. Patent 3,622,521, 1971.
(172) Horvath, B. U.S. Patent 3,625,864, 1971.
(173) Hoff, R. E.; Pullukat, T. J.; Shida, M. *J. Appl. Polym. Sci.* **1981**, *26*, 2927.
(174) Bordiga, S.; Buzzoni, R.; Geobaldo, F.; Lamberti, C.; Giamello, E.; Zecchina, A.; Leofanti, G.; Petrini, G.; Tozzola, G.; Vlaic, G. *J. Catal.* **1996**, *158*, 486.
(175) Berlier, G.; Spoto, G.; Fisicaro, P.; Bordiga, S.; Zecchina, A.; Giamello, E.; Lamberti, C. *Microchem. J.* **2002**, *71*, 101.
(176) Lamberti, C.; Spoto, G.; Scarano, D.; Paze, C.; Salvalaggio, M.; Bordiga, S.; Zecchina, A.; Turnes Palomino, G.; DAcapito, F. *Chem. Phys. Lett.* **1997**, *269*, 500.
(177) Turnes Palomino, G.; Fisicaro, P.; Bordiga, S.; Zecchina, A.; Giamello, E.; Lamberti, C. *J. Phys. Chem. B* **2000**, *104*, 4064.
(178) Llabres i Xamena, F. X.; Fisicaro, P.; Berlier, G.; Zecchina, A.; Turnes Palomino, G.; Prestipino, C.; Bordiga, S.; Giamello, E.; Lamberti, C. *J. Phys. Chem. B* **2003**, *107*, 7036.
(179) Miller, R. M.; Tinti, D. S.; Case, D. A. *Inorg. Chem.* **1989**, *28*, 2738.
(180) Bensalem, A.; Weckhuysen, B. M.; Schoonheydt, R. A. *J. Phys. Chem. B* **1997**, *101*, 2824.
(181) Weckhuysen, B. M.; Schoofs, B.; Schoonheydt, R. A. *J. Chem. Soc., Faraday Trans.* **1997**, *93*, 2117.
(182) Weckhuysen, B. M.; Schoonheydt, R. A. *Catal. Today* **1999**, *49*, 441.
(183) Weckhuysen, B. M.; Verberckmoes, A. A.; Debaere, J.; Ooms, K.; Langhans, I.; Schoonheydt, R. A. *J. Mol. Catal. A* **2000**, *151*, 115.
(184) Puurunen, R. L.; Beheydt, B. J.; Weckhuysen, B. M. *J. Catal.* **2001**, *204*, 253.
(185) Cieslak-Golonka, M. *Coord. Chem. Rev.* **1991**, *109*, 223.
(186) Finch, J. N. *J. Catal.* **1976**, *43*, 111.
(187) Zecchina, A.; Garrone, E.; Morterra, C.; Coluccia, S. *J. Phys. Chem.* **1975**, *79*, 978.
(188) Figgis, B. N. *Introduction to Ligand Fields*; John Wiley & Sons: New York, 1966.
(189) Note that this is not the first time that a ligand displacement has been hypothesized to explain the evolution of the UV−vis and IR spectra of adsorbed species upon increasing the equilibrium pressure of the probe molecule. See, e.g., Berlier, G.; Spoto, G.; Bordiga, S.; Ricchiardi, G.; Fisicaro, P.; Zecchina, A.; Rossetti, I.; Selli, E.; Forni, L.; Giamello, E.; Lamberti C. *J. Catal*. **2002**, *208*, 64−82.
(190) Espelid, O.; Borve, K. J. *Catal. Lett.* **2001**, *75*, 49.
(191) Espelid, O.; Borve, K. J. *J. Catal.* **2002**, *205*, 177.
(192) Zecchina, A.; Otero Arean, C. *Chem. Soc. Rev.* **1996**, *25*, 187.
(193) Yermakov, Y. I.; Zacharov, V. A. *Adv. Catal.* **1975**, *24*, 173.
(194) Lupinetti, A. J.; Frenking, G.; Strauss, S. H. *Angew. Chem. Int. Ed.* **1998**, *37*, 2113.
(195) Strauss, S. H. *J. Chem. Soc., Dalton* **2000**, 1.
(196) Xu, Q. *Coord. Chem. Rev.* **2002**, *231*, 83.
(197) Willner, H.; Aubke, F. *Angew. Chem. Int. Ed.* **1997**, *36*, 2403.
(198) Zecchina, A.; Bordiga, S.; Turnes Palomino, G.; Scarano, D.; Lamberti, C.; Salvalaggio, M. *J. Phys. Chem. B* **1999**, *103*, 3833.
(199) Bolis, V.; Barbaglia, A.; Bordiga, S.; Lamberti, C.; Zecchina, A. *J. Phys. Chem. B* **2004**, *108*, 9970.
(200) Gaspar, A. B.; Martins, R. L.; Schmal, M.; Dieguez, L. C. *J. Mol. Catal. A* **2001**, *169*, 105.
(201) Gaspar, A. B.; Brito, J. L. F.; Dieguez, L. C. *J. Mol. Catal. A* **2003**, *203*, 251.
(202) Scarano, D.; Spoto, G.; Bordiga, S.; Zecchina, A.; Lamberti, C. *Surf. Sci.* **1992**, *176*, 281.
(203) Scarano, D.; Spoto, G.; Bordiga, S.; Carnelli, L.; Ricchiardi, G.; Zecchina, A. *Langmuir* **1994**, *10*, 3094.
(204) Braterman, P. S. *Metal Carbonyl Spectra*; Academic Press: London, 1975.
(205) Lamberti, C.; Bordiga, S.; Salvalaggio, M.; Spoto, G.; Zecchina, A.; Geobaldo, F.; Vlaic, G.; Bellatreccia, M. *J. Phys. Chem.* **1997**, *101*, 344.
(206) Lamberti, C.; Turnes Palomino, G.; Bordiga, S.; Berlier, G.; D'Acapito, F.; Zecchina, A. *Angew. Chem., Int. Ed.* **2000**, *39*, 2138.
(207) Bordiga, S.; Turnes Palomino, G.; Arduino, D.; Lamberti, C.; Zecchina, A.; Otero Areán, C. *J. Mol. Catal. A* **1999**, *146*, 97.
(208) Kettle, S. F. A.; Paul, I. In *Advances in Organometallic Chemistry*; Stone, F. G. A., West, R., Eds.; Academic Press: New York, 1972; Vol. 10, p 199.
(209) Bordiga, S.; Bertarione, S.; Damin, A.; Prestipino, C.; Spoto, G.; Lamberti, C.; Zecchina, A. *J. Mol. Catal. A* **2003**, *204*, 527.
(210) Zecchina, A.; Bordiga, S.; Spoto, G.; Marchese, L.; Petrini, G.; Leofanti, G.; Padovan, M. *J. Phys. Chem.* **1992**, *96*, 4991.
(211) Bordiga, S.; Escalona Platero, E.; Otero Arean, C.; Lamberti, C.; Zecchina, A. *J. Catal.* **1992**, *137*, 179.
(212) Zecchina, A.; Bordiga, S.; Lamberti, C.; Spoto, G.; Carnelli, L.; Otero Arean, C. *J. Phys. Chem.* **1994**, *98*, 9577.
(213) Bordiga, S.; Scarano, D.; Spoto, G.; Zecchina, A.; Lamberti, C.; Otero Arean, C. *Vib. Spectrosc.* **1993**, *5*, 69.
(214) Lamberti, C.; Morterra, C.; Bordiga, S.; Cerrato, G.; Scarano, D. *Vib. Spectrosc.* **1993**, *4*, 273.
(215) Lamberti, C.; Bordiga, S.; Cerrato, G.; Morterra, C.; Scarano, D.; Spoto, G.; Zecchina, A. *Comput. Phys. Commun.* **1993**, *74*, 119.
(216) Rebenstorf, B. *Acta Chem. Scand. A* **1991**, *45*, 1012.
(217) Adamo, C.; Barone, V.; Fortunelli, A. *J. Chem. Phys.* **1995**, *102*, 384.
(218) Geerlings, P.; De Proft, F.; Langenaeker, W. *Chem. Rev.* **2003**, *103*, 1793.
(219) Becke, A. D. *J. Chem. Phys.* **1993**, *98*, 1372.
(220) Becke, A. D. *J. Chem. Phys.* **1993**, *98*, 5648.
(221) Lee, C.; Yang, W.; Parr, R. G. *Phys. Rev. B* **1988**, *37*, 785.
(222) Civalleri, B.; Garrone, E.; Ugliengo, P. *Chem. Phys. Lett.* **1998**, *294*, 103.
(223) Espelid, O. Theoretical models of active sites at Cr/Silica Phillips type catalysts for ethylene polymerization. Ph.D. Thesis in Chemistry, Bergen, Norway, 2001.
(224) Vitillo, J. G. Ab initio modeling of silica-supported Cr(II) sites active in the ethylene polymerization. Degree Thesis in Materials Science, Torino, Italy, 2002.
(225) Vitillo, J. G.; Damin, A.; Zecchina, A.; Lamberti, C.; et al. Manuscript in preparation.
(226) Andrews, L.; Zhou, M. F.; Gutsev, G. L.; Wang, X. F. *J. Phys. Chem. A* **2003**, *107*, 561.
(227) Zhou, M. F.; Andrews, L.; Bauschlicher, C. W. *Chem. Rev.* **2001**, *101*, 1931.
(228) Leofanti, G.; Marsella, A.; Cremaschi, B.; Garilli, M.; Zecchina, A.; Spoto, G.; Bordiga, S.; Fisicaro, P.; Berlier, G.; Prestipino, C.; Casali, G.; Lamberti, C. *J. Catal.* **2001**, *202*, 279.
(229) Berlier, G.; Spoto, G.; Bordiga, S.; Ricchiardi, G.; Fisicaro, P.; Zecchina, A.; Rossetti, I.; Selli, E.; Forni, L.; Giamello, E.; Lamberti, C. *J. Catal.* **2002**, *208*, 64.
(230) Connelly, N. G. *Inorg. Chem. Acta Rev.* **1972**, *6*, 47.
(231) Hoffmann, R.; Chen, M. M. L.; Elian, M.; Rossi, A. R.; Mingos, D. M. P. *Inorg. Chem.* **1974**, *13*, 2666.
(232) Hardcastle, F. D.; Wachs, I. E. *J. Mol. Catal.* **1988**, *46*, 173.
(233) Deo, G.; Wachs, I. E. *J. Phys. Chem.* **1991**, *95*, 5889.
(234) Kim, D. S.; Tatibouet, J. M.; Wachs, I. E. *J. Catal.* **1992**, *136*, 209.
(235) Weckhuysen, B. M.; Wachs, I. E. *J. Phys. Chem.* **1996**, *100*, 14437.
(236) Weckhuysen, B. M.; Wachs, I. E. *J. Chem. Soc., Faraday Trans.* **1996**, *92*, 1969.
(237) Weckhuysen, B. M.; Wachs, I. E. *J. Phys. Chem. B* **1997**, *101*, 2793.
(238) Dines, T. J.; Inglis, S. *Phys. Chem. Chem. Phys.* **2003**, *5*, 1320.
(239) Mattes, R. Z. *Z. Anorg. Allg. Chem.* **1971**, *362*, 163.

(240) Hope, E. G.; Levason, W.; Ogden, J. S.; Tajik, M. *J. Chem. Soc., Dalton Trans.* **1986**, 1587.
(241) Cimino, A.; Cordischi, D.; Febbraro, S.; Gazzoli, D.; Indovina, V.; Occhiuzzi, M.; Valigi, M.; Boccuzzi, F.; Chiorino, A.; Ghiotti, G. *J. Mol. Catal.* **1989**, *55*, 23.
(242) Kim, D. S.; Wachs, I. E. *J. Catal.* **1993**, *142*, 166.
(243) Vuurman, M. A.; Wachs, I. E. *J. Phys. Chem.* **1992**, *96*, 5008.
(244) Groppo, E.; Damin, A.; Bonino, F.; Zecchina, A.; Bordiga, S.; Lamberti, C. *J. Am. Chem. Soc.*, submitted.
(245) Li, C.; Xiong, G.; Xin, Q.; Liu, J.; Ying, P.; Feng, Z.; Li, J.; Yang, W.; Wang, Y.; Wang, G.; Liu, X.; Lin, M.; Wang, X.; Min, E. *Angew. Chem., Int. Ed.* **1999**, *38*, 2220.
(246) Li, C.; Xiong, G.; Liu, J. K.; Ying, P. L.; Xin, Q.; Feng, Z. C. *J. Phys. Chem. B* **2001**, *105*, 2993.
(247) Yu, L.; Xiong, G.; Li, C.; Xiao, F.-S. *J. Catal.* **2000**, *194*, 487.
(248) Xiong, G.; Li, C.; Li, H. Y.; Xin, Q.; Feng, Z. C. *Chem. Commun.* **2000**, 677.
(249) Wei, D.; Wang, H.; Feng, X. B.; Chueh, W. T.; Ravikovitch, P.; Lyubovsky, M.; Li, C.; Takeguchi, T.; Haller, G. L. *J. Phys. Chem. B* **1999**, *103*, 2113.
(250) Li, C.; Stair, P. C. *Stud. Surf. Sci. Catal.* **1996**, *101*, 881.
(251) Vuurman, M. A.; Stufkens, D. J.; Oskam, A.; Moulijn, J. A.; Kapteijn, F. *J. Mol. Catal.* **1990**, *60*, 83.
(252) Wachs, I. E. *Catal. Today* **1996**, *27*, 437.
(253) Lee, P. A.; Citrin, P. H.; Eisenberger, P.; Kincaid, M. *Rev. Mod. Phys.* **1981**, *53*, 769.
(254) Bart, J. C. J.; Vlaic, G. *Adv. Catal.* **1987**, *35*, 1.
(255) Bertagnolli, H.; Ertel, T. S. *Angew. Chem. Int. Ed.* **1994**, *33*, 45.
(256) Bianconi, A. XANES Spectroscopy. In *X-ray Absorption: Principles, Applications, Techniques of EXAFS, SEXAFS and XANES*; Koningsberger, D. C., Prins, R., Eds.; John Wiley & Sons: New York, 1988; Vol. 92, p 573.
(257) Lamberti, C.; Prestipino, C.; Bonino, F.; Capello, L.; Bordiga, S.; Spoto, G.; Zecchina, A.; Moreno, S. D.; Cremaschi, B.; Garilli, M.; Marsella, A.; Carmello, D.; Vidotto, S.; Leofanti, G. *Angew. Chem. Int. Ed.* **2002**, *41*, 2341.
(258) Lamberti, C.; Bordiga, S.; Bonino, F.; Prestipino, C.; Berlier, G.; Capello, L.; D'Acapito, F.; Llabres i Xamena, F. X.; Zecchina, A. *Phys. Chem. Chem. Phys.* **2003**, *5*, 4502.
(259) Prestipino, C.; Berlier, G.; Llabres i Xamena, F. X.; Spoto, G.; Bordiga, S.; Zecchina, A.; Turnes Palomino, G.; Yamamoto, T.; Lamberti, C. *Chem. Phys. Lett.* **2002**, *363*, 389.
(260) Wong, J.; Lytle, F. W.; Messmer, R. P.; Maylotte, D. H. *Phys. Rev. B* **1984**, *30*, 5595.
(261) Garcia, L.; Benfatto, M.; Natoli, C. R.; Bianconi, A.; Davoli, I.; Marcelli, A. *Solid. State Commun.* **1986**, *58*, 595.
(262) Pantelouris, A.; Modrovw, H.; Pantelouris, M.; Hormes, J.; Reinen, D. *Chem. Phys.* **2004**, *300*, 13.
(263) Bianconi, A. *Phys. Rev. B* **1982**, *26*, 2741.
(264) Mehadji, C.; Nour, S.; Chermette, H.; Cartier, C.; Menage, S.; Verdaguer, M. *Chem. Phys.* **1990**, *148*, 95.
(265) Bordiga, S.; Coluccia, S.; Lamberti, C.; Marchese, L.; Zecchina, A.; Boscherini, F.; Buffa, F.; Genoni, F.; Leofanti, G.; Petrini, G.; Vlaic, G. *J. Phys. Chem.* **1994**, *98*, 4125.
(266) Weidemann, C.; Rehder, D.; Kuetgens, U.; Hormes, J.; Vilter, H. *Chem. Phys.* **1989**, *136*, 405.
(267) Wolfsberg, M.; Helmholtz, L. *J. Chem. Phys.* **1953**, *20*, 837.
(268) Jousseaume, C.; Ribot, F.; Kahn-Harari, A.; Vivien, D.; Villain, F. *Nucl. Instrum. Methods B* **2003**, *200*, 425.
(269) Jousseaume, C.; Vivien, D.; Kahn-Harari, A.; Derouet, J.; Ribot, F.; Villain, F. *J. Appl. Phys.* **2003**, *93*, 6006.
(270) Arcon, I.; Mirtic, B.; Kodre, A. *J. Am. Chem. Soc.* **1959**, *81*, 222.
(271) Thune, P. C.; Verhagen, C. P. J.; vandenBoer, M. J. G.; Niemantsverdriet, J. W. *J. Phys. Chem. B* **1997**, *101*, 8559.
(272) Thune, P. C.; Linke, R.; van Gennip, W. J. H.; de Jong, A. M.; Niemantsverdriet, J. W. *J. Phys. Chem. B* **2001**, *105*, 3073.
(273) Wang, Y.; Ohishi, Y.; Shishido, T.; Zhang, Q. H.; Yang, W.; Guo, Q.; Wan, H. L.; Takehira, K. *J. Catal.* **2003**, *220*, 347.
(274) Pak, C.; Haller, G. L. *Microporous Mesoporous Mater.* **2001**, *48*, 165.
(275) Zecchina, A.; Groppo, E.; Damin, A.; Prestipino, C. *Top. Organomet. Chem.*, in press.
(276) Espelid, O.; Borve, K. J. *J. Catal.* **2002**, *205*, 366.
(277) Stephens, J. S.; Cruickshank, D. W. J. *Acta Crystallogr. B* **1970**, *26*, 222.
(278) Finger, L. W.; Hazen, R. M. *J. Appl. Phys.* **1980**, *51*, 5362.
(279) Lamberti, C.; Prestipino, C.; Bordiga, S.; Berlier, G.; Spoto, G.; Zecchina, A.; Laloni, A.; La Manna, F.; D'Anca, F.; Felici, R.; D'Acapito, F.; Roy, P. *Nucl. Instrum. Methods B* **2003**, *200*, 196.
(280) Liu, B. P.; Nakatani, H.; Terano, M. *J. Mol. Catal. A* **2003**, *201*, 189.
(281) Mori, H.; Hasebe, K.; Terano, M. *J. Mol. Catal. A* **1999**, *140*, 165.
(282) dos Santos, J. H. Z.; Ban, H. T.; Teranishi, T.; Uozumi, T.; Sano, T.; Soga, K. *J. Mol. Catal. A* **2000**, *158*, 541.
(283) Liu, B. P.; Terano, M. *J. Mol. Catal. A* **2001**, *172*, 227.
(284) Thune, P. C.; Loos, J.; Lemstra, P. J.; Niemantsverdriet, J. W. *J. Catal.* **1999**, *183*, 1.
(285) Thune, P. C.; Loos, J.; de Jong, A. M.; Lemstra, P. J.; Niemantsverdriet, J. W. *Top. Catal.* **2000**, *13*, 67.
(286) Thune, P. C.; Loos, J.; Wouters, D.; Lemstra, P. J.; Niemantsverdriet, J. W. *Macromol. Symp.* **2001**, *173*, 37.
(287) van Kimmenade, E. M. E.; Kuiper, A. E. T.; Tamminga, Y.; Thune, P. C.; Niemantsverdriet, J. W. *J. Catal.* **2004**, *223*, 134.
(288) Rahman, A.; Mohamed, M. H.; Ahmed, M.; Aitani, A. M. *Appl. Catal., A* **1995**, *121*, 203.
(289) Abbenhuis, H. C. L.; Vorstenbosch, M. L. W.; van Santen, R. A.; Smeets, W. J. J.; Spek, A. L. *Inorg. Chem.* **1997**, *36*, 6431.
(290) Grunert, W.; Shpiro, E. S.; Feldlaus, R.; Anderes, R.; Antoshin, G. V.; Minachev, K. M. *J. Catal.* **1986**, *100*, 138.
(291) Liu, B.; Nakatani, H.; Terano, M. *J. Mol. Catal. A* **2002**, *184*, 387.
(292) Schmidt, H.; Riederer, W.; Krauss, H. L. *J. Prak. Chem.-Chem. Ztg.* **1996**, *338*, 627.
(293) McDaniel, M. P.; Johnson, M. M. *J. Catal.* **1986**, *101*, 446.
(294) McDaniel, M. P.; Johnson, M. M. *Macromolecules* **1987**, *20*, 773.
(295) Bensalem, A.; Weckhuysen, B. M.; Schoonheydt, R. A. *J. Chem. Soc., Faraday Trans.* **1997**, *93*, 4065.
(296) Ellison, A.; Overton, T. L.; Bencze, L. *J. Chem. Soc., Faraday Trans.* **1993**, *89*, 843.
(297) Zacharov, V. A.; Yermakov, Y. I. *J. Polym. Sci. A* **1971**, *9*, 3129.
(298) Zacharov, V. A.; Yermakov, Y. I.; Kushnareva, E. G. *J. Polym. Sci. A* **1971**, *9*, 771.
(299) McDaniel, M. P.; Martin, S. J. *J. Phys. Chem.* **1991**, *95*, 3289.
(300) Grayson, M. E.; McDaniel, M. P. *J. Mol. Catal.* **1991**, *65*, 139.
(301) Choi, K. Y.; Tang, S. H. *J. Appl. Polym. Sci.* **2004**, *91*, 2923.
(302) Wang, S. M.; Tait, P. J. T.; Marsden, C. E. *J. Mol. Catal.* **1991**, *65*, 237.
(303) Zacharov, V. A.; Yermakov, Y. I. *Catal. Rev.-Sci. Eng.* **1979**, *19*, 67.
(304) Eden, C.; Feilchenfeld, H.; Haas, Y. *J. Catal.* **1968**, *11*, 263.
(305) Myers, D. L.; Lunsford, J. H. *J. Catal.* **1985**, *92*, 260.
(306) Eden, C.; Feilchenfeld, H.; Haas, Y. *J. Catal.* **1967**, *9*, 367.
(307) Amor Nait Ajjou, J.; Rice, G. L.; Scott, S. L. *J. Am. Chem. Soc.* **1998**, *120*, 13436.
(308) Amor Nait Ajjou, J.; Scott, S. L. *Organometallics* **1997**, *16*, 86.
(309) Amor Nait Ajjou, J.; Scott, S. L.; Paquet, V. *J. Am. Chem. Soc.* **1998**, *120*, 415.
(310) McDaniel, M. P.; Welch, M. B. *J. Catal.* **1983**, *82*, 98.
(311) Margl, P.; Deng, L. Q.; Ziegler, T. *J. Am. Chem. Soc.* **1999**, *121*, 154.
(312) Karol, F. J.; Karapinka, G. L.; Wu, C.; Dow, A. W.; Johnson, R. N.; Carrick, W. L. *J. Polym. Sci., Part A: Polym. Chem.* **1972**, *10*, 2621.
(313) Keii, T., *Kinetics of Ziegler−Natta Polymerization*; Chapman & Hall: London, 1972.
(314) Scott, S. L.; Amor Nait Ajjou, J. *Chem. Eng. Sci.* **2001**, *56*, 4155.
(315) Kim, C. S.; Woo, S. I.; Jeong, D. J.; Oh, J. S. *Polym. Bull.* **1992**, *29*, 205.
(316) Di Croce, P. G.; Aubriet, F.; Chety-Gimondo, R.; Muller, J. F.; Grange, P. *Rapid Commun. Mass Spectrom.* **2004**, *18*, 601.
(317) Kantcheva, M.; Bushev, V.; Klissurski, D. *J. Catal.* **1994**, *145*, 96.
(318) Bade, O. M.; Blom, R.; Dahl, I. M.; Karlsson, A. *J. Catal.* **1998**, *173*, 460.
(319) Rebenstorf, B. *Chem., Z. A. A.* **1984**, *513*, 103.
(320) Szymura, J. A.; DallaLana, I. G.; Fiedorow, R.; Zielinski, P. A. *Macromolecules* **1996**, *29*, 3103.
(321) Hogan, J. P. In *Copolymerization*; Ham, G. E., Ed.; Interscience: New York, 1964; p 103.
(322) Painter, P. C.; Coleman, M. M.; Koenig, J. L. *The Theory of Vibrational Spectroscopy and Its Application to Polymeric Materials*; Wiley: New York, 1982.
(323) Ghiotti, G.; Garrone, E.; Coluccia, S.; Morterra, C.; Zecchina, A. *J. Chem. Soc. Chem. Commun.* **1979**, 1032.
(324) Artioli, G.; Lamberti, C.; Marra, G. L. *Acta Crystallogr. B* **2000**, *56*, 2.
(325) Cossee, P. *J. Catal.* **1964**, *3*, 80.
(326) Ivin, K. J.; Rooney, J. J.; Stewart, C. D.; Green, M. L. H.; Mahtab, J. R. *J. Chem. Soc. Chem. Commun.* **1978**, 604.
(327) Zecchina, A.; Bertarione, S.; Damin, A.; Scarano, D.; Lamberti, C.; Prestipino, C.; Spoto, G.; Bordiga, S. *Phys. Chem. Chem. Phys.* **2003**, *5*, 4414.
(328) Krauss, H. L.; Hagen, K.; Hums, E. *J. Mol. Catal.* **1985**, *28*, 233.
(329) Candlin, J. P.; Thomas, H. *Adv. Chem. Ser.* **1974**, *132*, 212.
(330) Freundlich, J. S.; Schrock, R. R.; Cummins, C. C.; Davis, W. M. *J. Am. Chem. Soc.* **1994**, *116*, 6476.
(331) Giannini, L.; Solari, E.; Floriani, C.; Chiesi-Villa, A.; Rizzoli, C. *J. Am. Chem. Soc.* **1998**, *120*, 823.
(332) Ayscough, P. B.; Eden, C.; Steiner, H. *J. Catal.* **1965**, *4*, 278.
(333) Groeneveld, C.; Wittgen, P. P. M. M.; Swinnen, H. P. M.; Wernsen, A.; Schuit, G. C. A. *J. Catal.* **1983**, *83*, 346.
(334) Amor Nait Ajjou, J.; Scott, S. L. *J. Am. Chem. Soc.* **2000**, *122*, 8968.
(335) Ystenes, M. *J. Catal.* **1991**, *129*, 383.

(336) Blom, R.; Follestad, A.; Noel, O. *J. Mol. Catal.* **1994**, *91*, 237.
(337) Espelid, O.; Borve, K. J. *J. Catal.* **2000**, *195*, 125.
(338) Espelid, O.; Borve, K. J. *J. Catal.* **2002**, *206*, 331.
(339) Jozwiak, W. K.; Lana, I. G. D.; Fiedorow, R. *J. Catal.* **1990**, *121*, 183.
(340) Krauss, H. L.; Hums, E. *Z. Naturforsh., B: Anorg. Chem., Org. Chem.* **1979**, *34B*, 1628.
(341) McDaniel, M. P.; Kantor, D. M. *J. Polym. Sci., Part A: Polym. Chem.* **1983**, *21*, 1217.
(342) Al-Mashta, F.; Davanzo, C. U.; Sheppard, N. *J. Chem. Soc. Chem. Commun.* **1983**, 1258.
(343) Al-Mashta, F.; Sheppard, N.; Davanzo, C. U. *Mater. Chem. Phys.* **1985**, *13*, 315.
(344) Turner, H. W.; Schrock, R. R.; Fellman, J. D.; Holmes, S. J. *J. Am. Chem. Soc.* **1983**, *105*, 4942.
(345) Schmid, R.; Ziegler, T. *Can. J. Chem.* **2000**, *78*, 265.
(346) Emrich, R.; Heinemann, O.; Jolly, P. W.; Kruger, C.; Verhovnik, G. P. J. *Organometallics* **1997**, *16*, 1511.
(347) Ruddick, V. J.; Badyal, J. P. S. *J. Phys. Chem. B* **1998**, *102*, 2991.
(348) Huang, C. Z.; Ahn, J.; Kwon, S.; Kim, J.; Lee, J.; Han, Y. H.; Kim, H. *Appl. Catal. A* **2004**, *258*, 173.
(349) Smith, G. D.; Palmer, R. A. Fast time-resolved mid-infrared spectroscopy using an interferometer. In *Handbook of Vibrational Spectroscopy*; Chalmers, J. M., Griffiths, P. R., Eds.; J. W. Sons: Chichester: 2002; Vol. 1, p 625.
(350) Otero Arean, C.; Escalona Platero, E.; Spoto, G.; Zecchina, A. *J. Mol. Catal.* **1989**, *56*, 211.
(351) Escalona Platero, E.; Otero Arean, C.; Scarano, D.; Spoto, G.; Zecchina, A. *Mater. Chem. Phys.* **1991**, *29*, 347.
(352) Geobaldo, F.; Spoto, G.; Bordiga, S.; Lamberti, C.; Zecchina, A. *J. Chem. Soc., Faraday Trans.* **1997**, *93*, 1243.
(353) Spoto, G.; Bordiga, S.; Ricchiardi, G.; Scarano, D.; Zecchina, A.; Borello, E. *J. Chem. Soc., Faraday Trans.* **1994**, *90*, 2827.
(354) Vikulov, K.; Spoto, G.; Coluccia, S.; Zecchina, A. *Catal. Lett.* **1992**, *16*, 117.
(355) Lamberti, C.; Groppo, E.; Spoto, G.; Bordiga, S.; Zecchina, A. *Adv. Catal.*, invited contribution to appear in 2005.

CR040083S